Technical Report Documentation Page

1. Report No.	2. Government Accession No.	3. Recipient's Catalog No.
FHWA/TX-14/0-6656-1		

4. Title and Subtitle	5. Report Date
ASR TESTING: A NEW APPROACH TO AGGREGATE CLASSIFICATION AND MIX DESIGN VERIFICATION: TECHNICAL REPORT	Published: April 2014
	6. Performing Organization Code

7. Author(s)	8. Performing Organization Report No.
Anal K. Mukhopadhyay and Kai-Wei Liu	Report 0-6656-1

9. Performing Organization Name and Address	10. Work Unit No. (TRAIS)
Texas A&M Transportation Institute College Station, Texas 77843-3135	11. Contract or Grant No. Project 0-6656

12. Sponsoring Agency Name and Address	13. Type of Report and Period Covered
Texas Department of Transportation Research and Technology Implementation Office 125 East 11th St. Austin, Texas 78701-2483	Technical Report: September 1, 2010–August 31, 2013
	14. Sponsoring Agency Code

15. Supplementary Notes

Project performed in cooperation with the Texas Department of Transportation and the Federal Highway Administration.

Project Title: ASR Testing: A New Approach to Aggregate Classification and Mix Design Verification

URL: http://tti.tamu.edu/documents/0-6656-1.pdf

16. Abstract

The main objective of this study was to develop a fast, reliable test method to determine the aggregate alkali-silica reactivity (ASR) with respect to the overall alkalinity of the concrete. A volumetric change measuring device (VCMD) developed at the Texas A&M Transportation Institute was used in this research. The VCMD simulates the aggregate–pore solution reaction in concrete and measures free solution volume contraction due to ASR over time. The solution volume change over time at multiple temperatures is modeled to determine activation energy (E_a) based on the rate theory. The VCMD-based test can reliably predict aggregate alkali silica reactivity in a short period of time (5 days) in terms of measuring activation energy. A representative E_a can be determined by testing as-received aggregates (i.e., field aggregates) with 0.5N NaOH + Ca(OH)2 solution (similar to concrete pore solution) and with permissible repeatability. Researchers have developed an E_a-based aggregate classification system, which can serve as a potential screening parameter in an aggregate quality control program. A relationship between E_a and alkalinity is developed, which became the basis to determine threshold alkalinity. The proposed method has the potential to be considered as an alternative method to the current AMBT method.

An effective way of tailoring mix design depending on the level of protection needed is developed based on activation energy, threshold alkalinity, pore solution chemistry, and concrete validation testing. A new accelerated concrete cylinder test (ACCT) using VCMD (60°C, leaching-proof conditions) was developed to test concrete mixes in a short time. Although the testing period is not yet fully established, the ACCT method takes around 1 month to test a reactive straight cement concrete mix with varying alkali loadings (i.e., 8.9–4.5 lb/yard^3) and around 3–4 months to test a slowly reactive straight cement mix with lower alkali loadings (e.g., 3.0–4.0 lb/yard^3). The ACCT method has the ability to emerge as a potential method to test job mix.

17. Key Words	18. Distribution Statement
Alkali Silica Reaction, Volumetric Expansion Measuring Device, Aggregate, Alkaline Test Solution, Solution Volume Contraction, Activation Energy, Threshold Alkalinity, Pore Solution Alkalinity, Accelerated Concrete Cylinder Test, Mix Design Validation	No restrictions. This document is available to the public through NTIS: National Technical Information Service Alexandria, Virginia 22312 http://www.ntis.gov

19. Security Classif. (of this report)	20. Security Classif. (of this page)	21. No. of Pages	22. Price
Unclassified	Unclassified	200	

Form DOT F 1700.7 (8-72) **Reproduction of completed page authorized**

ASR TESTING: A NEW APPROACH TO AGGREGATE CLASSIFICATION AND MIX DESIGN VERIFICATION: TECHNICAL REPORT

by

Anal K. Mukhopadhyay, Ph.D.
Associate Research Scientist
Texas A&M Transportation Institute

and

Kai-Wei Liu
Graduate Assistant Researcher, Texas A&M Transportation Institute

Report 0-6656-1
Project 0-6656
Project Title: ASR Testing: A New Approach to Aggregate Classification and Mix Design Verification

Performed in cooperation with the
Texas Department of Transportation
and the
Federal Highway Administration

Published: April 2014

TEXAS A&M TRANSPORTATION INSTITUTE
College Station, Texas 77843-3135

DISCLAIMER

This research was performed in cooperation with the Texas Department of Transportation (TxDOT) and the Federal Highway Administration (FHWA). The contents of this report reflect the views of the authors, who are responsible for the facts and the accuracy of the data presented herein. The contents do not necessarily reflect the official view or policies of the FHWA or TxDOT. This report does not constitute a standard, specification, or regulation. The scientist in charge of the project was Dr. Anal K. Mukhopadhyay.

ACKNOWLEDGMENTS

This project was completed in cooperation with TxDOT and FHWA. The authors wish to express their appreciation to the Texas Department of Transportation personnel for their support throughout this study, as well as the Federal Highway Administration. Special thanks are extended to Lisa Lukefahr as the project director, Andy Naranjo and Ryan Barborak for serving as project coordinators, and Dr. German Claros, TxDOT as project advisor. Acknowledgment is also due to the staff personnel at Texas A&M Transportation Institute. We would like to thank Dr. Dan Zollinger, Dr. Andrew Wimsatt, and Dr. Chang-Seon Shon, TTI, Texas A&M University for their support in different stages of this project.

Table of Contents

List of Figures

Figure **Page**

List of Tables

Table **Page**

CHAPTER 1: INTRODUCTION

1.1 BACKGROUND AND SIGNIFICANCE OF WORK

Alkali-silica reaction (ASR) is recognized as a major concern for the Texas Department of Transportation (TxDOT). New cases of ASR are continuously being reported despite the advancement of the last decades. Prior to the early 1990s, ASR was not considered an issue in TxDOT, although cases of ASR in prestressed and cast-in-place concrete were at least visually observed. In 1999, a rigorous ASTM C 1260 testing of virtually every concrete aggregate source was initiated, which resulted in the preparation of SP 421-024 in March 2000. The special provision recommended using one of the mix-design options (1–8) if the cementitious material content exceeds 520 lb/yard^3. Options 1–5 cover the use of Class F ash (20–35 percent), Class C ash, ground granulated blast-furnace slag (GGBS) (35–50 percent), silica fume (10 percent), ultrafine fly ash (UFFA), metakaolin, etc. Option 7 recommended that the total alkali contribution from cement in the concrete should not exceed 4.00 lb (calculated by the amount of cement [pound per cubic yard] × $Na_2O_{eq.}$ in cement) per cubic yard of concrete when using hydraulic cement alone. Option 8 recommended that 14 days of ASTM C 1260 expansion should not exceed 0.10 percent if any deviation from options 1–7 occurred. TxDOT Research Project 0-4085 was launched in 2000 and continued until 2005.

In 2004, the specification book was updated by adding an additional option, and the measures in the special provision were thought to be adequate in order to avoid ASR distress. In spring 2008, exposure blocks cast as part of Project 0-4085 in 2001 started showing ASR cracking. In early 2008, prestressed girders in Central Texas (cast in 2004) showed ASR cracking, although one mix had 20 percent Class F ash and another mix had less than the required total alkali limit (option 7). TxDOT realized that some Texas aggregate sources would not be sufficiently limited by 4.0 lb/yard^3 of alkali and could fool C 1567. As a result, in January 2008, SP 421-031 created an exclusion list for option 7 (straight cement) and option 8 (ASTM C 1567 testing). Subsequently, the item 421-034 special provision was developed, where the total alkali contribution from cement changed from 4.0 lb to 3.5 lb/yard^3 of concrete (change of option 7), and the 14-day ASTM C 1567 expansion limit went from 0.10 percent to 0.08 percent (change of option 8). In May 2008, SP 424-001 was issued to disallow options 6–8 for major prestressed members and raise the minimum Class F ash content to 25 percent. In July 2008, additional aggregates from the Austin area were added to the option 7 exclusion list. In early 2009, girders (fabricated mostly in 2007 with a few in 2005–2006 using option 7) in a Waco prestressed plant began showing signs of distress. The fine aggregates were tested by petrography, x-ray diffraction (XRD), ASTM C 1260, and the acid insoluble percentage; identified as reactive; and added to the exclusion list.

From the above discussion, it is clear that options 7 and 8 in SP 421 did not provide enough protection, and some aggregates have been found to produce expansive gel even at low alkali loadings. The possible options that were suggested to minimize the occurrence of ASR are:

- Create a stratified aggregate classification system using a new testing approach that will address reactivity and source variability in an efficient manner.

- Define the testing frequency for pits/stockpiles (an important item to address source variability).
- Change the alkali loading equation to account for Na_2O and K_2O effects separately.
- Investigate alkali levels in pore solution.
- Change the lithium dosage for option 6.
- Encourage plants to acquire silos for fly ash if they do not currently have one. Using fly ash (25-35 percent) should be considered as a required item.

It would be beneficial to accurately, fairly, and rapidly assess the ASR potential of each aggregate at various alkali loadings. An effective way of tailoring mix design depending on the level of protection needed is warranted. This will ensure valuable resource conservation and avoid paying for premium ASR protection when only minor protection is needed.

Since the ASR-related problems were identified in the early 1940s, extensive work has been carried out on ASR over the decades. One of the main areas of research was to develop a quick and reliable test method to access ASR potential of aggregates and concrete through a simulative type of approach. The main purpose of an ASR test method is to measure aggregate reactivity prior to their use in concrete structures and develop ASR-resistant mixes. The current approach of ASR testing and mitigating damaging ASR heavily depends on mortar-bar tests (AMBT) and concrete prism tests (CPT). Although these approaches have resulted in significant advances in the avoidance of ASR damage in concrete structures, there were limitations and drawbacks. The test conditions of AMBT are severe and the test results are unrelated to field performance. CPT has been considered as the best index for field performance, but the test duration imposes a major limitation. Therefore, there is a strong need for developing a rapid and reliable ASR test method.

A device called volumetric change measuring device (VCMD) has been developed at Texas A&M Transportation Institute (TTI) where as-received aggregates were immersed in alkaline solution of varying concentrations and allowed to react at different temperatures. The device measures solution volume contraction over time (till 4–5 days) as the reaction between aggregate and solution proceeds. A new model has been developed that characterizes the measured volume change over time and calculates reaction rate. The reaction rates at multiple temperatures allowed to calculate ASR activation energy (E_a) based on Arrhenius rate theory. E_a is used as a measure of alkali silica reactivity of aggregate.

1.2 RESEARCH OBJECTIVES

The main objective of this study was to develop a fast, reliable test method to determine aggregate alkali silica reactivity based on the time-dependent nature of the onset and speed of reaction. The test method should also determine the aggregate sensitivity to the overall alkalinity of the concrete. The VCMD was identified as a potential method to fulfill these requirements. The specific objectives of the proposed research were:

- Selecting aggregates (both coarse and fine aggregates) from both the exclusion list (poor performance) and approved list (satisfactory performance) covering different types of aggregates with a wide range of reactivity
- Testing the selected aggregates by VCMD-based aggregate-solution test and measure compound activation energy. Activation energy is considered as a single fundamental material property to represent aggregate alkali-silica reactivity.
- Monitoring soak solution chemistry changes and microstructural studies on the reaction products were proposed as supporting tools for the VCMD test.
- Developing an aggregate ASR classification system based on compound activation energy.
- Highlighting the benefits of the proposed method by establishing a comparative assessment between ASTM C 1260 and the proposed test method. The expected benefit was consistent identification of the aggregate belonging to false positives and negatives categories in a short period of time.
- Development of a procedure to determine alkali threshold of aggregate based on aggregate-solution test at multiple levels of alkalinity.
- Development of a chemical method based on activation energy, threshold alkalinity, and pore-solution alkalinity to formulate/verify/adjust mix design with the expectation that the verified mixes will either not show any ASR or little ASR with no visible or measurable distress during the expected service life.
- Mix-design validation through direct concrete testing. It was proposed that an attempt will be made to develop an accelerated concrete cylinder test (ACCT) that can be used to:

    - Test a mix at varying levels of alkalinity and determine aggregate reactivity to the overall alkalinity of concrete.
    - Test a job mix with or without alkali boosting.

In the past 5.5 years, TxDOT has already paid approximately $2 million for recasting precast concrete products. Hundreds of other precast elements with the same mix designs were placed in the past, and future maintenance costs are expected to increase for these structures. It is expected that the proposed fast, reliable test method will eventually replace ASTM C 1260/1567 and improve the protection provided under option 8 of item 421. This option is more commonly used as Class F ash becomes increasingly unavailable. An activation-energy-based classification system in conjunction with ASTM C 1260 data will be used to create stratified lists of aggregate reactivity, allowing for progressive mitigation options to be used. Recommendations for specification changes will be provided. An effective way of tailoring mix design depending on the level of protection needed will be developed, which will ensure valuable resource conservation and help TxDOT avoid paying for premium ASR protection when only minor protection is needed. The locally available aggregate and supplementary cementitious materials (SCMs) can be judiciously used with the proposed approach, thus minimizing the number of aggregates in the exclusion list.

1.3 ORGANIZATION OF THE REPORT

The work that was performed under different tasks (according to the original proposal) is presented in this report as chapters.

Chapter 1 is an introduction addressing the research background and objectives, followed by a description of report organization.

Chapter 2 provides the background information based on a literature review relevant to the proposed study. The current test methods and their limitations are highlighted.

Chapter 3 presents the basis of aggregate material selection and characterization (petrographic examination).

Chapter 4 describes the evolution of test equipment and protocol validation.

Chapter 5 presents all aggregate testing results (activation energy, soak solution chemistry, and microstructures, etc.) and a new ASR aggregate classification system based on compound activation energy (E_a). A comparative assessment between E_a-based classification system and ASTM C 1260 / C 1293 is also presented and discussed in this chapter.

Chapter 6 presents a step-by-step approach to develop an ASR-resistant mix, i.e., (a) formulation/verification of a mix based on compound E_a, threshold alkalinity, and pore solution alkalinity, and (b) validation through concrete testing. A rapid concrete cylinder test was developed in this study and used for concrete validation testing. This chapter also presents a detailed description of this new rapid concrete testing.

Finally, Chapter 7 provides summary and conclusions based on the research findings from this study and potential recommendations for future research and implementation.

CHAPTER 2: LITERATURE REVIEW

This chapter provides a comprehensive literature review on alkali-silica reaction (ASR) relevant to this study in four sections. The first section describes the factors that initiate and sustain ASR. The second section deals with the current reaction and expansion mechanisms of ASR. The third section provides a brief background on the current test methods for predicting the ASR potential of aggregates along with some discussions on the usefulness and limitations of these methods. The current kinetic approaches for determining ASR aggregate reactivity are summarized in the last section.

2.1 INTRODUCTION

ASR in Portland cement concrete is a deleterious chemical reaction that induces expansive stress in the presence of sufficient moisture. Since the identification of ASR-related problems in the early 1940s, extensive research has been carried out on ASR over the decades. The development of ASR test methods to assess ASR potential of aggregates and concrete through a simulative type of approach was one of the main portions of that research. The other areas of research include:

- A better understanding of both reaction and expansion mechanisms.
- Development of specifications for preventing ASR in new concrete.
- Management guidelines for existing ASR-induced damaged concrete structures.

The main purpose of an ASR test method is to measure aggregate reactivity prior to their use in concrete structures. The most commonly used ASR testing heavily depends on the accelerated mortar bar test (AMBT, ASTM C 1260) and concrete prism test (CPT, ASTM C 1293). The AMBT is rapid (i.e., 14 days) but the test conditions (i.e., 1N NaOH and 80°C) are severe and the test results are sometimes unrelated to field performance. The CPT has been considered as the best index for field performance but the long testing time (i.e., 1 year min.) and alkali leaching are some of the limitations.

ASR is a kinetic type of chemical reaction. It is known that some threshold values of alkalinity and moisture need to be satisfied in order to initiate ASR and make ASR expansive. Activation energy (E_a) of ASR can serve as a single chemical material parameter to represent the combined effects of alkalinity, temperature, and moisture and can be used as a measure of alkali silica reactivity of aggregate. Many researchers in the past have applied kinematic type models to characterize mortar bar expansion over time and determine a constant that was used to differentiate between reactive and non-reactive aggregates effectively (Uomoto et al. 1992; Johnston et al. 2000). The main purpose was to provide a better interpretation of the AMBT data through kinematic approach but not intended to improve the test procedure. There is a growing demand for a rapid and reliable ASR test method.

It is important to understand the basics of ASR, responsible factors, expansion mechanisms, some limitations of the current test methods, and effectiveness of the remedial measures in order to identify the more effective test method. A brief discussion on these topics is given below.

2.2 FACTORS INFLUENCING ALKALI-SILICA REACTION (ASR)

ASR is a chemical reaction between alkali hydroxides in a pore solution and the reactive form of silica in aggregates. It is widely accepted that three essential conditions (see Figure 2.1) are necessary in order to create ASR-induced damage in concrete structures:

1. Sufficient availability of OH^- ions and alkalis (Na^+ and/or K^+) – a highly alkaline concrete pore solution (pH > 13.2) ensures enough supply of alkali hydroxides.
2. Presence of a reactive siliceous component(s) in aggregates (both coarse and fine aggregates) at optimum level (i.e., pessimum proportion).
3. Sufficient moisture (> 80 percent RH) (Chatterji et al. 1989; Ponce and Batic 2006; and Mukhopadhyay et al. 2006).

The optimum combination of conditions 1 and 2 is essential to initiate ASR, whereas condition 3 is essential to make ASR expansive (i.e., deleterious). If any one of the three factors is not present in the concrete, then the reaction will either not proceed or not become deleterious. The higher the temperature the higher the rate of ASR is. Increasing temperature causes higher expansion at early age but lower ultimate expansion (Diamond et al. 1981). The product of this reaction is a gel known as ASR gel. In the presence of sufficient moisture (> 80 percent RH), the gel absorbs moisture due to its hygroscopic nature and swells. Swelling leads to tensile stresses in concrete. When these stresses exceed the tensile strength of concrete, cracks develop. Typical visual manifestation of ASR includes map cracking (see Figures 2.2 and 2.3), misalignment of structural elements, and expansive features such as joint closure and heaving/blow-ups, etc. ASR cracks act as open passages for moisture and other chemicals (chloride ions, sulfate ions, etc.), leading to more damage. In addition to the three requirements listed above, the presence of calcium hydroxide [$Ca(OH)_2$] in concrete pore solution also found to be an important factor. Chatterji et al. (1989) believed that sufficient Ca^{2+} concentration in the pore solution (vicinity of the aggregate) is needed for ASR gel to be expansive inside aggregate.

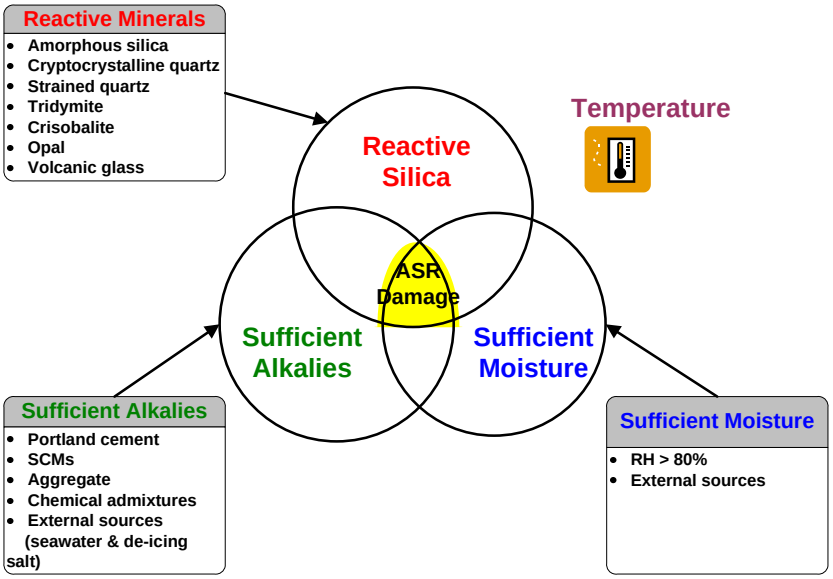

Figure 2.1. Three Essential Factors that Initiate ASR and Make ASR Expansive in Concrete.

Figure 2.2. Prestressed Concrete Box Beams Cast in 1991 Started Showing Cracking in 1993 while Still in Storage.

Figure 2.3. ASR Cracking in Cast-in-Place Elements.

2.2.1 Reactive Siliceous Components in Aggregates

The occurrence of silica or silicate minerals in aggregates (both coarse and fine) is a common feature. Aggregate alkali-silica reactivity is a function of the form/degree of crystallinity, grain size, texture, and proportion of the reactive silica within the reactive aggregate (Stanton 1940, Mindess 2003). Not all forms of silica are ASR-reactive. The more disordered the structure of the silica phase, the greater the reactivity. The basic structure of silicates involves a framework of silicon-oxygen tetrahedron. Each oxygen atom is shared between two silicon atoms, where each silicon atom is bonded to four oxygen atoms (called siloxane bridge). A regular (ordered) arrangement of the basic Si-O tetrahedron creates a crystalline structure (see Figure 2.4a, e.g., quartz) whereas an irregular (disordered) arrangement of the tetrahedron creates poorly crystalline (e.g., chalcedony) to amorphous structure (e.g., opal, Figure 2.4b), depending on the degree of irregularity. Diamond (1976), Tatematsu and Sasaki (1989), and Mehta and Monteiro (1992) have designated the degree of reactivity of these reactive forms of silica, with decreasing order as follows:

- Opal.
- Crystobalite.
- Tridymite.
- Microcrystalline quartz.
- Cryptocrystalline quartz.
- Chalcedony.
- Chert.
- Volcanic glass.
- Strained quartz.

The crystalline quartz (e.g., present in igneous rocks) is not considered susceptible to ASR, whereas strained quartz (e.g., present in metamorphic rocks) is reactive.

Mindess et al (2003) summarize the forms of reactive silica in aggregates that can participate in ASR (see Table 2-1). In general, the metastable types of silica [e.g., opal,

chalcedony, tridymite, crisobalite, and some disordered forms of quartz (cryptocrystalline and strained quartz)] and alumina–silicate glasses (e.g., acid volcanic glass) are known to be highly reactive with the alkalis in concrete (Gillott et al. 1973; John et al. 1998; Broekmans 2002; Fernandes and Noronha 2004).

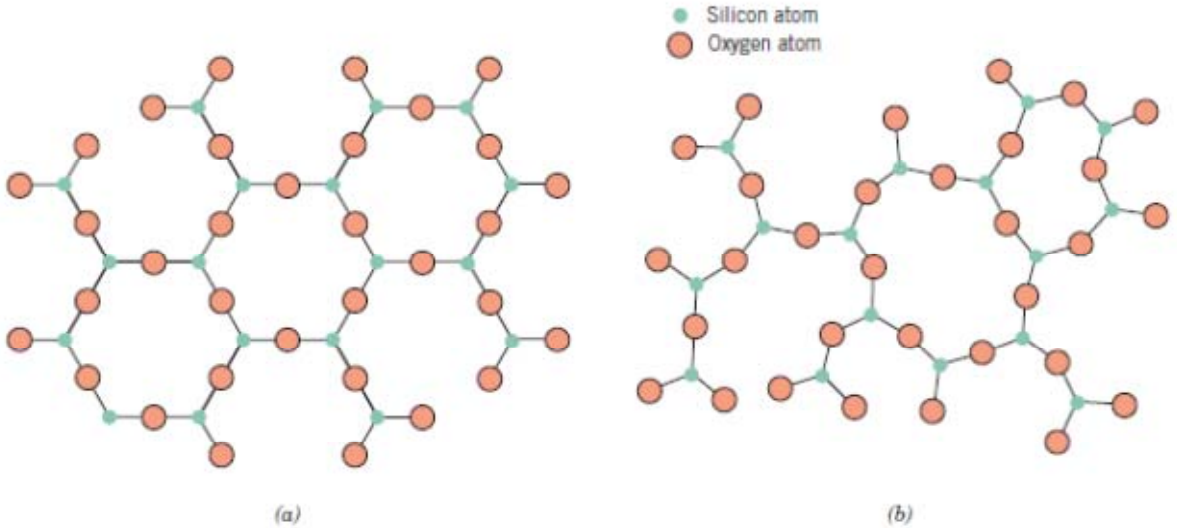

Figure 2.4. Two-Dimensional Schemes for the (a) Crystalline and (b) Non-Crystalline SiO_2 (Callister 2007).

The degree of crystallinity and amount of defects in the lattice affect the potential alkali reactivity and solubility of siliceous aggregates (Grattan-Bellew 2001). However, the form of silica is not the only parameter that determines alkali reactivity of an aggregate. The other important factors that determine aggregate reactivity are as follows:

- Amount and nature of distribution of the reactive constituents inside aggregates.
    - Homogeneous or inhomogeneous distribution.
    - Whether the whole aggregate particle is reactive (e.g., acid volcanic rock) or certain reactive constituent(s) inside an aggregate is reactive.
    - In certain sandstones, the fine cementing material is reactive, but the coarser grains are nonreactive.
- Role of aggregate porosity, pore connectivity and other internal structures (e.g., layering, schistose/foliated structures, etc.) on ingress of OH^-, Na^+, K^+ ions into the aggregates.
    - High porosity/pore connectivity can enhance the ingress of ionic species and increase the chance for ASR to occur with a much faster rate, provided enough reactive constituents are present (Gogte 1973; John 1998; Broekmans 2002; Wenk et al. 2008).

Table 2.1. Forms of Reactive Silica in Aggregates Susceptible to ASR (Mindess et al. 2003).

Reactive Component	Physical Form	Rock Type in which It is Found	Occurrence
Opal	Amorphous	Opaline limestone (e.g., Spratt limestone), chert, shale, flint	Common as a minor constituent in sedimentary rocks
Silicate glass		Volcanic glasses (rhyolite, andesite, dacite) and tuffs; synthetic glasses	Regions of volcanic origin; river gravels originating in volcanic areas; container glass
Chalcedony	Microcrystalline quartz	Siliceous limestones and sandstones, cherts, and flints	Widespread
Cristobalite (Tridymite)	Crystalline but metastable	Opaline rocks, fired ceramics	Uncommon
Strained Quartz	Disordered due to strain effects	Metaquartzite, sands, gravel, sandstones, many metamorphic rocks (e.g., granite gneiss and schists)	Common

Petrographic studies play an important role in understanding the above additional factors related to aggregate reactivity. It is unlikely that mineralogy and percentage of reactive constituent will remain the same for a particular quarry/pit (especially for an aggregate with high source variability) over time, and therefore users may not be able to confidently use aggregates from sources that have performed satisfactorily in the past without re-testing. The frequency of aggregate testing as a function of source variability is an important item that needs to be addressed.

2.2.1.1 Pessimum Effect Related to the Quantity of Reactive Constituent(s)

A pessimum effect is defined as increasing expansion with increasing reactive silica content in aggregate up to a certain level (i.e., the pessimum proportion) followed by decreasing expansion with increasing reactive silica content (Hobbs, 1988, see Figure 2.5). Concrete prism tests with different types of aggregates have shown that a maximum expansion occurs at a particular amount of the reactive siliceous constituent in aggregates (Gillott 1975, Hobbs 1988, Grattan-Bellew 2001, and RILEMTC AAR-1 2003). However, the pessimum proportion effect differs for various reactive constituents. For example, for aggregates containing opal, the maximum expansion occurs for the reactive silica content below 10 percent (Vivian 1947, Shayan 1992, and Bektas et al. 2004). Slowly reactive aggregates don't even show a pessimum effect. It was reported that as little as 2 percent of reactive silica is enough to observe distress in concrete structures (Swamy 1992).

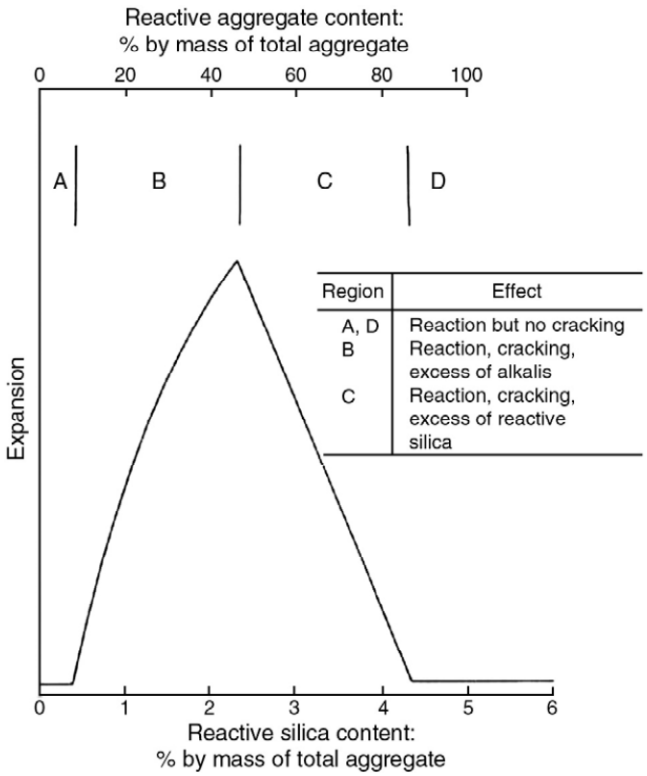

Figure 2.5. Pessimum Curve of Pure Siliceous Aggregate (Hobbs 1988).

Garcia-Diaz et al. (2010) investigated the ASR pessimum behavior of the siliceous limestone aggregates. The results show that high alkali content in concretes containing reactive siliceous limestone aggregates (both fine and coarse aggregates) have less expansion than concretes containing fine reactive siliceous limestone aggregates and non-reactive coarse aggregates.

The pessimum effect is based on the assumption of limited amount of alkali hydroxide in the system so that it will not be expected to occur if the concrete is immersed in a continuously alkali hydroxide-supplied system (Ichikawa 2009). However, Bleszynski and Thomas (1998) observed that expansion of concrete containing reactive flint sand and inert limestone reached maximum at the proportion of 25 percent flint when the concrete was stored in an alkaline solution for two to three years.

2.2.1.2 Pessimum Effects Related to Aggregate Size

In general, expansion increases as particle size decreases (i.e., surface area increases) if the reaction occurs at the surface of the reactive particles. Researchers have investigated the effects of aggregate size to achieve maximum/insignificant mortar bar or concrete prism ASR expansion (see Table 2.2).

Table 2.2. Mortar Bar/Cconcrete Prism ASR Expansion as a Function of Aggregate Size.

Researchers	Max. ASR Expansion with the Size Ranges	Insignificant ASR Expansion with the Size Ranges	Type of Materials / Test
Stanton, 1940	0.17–0.6mm		Siliceous magnesium limestone containing opal and chalcedony (Mortar bar / concrete prism)
Woods, 1968	0.07–0.85mm		Opaline aggregate particles in mortar bar
Zhang, 1999	0.15mm		Mortar bars made of siliceous aggregates
Kuroda et al. (2000 and 2004)	0.48mm		Mortar bars made of only reactive aggregates
	0.15–0.30 mm		Using both reactive and nonreactive aggregates in mortar bars
Hobbs and Gutteridge 1979, Han and Tang 1984		Less than 0.02 mm	Mortar bar expansion
Kawamura et al. 1983, Zhang et al. 1990, Shayan 2002, and Multon et al. 2008		Less than 0.05-0.15mm	
Shao et al. 2000, Shayan 2002, and Moisson et al. 2004		Up to 0.1 mm (Counteract the effect of ASR)	Mortar bar

Table 2.2 indicates that different results pertaining to the aggregate size that yields maximum ASR expansion are reported by different researchers. Some of the explanations for these differences in results are:

- ASR expansion not only depends on the aggregate size but also depends on the nature and composition of the aggregate.
- If the ASR occurs within the particle, the expansion is independent of the aggregate size (Hobbs and Gutteridge 1979).
- Ramyar et.al. (2005) has reported that aggregate with intermediate angular size fractions gives higher mortar bar expansion than that made of rounded aggregates of the same size based on their work on the effect of angularity and size of crushed aggregates on mortar-bar expansion.
- Crushing certain types of aggregates (especially for reactive aggregates) for laboratory tests changes their reactivity characteristics (Lindgard et al. 2012).

Gao et al. (2013) also found the pessimum effect of ASR expansion with specimen to aggregate size ratio. The expansion rate is slower in all sizes of specimens containing the largest aggregates due to a delay in the diffusion of the hydroxyl ions into the reactive silica in

aggregates. This pessimum effect is not an intrinsic phenomenon but depends on specimen-to-aggregate size ratio.

2.2.2 Role of Concrete Moisture

Moisture is an essential ingredient for ASR to occur and become expansive. Water is the main carrier of hydroxyl and cations in a form of pore solution to the reaction site, thus facilitating ASR to occur. Subsequently, the reaction product (i.e., ASR gel) absorbs moisture, causing swelling. The swelling causes high stress inside aggregates, resulting in aggregate cracking and subsequent concrete deterioration. Although concrete looks dry during its service years, it can still maintains relative humidity (RH) in the range of 80–90 percent in the inner portions (Mukhopadhyay 2009). Pedneault (1996) found that concrete displayed very small expansion at an RH less than 80 percent, and expansion increases exponentially when RH increases above 80 percent.

The moisture level might be reduced below 80 percent in concrete by limiting the exposure of concrete structures to moisture or the use of low permeability (concrete with low water to cement ratio) concrete. In addition, improving drainage conditions can also be applied as an effective way to reduce the availability of external moisture. A higher w/c can cause both increasing and decreasing of expansion due to ASR. The following phenomena can cause increase of expansion:

- Higher porosity/permeability causing higher ionic mobility and more reaction.
- Greater availability of free (capillary) water to make the gel more expansive.

The possible mechanisms that may cause reduction in expansion are:

- Higher available space (high capillary porosity due to high w/c) for gel accommodation.
- Relatively lower pore solution concentration (dilution effects due to high w/c) may cause slower expansion rate and lower level of expansion.

It seems that higher ionic mobility and greater availability of free water are the dominant factors for ASR and hence the net expansion should be higher with high w/c than the concrete with low w/c.

2.2.3 Alkalinity

Concrete consists of innumerable pores that are filled with solution containing OH^- and alkali ions (i.e., Na^+ and K^+), which play an important role in developing ASR. The primary source of alkali in concrete is cement. The alkalis primarily present in cement clinker as alkali sulfates with minor bounded alkalis in the crystal structure of the silicate phases. Alkalis are immediately released from alkali sulfates in pore solution when portland cement is mixed with water. Other sources, such as SCMs (Buck and Mather 1987; Diamond 1981), certain aggregates (e.g. mica, clay minerals, alkali feldspars, etc.) (Grattan-Bellew 1994; Berube et al. 2002; Constantiner and Diamond 2003), chemical admixtures (e.g., superplasticizers) (Mukhopadhyay

et al. 2009), seawater-contaminated aggregates or concrete, and de-icing chemicals can also contribute additional alkalis other than cement alkalis and enhance the pH of the pore solution.

The concentration of OH^-, Na^+, and K^+ in a mature cement paste (water-to-cementitious ratio = 0.5, Type I cement with 0.91 percent Na_2O_e) was reported as 0.8N, 0.2N, and 0.4N, respectively, with a negligible concentration of Ca^{2+} (Diamond 1983). Diamond (1983) suggested that a threshold concentration required to initiate and sustain ASR is 0.25M (pH=13.4). Kolleck et al. (1986) found that the threshold concentration to initiate ASR is 0.2M (pH=13.3). Several other authors (Kollek et al. 1986; Rivard et al. 2003; Kagimoto et al. 2004; Thomas et al. 2006; Shehata and Thomas 2006) have also reported the threshold concentration of hydroxyl ions in the pore solution in the range between 0.2 (pH=13.3) to 0.3 M (pH=13.5). Kawamura and Iwahori (2004) observed that the expansive pressure is approximately proportional to the amount of ASR gel formed, provided the alkali content of the ASR gel is less than a critical value. Different aggregates have different threshold values to initiate the reaction, which largely depends on the aggregate reactivity (Sibbick and Page 1992). If the whole aggregate is reactive and the aggregate is homogeneous, the threshold may be lower. On the other hand, if the aggregate is heterogeneous and reactive constituents occur as isolated pockets within the non-reactive phases, the threshold level may be high as the non-reactive phases (i.e., physical adsorption) may consume some alkalis. The porous aggregate may have lower threshold than less porous and low defects aggregates. A reactive aggregate may not react or have low potential to react when the alkali level in the system is below the threshold concentration. Therefore, assigning a common total concrete bulk alkali (e.g., 4 lb/yard^3 as in option 7 of item 421) irrespective of aggregate reactivity may not provide enough protection.

Cement having a Na_2O_e of less than 0.6 percent is generally considered as low-alkali cement. However, this kind of low alkali level in cement found to be sufficient to cause ASR in highly reactive aggregate. The bulk $NaO_{eq.}$ of cement (0.6 percent requirement) may not always accurately define the potential of cement alkali to cause ASR and might be misleading in certain cases. Cements with similar $Na_2O_{eq.}$ can have different K/Na ratios and are found to be the reason for the observed differences in concrete expansion (Leeman and Lothenbach 2008). The amount of alkalis that are soluble in the concrete pore solution and hence available for the reaction is more important than the total bulk alkali content of the concrete materials. The approach of using low-alkali cement alone does not necessarily prevent ASR-induced damage because the contribution of alkalis from other sources is not considered. Alkalis may also become concentrated in a portion of the concrete through migration with moisture. Therefore, many agencies and countries specified total permissible alkali between 2.5 and 4.5 kg/m^3 (4.21 and 7.58 lbs /yard^3), and stated that the boundary of total permissible alkali is not rigid but depends on the aggregate reactivity (Nixon and Sims 1992). Sibbick and Page (1992) advocated that the alkali threshold based on CPT test is between 3 to 5 kg/m^3 (5.05 and 8.43 lbs/yard^3) for reactive aggregates but is lower for highly reactive aggregates. A value of 3.0 kg/m^3 (5.05 lbs/yard^3) was reported as threshold concrete alkali based on the relationship between 2 years CPT expansion and concrete alkali content (see Figure 2.6). However, the occurrence of ASR expansion has also been reported even with the total concrete alkali content less than 3 kg/m^3 (Folliard et.al. 2007).

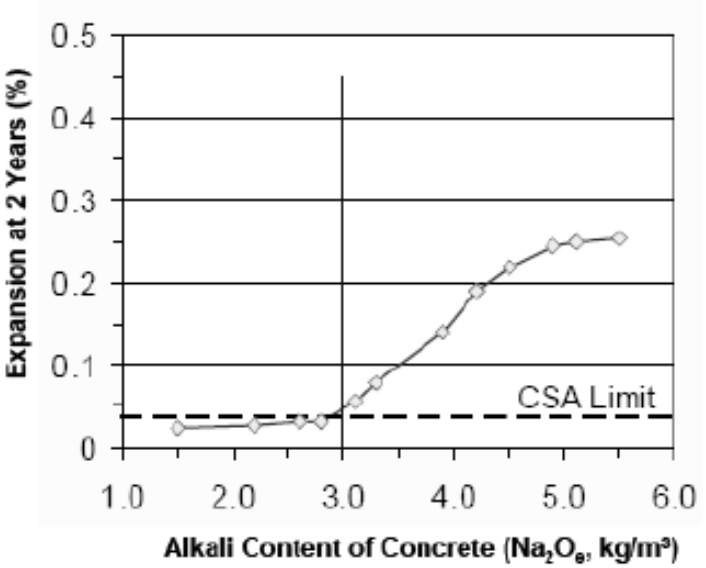

Figure 2.6. Effects of Alkali Content on Expansion of Prisms Stored over Water at 38°C (Folliard et al. 2007).

2.2.4 Environmental Effects / External Factors

The two main environmental factors that affect ASR are:

- Variation of moisture content and temperature and associated alkali redistribution inside concrete due to seasonal climatic variations (e.g., temperature and wetting/drying cycles).
- Penetration of alkalis from external sources (e.g., seawater and deicers).

It has been reported that wetting and drying cycles enhance ASR (Mukhopadhyay et al. 2009). The concentration of alkalis in pore solution increases during drying and can concentrates locally in certain portion of the concrete elements. ASR can occur in those alkali-enriched portions, although total concrete alkali loading may be reasonably low. During the next wetting cycle, rewetting causes dilution of alkali-rich portions (making ASR slow in those areas), but it creates favorable situation for swelling of the gels that already formed during the drying cycle.

During laboratory performance testing, researchers have found that higher temperature accelerates ASR. Hobbs (1992) found that the reaction occurred for specimens stored at 38°C was seven times faster than those stored at a temperature of 9°C, and was four times faster than those stored at 20°C. Nilsson (2006) reported that an increase in temperature raises internal RH for small concrete prisms (w/c 0.4) stored over water in a sealed container. The internal RH increases approximately 0.25 percent/°C, but the effect decreases when w/c increases. Therefore, when the concrete temperature increases from 25 °C to 45 °C, the internal RH might be increased by approximately 5 percent.

RH values higher than 80 percent are able to sustain expansive ASR in most of the pavement below the top surface layer, even in the summer in a hot desert climate (SHRP-C-342, 1993). The data also show that humidity conditions are sufficiently moist to support expansive

ASR in much of the concrete in pavements and structures for at least part of each year in most of the continental United States.

One reactive aggregate with conventional mix design mitigation measures may perform well in one geographic locations with mild environmental effects (e.g., low rainfall, low T, and low RH and T variation) but may show ASR distress in another geographic location with severe environmental factors (e.g., high rainfall, high T, and high T and RH variation etc.). Therefore, lowering concrete total alkali loading alone might not provide enough protection for a concrete under severe ambient conditions. Applying additional protection measures depending on the severity of environmental factors is highly recommended.

2.2.5 Role of Supplementary Cementitious Materials (SCMs)

In general, SCMs such as fly ash, GGBS, and condensed silica fume are all used to reduce ASR expansion in concrete. The mechanisms are not well understood, but it is agreed that the reactive silica in SCMs combines with the cement alkalis (i.e., Na and K) more readily through pozzolanic reaction than the siliceous phase(s) in aggregate. Therefore, alkalis are rapidly consumed, and the level of hydroxyl ions is reduced to a level at which aggregates react very slowly or not at all (Carrasquillo and Farbiaz 1988, Diamond and Penko 1992). Furthermore, the pozzolanic reaction results in the formation of alkali-calcium-silicate-hydrates, which is non-expansive, unlike the water-absorbing expansive ASR gels. However, not all SCMs increase ASR resistance. Some SCMs can be a source of additional alkalis. Diamond (1981) reported that Class F fly ash is more effective in controlling ASR than Class C fly ash. Shehata and Thomas (2000) and Shon et al. (2003, 2004) supported that Class C fly ashes are less effective than Class F fly ashes in controlling ASR because some Class C fly ashes (those with $Na_2O_{equivalent}$ greater than the cement) actually enhance alkali ions (e.g., Na^+ and K^+) and OH^- in pore solution.

2.3 CURRENT MECHANISMS OF ASR

2.3.1 Reaction Mechanisms

ASR is the reaction between the hydroxyl (OH^-) ions present in pore solution and reactive siliceous component(s) in aggregates. The alkali cations (i.e., Na^+, K^+, Ca^{2+}, etc.) are important because their presence in high concentration leads to an equally high concentration of hydroxyl to maintain equilibrium in the pore solution. When they are incorporated into the ASR gel, the role of alkali becomes relevant.

In general, there are four steps in the chemical reaction mechanism of ASR (Glasser et al. 1981, Wang et al. 1991, Poole 1992, and Garcia-Diaz et al. 2010).

Step 1: Neutralization of surface silanols of the reactive silica by the alkali base:

$$SiO5/2H + Na^+/K^+ + OH^- \rightarrow SiO5/2(K, Na) + H_2O$$

Step 2: Breaking up of siloxane bonds (Q_4) by hydroxyl ions to form Q_3 tetrahedrons:

$$SiO2 + Na^+/K^+ + OH^- \rightarrow SiO5/2(K, Na) + ½\ H_2O$$

In this step, the OH^- reacts with Si-O-Si bonds to form silanol bonds:

$$\text{Si-O-Si} + H_2O \text{ –> Si-OH….OH-Si}$$

Step 3: Dissolution of silica due to continued hydroxyl ions attack on the Q_3 tetrahedron to form silica ions and small polymers:

$$SiO5/2(K,Na) + Na^+/K^+ + OH^- + ½\ H_2O \rightarrow H_2SiO_4^{2-} + 2(Na^+/K^+)$$

Step 4: "Gelation" of expansive ASR silica gels from the silica saturated pore solution.

The products of the above acid base reaction (Step 2) are a molecule of water and the negatively charged Si-O-. These negative charges attract positive alkali cations such as sodium, potassium, and calcium and form ASR gel (Steps 3 and 4). The number of positive cations should be sufficient enough to maintain charge balance in the system. Dent-Glasser and Kataoka (1981) summarized the entire ASR chemical reaction as:

$$H_{0.38}SiO_{2.19} + 0.38Na_2O \rightarrow Na_{0.38}SiO_{2.19} + 0.38H_2O$$

As shown in the above equation, sodium was involved to achieve charge balance, but in reality other cations (e.g., K^+, Ca^{2+}) also participate in charge balancing. The product of the above reaction is called ASR gel and composed of SiO_2, Na_2O, K_2O, CaO, and water. According to many researchers, ASR may take the form of either a gel or poorly crystalline material (Stewart 2005). The ASR product by itself is not deleterious; however, the problem occurs when this gel absorbs water, resulting in greater volume than the one that it replaces, and creating high swelling pressure and expansion. Studies have shown that these gels maintained quasi-state equilibrium with water. During drying cycles, the alkali concentration increases and therefore the ionic content of the gel increases. On the other side, during wet cycles, the reverse reaction happens. Since these gels have different chemical composition and different densities at different periodic cycles, the amount of swelling is extremely difficult to predict (Swamy 1992).

2.3.2 Expansion Mechanisms

Although the chemical reaction mechanisms that govern ASR are well understood, the expansion mechanisms still remain unclear and are a point of controversy. The most common and circulated theories in the literature regarding ASR expansion mechanism are briefly described below:

Formation of Osmotic Pressure Cell

Hansen (1944) proposed that the cracking that occurred in the concrete was due to the formation of an osmotic pressure cell surrounding the aggregate. In the theory, hardened cement paste act as a semi-permeable membrane on silicate ions passage. The membrane allows water molecules and alkali hydroxides to diffuse in, but prevents silicate ions to diffuse

out. The alkali-silicate that formed on the surface on an aggregate surface would draw solution from the cement paste to form a liquid-filled pocket. The liquid that was drawn in would then exert an osmotic pressure against the confining cement paste, leading to cracking.

Swelling Theory

McGowan and Vivian (1952) postulated that cracking in concrete should relieve the osmotic pressure and prevent any further expansion. Instead, they proposed the "Swelling theory" in which alkali silica gel (a product of reacted aggregates) absorbs water, leading to swelling in the gel, which causes expansive pressure and eventually causes concrete cracking. Other researchers (Tang 1981) also agreed with this theory.

Swelling Theory Controlled by Lime

Powers and Steinour (1955) believed that the theories that both Hansen (1944) and McGowan and Vivian (1952) proposed were fundamentally similar. They thought that the primary damage mechanism was swelling of the solid reaction product as controlled by the amount of lime it contained, but the osmotic pressure might also develop. When a silica particle is exposed to a strong base, the hydroxyl ions attack the surface and gradually penetrate the particle. If the attack occurs in the presence of excess lime, then a non-swelling lime-alkali-silica complex is formed when chemical equilibrium with the lime is reached. However, if the alkali-silica complex is not in equilibrium with the lime, then swelling will occur. When the alkali-silica complex imbibes water, the researchers believe that the swelling is due to the displacement of colloidal units with respect to one another.

One cause of insufficient lime is that alkalis in the solution depressed the lime, so not enough lime may be available at the reaction site to form the non-expansive gel. Another cause is that the lime-alkali-silica complex can hinder the diffusion of the calcium ion to the reaction site while allowing the other ions to diffuse to form additional gel that can swell. For the osmotic pressure to buildup, the researchers explained that water within concrete would tend to move to regions where it has the lowest free energy. The water that the alkali-silica complex held has lower free energy than water external to the complex. As the strength of the solution within the alkali-silica complex increases, greater osmotic pressure is required to prevent the entry of additional water into the complex. If the alkali-silica complex is fluid and confined, then osmotic pressure may be generated. If the alkali-silica complex is solid, the swelling of the reaction rim may still generate pressure.

Diffusion Theory Controlled by Calcium

Chatterji et al. (1986, 1989) proposed that when hydroxyl ions are placed in a solution with a pH of 7 or greater, these ions penetrate reactive siliceous particles, in amounts increasing with solution pH and ionic strength. At a constant solution pH and ionic strength, the absorption of OH^- decreases with the increasing size of the associated hydrated cation (OH^- absorption decreases in the series K^+, Na^+, Li^+, Ca^{2+}). In a pore solution with mixed ionic species

(e.g., $Ca(OH)_2$ and NaCl), the cations will penetrate into the reactive silica grain following the penetrating OH- ions; however, more of the smaller hydrated cations will do so than the larger ones (in this example, hydrated Na+). After that, penetrating OH^- ions attack siloxane bonds, and this reaction further opens up the reactive silica grain to attack. Silica ions are liberated from their original sites, enabling them to diffuse out of the reactive grains. Ca^{2+} controls the rate of silica diffusing out of reacting grains in the immediate vicinity. A higher Ca^{2+} ion concentration lowers or impedes silica diffusion away from the reactive grains. Finally, when the net amount of materials (Na^+, K^+, Ca^{2+}, OH^-, and H_2O) entering a reactive silica grain exceeds the amount of materials leaving (SiO_2^{2-}), expansion occurs.

Diffuse Double Layer Theory

A theory was proposed citing electrostatic repulsion between diffuse double layers (DDLs) as responsible for generating expansive forces (Prezzi 1997 and Rodrigues et al. 1999). Very high negative charges are observed at the surface of the silica grains (Bolt 1957 and Rodrigues et al. 1999). To counterbalance the negative silica charges, an electric double layer of positive charges (cations) develop and adsorb around the silica surface. Two layers defined as the Gouy-Chapman layer or the Stern layer has a collective thickness of a few nanometers that can be calculated from the ionic strength of the pore solution electrolyte. The double layers are composed of calcium, potassium and sodium, and some other anions, but the net charge of the whole system (sum of negative charges of silica + anions + sum of all cations) is equal to 0. This system will form a colloidal suspension and then conglomerate into a gel (Prezzi 1997). The chemistry of this gel depends on the chemistry of the pore solution, the pore structure in the concrete, and the environmental condition. The amount of repulsive forces and the thickness of the electric double layer depend on the valence of the cations in the gel and their concentration in the double layer (Prezzi 1997 and Rodrigues et al. 2001). Consequently, bivalent ions (Ca^{++}) will generate more repulsive forces and a larger electric double layer thickness than monovalent ions (Na^+). Therefore, gels with a high concentration of calcium will produce lower expansive forces than those containing a high amount of sodium and vice versa (Rodrigues et al. 1999). Diamond (1989) indicated that the expansive pressures because of gel swelling are in the range 6–7 MPa, but expansive pressure of 10.3 MPa was calculated using conventional double layer equations (Rodrigues et al. 1999).

Expansive Pressure Theory due to the Formation of Reaction Rim

In 2007, Ichikawa and Miura conducted research on the effect of ASR-generated hydrated alkali silicate on the development of expansive pressure inside aggregates. The results show that the alkali silicate does not develop expansive pressure unless an insoluble, dense reaction rim surrounds the aggregate. ASR consumes alkali hydroxide and then induces the dissolution of Ca^{2+} ions into pore solution. The Ca^{2+} ions react with alkali silicate to form an insoluble reaction rim. The reaction rim acts like a barrier, which allows the penetration of alkaline solution but prevents the leakage of alkali silicate. This accumulates the formation of viscous alkali silicate by ASR in the aggregate to develop an expansive pressure enough to crack the aggregate and the surrounding cement paste.

Aggregate Swelling Associated with Siloxane Bond Breaking (Q4 to Q3 Transformation)

Garcia-Diaz et.al. (2006) proposed a novel mechanism for the ASR damage. Two reaction steps are taken into account in the mechanism: the Q_3 tetrahedrons formation by breaking up siloxane bonds and the dissolution of these Q_3 tetrahedrons. They demonstrated that the Q_3 tetrahedrons formation in the aggregate prevails over dissolution during the swelling step and contributes to an internal silica gel generation (may not be similar to conventional ASR gel). The Q_4 to Q_3 transition is expansive and is responsible for the swelling and cracking of the aggregate. They observed significant increase of the aggregate pore volume associated with this transition. They observed a linear relationship between the mortar bar swelling and the aggregate swelling due to this transition.

2.4 CURRENT TEST METHODS FOR PREDICTING ASR POTENTIAL

The section provides an overview of the main laboratory test methods that are currently used to evaluate alkali silica reactivity of aggregates. Figure 2.7 shows several of the current test methods to assess ASR prior to their use in concrete structures. The current test methods are classified into three categories: (a) aggregate testing, (b) cement-aggregate combination testing, and (c) gel identification testing.

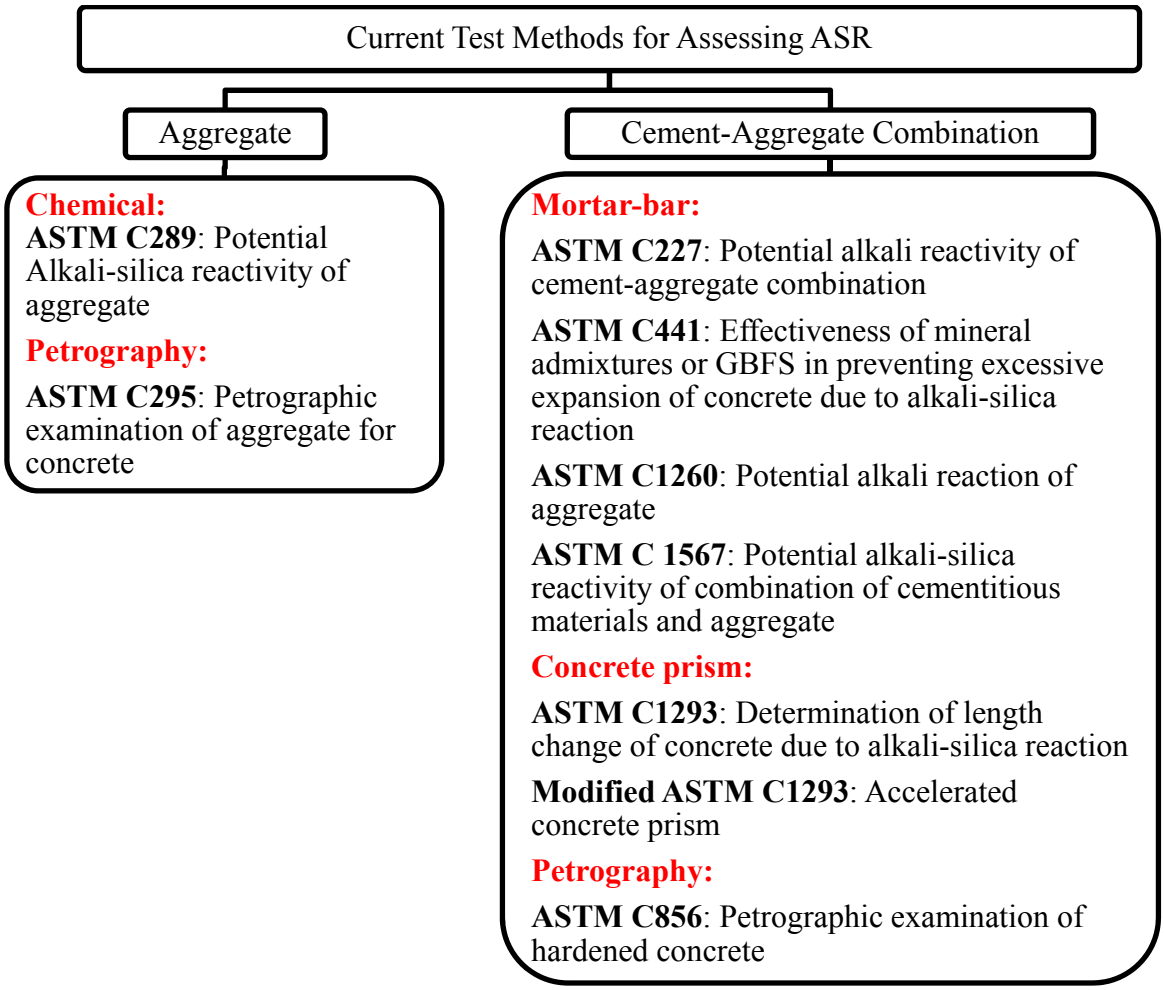

Figure 2.7. Current Test Methods for Assessing ASR.

The most commonly used tests for assessing aggregate ASR potential are ASTM C 1260 and ASTM C 1567 (accelerated mortar bar test [AMBT]) and ASTM C 1293 (concrete prism test [CPT]). A brief description of the procedure along with its usefulness and limitations of AMBT and CPT are summarized below.

ASTM C 1260: Standard Test Method for Potential Alkali Reactivity of Aggregates (Mortar-Bar Method)

This test is a modification of ASTM C 227 for assessing the potential reactivity of aggregates. Aggregates are crushed to meet specific grading requirements. Prepared mortar bars are soaked in 1N NaOH solution at 80°C for 14 days. The purpose of using severe test conditions such as high level of alkalinity and temperature along with crushing aggregate is to accelerate ASR in mortar bars. As a result, expansions of mortar bars are obtained within as little as 16 days. The test method was developed because of the shortcomings of ASTM C 227 and ASTM C 289.

Several researchers and agencies have also referred to the ASTM C 1260 method as the accelerated mortar bar test method.

Earlier research indicates that the AMBT method should be used with caution when rejecting aggregates. The test conditions (i.e., 1N NaOH and 80°C) are severe and the test results are unrelated to field performance. Aggregates with a good field track record in terms of ASR can sometimes be classified as reactive when tested according to this method. This is supported by the observation that some aggregates failed by the AMBT method actually passed by the CPT method (i.e., false negatives). A heterogeneous distribution of reactive constituents within the aggregate is common for certain aggregates (e.g., reactive cementing materials in sandstone, reactive siliceous impurity in limestone, etc.). Losing the reactive phases during crushing and sieving of these aggregates (part of sample preparation in C 1260) sometimes causes aggregates passed by the AMBT but failed by the CPT (i.e., false positives).

ASTM C 1293: Standard Test Method for Concrete Aggregates by Determination of Length Change of Concrete due to Alkali Silica Reaction

This method involves measuring length change of concrete prisms made with the coarse or fine aggregates under investigation. A non-reactive fine aggregate is used when the coarse aggregate is reactive and vice-versa. Additional alkali (NaOH) is added to the concrete mixture in order to elevate the alkali level (1.25 percent Na_2O_e by mass of cement) of the concrete. De-molded prisms are stored above water at 38°C in a sealed container.

Test method ASTM C 1293 is considered the best index for field performance, but the duration of the test (a year or more) represents a major drawback. Experience has shown that a higher level of alkali is required to initiate expansion in the CPT than in field concrete produced with the same aggregate. Quick reduction in pH of the pore solution as a result of significant alkali leaching is reported in the CPT than it does in actual field concrete. Moreover, no wetting or drying takes place in this test method. As a result, this test tends to underestimate the extent of the reaction that would take place in a field concrete made with the same mix as the test. Berube et al. (2000) suggested that the test conditions are too severe as the concrete prism test may identify some aggregates with generally good field performance as being potentially reactive. Moreover, both the CPT and the AMBT tests are conducted at a single alkali level, which is quite high compared to the field concrete. As a result, these methods cannot study the effects of cement alkali and threshold alkalinity cannot be determined. The CPT method is not capable of evaluating field mixes (i.e., job mixes) as the CPT prescribes a standard mix design. Similarly, there are no provisions to test differently, or to use different limits for different exposure or service conditions. And thus for many situations, the level of prevention that will satisfy the test may be overly conservative. It can be generalized that the AMBT is harsher than field service, while the CPT is milder than field service.

The primary requirements for any accelerated ASR test method are:

- It should be able to predict correctly the potential reactivity of aggregate in over 95 percent of the cases (Grattan-Bellew 1989 and 1997).
- Inter-laboratory coefficient of variation should be low, preferably less than 12 percent.

Owing to the complexity and variability in composition and grain size of aggregates, it is unlikely that a single test method can correctly evaluate all types of aggregates. Researchers and agencies worldwide have proposed some of the new methods or modifications of existing methods to overcome some of the limitations associated with aggregate crushing, alkali content, storage conditions (alkalinity of test solution and temperature), and leaching. However, current test procedures are largely empirical and yield test results that are applicable to a narrow band of conditions. It is clear that there is a lack of a unified approach to address how different combinations of concrete materials may interact to affect ASR behavior and warrant a different approach for ASR testing. A fast and reliable testing protocol that can measure aggregate reactivity matching with field levels of alkalinity and temperature is warranted.

2.5 KINETIC APPROACHES FOR THE DETERMINATION OF ASR AGGREGATE REACTIVITY

ASR is a chemical reaction where some initial conditions related to alkalinity, aggregate reactivity, moisture, and temperature conditions must be met to initiate ASR. ASR is a kinetic type of chemical reaction that integrates the combined effects of temperature, alkalinity, moisture, and time relative to the kinetics of ASR expansion.

Kawamura and Iwahori (2004) found that the expansive pressure is approximately proportional to the amount of ASR gel formed provided the alkali content of ASR gel is less than a critical value. The authors also found that even when AMBT greatly expanded in tests without restraint, mortar bars containing ASR gel with higher alkali content (similar to ASTM C 1260) than the critical value showed extremely low expansive pressure. The authors, therefore, concluded that in existing ASR-affected concrete structures containing gels with higher alkali content than a critical value, damages due to the secondary stresses caused by restraint might not be so significant, even if reactive aggregates used in the concrete have showed greater expansions in mortar bar tests in the laboratory. This knowledge allows for greater understanding of the kinetics involved with the formation of gel and its subsequent expansion. Therefore, kinetic-type models can be used to derive characteristic material properties and assess ASR fundamentally. In the past, researchers have investigated the use of a kinetic-type ASR model for either the prediction of mortar bar expansion (T. Uomoto, Y. Furusawa, and H. A. Ohga, 1992) or for better interpretation of the existing test methods (Johnston et al. 2000). A brief discussion on previous kinetic type approaches and applications follows.

French kinetic chemical test

Sorrentino et. al. (1992) introduced the French kinetic chemical test similar to the ASTM C 289 chemical method. The method consists of measuring the amount of silica dissolved into 1N NaOH solution at 80^{o}C for 96 hours, which includes the time parameter. After conducting many tests, the authors suggested a chart (see Figure 2.8) displaying different degree of ASR reactivity with zones representing deleterious and innocuous aggregates. They also mentioned that based on the test results, their new test procedure was able to detect aggregates that displayed a pessimum effect.

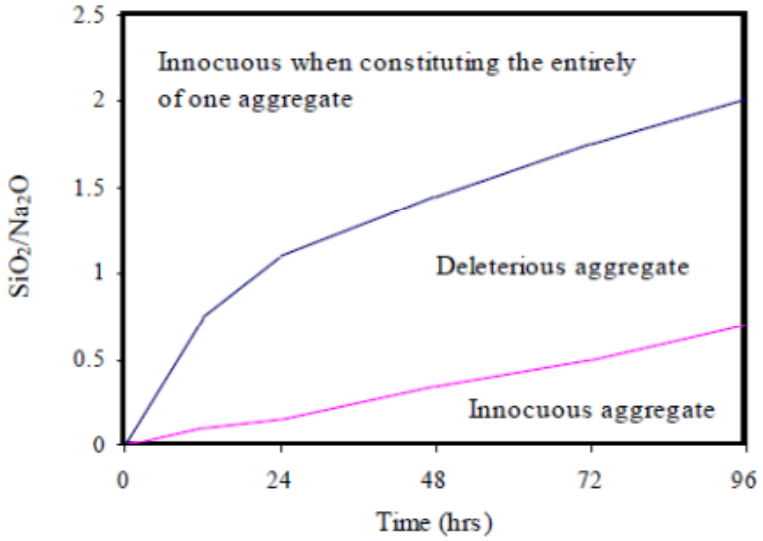

Figure 2.8. Chart of the Kinetic Test (Sorrentino et al. 1992).

Kinematic Model to Predict Mortar Bar Expansions

Uomoto et.al. (1992) introduced a kinetic model to predict the expansion behaviors of mortar bars. The expansion behaviors were calculated by alkali diffusion coefficients in aggregates and alkali-silica ratio (RS) of reaction products. The alkali diffusion coefficients and RS were determined by the leaching test in accordance with ASTM C289. However, the model is based on many assumptions without experimental verification. Thus, experiments are needed in order to improve the model.

Application of Kolmogorov-Avrami-Mehl-Johnson Kinematic Model to the Motor Bar Expansion Data

Using the Kolmogorov-Avrami-Mehl-Johnson model, Johnston et al. (2000) proposed a kinetic-based approach to overcome some of the deficiencies in specifying the percentage of expansion to distinguish between reactive and non-reactive aggregates in ASTM C 1260. This procedure is based on growth and nucleation where the power of time and the percent expansion are related to each other exponentially as follows (Equation [2.1]):

$$\alpha = \alpha_0 + (1-\alpha_0)(1-\exp(-k(t-t_0)^M)) \qquad \text{Equation (2.1)}$$

where

α_0 is the degree of reaction at time t_0

k is the rate constant

t_o is the time when growth and nucleation are dominant

M is exponential factor.

By applying a least square fit to the logarithmic form of the kinetic model, two parameters [ln(k) and M] were generated. Figure 2.9 shows two distinctive areas by plotting M against ln(k). The test results show that reactive aggregates are associated with ln(k) > -6 and non-reactive aggregates are associated with ln(k) < -6. This method was effective in determining the amount of mineral admixtures necessary to mitigate ASR. The main disadvantage of this procedure is that the analysis was done using AMBT, which only takes 16-day testing periods. However, the aggregates needed to be crushed and therefore the surface area and the reactivity of the aggregate were altered and no longer represented real concrete.

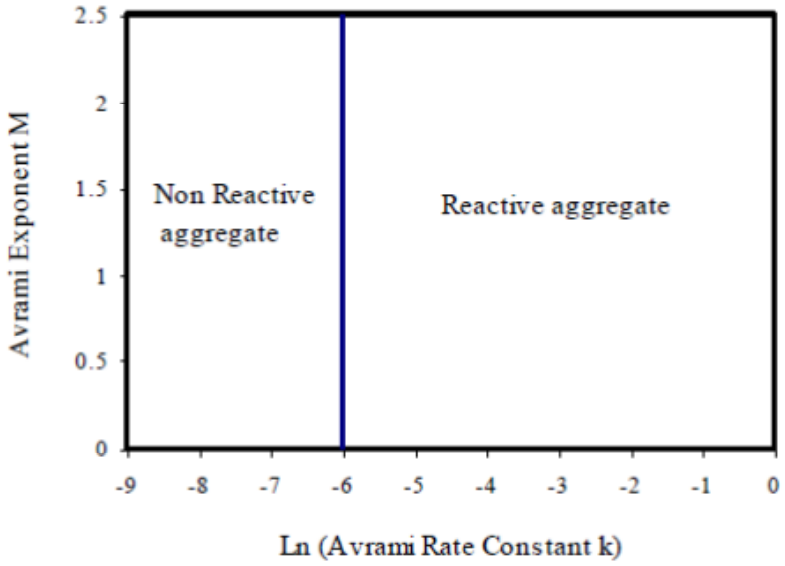

Figure 2.9. Avrami Exponent vs. Rate Constant (Johnston et al. 2000).

CHAPTER 3: MATERIAL CHARACTERIZATION

This chapter presents aggregate selection, collection and characterization. It was proposed to select aggregates after critically evaluate the past record of alkali silica reactivity of aggregates based on the current methods (e.g., ASTM C 1260 and C 1293) and field performance (as much as available from beams/blocks, precast girders, field structures, etc.) data. It was proposed that the selected aggregates (both coarse and fine aggregates) should cover a wide range of reactivity, mineralogy and geographic locations. It was also proposed to give more emphasis to select aggregates from the exclusion list as well as aggregates belong to false positives / negatives categories. The selected and collected aggregates were evaluated in terms of overall mineralogical composition, type, and distribution of the reactive components through petrographic examination of thin sections (ASTM C 295).

3.1 MATERIALS SELECTION AND COLLECTION

Aggregates from both the exclusion list (TxDOT option 7 of item 421 exclusion lists) and the approved list were selected. The RS proposed that at least 15 aggregates (both coarse and fine aggregates) will be tested with full factorial experimental design (Chapter 5). All the aggregate sources were identified after critically analyzing the past ASR records and obtaining feedback from the Project Director (PD) and other project members from the TxDOT. For each source, the required amount of materials (determined based on the full factorial experimental design discussed in Chapter 5) have been collected. It was decided to test borosilicate glass balls (pure phase) using the proposed test methods for validation purposes (as a proof of concept). The required amounts of highly reactive borosilicate glass balls were also collected.

Table 3.1 provides detailed information on the 15 selected aggregate sources. The ASTM C 1260 (AMBT) passed the CA6 and CA7 coarse aggregates, but the ASTM C 1293 (CPT) failed them. On the other hand, the ABMT method passed the CA5 coarse aggregate, but the CPT method passed it.

Table 3.1. List of Selected Aggregates.

Aggregate	Type	TxDOT Exposure/4085 ID	ASTM C1260	ASTMC1293 (38°C)	Modified ASTM C1293 (60°C)	Block 0.95/1.25 Na_2O_e
FA1	Fine	FA1/-	0.554	-	-	-/-
FA2	Fine	FA10/F7	0.334	0.21	0.171	0.5492/0.9064
FA3	Fine	-/-	0.317	-	0.058	-/-
FA4	Fine	FA3/F14	0.242	-	0.043	-/-
FA5	Fine	FA2/F6	0.079	0.01	0.035	0.0026/-
CA1	Coarse	-/C2	0.417	0.11	0.078	-/0.2609
CA2	Coarse	CA2/-	0.250	-	0.047	-/-
CA3	Coarse	CA3/-	0.227	-	0.071	-/-
CA4	Coarse	CA6/C9	0.179	0.15	0.149	0.004/0.1864
CA5	Coarse	C4/-	0.140	0.02	0.02	0.165/0.0697
CA6	Coarse	CA7/-	0.100	-	-	-/-
CA7	Coarse	CA5/-	0.040	-	0.129	-/-
CA8	Coarse	CA1/C6	0.012	0.01	0.027	0.0026/-
FA6	Fine	-/-	0.474	-	0.391	-/-
FA7	Fine	-/-	0.019	-	-	-/-

Note: FA: fine aggregate; CA: coarse aggregate

For comparison purposes, the gradations for coarse and fine aggregates were kept as a fixed parameter and met ASTM C33 specification (see Figure 3.1). Grading requirements for coarse aggregates are based on nominal size from 1 inch to No. 4. Additionally, all aggregate-related properties (i.e., dry unit weight, specific gravity, and absorption capacity), were also measured using ASTM C127, C128, and C138, and summarized in Table 3.2.

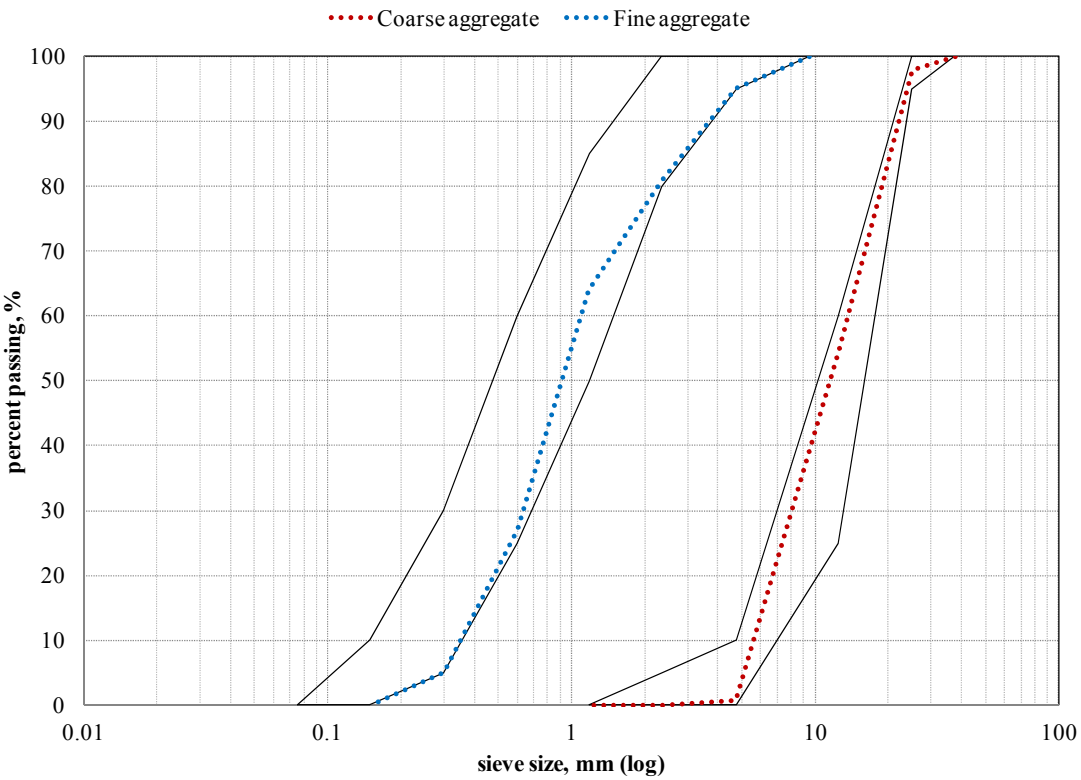

Figure 3.1. Gradation Curves of Aggregates.

Table 3.2. Properties of Aggregates.

Aggregate	DRUW, lb/ft^3	AC	SGod	SGssd
FA1	108.627	1.98%	2.56	2.61
FA2	109.148	2.22%	2.52	2.58
FA3	108.515	1.32%	2.59	2.62
FA4	103.855	1.08%	3.08	3.11
FA5	102.542	6.18%	2.34	2.48
CA1	102.447	0.86%	2.58	2.60
CA2	109.751	1.45%	2.58	2.62
CA3	96.134	1.43%	2.57	2.61
CA4	100.209	0.87%	2.57	2.59
CA5	97.103	1.30%	2.57	2.61
CA6	95.119	0.98%	2.71	2.73
CA7	102.575	0.60%	2.56	2.58
CA8	95.317	2.47%	2.50	2.56
FA6	110.777	2.69%	2.52	2.59
FA7	109.685	2.33%	2.52	2.58

Note: DRUW: dry unit weight; AC: absorption capacity; SG: specific gravity

3.2 AGGREGATE CHARACTERIZATION

The objective of this task was to evaluate the aggregates that were collected (Table 3.1) in terms of overall mineralogical composition, type, and distribution of the reactive components through petrographic examination of thin sections (ASTM C 295). The type (mineralogy), nature of distribution, and content of the reactive constituent(s) determine the reactivity of an aggregate. Aggregate alkali-silica reactivity is a function of the form/degree of crystallinity, grain size, texture, and proportion of the reactive silica within the reactive aggregate. Not all forms of silica are ASR reactive. The more disordered the structure of the silica phase, the greater the reactivity. In general, the metastable types of silica (e.g., opal, chalcedony, tridymite, crisobalite, and some disordered forms of quartz [cryptocrystalline and strained quartz]) and alumina-silicate glasses (e.g., acid volcanic glass) are known to be reactive with the alkalis in concrete. The crystalline quartz (e.g., present in igneous rocks) is not considered susceptible to ASR, whereas strained quartz (e.g., present in metamorphic or sedimentary rocks) is reactive.

The petrographic characterization of an aggregate in terms of determining (i) mineralogy, (ii) type, and (iii) distribution of reactive constituent(s) by optical microscope is the first step in assessing aggregate reactivity (ASTM C 295). An effective use or better interpretation of any ASR testing can only be possible if the above aggregate characterization parameters are known. For example, petrographic observations can provide very useful information to explain why an aggregate passes by ASTM C 1260 but fails by ASTM C 1293 (e.g., sandstone aggregate). Aggregate porosity can have considerable influence on the ultimate expansion of concrete. Studies done on Demark flint aggregates have shown this effect (Broekmans 2002). Migration of reactive ions (Na^+, K^+, Ca^{2+}, and OH^-) can be facilitated by interconnected pores as well as layered structures and other weak planes in aggregates. Certain aggregates, such as granite, glassy volcanic rocks, and clay minerals in siliceous limestone can contribute additional alkalis in pore solution, which can be considered one of the factors for ASR, even with low-alkali cement.

3.2.1 Sample Preparation

Representative particles of different sizes were selected for each aggregate to prepare thin section. The thin sections (50 × 75 mm or 2″ x 3″) for all the aggregates were prepared with blue dye impregnation to highlight the pores and microcracks. A Nikon Labophot 2-POL transmitted light microscope with magnification range 4–40X was used to observe the thin sections. A Lumenera Infinity 1-3C digital camera at 3 megapixel resolutions was used to acquire digital micrographs. A scanning electron microscope with field-emission gun (SEM-FEG) attached with a FEI Quanta 600 EDS was used to perform higher magnification observation of some selective aggregates. Aggregates were coated with 8nm Pt/Pd before being examined in secondary electron mode (SE). The operating conditions were set at 10 kV with beam current greater than 100 nA.

Based on the thin section observations, the reactive constituents for each aggregate were identified (see Table 3.3). The representative photomicrographs of the reactive constituent(s) for each aggregate are presented in Figures 3.2 to 3.16. Figure 3.17 is the Scanning Electron Microscope (SEM) images of borosilicate glass and an acid volcanic particle from a fine aggregate (FA1).

Table 3.3. Reactive Component (s), Mineralogy, and Other Relevant Material Data.

Aggregate	Rock type	Type	Reactive Constitute
FA1	RG (Volcanics, Cherty)	Fine	Acid volcanic, chert, strained QTZ (Figure 3.2)
FA2	RG	Fine	Mainly chalcedony, chert, strained QTZ (Figure 3.3)
FA3	RG	Fine	Strained QTZ, chert, chalcedony (Figure 3.4)
FA4	LS	Fine	Chert, strained QTZ, siliceous inclusions (Figure 3.5)
FA5	LS	Fine	NR w/ few siliceous inclusions (Figure 3.6)
CA1	RG (Volcanics, Cherty)	Coarse	Acid volcanic, chert, QTZ (Figure 3.7)
CA2	LS	Coarse	Chert, strained QTZ, siliceous inclusions (Figure 3.8)
CA3	LS	Coarse	Chalcedony (Figure 3.9)
CA4	RG	Coarse	Chalcedony, chert, QTZ (Figure 3.10)
CA5	LS	Coarse	Separate chert particle (Figure 3.11)
CA6	LS	Coarse	Strained QTZ, siliceous inclusions (Figure 3.12)
CA7	RG	Coarse	Chalcedony, chert, QTZ (Figure 3.13)
CA8	LS	Coarse	NR w/ few siliceous inclusions (Figure 3.14)
FA6	RG	FA	Acid volcanic, chert, QTZ (Figure 3.15)
FA7	LS	CA	NR w/ few siliceous inclusions (Figure 3.16)

Note: LS: limestone; RG: river gravel; QTZ: quartz; NR: non-reactive.

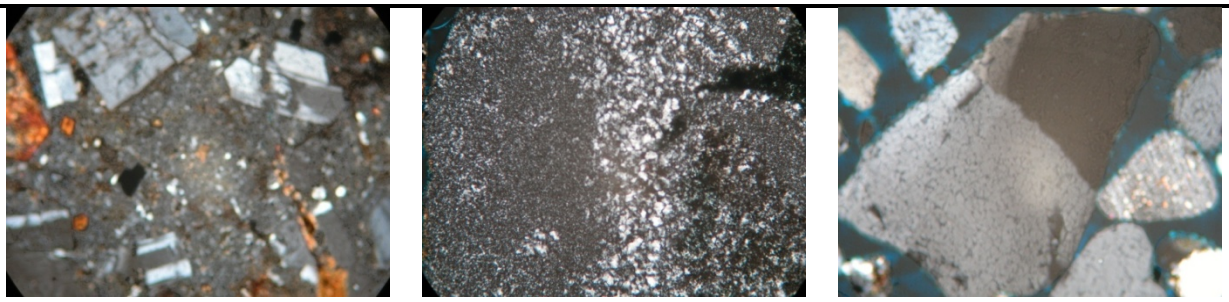

Acid volcanic | Microcrystalline quartz/Chert | Strained quartz

Figure 3.2. Petrographic Observations of FA1.

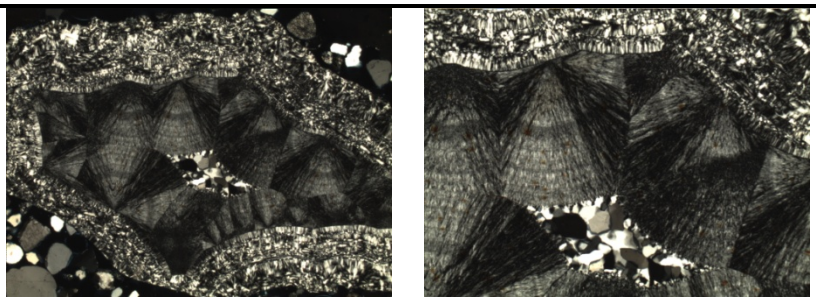

Mainly chalcedony

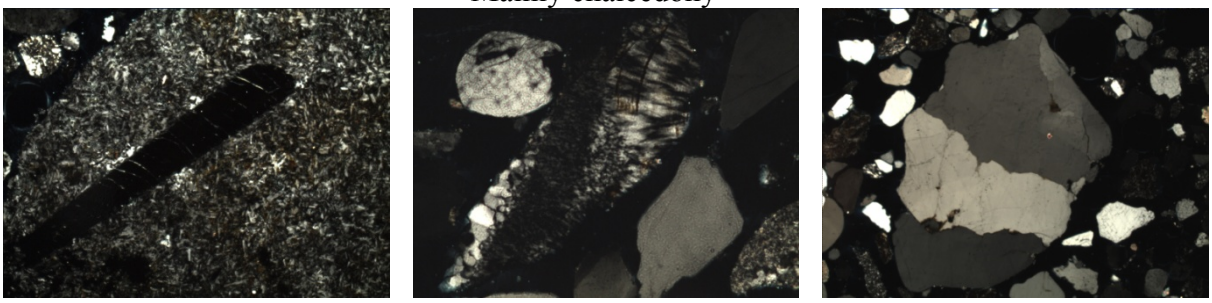

Chert | Chert | Strained quartz

Figure 3.3. Petrographic Observations of FA2.

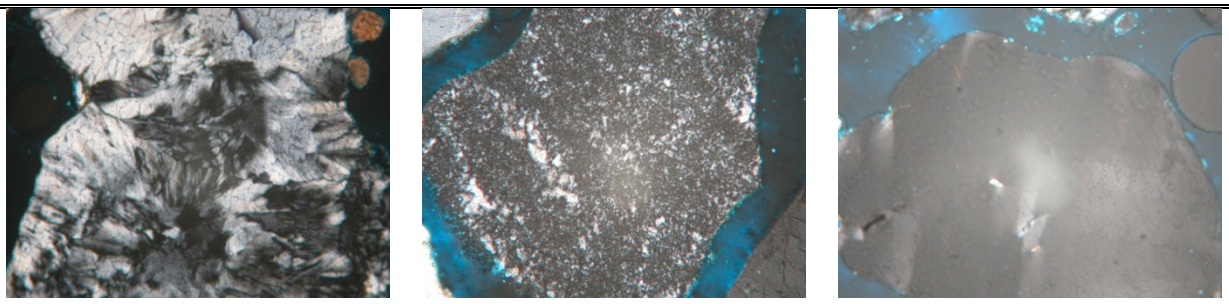

Chalcedony/chert | Micro-crystalline quartz/chert | Strained quartz

Figure 3.4. Petrographic Observations of FA3.

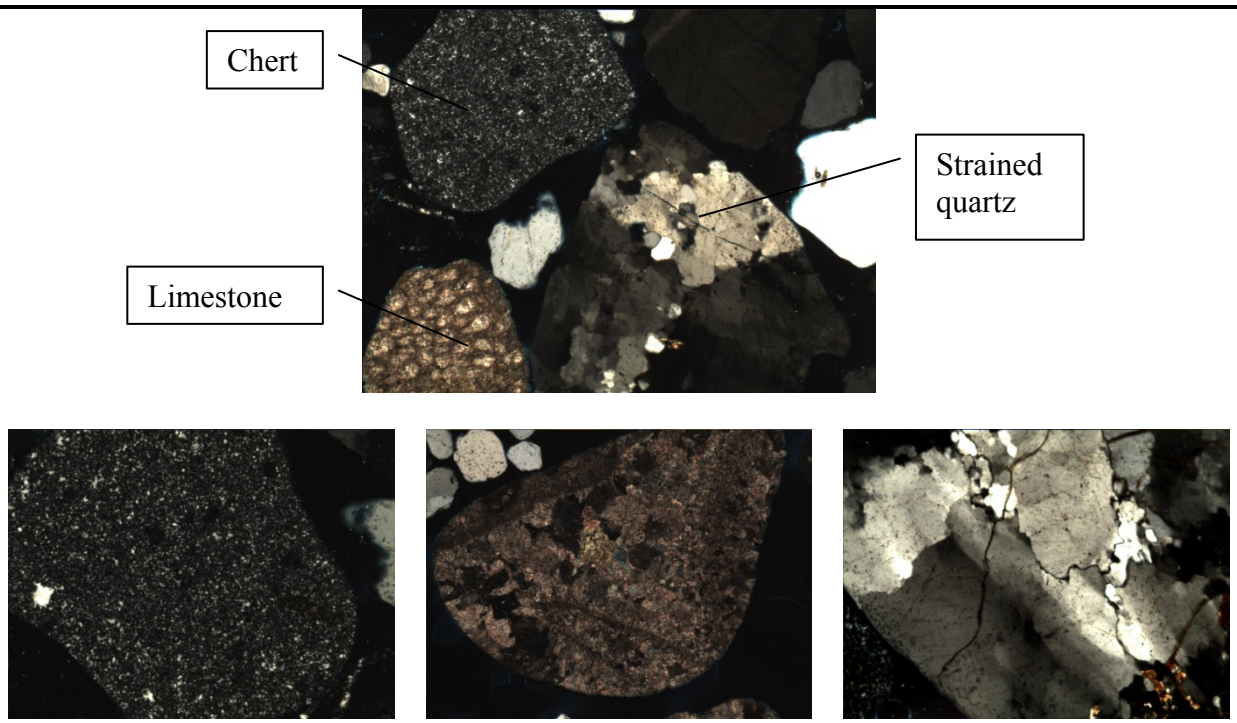

Figure 3.5. Petrographic Observations of FA4.

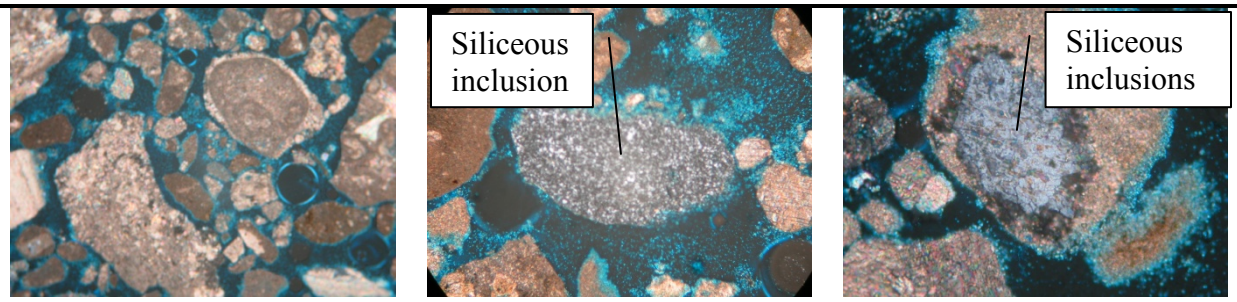

Figure 3.6. Petrographic Observations of FA5.

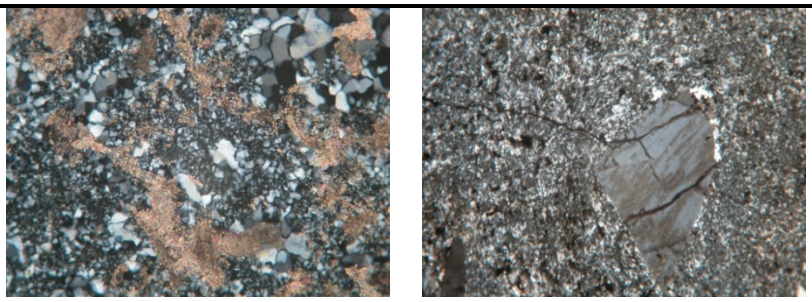

Figure 3.7. Petrographic Observations of CA1.

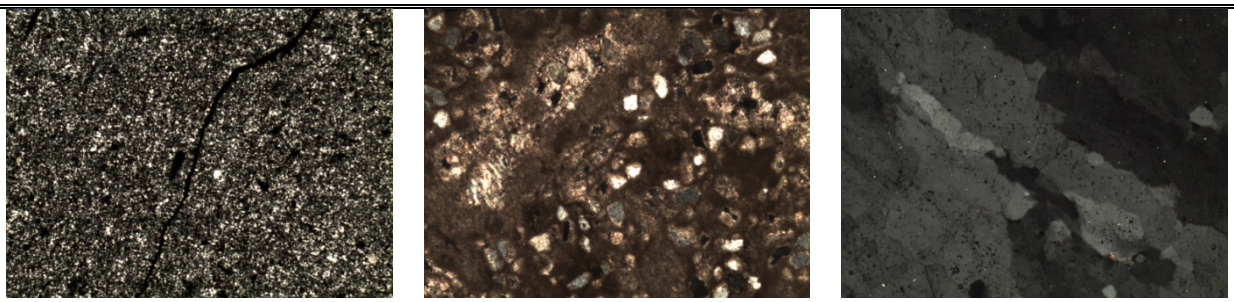

Chert | Siliceous inclusions in Lst | Strained quartz

Figure 3.8. Petrographic Observations of CA2.

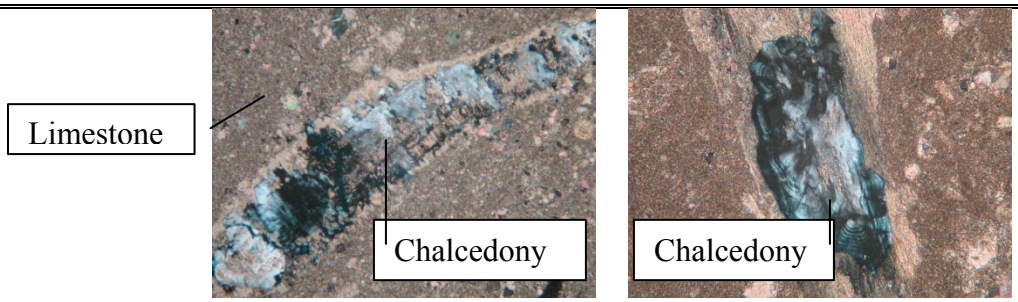

Chalcedony within limestone

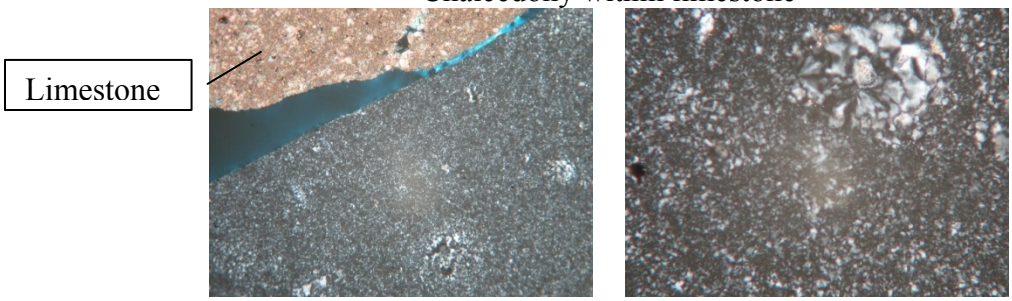

Separate Chert particles

Figure 3.9. Petrographic Observations of CA3.

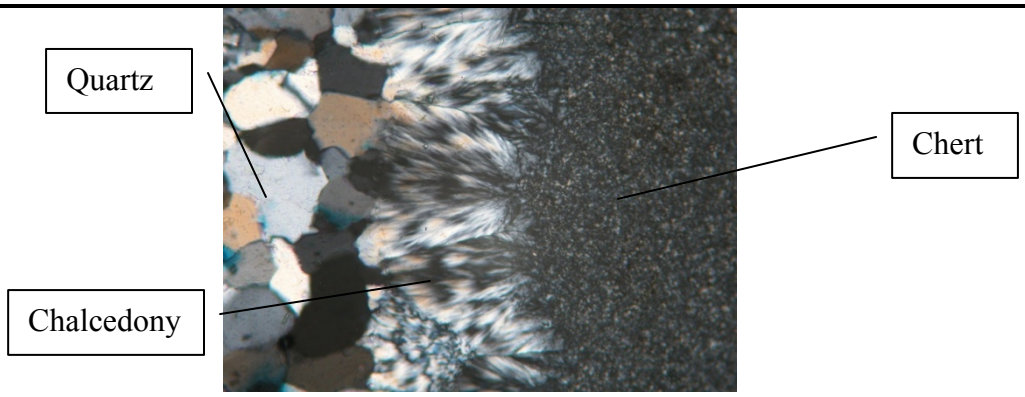

Quartz/Chalcedony/Chert

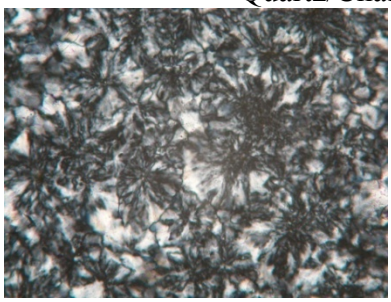

Chalcedony/chert

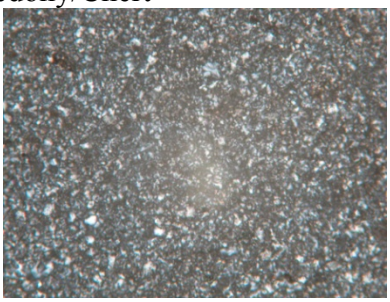

Micro-crystalline quartz/chert

Figure 3.10. Petrographic Observations of CA4.

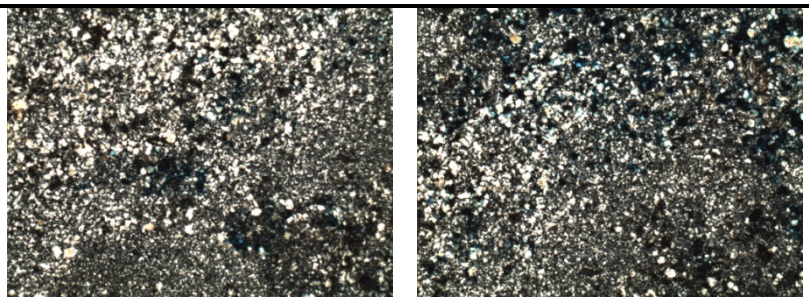

Separate chert particles

Figure 3.11. Petrographic Observations of CA5.

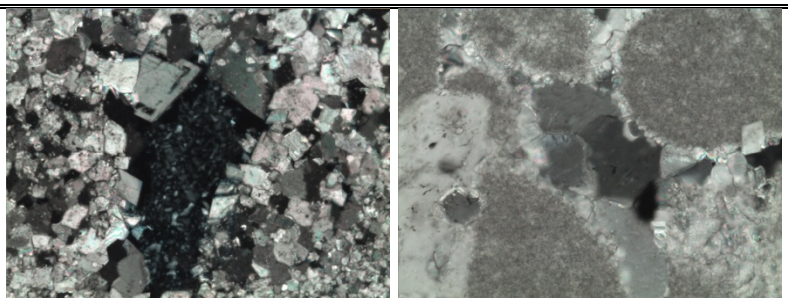

Siliceous inclusions Strained quartz

Figure 3.12. Petrographic Observations of CA6.

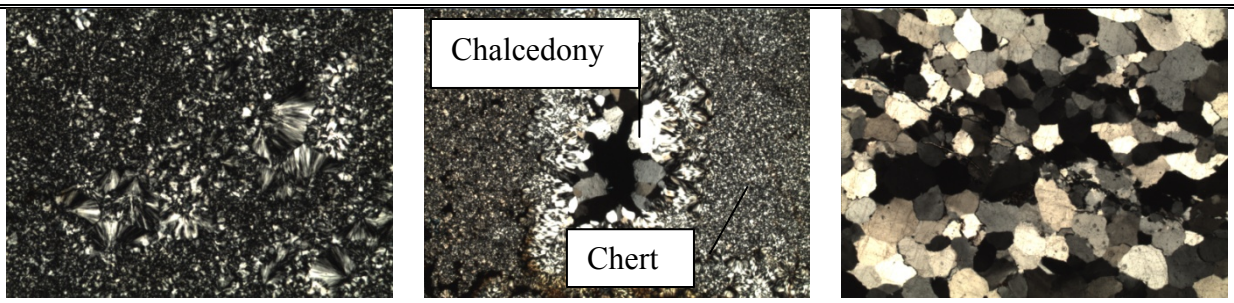

Chert Chalcedony/Chert Multigrain quartz

Figure 3.13. Petrographic Observations of CA7.

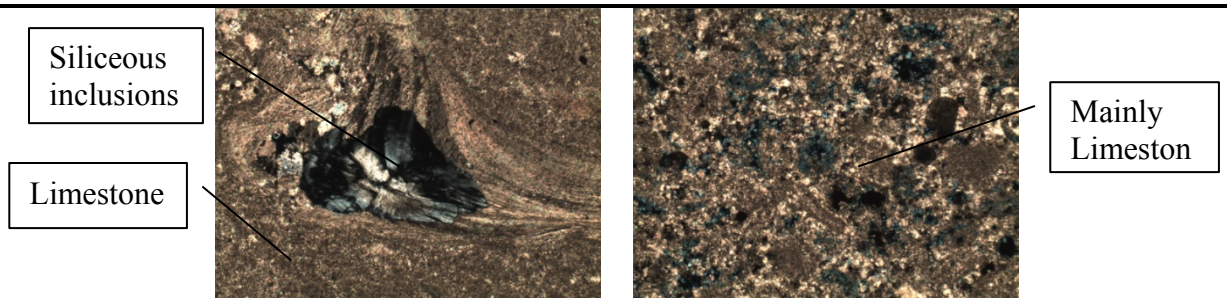

Mainly Limestone (nonreactive) with few siliceous inclusions

Figure 3.14. Petrographic Observations of CA8.

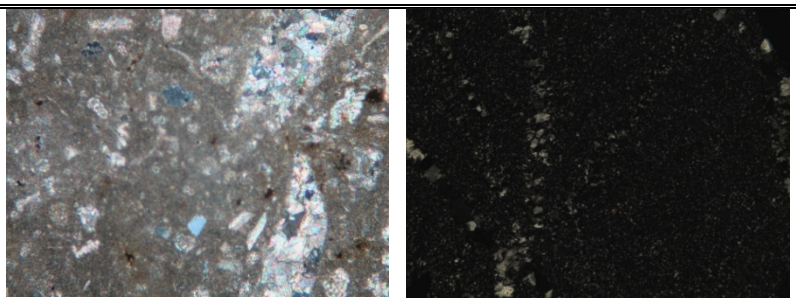

Acid volcanic Quartz/Chert

Figure 3.15. Petrographic Observations of FA6.

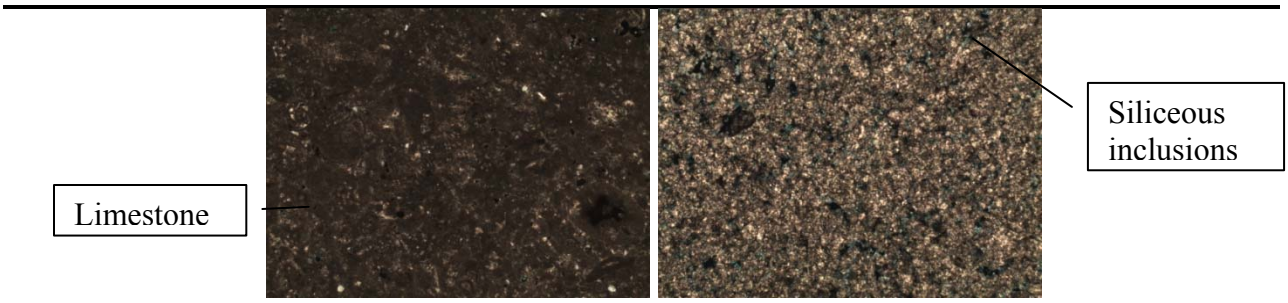

Figure 3.16. Petrographic Observations of FA7.

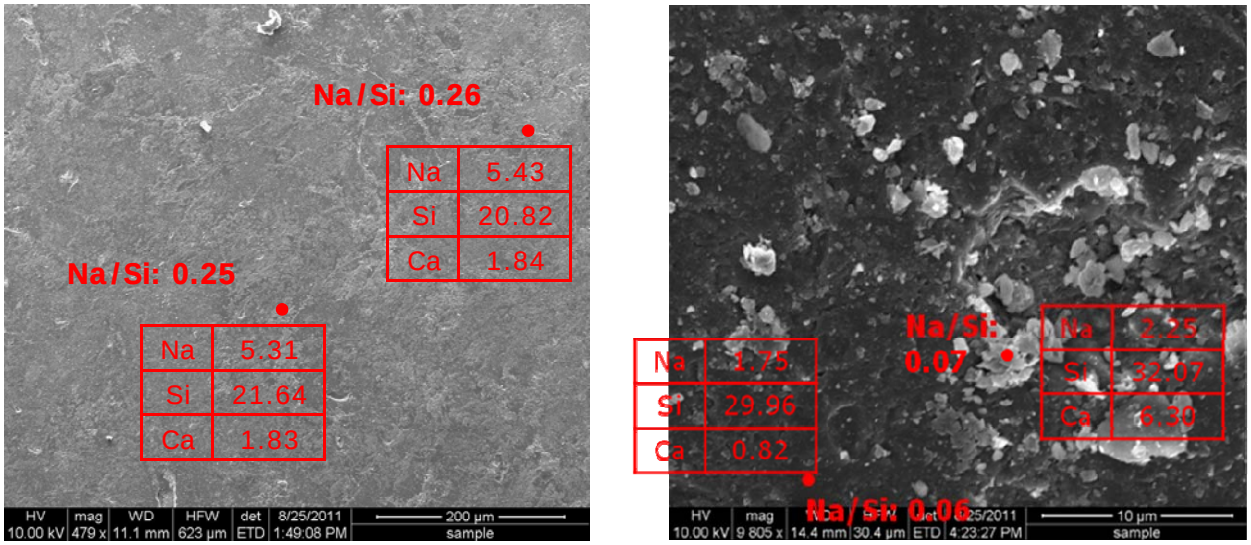

Figure 3.17. Secondary Electron Images and EDS of (a) A Borosilicate Glass Ball, (b) A Reactive Particle in Fine Aggregate (FA1).

Note: Even at high magnification, the presence of micro-crystalline structure is not observed in Fig. 3.17(b). This kind of particle will be highly reactive in alkaline solution.

Aggregates containing acid volcanic glass are considered highly reactive (Barringer 2000), and strained quartz and chalcedony are susceptible to alkali attack due to its poor crystal structure (Roger 1999). If the aggregates contain microcrystalline quartz/ chert inclusions, they are considered slow/late reactive aggregates (Gillott et al.1973). Based on the Petrographic observations, an attempt has been made to predict the reactivity of each aggregate (see Table 3.4 for the summary). In general, aggregates that have high expansion from ASTM C1260 14-days AMBT testing contain more than one reactive constituent, e.g., (a) silica minerals with poorly crystalline structure (e.g. chert with predominantly chalcedony [cryptocrystalline silica with fibrous structure]), (b) strained quartz, and (c) acid volcanic rocks. For the aggregate passes by ASTM C1260 but fails by ASTM C1293 (e.g. CA7), quartzite particles along with chalcedony and cherty materials were identified. Some of the reactive constitutes (e.g., cementing materials in quartzite) might have been lost during crushing, which explains why this aggregate was passed by 1260. Aggregates with high porosity enhance the ASR reactivity due to increased permeability and easier access to concrete pore solution (John et al.1998 and Broekmans 2002). For the aggregate

passes by ASTM C1293 but fails by ASTM C1260 (e.g., CA5), chert particles mostly occur as inclusions within limestone, which is considered to be slowly reactive constitute. The low porosity of the aggregate along with slowly reactive siliceous inclusion might be the reason why ASTM C 1293 gave a passing mark.

3.3 SUMMARY

The degree of ASR and associated distress in the field not only depends on the type of siliceous component but also other field-related parameters (threshold alkalinity and extra alkali sources, moisture, temperature, load capacity, etc.). The field performance of aggregates containing strained quartz shows the occurrence of ASR after decades, and some of the laboratory tests are ineffective (Fernandes et al. 2004 and Shayan et al. 2008) to identify these aggregates as reactive. Therefore, the petrographic techniques should be considered as a good supporting tool at best. A correlation between petrographic observations (Table 3.4) and the reactivity prediction based on volumetric change measuring device (VCMD) (Chapter 5) will be established.

Table 3.4. ASR Aggregate Reactivity Based on Petrography Observations.

Aggregate	1260 Value (14D)	Modified 1293 Value (1YR)	Dominated Reactive Constitute	ASR Reactivity
FA1	0.554	-	Acid volcanic (HR) + high strain QTZ (HMR) + Chert (SR)	Highly reactive
CA1	0.417	0.078	Acid volcanic (HR) + Chert (SR)	
FA6	0.381	0.391	Acid volcanic (HR) + Chert (SR)	
FA2	0.334	0.171	High strained QTZ (HMR) + Chalcedony (HMR) + chert (SR)	
FA3	0.317	0.058	Low strained QTZ (MR) + Chalcedony (HMR) + Chert (SR)	
CA2	0.250	0.047	High strained QTZ (HMR) + Chert (SR)	Medium reactive
FA4	0.242	0.043	High strained QTZ (HMR) + Chert (SR)	
CA3	0.227	0.071	Chalcedony (HMR) + Chert (SR)	
CA4	0.179	0.149	Chalcedony (HMR) + Chert (SR)	
FA5	0.079	0.035	Few siliceous (e.g., Chert) inclusions	Nonreactive, but depending on the concentration of the siliceous
CA8	0.012	0.027	Few siliceous (e.g., Chert) inclusions	

FA7	0.019	-	Few siliceous (e.g., Chert) inclusions	inclusions, some batches of sample may be identified as slowly reactive
CA7*	0.04	0.129	chalcedony (HMR) + chert (SR)	Medium reactive
CA6*	0.1	-	Low strained QTZ (MR) + siliceous inclusions	Medium reactive
CA5**	0.14	0.02	limestone (NR) + limited separate Chert (SR)	Nonreactive or Slowly reactive

*Note: *: Passed by 1260 but failed by 1293; **: Failed by 1260 but passed by 1293; QTZ: quartz; HR: highly reactive; MR: medium reactivity; SR: slowly reactive; NR: non-reactive; HMR – high to medium reactivity*

CHAPTER 4: TEST EQUIPMENT AND PROTOCOL VALIDATION

The previous chapter explained that ASR is a kinetic type of chemical reaction that integrates the combined effects of temperature, alkalinity, moisture, and time relative to the kinetics of ASR expansion. Activation energy can serve as a single chemical material parameter to represent this kinetic type of combined effect and can be used to evaluate the ASR susceptibility of aggregates. A simple chemical test by simulating the aggregate–pore solution reaction that exists in concrete will be appropriate to determine ASR activation energy. Previously, the research team had developed a test method based on a volumetric change measurement device (VCMD) through an Innovative Pavement Research Foundation (IPRF)–sponsored research project (Mukhopadhyay et al. 2009) at the Texas A&M Transportation Institute. The VCMD simulates the aggregate-pore solution reaction that exists in concrete and measures net solution volume change due to ASR over time. This test is performed with as-received aggregates (the error due to crushing is eliminated) and within a short period of time (approximately 5 days including sample preparation). By fitting a kinetic type of performance model to measured volume change data over time, rate constant (β) is calculated. Rate constants at multiple temperatures (a minimum of three temperatures, e.g., 60°C, 70°C, and 80°C) are then determined, and the activation energy (E_a) is calculated by plotting ln(β) versus (1/T). Based on the rate theory (Callister 2007), the slope of the linear regression is equal to ($-E_a/R$) where R is the universal gas constant and E_a is the activation energy. The VCMD has been used to measure the alkali-silica reactivity of selective minerals and aggregates in terms of their activation energy (Mukhopadhyay et al. 2006, Shon et al. 2007). The same VCMD-based procedure was used in this project to measure activation energy of the collected aggregate materials (presented in Chapter 3.

This chapter describes the upgradation of the previously developed VCMD test equipment and protocol development through:

- Identification of areas of reconditioning and upgradation of the devices.
- Fine-tuning the calibration and test procedure.
- Testing a pure phase material (e.g., non-porous borosilicate glass balls) as a proof of concept to verify that VCMD actually measures net solution volume contraction over time (solution curve) due to ASR.
- Verification of deducting water curve (water volume change over time from a parallel aggregate-water test) from the solution curve as a procedure to determine expansion (solid volume increase) indirectly. Earlier, it was observed that deducting the water curve from the solution curve for the same aggregate material (mainly coarse aggregate) provides a way to measure expansion (i.e., solid volume increase) indirectly.
- Further reduction of testing period.

4.1 TEST EQUIPMENT

A detailed description of the VCMD and the test procedure to measure net solution volume change from aggregate-solution test is presented in Appendix A. A brief description of the equipment and the test procedure is given below.

The VCMD consists of a pot, a Teflon®-coated brass lid, a hollow tower, and a steel float. The pot and tower are made of stainless steel whereas the lid is made of naval brass. At the top of the tower, a casing is installed to ensure proper alignment of the linear variable differential transducer (LVDT) and the float. The LVDT used is the Schaevitz® Model HCA-1000 HCA, which has a maximum range of 2 inches. The LVDT is placed with an O-ring located at the bottom of the casing and secured with six set screws though the side of the cylinder. In Appendix A, Figures A-1–A-5 show detailed drawings of the separate and assembled parts of the VCMD. Currently, TTI has eight VCMDs , eight LVDTs, one data acquisition system (nine channels), and two ovens.

As the chemical reaction between aggregate and the test solution [NaOH + saturated $Ca(OH)_2$] progresses, the volume of test solution in the pot changes and the float sitting in the solution also moves. As the float moves, the stainless steel rod moves inside the LVDT and generates electrical signals (Figure 4.1). Therefore, the physical phenomenon (i.e., movement of the rod) is converted into a measurable signal. All LVDT signals are amplified through the use of signal conditioners and then transferred though a USB cable to a workstation where a program in LabVIEW was developed to display, analyze, and store the generated data (see Figure 4.1).

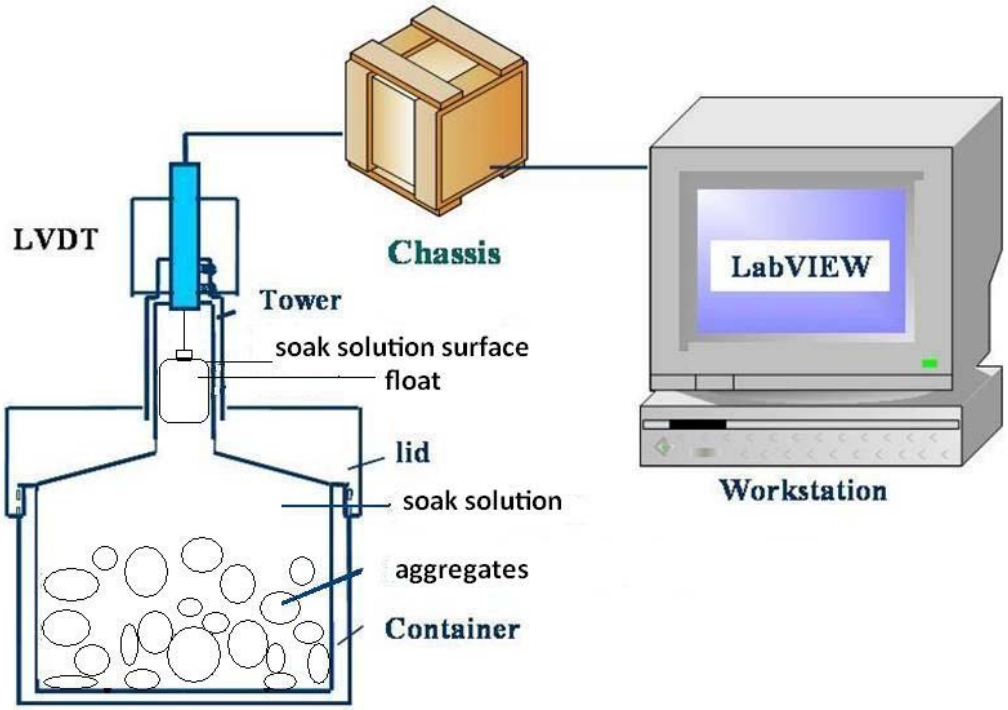

Figure 4.1. VCMD Test Setup.

4.1.1 Equipment Upgradation and Reconditioning

The towers of the three devices out of the total eight VCMDs had the old design, so efforts have been made to make all the devices identical. To achieve this, the towers of the three old VCMDs were modified. In the earlier version of the VCMD (see Figure 4.2), LVDT housing

on the top of the tower was not introduced. Application of glue at the junction between the LVDT and the tower was the common practice to seal the junction. However, this practice sometimes causes evaporation of the solution after several tests. Therefore, the old towers in these three old VCMDs were replaced by the new towers with LVDT housing (see Figure 4.3).

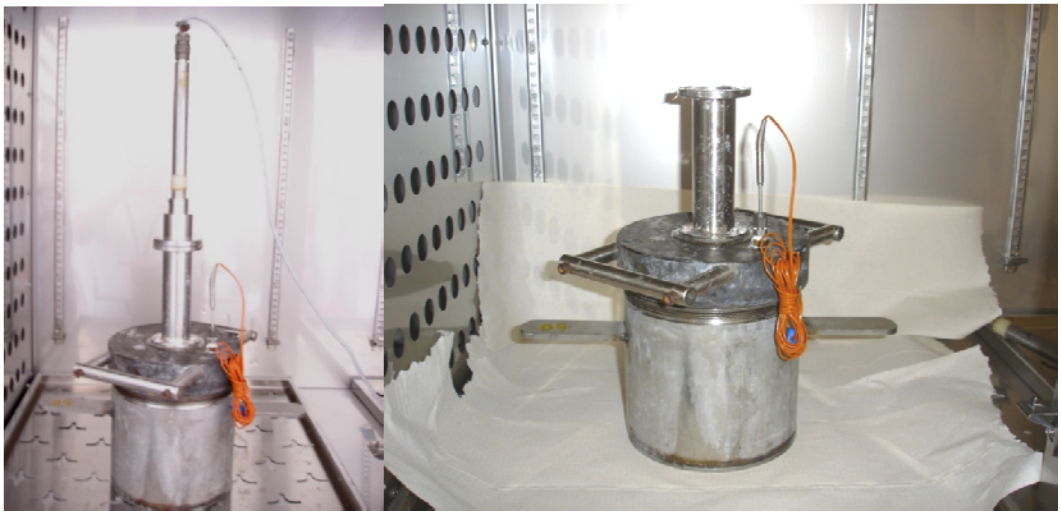

Figure 4.2. An Old VCMD.

Figure 4.3. A Modified VCMD with LVDT Housing.

The researchers reconditioned the inside of the tower and lid to make them smooth, which eliminates/reduces the chances of float sticking issues. Figure 4.4 shows the polishing done inside the tower to create a smooth surface. The team also reconditioned the towers to achieve identical inside diameter for all the VCMDs (see Figure 4.5).

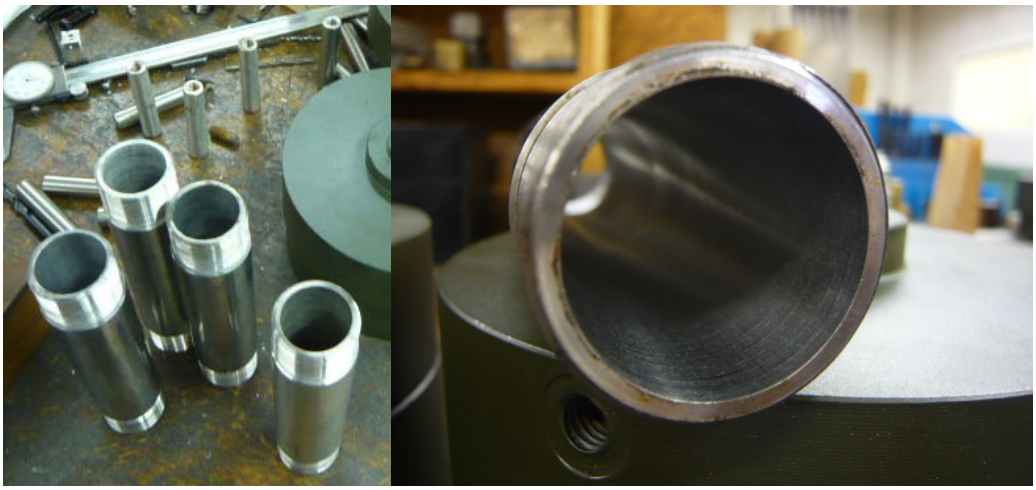

Figure 4.4. Polishing inside the Tower.

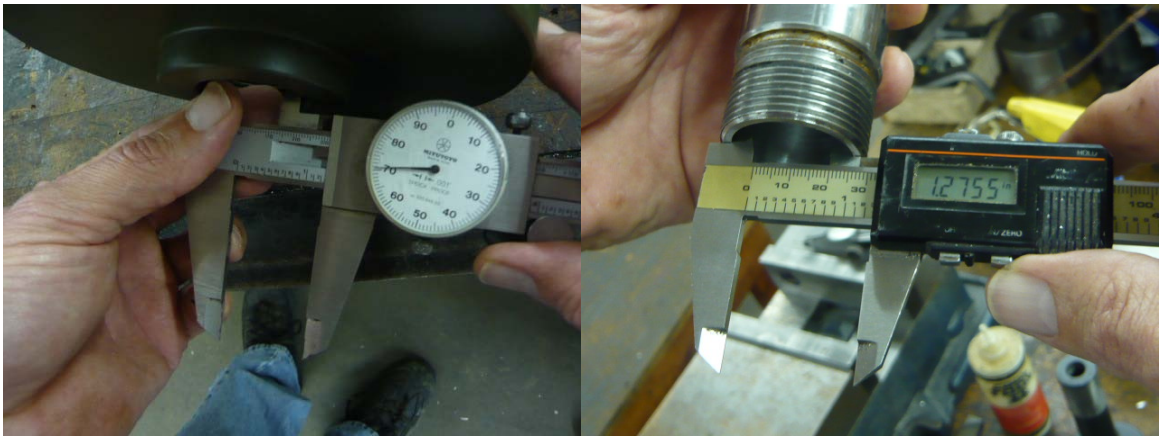

Figure 4.5. Tower Reconditioning to Make the Same Tower Diameter for All the VCMDs.

4.1.2 Equipment Calibration

To check smooth float movement and ensure that the devices are leak-proof, it is recommended to conduct water testing at 80°C with the same testing duration for all the VCMDs. Each VCMD was filled up with water, vacuumed with vibration (to remove air bubbles), and then placed inside the oven where it experienced a temperature change from the starting temperature (45-55°C) to 80°C. The water in the pot experiences thermal expansion due to the temperature increase, which makes the float move upward. The float displacements (in inches) and solution temperatures data for all the eight VCMDs were recorded over four days and are presented in Figure 4.6. The figure shows that when the temperature reaches 80^{o}C, the float also reaches a stable displacement level in all the VCMDs. The float movement doesn't change thereafter. This verifies that the devices are leak-proof and no measurable evaporation loss situation during the 4-day test duration.

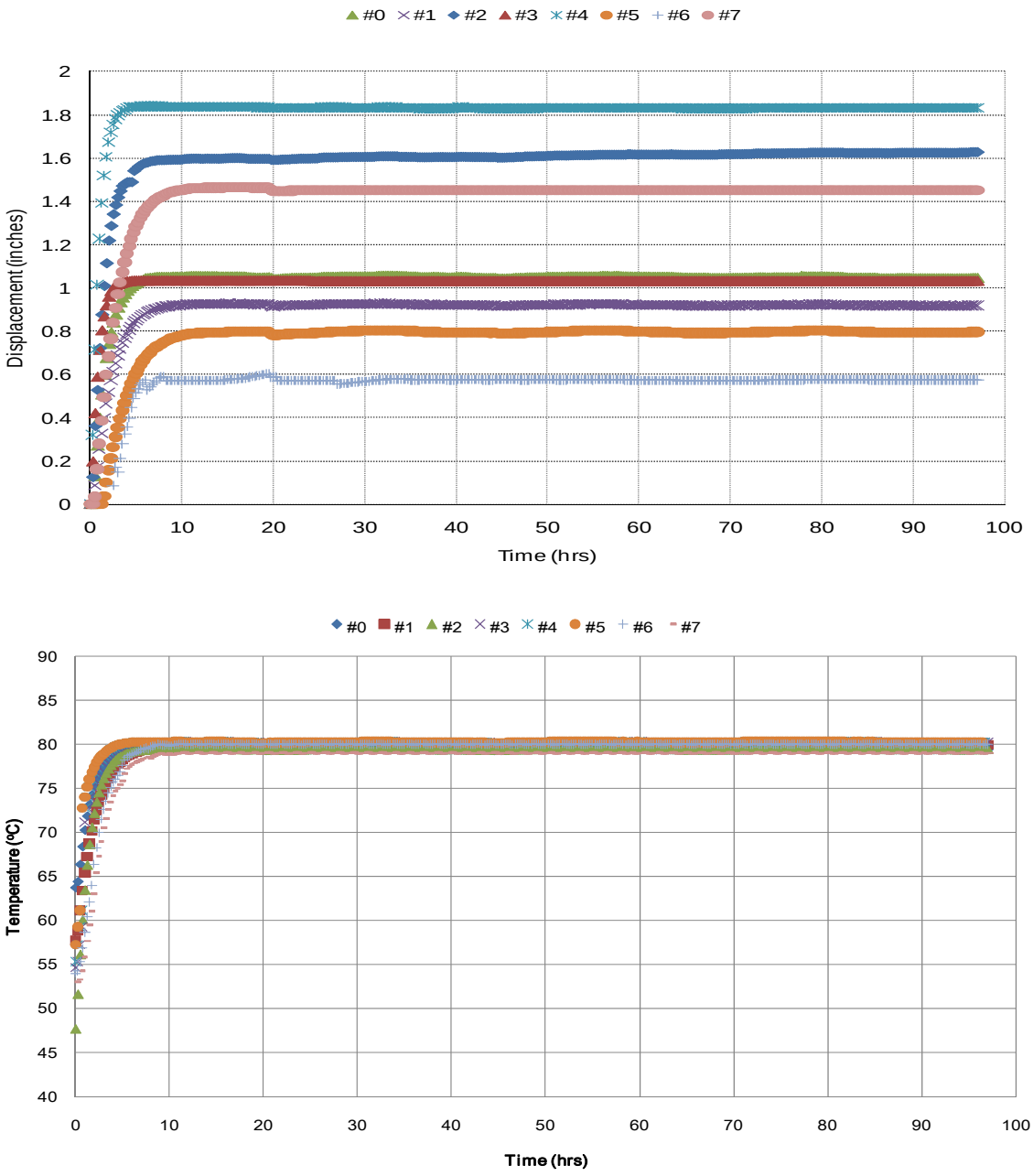

Figure 4.6. Float Displacements and Water Temperatures over Time in all the VCMDs from Water Tests.

To verify smooth float movement, each VCMD was filled up with water, followed by vacuuming with vibration and placed inside the oven where it experienced a temperature increase from 40°C to 60°C. The temperature of water inside the VCMD and the LVDT displacement due to volume expansion (thermal) of water were continuously recorded through the data acquisition system. The initial and final positions of LVDT are taken from the average of 2-hour displacement data at a stable initial temperature (i.e., 40°C) and final temperature (i.e., 60°C) respectively. The difference between average final and initial LDVT readings represent the total LVDT displacement (ΔH) due to thermal expansion (ΔT, i.e., 20°C). The coefficient of

variation (COV) of ΔH for each VCMD (3 tests for each VCMD) is under 2 percent, whereas the COV of ΔH between VCMDs is around 6 percent. The relatively higher COV between VCMDs is possibly due to the combined effects of slight differences in float weight, initial water weight, volume of the pot, and temperature change (ΔT) for each VCMD. Based on these results, it can be concluded that the smooth float movement was achieved in all the VCMDs.

A one-time calibration testing should be sufficient. However, it is recommend to perform the above calibration testing whenever there is:

- A change in float.
- A repair in the device.
- An abnormal LVDT reading during data collection.

4.2 TEST SOLUTION

The 1 N, 0.5N and 0.25N NaOH (NH) solutions are prepared by diluting 40, 20 and 10g of sodium hydroxide crystals into 0.9 liter of distilled water. Water is added to raise the total volume of solution to 1 liter. $Ca(OH)_2$ (CH) crystals are then added (1g per liter solution) to the above respective NaOH solutions slightly above saturation in order to prepare an alkaline solution saturated with calcium hydroxide. Adding CH crystals slightly above the saturation point ensures presence of undissolved CH crystals, which represents a situation similar to concrete pore solution. Thorough mixing ensures homogeneity of all the prepared solutions.

4.3 TEST PROCEDURE TO MEASURE SOLUTION VOLUMN CHANGE DUE TO ASR

The VCMDs are filled up with as-received aggregate (approximately 8–9 lbs) and alkaline solution of different concentrations [e.g., 1N, 0.5N, and 0.25N NH + CH] and tested at different temperatures (e.g., 60°, 70°, and 80°C) inside an oven according to the experimental design in Section 4.4.1. The weight of the oven-dried material corresponded to the 80 percent volume of the VCMD pot. Researchers used a constant aggregate/solution volume ratio and gradation for all the aggregate testing in Section 4.4.1.

The VCMD test procedure is summarized below (Appendix A gives a detailed procedure):

- Keep the VCMD filled up with clean and dried aggregate and alkaline solution overnight at room temperature to allow maximum saturation of voids in the alkaline solution.
- Place the VCMD on a vibrating table and conduct vacuuming under vibration for 2 hours in the next day to mainly remove entrapped air bubbles in the solution. This also helps to saturate the unfilled voids (likely to be present) in aggregates after overnight saturation.
- Place the VCMD inside an oven and heat it to the selected target temperature (~ 2.5 hours).
- Apply a second stage vacuuming under vibration of around 45 minutes to facilitate further removal of air bubbles (may be generated during heating at target temperature) from solution.

- The VCMD was placed inside an oven, whose temperature was then raised to the selected target temperature (i.e. 60 or 70 or 80°C). It takes around 4–5 hours to reach the target temperature.
- Solution volume changes as the chemical reaction between aggregate and alkaline solution progresses; make the float move. As the float moves inside the tower, the stainless steel rod attached with the float also moves inside the LVDT. Through the data acquisition system, the computer records LVDT displacement readings over time.

LVDT displacement readings at the stable target temperature represents the reference (initial) LVDT reading for calculating displacement due to ASR. This ensures separation of thermal solution volume expansion from solution volume change due to ASR. All subsequent LVDT readings (i.e., after reference reading) minus the reference LVDT reading represent displacement due to ASR over time. The percent volume change of solution due to ASR is calculated by using Equation 4.1.

$$V(\%) = \frac{\Delta V_{ASR}}{V_{Aggregate}} \times 100 \qquad \text{(Equation 4.1)}$$

V(%)= Percent volume change of solution due to ASR
ΔV_{ASR}= Solution volume change due to ASR
$V_{Aggregate}$= Initial volume of aggregate

4.4 AGGREGATE AND PURE PHASE MATERIALS TESTING

Pure phase material (e.g., borosilicate glass balls) and aggregates (both fine and coarse) (see Table 3.1 in Chapter 3) were tested using the above updated devices and procedures. The design of experiments and the test results are presented below:

4.4.1 Design of Experiment

Table 4.1 presents the design of experiments, i.e., the effective factors and their levels. Fifteen aggregates with different types of reactive silica and varying ranges of reactivity were selected (see Chapter 3, Table 3.1). For each aggregate, researchers conducted a total of 18 test runs (three levels of temperatures and a minimum of two levels of alkalinities with three replicas).

Table 4.1 Factors and Levels in the Design of Experiments

Factors	No. of Levels	Level Description
Material type	1 pure phase + 15 aggregates	Borosilicate glass + 15 aggregates in Table 3.1
Temperature	3	(1) 60°C, (2) 70°C, and (3) 80°C
Solution normality	2/3	(1) 0.5N and (2) 1N NH with CH (3) 0.25N NH with CH for some selected aggregates

4.4.2 Testing Pure Phase Material

The use of borosilicate glass as a highly alkali silica reactive material has been reported both in conducting ASR research and ASR test developments (Ostertag et. al. 2007, ASTM C 441). The composition of the borosilicate glass balls is composed of SiO_2: 81 percent, Na_2O: 4 percent, Al_2O_3: 2 percent, B_2O_3: 13 percent. This is a non-porous material. Borosilicate glass balls were tested at three levels of temperatures and at 0.5N NaOH (NH) + $Ca(OH)_2$ [CH], 1N NH + CH, and 1N (NaOH + KOH) + CH alkalinities. Three tests (corresponding to three different temperatures) at each alkalinity with total 3 alkalinities gives total 9 test runs. Figure 4.7 shows the net solution volume changes in a form of contraction over time at three levels of temperatures and at 1N NH + CH for borosilicate glass balls–solution tests as an example. The remaining data are presented in Appendix B. A net solution volume contraction over time due to ASR between glass balls and alkaline solution was invariably observed for all the tests at different levels of temperatures and alkalinities. Note that glass balls are non-porous and there was no effect of absorption on the measured net solution volume contraction over time. This observation suggests that the VCMD in closed system set up measures net solution volume contraction over time due to ASR. The glass ball solid volume increases but the net solution volume decreases.

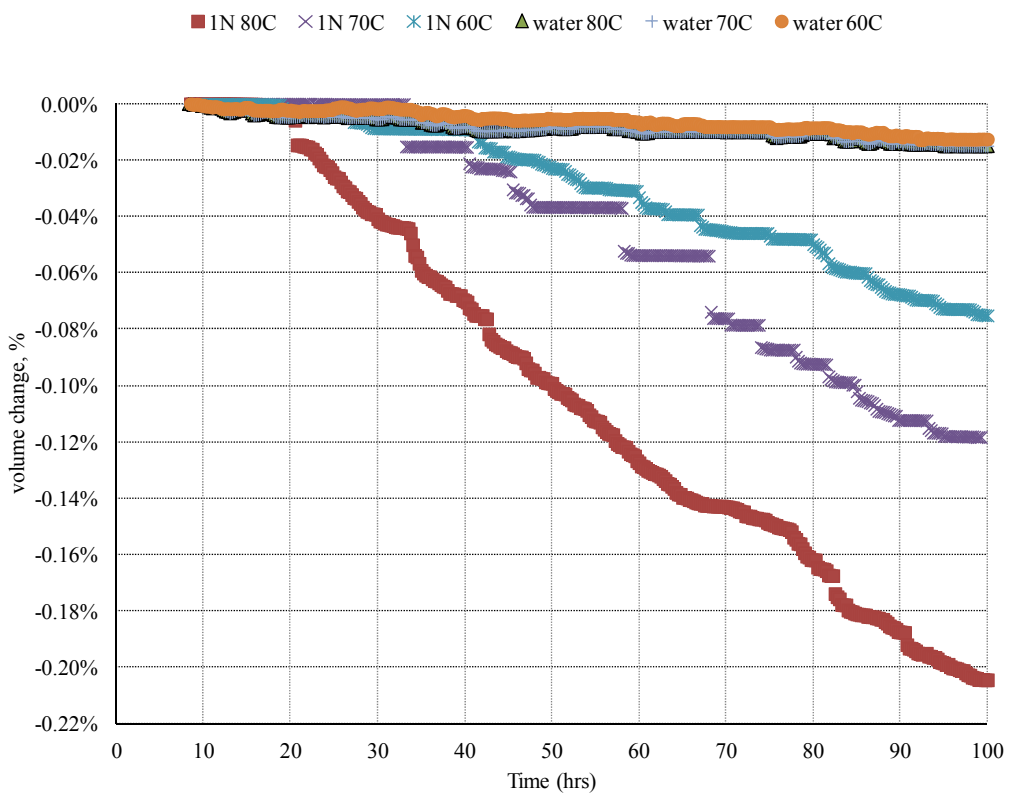

Figure 4.7. Net Solution Volume Change from Borosilicate Glass Balls at 1N NH + CH Solution at Three Temperatures.

4.4.3 Testing Aggregates

For each aggregate, researchers conducted 18 test runs (three temperatures, two levels of alkalinities, and three replicas). Eight VCMDs were simultaneously run inside an oven for five days. The approximate total time to complete all 18 test runs is 15 days without any interruption. All aggregates were tested using the VCMD according to the experimental design in Table 4.1 and net solution volume change over time was measured. Figure 4.8 shows the measured volume change over time at three levels of alkalinity and temperatures (60°, 70°, and 80°C) for FA1 as an example. The data for all the aggregates at different levels of alkalinities and temperatures are presented in Appendix B. Note that net solution volume contraction over time was also invariably measured for all the tested aggregates (irrespective of coarse or fine aggregates). This is in agreement with earlier findings in the previous project.

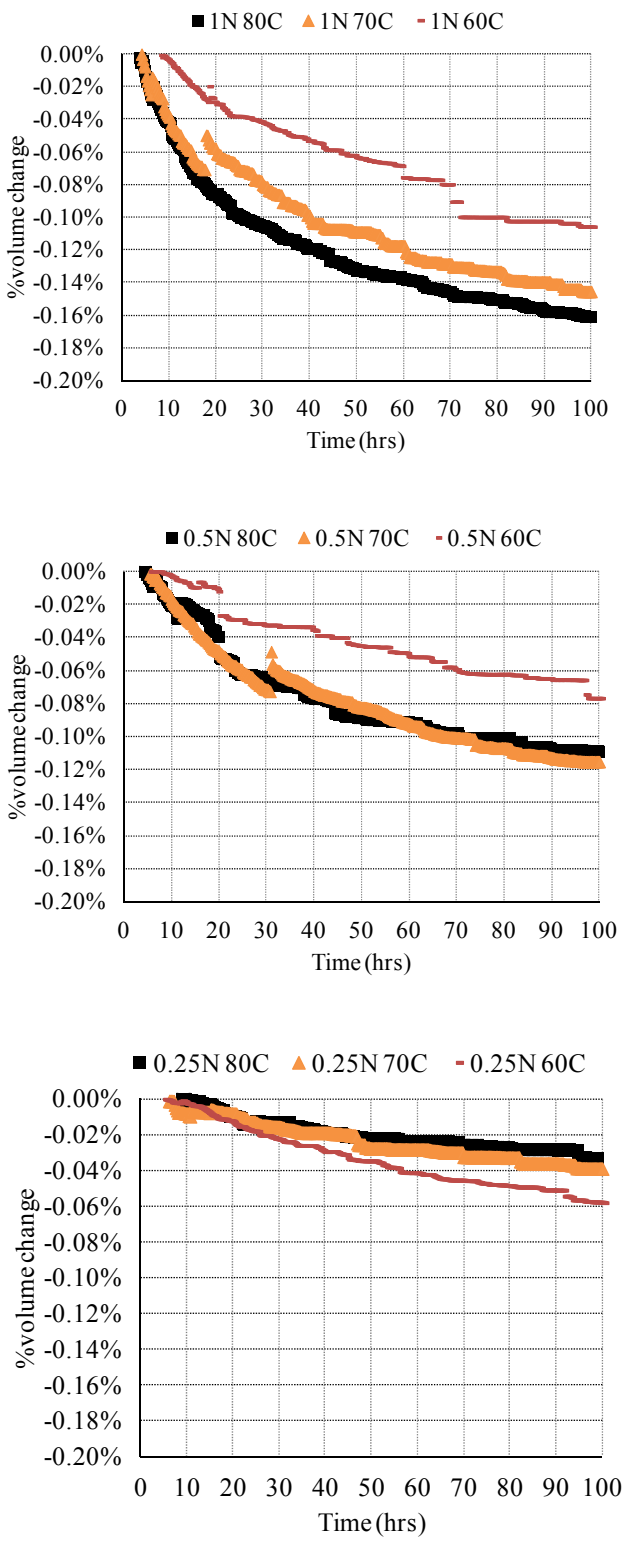

Figure 4.8. Solution Volume Change with Different Levels of Alkaline Solutions (1N, 0.5N, and 0.25N NH + CH) at Three Temperatures (60°, 70°, and 80°C) for FA1.

Concrete aggregates that have high absorption capacity (AC) reach 85 percent of their total absorption capacity in less than 30 minutes of soaking in water, and reach 95 percent of their AC within 24 hours of soaking in water (Adam et al. 2012). The total submerged time of aggregate in alkaline solution before achieving the stable target temperature in the VCMD test is around 24 hours. Moreover, the two-stage vacuum saturation is a part of the VCMD sample prepation procedure, which enhances absorption (should be more than 95 percent). It is observed that aggregates attain the maximum possible saturation by the end of the second stage of vacuuming, which ensure no or very negligible further aggregate saturation during testing. It is extremely difficult to fully saturate (i.e., achieving 100 percent AC) an aggregate by prolonging soaking time. Therefore, it is unlikely that the saturation (pore filling by solution) will continue during the VCMD testing (i.e., four days). Even if this continues, it would be very negligible. Therefore, the effect of aggregate absorption in measuring net solution volume change in the VCMD test would be very negligible. The dominant phenomenon is net solution volume contraction due to ASR.

Measuring chemical shrinkage in fine aggregate-alkaline solution system over time has been reported earlier (Geiker and Kundsen 1986). In Geiker and Kundsen's procedure, a flask is filled up with sand samples and 10N NaOH solution, and then stored in a thermostatic bath at 50°C. The researchers used the data solution volume change over time (recorded manually) to calculate chemical shrinkage due to ASR over time. The chemical shrinkage was used as a measure of aggregate reactivity, i.e., the higher the chemical shrinkage, the more reactive the aggregate is. The authors stated that the measured chemical shrinkage in their test procedure is very similar to the cement hydration. The total volume (cement and water) decrease and the volume of solids increase during cement hydration. Similarly, when ASR occurs in concrete, water coming from outside the system allows the ASR gel to expand and to occupy a volume greater than the amount of water in the reaction. This test was widely used in Demark.

The measurement of solution volume contraction over time was also commonly observed in our previous study (Mukhopadhyay et. al. 2009). Interestingly, an approach of subtracting water curves (i.e., net water volume change over time in parallel aggregate-water test) from the solution curves (i.e., net solution volume change over time in aggregate-solution test) was used to determine net solid volume increase (expansion) due to ASR indirectly in the previous study. A net upward displacement was observed based on limited coarse aggregate testing and interpreted as a measure of solid volume increase, i.e., expansion. In this study, aggregate-water tests at the three selected temperatures were conducted for all the aggregates in Table 3.1. Deductions of water curves from solution curves are performed and the net displacements after water curve deduction are summarized in Table 4.2.

Table 4.2. Net Displacement after Water Deduction for All Aggregates.

	CA			**FA**			**All Aggregates**		
Net displacement	U	D	LC	U	D	LC	U	D	LC
Occurrence, %	60	34	6	14	75	11	41	51	8

Note: U: Upward, D: Downward; LC: Little Change

Table 4.2 shows that the consistent trend of upward movement after deducting the water curves from solution curves is not obtained. In fact, the net displacements remain downward in most of the cases. The coarse aggregates shows higher percentage of net upward displacements (sometimes with very less upward movement) than the fine aggregates. Based on these findings (inconsistent trends), it is concluded that simply deducting water curves from solution curves does not necessarily provide direct measurement of solid volume change (i.e., expansion). The water curve can be considered a perfect reference curve if the aggregate-water system remains totally inert (i.e., no reaction between tested aggregates and water at high tested temperatures). However, the following discussion indicates that this assumption may not be correct.

Researchers found that the solubility of amorphous silica depends on both temperature and pH value. Morey et al. (1964) and Alexander et al. (1954) observed that the solubility of amorphous silica in water increases with an increase of temperature shown in Figure 4.9 (a). Alexander et al. (1954) also concluded that the solubility was about 0.012 to 0.014 in the pH range 5 to 8 at 25 ^{o}C and increased at high pH (pH > 8) [shown in Figure 4.9 (b)] because of the formation of silicate ion in addition to $Si(OH)_4$ in solution. Therefore, it is unlikely that aggregate-water system remains inert at high temperatures and water curves obtained from aggregate-water tests may not serve as a good reference curves. This explains the inconsistency of the results in Table 4.2.

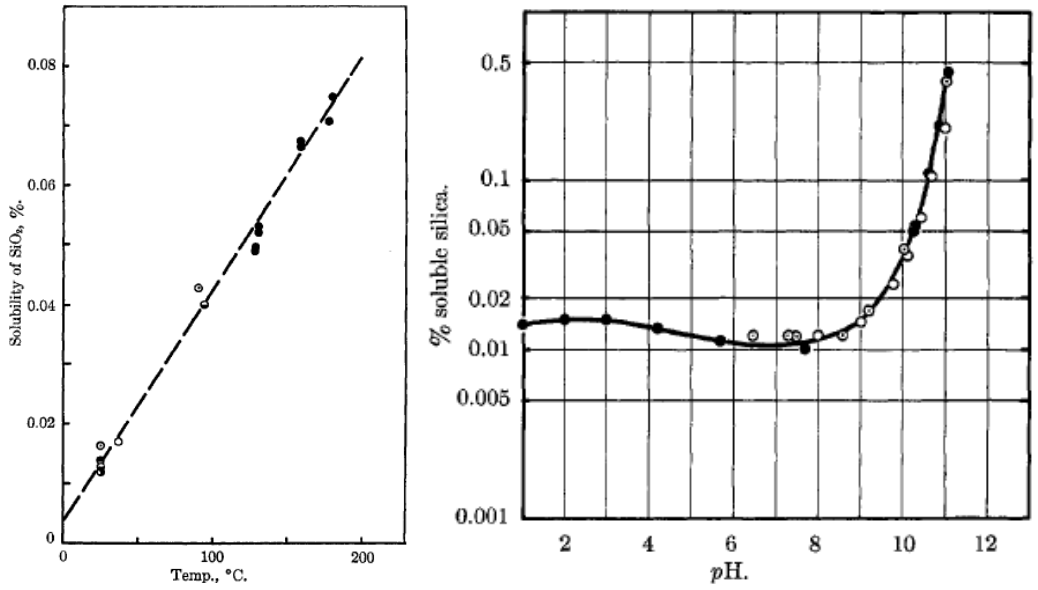

(a) (b)

Figure 4.9. Solubility of Amorphous Silica in (a) Water and (b) Different pH Solution at 25^{o}C (Alexander et al. 1954).

4.5 SUMMARY

The main observations based on the results and discussions in this chapter are summarized below:

- The experiments with pure glass balls support measuring net solution volume contraction over time in VCMD.
- A decrease of net solution volume is due to the combined effects of:

    - Si-O-Si bond breaking and dissolution (solution volume decreases).
    - Consumption of reactants such as water and ionic species (solution volume decreases).
    - Product formation and expansion (solution volume increases).
    - Solution goes into micropores (pores that developed due to the formation of high-volume less dense ASR products) and microcracks. The degree of micropore and microcrack formation is related to the degree of ASR (solution volume decreases).
    - Incomplete absorption (negligible but may be responsible for slight solution volume decrease) in a closed system condition of the VCMD.

- Deduction of water curves from solution curves does not provide an effective way to directly measure solid volume change (i.e., expansion). Therefore, the requirement of conducting parallel aggregate-water tests is no longer needed and facilitates reduction of total testing time.
- It is recommended to characterize the net solution volume contraction over time to determine rate constants at different temperatures followed by activation energy calculaiton, which is presented in the next chapter.

CHAPTER 5: DEVELOPMENT OF ACTIVATION ENERGY-BASED ASR AGGREGATE CLASSIFICATION SYSTEM

This chapter presents

- Determination of activation energy from net solution volume contraction measurements over time (presented in Chapter 4) at different temperatures and alkalinity for both borosilicate glass and all the tested aggregates.
- Developing an activation energy-based ASR aggregate classification system to categorize aggregates based on their reactivity.
- Establishing a characteristic trend between E_a and alkalinity and determine a threshold alkalinity (TH_A) for each aggregate.
- The use of monitoring test solution chemistry change and microstructural studies on the reacted aggregate particles by SEM-EDS as supporting tools for the VCMD test results is also presented.

5.1 MEASUREMENT OF ASR ACTIVATION ENERGY

A kinetic-type model (Equation 5.1) was developed to model measured non-linear type solution volume change data over time (Hassan et al. 2010). By fitting the model (Equation 5.1) to the measured data over time, the characteristics parameters (i.e., ε_0, β, t_0, ρ) are calculated.

$$\frac{1}{\varepsilon} = \frac{1}{\varepsilon_0}.e^{(\frac{\rho}{t-t_0})^{\beta}} \qquad \text{(Equation 5.1)}$$

ε_0 = Volume change due to ASR
β = Rate constant
t_0 = Initial time of ASR expansion (hr)
ρ = Time corresponding to a volume change (ε_0 /ε)

The β values at multiple temperatures (minimum 3 temperatures) are then determined and activation energy is calculated by plotting ln(β) versus (1/T). Based on rate theory (Callister 2007), the slope of the linear regression is equal to ($-E_a/R$) where R is the universal gas constant and E_a is the activation energy. For ASR, E_a is considered as the minimum energy required initiating ASR taking into account the combined effect of alkalinity, temperature and time. In analytical chemistry, activation energy (E_a) is defined as the minimum energy required for a chemical reaction to proceed (Ebbing et al. 2005). Consequently, it can be considered as an energy barrier. For ASR, E_a is considered as the minimum energy required to initiate ASR, taking into account the combined effect of alkalinity, temperature, and time. It is important here to mention that the ASR E_a should be considered as a compound activation energy as aggregate is a heterogeneous material that is often composed of different mineral phases, i.e., reactive phases (one or more phases) and non-reactive phases (crystalline minerals). The concept of ASR

activation energy was introduced as a representative single parameter of alkali silica reactivity of minerals and aggregates earlier (Mukhopadhyay et al., 2006, 2012).

5.1.1 Pure Phase Material

For borosilicate glass balls, the solution volume changes over time are measured at three temperatures and at 1N NH + CH, 0.5N NH + CH, and 1 N NH + KH + CH alkalinities (Chapter 4). The alkalinity of the test solution was selected in such a way so that the behavior of Na and K can be investigated separately. The NEWTON numerical approach was developed based on the model in Equation 5.1 to calculate solution volume change over time. Figure 5.1 shows the measured and calculated volume changes over time at three different temperatures (60°, 70°, and 80°C). At the best fit between the predicted and measured data over time (Figure 5.1), the characteristics parameters (i.e., ε_0, β, t_0, ρ) are determined (System Identification Method). The E_a calculation based on ln(β) versus (1/T) plot is also presented in Figure 5.2 for each level of alkalinity.

Solution Normality	Volume Change over Time and E_a Calculation	E_a (KJ/mole)
1N NH + CH	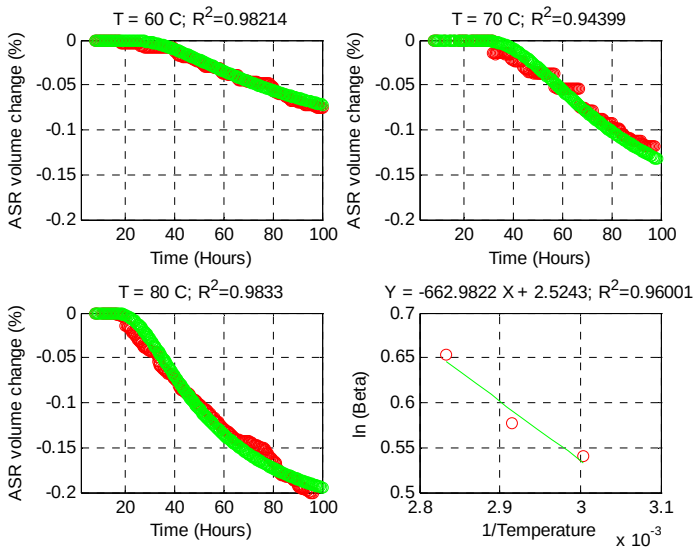	5.51

Figure 5.1. Measured (Red) and Modeled (Green) Solution Volume Change over Time and E_a Calculation for Borosilicate Glass at 1NH Solutions.

0.5N NH + CH	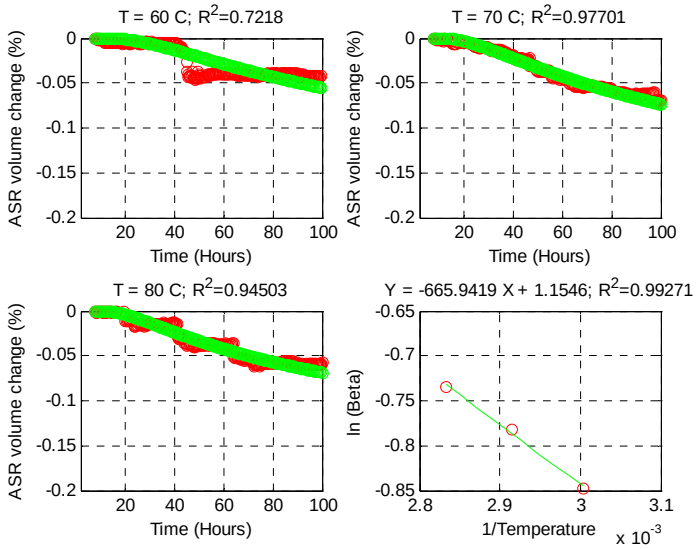	5.54
1N NH + KH + CH	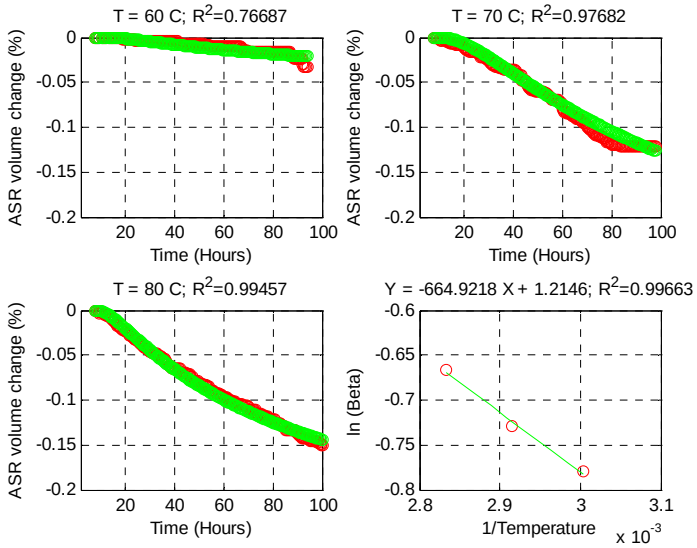	5.53

Figure 5.2. Measured (Red) and Modeled (Green) Solution Volume Change over Time and E_a Calculation for Borosilicate Glass at 0.5N NH and 1N NH + KH Solutions.

The measured E_as for highly-reactive borosilicate glass (Figures 5.1 and 5.2) at different alkali levels do not show much difference. In a pure phase system, Na and K show similar behavior in terms of ASR.

Bates et al. (1994) found that borosilicate glass alters differently from neutral to alkaline solutions. The formation of surface layers on glass is caused by constituent elements of the glass passing into solution, with the elements initially in solution diffusing into or being adsorbed onto the glass. This surface layer (usually called ASR gel) consists of:

- An innermost diffusion layer (partially hydrated and depleted of soluble elements (i.e., B and Na).

- An outermost precipitated layer (amorphous and crystalline phases).
- A gel layer (amorphous and crystalline phases) between them.

The structure and/or composition of the surface layer differ from the original glass and are formed by more than one reaction process (i.e., ion exchange, water diffusion, network hydrolysis and condensation, and precipitation) occurring simultaneously. Therefore, the measured E_a in this study possibly represents a combined effect of all the above processes and it would be better to call it as compound activation energy. These processes are similar to the different steps of the reaction mechanisms mentioned in Chapter 2. The measured net solution volume change in this study is a manifestation of the combined effects of different steps in the reaction mechanisms. Therefore, it is logical to say that the E_a of borosilicate glass measured represents a combined effect of multi-steps ASR reaction mechanisms with dissolution–precipitation possibly the dominating factor.

5.1.2 Aggregate

The net solution volume change over time for the tested aggregates at three levels of temperatures and alkalinities are presented in Appendix B. Any curve at a particular temperature and alkalinity in Appendix B represents an average of three replicas (i.e., repetition of the same test run three times). The same modeling approach (Section 5.1.1.) was applied to the average measured solution volume changes over time and representative E_a values at the studied levels of alkalinity were calculated. Figure 5.3 shows the measured (red) and calculated (green) volume change over time at three different temperatures (60°, 70°, and 80°C) and E_a calculation with different alkali levels for FA1 as an example. The data representing measured vs. predicted volume changes over time along with E_a calculation (same as Figure 5.3) for the remaining aggregates are presented in Appendix C. The activation energy for all the tested aggregates along with ASTM C1260 14-day expansion (%) and modified ASTM C1293 1-year expansion (%) are listed in Table 5.1 and graphically presented in Figure 5.4.

Solution Normality	Volume Change over Time and E_a Calculation	E_a (KJ/mole)
1N NH + CH	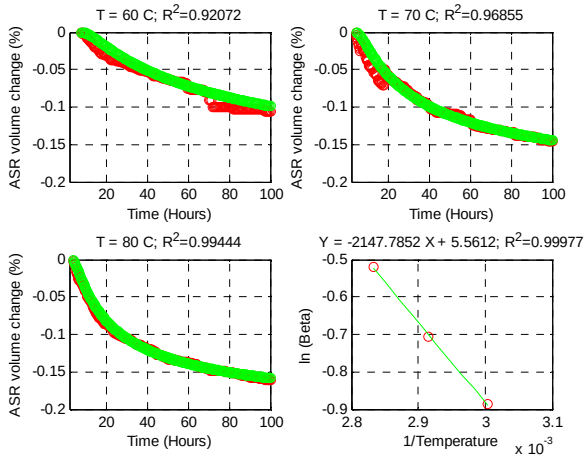	17.86
0.5N NH + CH	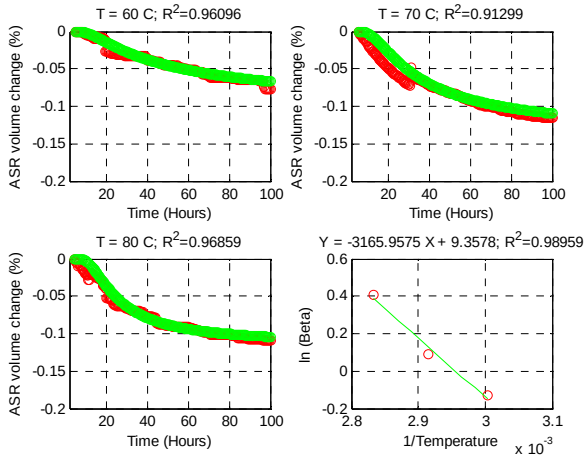	26.32
0.25N NH + CH	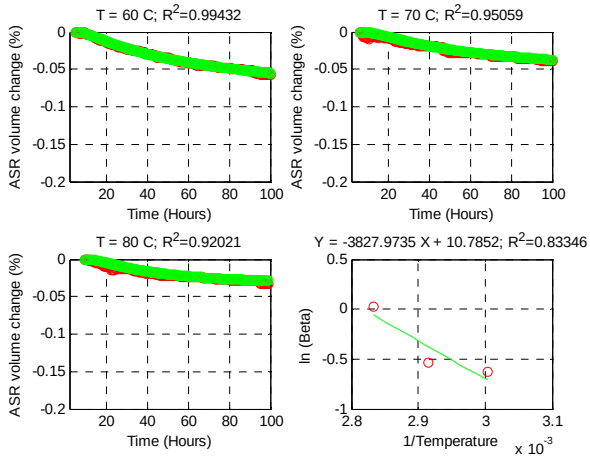	31.83

Figure 5.3. Measured (Red) and Modeled (Green) Solution Volume Change over Time and E_a Calculation for FA1 at 1N NH, 0.5N NH + CH, and 0.25N NH+CH Solutions.

Table 5.1. Measured ASR E_a as a Function of Alkalinity and Temperature.

Aggregate	E_a, KJ/Mol			Modified ASTM C1293 1YR Exp.%	ASTM C1260 14D Exp. %
	1N NH + CH	0.5N NH + CH	0.25N NH + CH		
Borosilicate Glass, 0.25″	5.512 5.528♣	5.537	-	-	-
NMR, CA	-	17.556	-	-	1.3
FA1	15.974	25.999	28.111	-	0.554
CA1	22.164	28.499	-	0.078	0.417
FA3	22.485	32.640	-	0.058	0.317
CA3	27.486	39.864	-	0.071	0.227
CA4	24.688	39.175	42.807	0.149	0.179
FA5	47.645	61.246	-	0.035	0.079
CA8	50.344	67.368	-	0.027	0.012
CA7*	33.641	35.655	-	0.129	0.040
CA5**	47.415	57.091	-	0.020	0.140
FA4	26.980	36.391	-	0.043	0.242
CA2	26.437	35.244	-	0.047	0.250
FA2	23.254	34.979	-	0.171	0.334
CA6*	24.783	27.602	-	-	0.100
FA6	19.947	26.961	-	0.391	0.381
FA7	-	Not measurable	-	-	0.019

Note: NH: NaOH; CH: $Ca(OH)_2$;KH: KOH; ♣ at 1N NH + KH + CH
**: Passed by ASTM C1260 but Failed by ASTM C1293; **: Failed by ASTM C1260 but Passed by ASTM C1293*

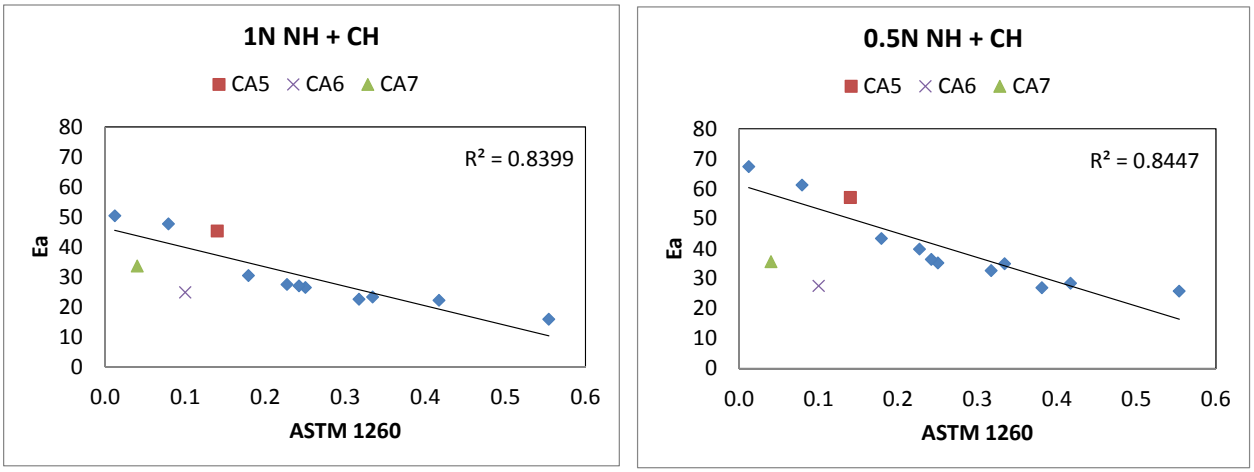

Figure 5.4. Correlation between ASR E_a of Aggregate and ASTM C1260 Expansion (14 days).

Here are some observations on Figure 5.4 and Table 5.1:

- Activation energy is a measure of aggregate reactivity. The lower the E_a values the higher the reactivity is.
- In general, C 1260 14 day expansion values are well correlated (negatively) with Ea values, i.e., Ea decreases with increasing C 1260 14 days expansion. A high reactivity is indicted by a lower value of Ea or higher C 1260 expansion. Similarly, a low reactivity is indicated by a higher value of Ea or lower C 1260 expansion. This indicates that a VCMD-based test procedure can reliably measure aggregate reactivity within a short period of time (i.e., 5 days).
- A representative Ea can be determined by testing aggregate with a test solution of 0.5N NaOH + $Ca(OH)_2$ alkalinity (close to concrete pore solution alkalinity), which offers a great advantage of the proposed method. The favorable points of testing with 0.5N + CH are

    - In general, solution volume change plots (Appendix B and D) at 0.5N NH + CH alkalinity are smoother than those with 1N NH + CH. The repeatability (discussed later) is better with 0.5N NH+CH than that with 1N NH + CH.
    - E_a values at 0.5NH+CH are well separated in comparison with E_a values at 1N NH + CH. This facilitates assigning effective E_a ranges to categorize aggregates based on their reactivity.
    - As 0.5N NH + CH is close to concrete pore solution alkalinity (field level of alkalinity), testing aggregate with 0.5N NH + CH solution is close to simulation of aggregate–pore solution reaction in concrete.
    - CA 6 and CA 7 aggregates are well separated with 0.5N NH + CH than that with 1N NH + CH.

- Consistently identified the aggregates belong to false positive and negative categories – For example, aggregates CA6 and CA7 are passed by C 1260 but failed by C 1293 (false positives) but these aggregates are identified as reactive based on E_a values. Similarly, CA5 aggregate is failed by C 1260 but passed by C 1293 (false negatives) but this aggregate is identified as non-reactive or slowly reactive based on E_a. Therefore, E_a based reactivity prediction shows better correlation with C 1293 than C 1260 for these mismatch aggregates. Therefore, the main benefits of the E_a based method is consistent identification of the aggregates belong to false positives and negatives in a short period of time.
- As the device measures the net combined effects of the different steps of ASR (i.e., breaking Si-O-Si bond, dissolution, product formation, swelling etc.) in a form of net solution volume change over time, it is better to use the term “compound activation energy”. Moreover, aggregates are multiphase and sometimes very heterogeneous materials. In general, the distribution of the reactive constituents inside aggregate is inhomogeneous in nature. This should not be confused with the activation energy of a single (one step) chemical reaction of a pure phase in Chemistry.

Each test run at a particular temperature and at a particular alkalinity was repeated three times to verify the repeatability (within the lab) of the VCMD test results. The solution volume

changes over time for all these replicas at different levels of temperatures and alkalinities are presented in Appendix D. Three rate constants (β) corresponding to the three replicas were used to calculate the coefficient of variation (COV) and the results are presented in Figure 5.5. The COV are mostly within 10 percent for the tested aggregates at all levels of alkalinity, which indicates that the results are highly repeatable.

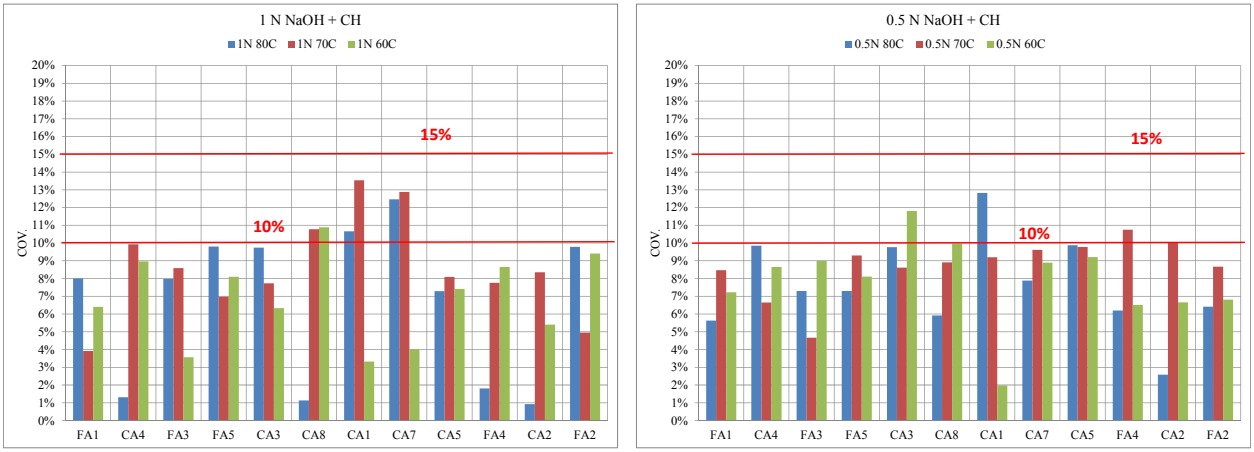

Figure 5.5. Coefficient of Variation (COV) Based on Reaction Constant (β) from the Repeated Tests for All the Tested Aggregates.

5.2 TEST-SOLUTION CHEMISTRY

Filtrates of test solution from VCMD tests are analyzed using the pH meter and induced couple plasma-mass spectrometry (ICP-MS) to determine pH and Na^+ concentration respectively in the test solution both before and after the test. The changes of pH and Na^+ concentrations (i.e., % reduction) in the test solution due to ASR in tested aggregates were calculated for all the test runs and the results are presented in Figures 5.6 to 5.9.

Here are some observations regarding Figures 5.6 to 5.9:

- The lower the activation energy, the higher the consumption of Na^+ and OH^- ions. The consumption of OH^- and Na^+ is more for highly reactive aggregates than that for slowly reactive aggregates.
- For non-reactive or slowly reactive aggregates (higher ranges of E_a), the consumption of Na^+ and OH^- ions are negligible (some consumption due to possibly physical adsorption without any measurable ASR).

Therefore, monitoring change of test-solution chemistry was served as a supporting tool for the VCMD test results.

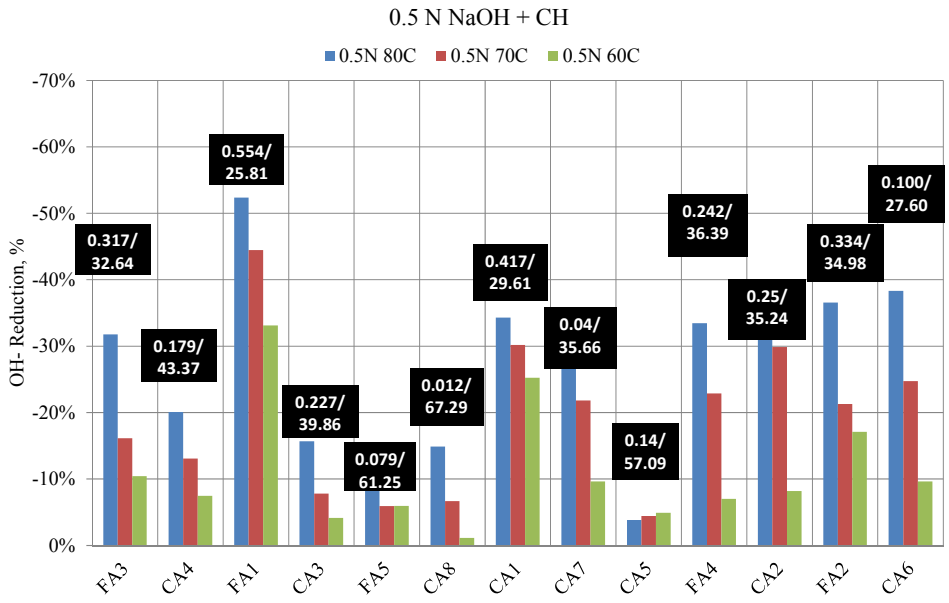

Figure 5.6. Percentage Reduction of OH^- at 0.5N NaOH + $Ca(OH)_2$. E_a and C1260 14D Expansion Values for Each Aggregate are Mentioned inside the Black Boxes.

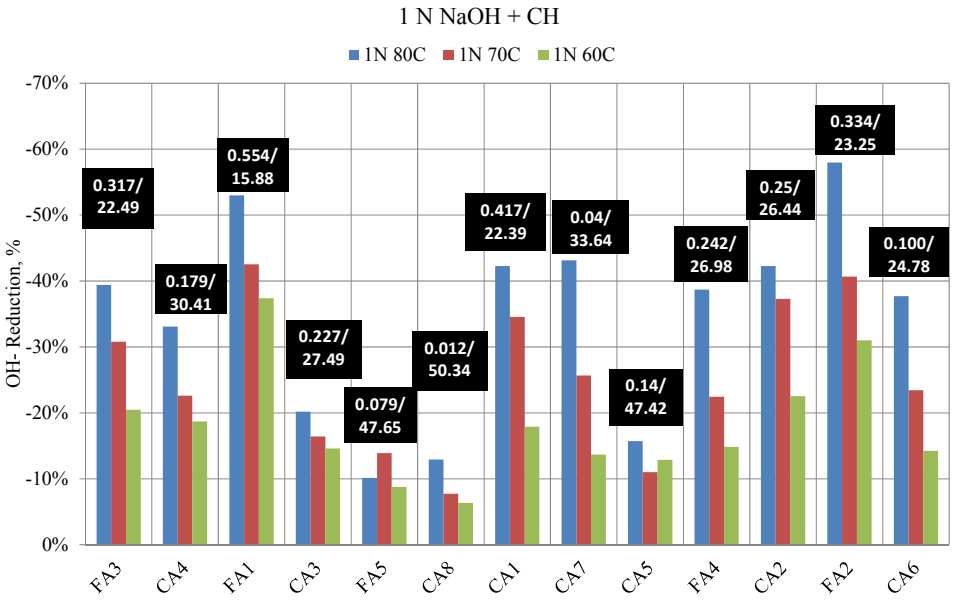

Figure 5.7. Percentage Reduction of OH^- at 1N NaOH + $Ca(OH)_2$. E_a and C1260 14D Expansion Values for Each Aggregate are Mentioned inside the Black Boxes.

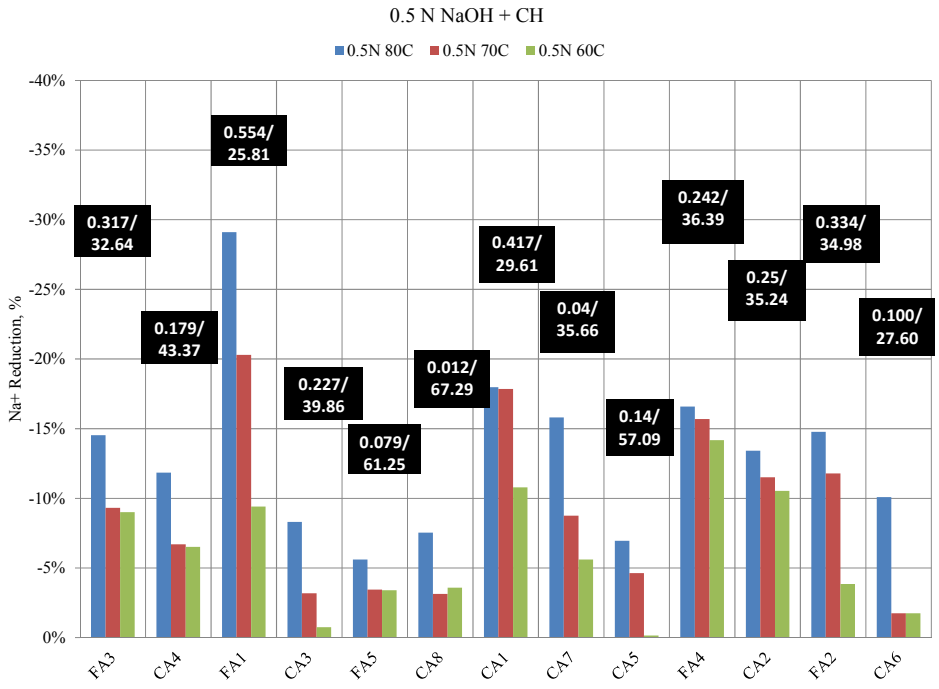

Figure 5.8. Percentage Reduction of Na^+ at 0.5N NaOH + $Ca(OH)_2$. E_a and C1260 14D Expansion Values for Each Aggregate are Mentioned inside the Black Boxes.

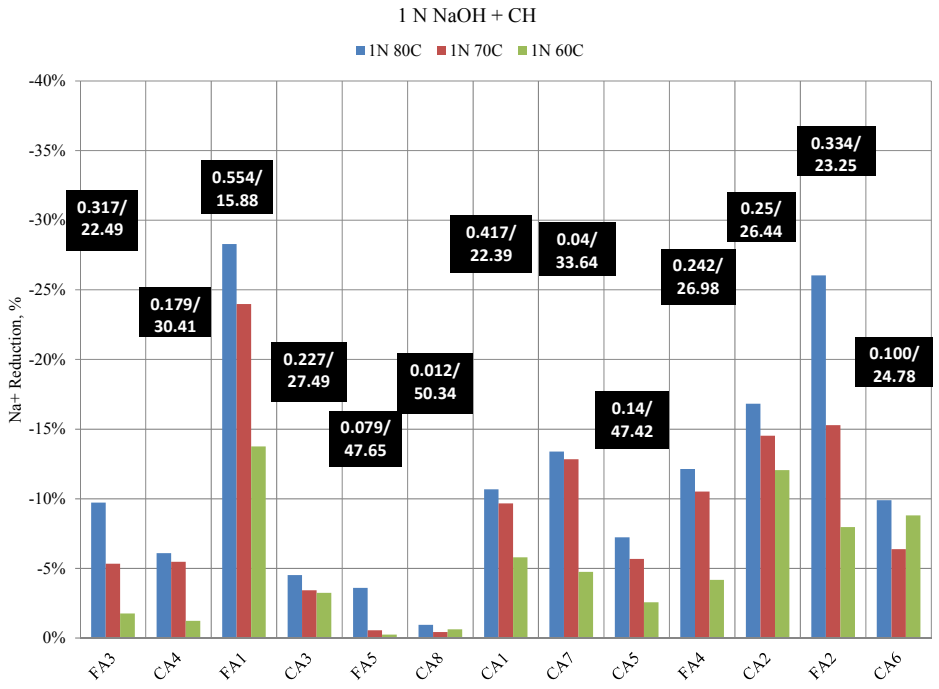

Figure 5.9. Percentage Reduction of Na^+ at 1N NaOH + $Ca(OH)_2$. E_a and C1260 14D Expansion Values for Each Aggregate are Mentioned inside the Black Boxes.

The samples of three different soak solutions from three different test runs (after each test run is terminated) were collected and analyzed to verify the repeatability of the soak solution chemistry determination. The COV was calculated using Na^+ and OH^- concentrations data from the three replicas corresponding to each test combination and the results are presented in Figures 5.10 and 5.11. The majority of COV is within 10 percent for the tested solution at all levels of alkalinity, which indicates that the procedure to collect solution sample and measure soak solution chemistry generate repeatable results.

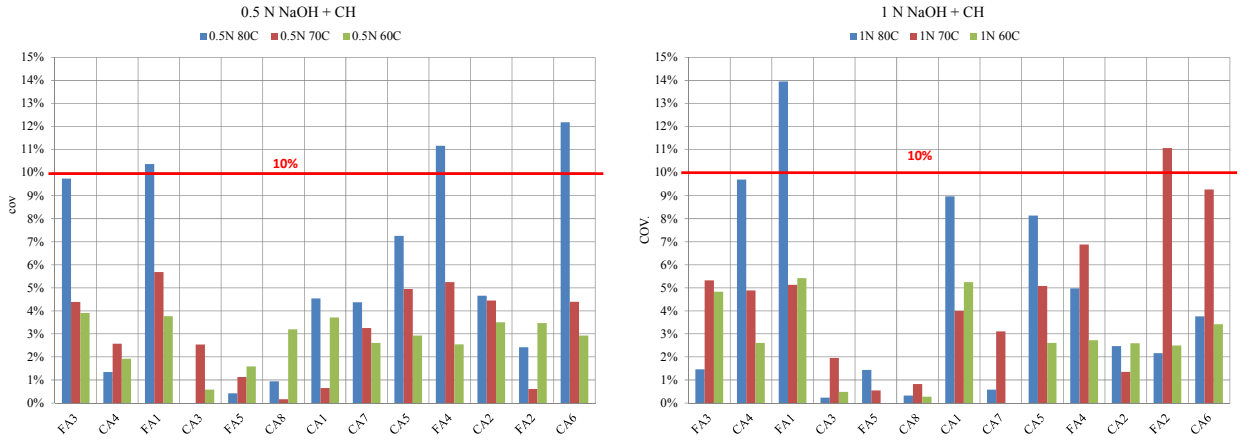

Figure 5.10. Coefficient of Variation (COV) Based on OH^- Concentrations at 0.5N and 1N NaOH + $Ca(OH)_2$.

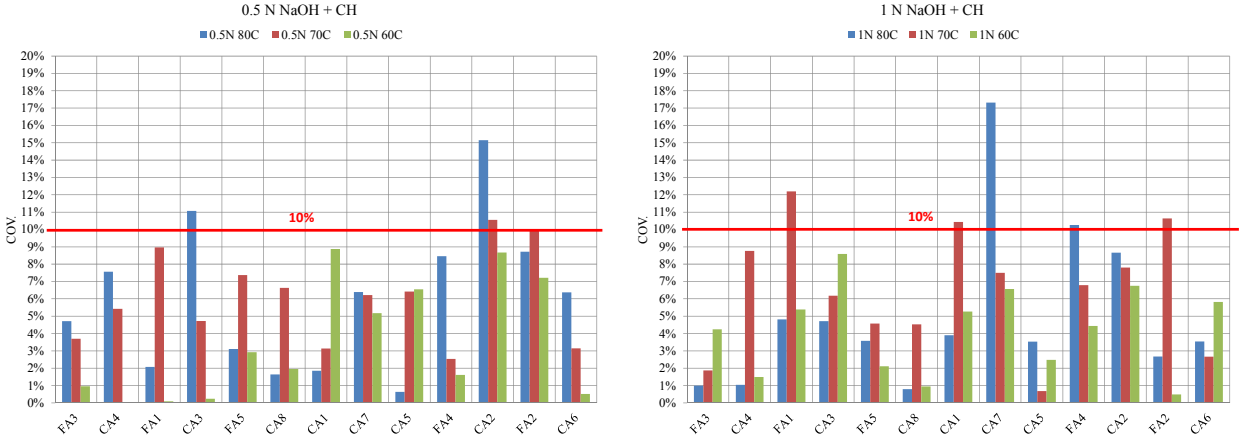

Figure 5.11. Coefficient of Variation (COV) of Na^+ Concentrations at 0.5N and 1N NaOH + $Ca(OH)_2$.

5.3 MICROSTRUCTURE OF REACTED AGGREGATES

Figure 5.12 shows the present of reaction product due to ASR on a borosilicate glass ball surface. The presence of mainly "Si" with some amount of "Na" was evident from SEM–EDS analysis. These observations suggest that ASR products (similar to ASR gel) formed on the aggregate surfaces due to ASR and the measurement of solution volume change in a form of

contraction in VCMD is due to the same ASR. The obvious presence of reaction products indicate occurrence of all the four steps of reaction mechanisms (i.e., Si-O-Si bond breaking, dissolution, and product formation through precipitation described in Chapter 2). It is expected that all the four steps will occur simultaneously at a much faster rate for a highly reactive aggregate and reaction products will be visible under SEM.

For highly reactive aggregates (e.g., FA1 and CA1) the presence of in-situ type reaction products were observed (Figures 5.13 and 5.14). For a slowly reactive aggregate, the presence of surface etching and cracking was observed with no obvious presence of gel within 4–5 days of the testing period. Note that Q_4 to Q_3 transformation (a swelling process, Garcia-Diaz et al. 2006, described in Chapter 2) can be responsible for aggregate volume expansion without forming any typical ASR gel. Therefore, it may be possible to measure some volume change due to ASR in VCMD with no obvious presence of ASR products in case of slowly reactive aggregates. From the above discussion, it is logical to claim that microstructural studies on the reacted aggregate particles by SEM-EDS support the activation energy-based reactivity prediction.

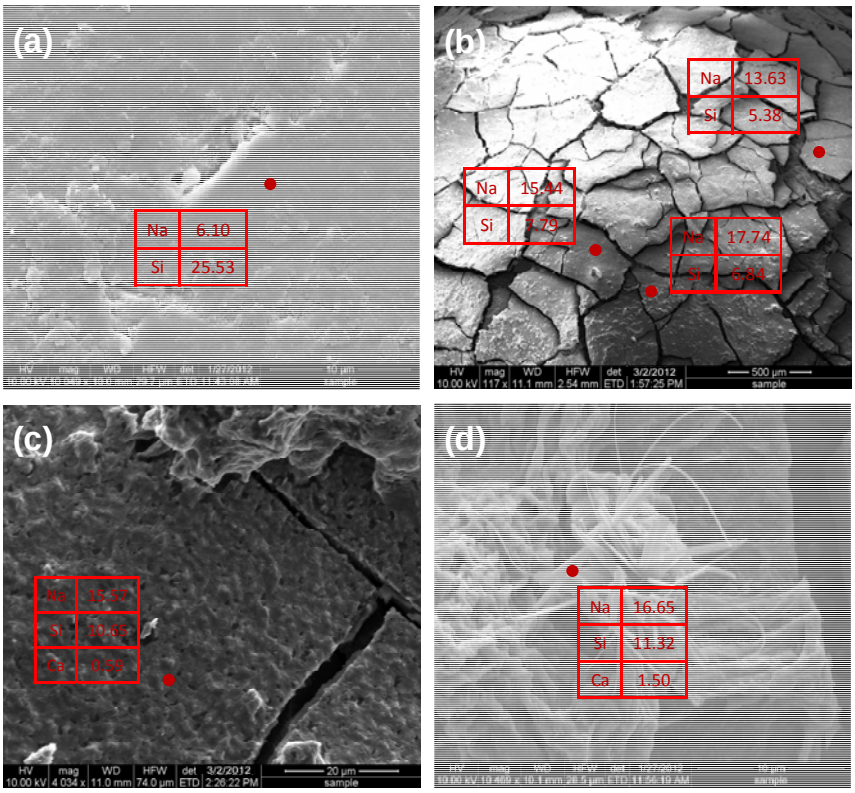

Figure 5.12. Secondary Electron Images of Reaction Products on a Borosilicate Glass Ball with Different Magnification: (a) Original, Na/Si:~0.25, (b)(c)(d) 1N NaOH + Ca(OH)2 at 96 hours, Na/Si: 1.46 to 2.59.

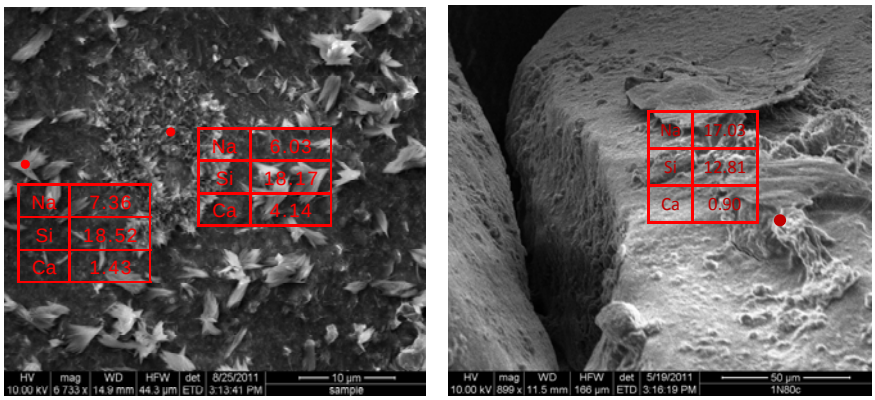

Figure 5.13. Secondary Electron Images of Reaction Products on Aggregate Particles at 1N NaOH + $Ca(OH)_2$ (80°C), FA1.

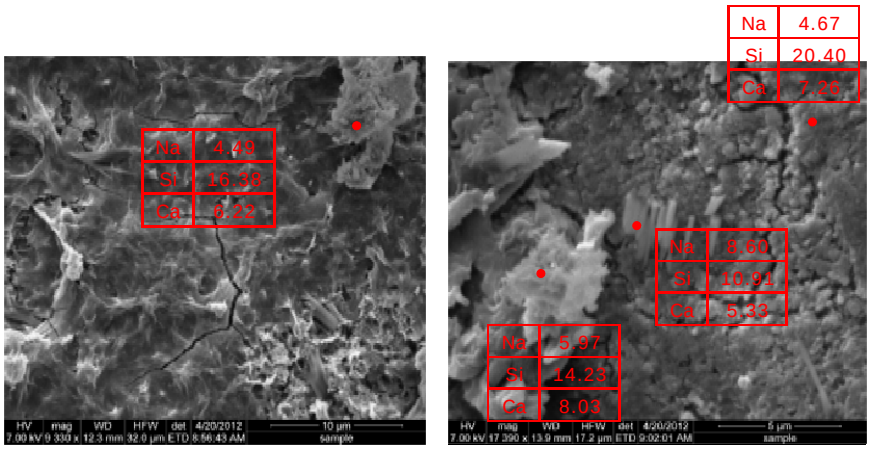

Figure 5.14. Secondary Electron Images of Reaction Products in Aggregate Particles at 1N NaOH + $Ca(OH)_2$ (80°C), CA1.

5.4 DETERMINATION OF THRESHOLD ALKALI LEVEL

An apparent relationship between compound activation energy (E_a) and alkalinity is evident from the results of the studied aggregates (Table 5.1). The higher the alkalinity, the lower the E_a. An attempt was made to establish a mathematical relationship between E_a and alkalinity. The following model (Equation 5.2) was used to establish a relationship between E_a and alkalinity:

$$E_a = E_{a_0} + \frac{C_1}{C^n} \qquad \text{(Equation 5.2)}$$

Where E_a is Activation energy (KJ/mol)
E_{ao} is Activation energy – theoretical threshold (KJ/mol)
C_1 is Activation energy curvature coefficient (KJ/(mol)$^{1-n}$
N is Activation energy curvature exponent

C is Alkalinity (mol)

The results are presented in Figures 5.15 to 5.17 for all the tested aggregates. The plots show that as alkalinity increases, the E_a decreases for all the aggregates. A good fit between the measured and predicted E_a values is manifested, and this demonstrates the applicability of the proposed model. The existence of a characteristic threshold alkalinity for each aggregate is manifested from the plots. A threshold value of alkalinity (TH_A) for each aggregate is mathematically calculated from the E_a vs. alkalinity plot and is summarized in Table 5.2. In general, the higher the reactivity, the lower the TH_A, except for Ca6 and CA7. The activation energy values for these two aggregates do not show a good relationship with alkalinity (a minor change in E_a for a large change in alkalinity), which caused the TH_A value moving towards lower side in Figure 5.17. The addition of one more data point at a relatively low alkalinity (e.g., 0.25N NH + CH) will possibly help to improve the TH_A determination for these two aggregates. Additionally, the effectiveness of calculating TH_A from E_a vs. alkalinity relationship needs further critical evaluation, which is continuing. The further work on

- Generating E_a at one more level of alkalinity (e.g., 0.25-0.3N NH + CH and/or 0.7N NH + CH).
- Further improvements in the TH_A calculation procedure are needed to increase the reliability of TH_A determination by this approach.

A reactive aggregate can practically behave as non-reactive or very slow reactive if concrete pore solution alkalinity can be maintained below the threshold level of alkalinity. The common approaches to achieve a low level of pore solution alkalinity are:

- Use of low alkali cement.
- Use of good quality fly ash with low alkali contents (lower than cement alkali contents).
- Use of ternary blends instead of fly ash alone.
- Ensuring minimum contribution of additional alkalis from external source(s).

Chapter 6 discusses these aspects in greater detail.

Table 5.2. Summary of Threshold Level of Alkalinity (TH_A).

Aggregate	TH_A (N)	E_a (1N)	E_a (0.5N)
CA1	0.37	22.392	29.610
FA1	0.27	15.882	25.811
CA7	0.17	33.641	35.655
CA4	0.52	30.409	43.365
FA3	0.47	22.485	32.640
CA3	0.5	27.486	39.864
CA2	0.59	26.437	35.244
FA4	0.46	26.980	36.391

CA5	0.49	47.415	57.091
CA6	0.20	24.783	27.602
FA2	0.46	23.254	34.979

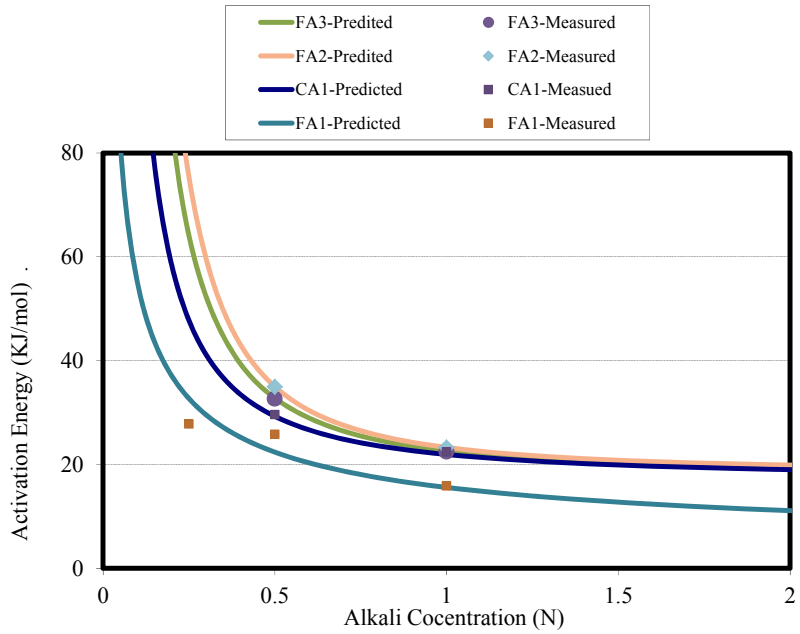

Figure 5.15. Alkalinity vs. E_a for the Highly Reactive Aggregates.

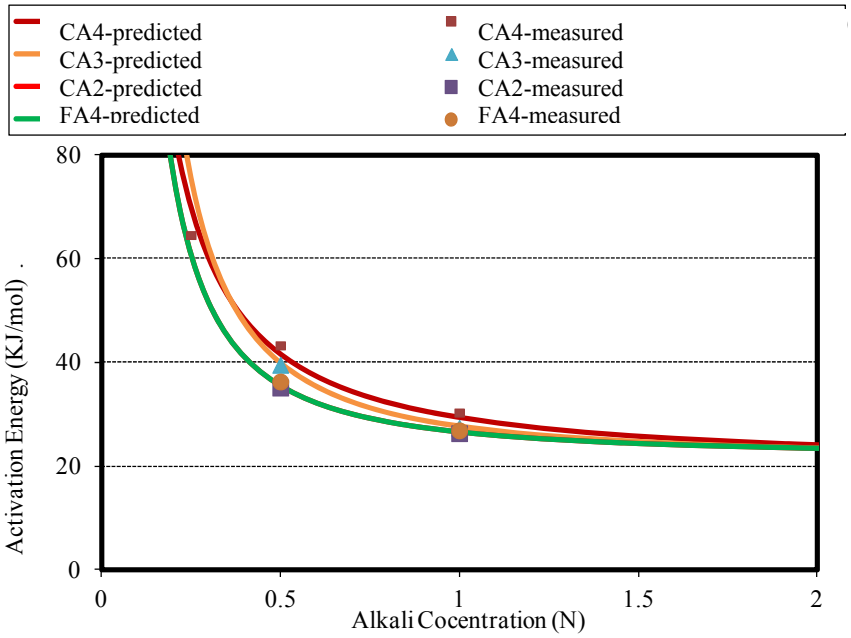

Figure 5.16. Alkalinity vs. E_a for the Aggregates with Medium Reactivity.

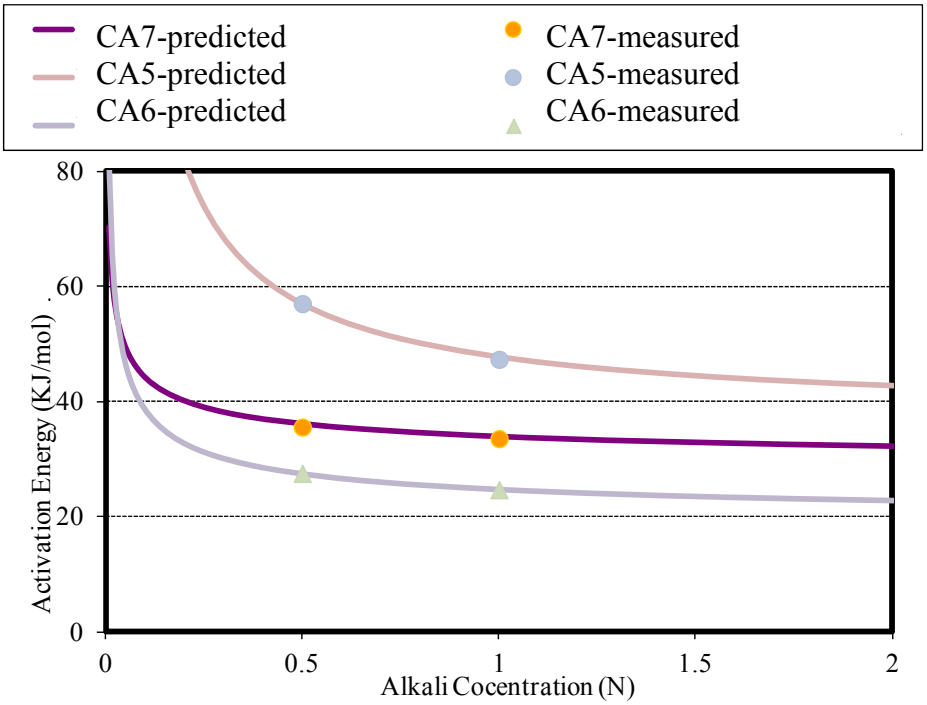

Figure 5.17. Alkalinity vs. E_a for the Aggregates Belonging to False Positive and Negative Categories.

5.5 DEVELOPMENT OF AN E_A-BASED ASR CLASSIFICATION SYSTEM

An activation energy-based aggregate classification system is developed based on the number of aggregates that are tested in this study and presented in Table 5.3. The ranges are arbitrary in nature at this time. To establish an effective ASR aggregate classification system, assignment of more refined activation energy ranges through testing greater number of aggregates is highly warranted. It is recommend to use the classification system based on activation energy at 0.5N NH + CH (close to concrete pore solution alkalinity, i.e., field levels of alkalinity) in all practical purposes.

Table 5.3. E_a-based Aggregate Classification System.

Activation Energy Range		Reactivity
1N NaOH + CH	0.5N NaOH + CH	
< 25	< 30	4 (highly reactive)
25–35	30–45	3 (reactive)
35–45	45–60	2 (potential/slow reactive)
> 45	> 60	1 (nonreactive)

The benefits of the activation-energy-based aggregate classification system are presented in Table 5.4. Case 1 and 2 are the examples where E_a and standard ASTM tests shows a very good match, which suggests that a VCMD-based method is a good choice as it takes less time

and produces data with higher repeatability than C 1260 test. Case 3 and 4 indicate the VCMD test method has the potential to overcome the limitations of the current test methods (especially ASTM C 1260) and has the ability to identify the aggregates that belong to false positive and negative categories (i.e., passed by ASTM C1260 but failed by ASTM C1293 and vice versa) reliably in a short period of time. AS previously described (Figure 5.4), aggregates CA6 and CA7 are passed by C 1260 but failed by C 1293 (false positives) but these aggregates are identified as reactive based on E_a values. Similarly, CA5 aggregate is failed by C 1260 but passed by C 1293 (false negatives) but this aggregate is identified as non-reactive or slowly reactive based on E_a. Therefore, Ea based reactivity prediction shows better correlation with C 1293 than C 1260 for these mismatch aggregates. In case 4, if C 1293 underestimates the reactivity (incidents of underestimation by C 1293 due to significant alkali leaching is reported) and that aggregate shows reaction in exposure blocks, the E_a-based classification system will identify that aggregate as a slowly/potentially reactive (2) and will not pass that aggregate. More number of aggregates belongs to false positive and negative categories need to be tested in order to establish the above benefits of the VCMD based procedure. Moreover, the VCMD test has the ability to test as-received aggregates (i.e., field aggregates) and determine reactivity matching with the field level of alkalinity (measuring E_a at 0.5N NH + CH).

Table 5.4. Comparison between E_a-Based Aggregate Classification System, Current Methods, and Field Performance.

Case #	ASTM C1260	ASTM C1293	Performance in Field or Exposure Blocks	E_a-Based Aggregate Reactivity (Table 5.3)
1	Passed	Passed	No ASR	1
2	Failed	Failed	Severe ASR	4
3	Passed	Failed	Considerable ASR	3, 4
4	Failed	Passed	No ASR or little ASR with no ASR distress	1, 2

5.6 SUMMARY

- The VCMD-based test can reliably predict aggregate alkali silica reactivity in a short period of time in terms of measuring activation energy. This test has the ability to test as-received aggregates (i.e., field aggregates) and determine activation energy (reactivity) matching with the field level of alkalinity [recommended to test aggregate with 0.5N NaOH + $Ca(OH)_2$ solution]. This reduces the gap between lab and field.
- The majority of COV based on rate constant is within 10 percent, which indicates the results are highly repeatable (Figure 5.5).
- The experiments with pure glass balls support solution volume contraction over time and used to validate the VCMD procedure.
- Measuring low E_a (high reactivity) of an aggregate using the VCMD is supported by higher consumption of Na^+ (Figures 5.8 and 5.9) and/or greater reduction of OH^- (Figures 5.6 and 5.7) in the test solution, which supports the VCMD test results.

- The formation of ASR product is observed by SEM-EDS on the reacted aggregate surfaces for the pure phase borosilicate glass and reactive aggregates (Figures 5.12 to 5.14). It is evident that microstructural studies on the reacted aggregate particles by SEM-EDS support the activation energy based reactivity prediction.
- The results in Figure 5.4 show that the aggregate that is failed by C 1260 but passed by C 1293 [i.e., CA5] has a relatively high E_a (slowly reactive or almost non-reactive). On the other hand, the aggregates that are passed by C 1260 (mortar bar method) but failed by C 1293 [i.e., CA6 and CA7] have a relatively low E_a (reactive). Therefore, The VCMD based test method has correctly identified the aggregates belong to false positives / negatives categories in a short period of time. This is the main benefit of the VCMD-based method. More aggregates that belong to the false positive and negatives categories need to be tested in order to establish the above benefit of the VCMD-based procedure.
- The ASR activation energy (E_a) will serve as a single chemical material parameter to represent alkali silica reactivity of aggregate. The E_a-based aggregate classification will serve as a potential screening parameter in aggregate quality control program.
- The VCMD-based test method can be used as an alternative to ASTM C 1260.

CHAPTER 6: DEVELOPMENT OF A PROCEDURE FOR MIX-DESIGN VERIFICATION

Determination of activation energy (E_a) and threshold alkalinity (TH_A) of the studied aggregates and development of an E_a-based aggregate classification system are presented in the previous chapter. This chapter presents a procedure for developing ASR resistant concrete mixes as well as verification of poorly performing mixes. The procedure involves:

- Formulation and adjustment of ASR resistant mix through a chemical method based on E_a and TH_A determined in the previous chapter and concrete pore-solution chemistry (will be presented in this chapter).
- Mix-design validation by using a rapid and reliable concrete test–a new concrete cylinder test using VCMD has been developed, which will also be presented in this chapter.

An attempt has been made to develop an effective way of tailoring mix design depending on the level of protection needed. This will ensure valuable resource conservation and avoid paying for premium ASR protection when only minor protection is needed.

6.1 PROCEDURES TO DESIGN AN ASR RESISTANT MIX

The procedures to design an ASR resistant concrete mix based on activation energy, threshold alkalinity, pore solution chemistry and concrete testing are presented in Table 6.1. The guidelines to select mix-design controls and special protection measures depending on E_a, TH_A ambient conditions are presented in Table 6.2. The different options and guidelines to develop ASR resistant mixes are briefly described below:

Option 1

Option 1 involves:

- Determination of E_a and TH_A from aggregate-solution test.
- Determination of pore solution alkalinity (PSA).
- Mix design adjustment based on TH_A–PSA relationship (i.e., PSA needs to be below TH_A in order to prevent / minimize ASR).
- Mix design validation through concrete testing. Each step is briefly described below:

1. Measuring E_a at multiple levels of alkalinity and determining TH_A (Chapter 5).
2. Development of an ASR-resistant mix by applying both mix design controls and special protection measures (as needed) depending on activation energy based reactivity prediction, TH_A and some consideration on the severity of ambient conditions (Table 6.2). Table 6.2 only shows two extreme combination of E_a, TH_A and ambient conditions as examples. Based on the two extreme combination

guidelines in Table 6.2, mix design controls and special protection measures (as needed) can be selected for all other possible case specific combinations.

3. Adjustment of the developed mix [step (ii)] based on pore solution alkalinity and TH_A.
   a. If the pore solution alkalinity (PSA) is lower than TH_A, the mix should perform well in the field without any ASR.
   b. If the PSA is higher than TH_A, the mix needs adjustment by both mix design controls (help to reduce the pore solution alkalinity) as well as special protection measures (help to make gel less expansive and/or increasing the space for gel accommodation) (Table 6.2).
   c. If the PSA is equal to TH_A, the mix may not need any further adjustment under mild ambient conditions. However, special protection measures may be needed under severe ambient conditions.
4. The adjusted mix [step 3] should perform well in the field without any ASR or with no measurable ASR distress. In order to verify the efficacy of the above chemical method to formulate ASR resistant mix, it is necessary to perform mix design validation through concrete testing. Validating the adjusted concrete mix [step 3] through a rapid and reliable concrete testing will be the ideal in order to recommend an ASR-resistant mix with high reliability. The ASTM C 1293 takes a year and doesn't serve the purpose if one can't wait that long. Efforts have been made by different researchers to develop a modified (accelerated) version of ASTM C 1293, which can be used provided the reliability of the modified version is established. Therefore, the demand of a rapid and reliable concrete test is still very high. The research team has developed a rapid concrete cylinder test which is presented in section 6.2 and used as a mix design validation method in this study along with modified C1293 data. Although testing period is not yet fully established, the proposed VCMD cylinder test takes around 1 month (21–35 days) to identify a reactive straight cement concrete mix with varying alkali loadings (i.e., 8.9–4.5 lbs/yard3). However, the time needed to test a slowly reactive straight cement mix with lower alkali loadings (e.g., 3.0–4.0 lbs/yard3) is relatively high and yet to be established. Validation by concrete testing is recommended till more concrete data are generated and a reasonably good correlation between the prediction based on pore solution–TH_A method and concrete performance testing is established. If a good positive correlation is established, the requirement of concrete validation testing will be minimized in future.
5. If the pore solution extraction method is not available, the dependency on concrete validation testing will be high in order to develop safe ASR-resistant mix with high reliability. As activation energy based reactivity prediction is reliable and dependable, an expert can design ASR resistant mix based on E_a-based reactivity, TH_A, knowledge gained based on concrete validation testing in step 4, and the

recommended guidelines on mitigation practices (Table 6.2) without pore solution data and concrete validation testing. This practice may be acceptable but some amount of risk will be involved.

As measuring activation energy is established as a reliable method to predict aggregate alkali silica reactivity, Option 1 is recommended for aggregates belonging to false positive and negative categories (i.e., critical aggregates) based on current ASTM C 1260 vs. C 1293 comparisons.

Option 2

Determination of E_a and TH_A based on the proposed VCMD concrete cylinder test without conducting aggregate –solution test is also possible. Measurement of expansion of concrete specimens at a minimum three levels of alkalinity (e.g., 4.5, 6.7, and 8.9 lb/yard^3) and three temperatures (e.g. 60°, 70°, and 80^{o}C) is needed in order to determine both E_a and TH_A. After determining E_a and TH_A, the same procedures for mix-design adjustment and validation as used for Option 1 (Table 6.1) can be applied. As generating concrete expansion data at multiple levels of temperatures and alkalinity involves in determining E_a and TH_A in this option, separate concrete mix-design validation testing may not be needed. If one feels more comfortable with the mix design development based on concrete testing alone, this is a good choice. Although, this approach provides reliable data but longer testing time may be a drawback.

Table 6.1. The Procedures to Design ASR Resistant Concrete Mixes.

	Test	Test Conditions	Duration	Measured Parameters	Adjustment/Validation Criteria
Development of ASR-Resistant Concrete Mix	VCMD Aggregate-Solution Test	Temperatures–60°, 70°, and 80°C. Soak solution alkalinity–1N, 0.5N, 0.25N.	15–20 days	Aggregate Reactivity based on E_a (Table 5.1). TH_A based on E_a @ multiple levels of alkalinity (Table 5.2).	If PSA < TH_A : mix should perform satisfactorily in the field with no symptoms of ASR. If PSA = TH_A : mix should perform well without any measurable ASR under mild ambient conditions (Table 6.2). If PSA > TH_A : stringent mix design controls as well as special protection measures are highly needed before concrete placement (Table 6.2).
	Pore Solution Extraction and Analysis by AAS–discussed in Section 6.2		10 days	Pore solution alkalinity (PSA) based on both Na^+ and K^+	
Mix-Design Validation	VCMD Concrete Cylinder Test (Section 6.2)	Temperature–60°C With or without alkali boosting	1–2 months	-Linear expansion % -Rate of expansion -Ultimate expansion	If the measured expansion at the recommended testing period is below the assigned limit: mix will perform satisfactorily in the field without any ASR. If the measured expansion is above the assigned limit: mix needs further adjustment.

Option 3

For the aggregates where the reactivity prediction based on the current test methods is satisfactory, activation energy measurement through aggregate-solution test may not be needed. In that situation, mix design verification / validation through direct VCMD concrete testing (Table 6.1) is recommended. The mix design based on the current test methods and mitigation practices can be tested with or without added alkalis and verify if the expansion stays below the assigned limits at the specified testing period. Addition of alkali (NaOH pellets) in the mix can accelerate the reaction but applicability / reliability needs to be verified (explained in details in Section 6.2). If the expansion is above the assigned limit, the mix needs further adjustment before placement.

Table 6.2. Guidelines through Examples for Development of ASR-Resistant Mixes.

E_a–Based Aggregate Reactivity (Table 5.1)	TH_A	Severity of Ambient Conditions	Mix-Design Controls	Special Protection Measures (SPM)
High	Low (i.e., low alkali tolerance)	High Example: High rainfall (high RH) ± high T ± seawater-contaminated aggregates ± use of deicers	• Low alkali cement • Relatively low cement factor (CF). • Higher amount (25–35%) of good quality fly-ash (soluble alkalis should be below the cement alkali) replacement. • Low w/c– o Create low permeability which reduces the ingress of external alkalis and moisture. o Less free water available for gel swelling. o Increase of PSA due to low w/c should be counteracted by high amount of good quality fly ash or ternary blends (SPM).	• Use of ternary / quaternary blends instead of fly ash alone (e.g., fly ash (FA) + GGBS, FA + silica fume (SF), FA + metakaolin, FA+SF+GGBS etc.). • Use of 100% or higher dosage of $LiNO_3$. • Use of porous light weight aggregate (LWA) and/or aggregate blend.
High	Low	Low Example: Low rainfall (low RH) ± low temperature ± no source of external alkalis	Low alkali cement, relatively low cement factor, higher amount (25–35%) of good quality fly-ash replacement	Use of: • LWA and/or aggregate blend. or • Use of lower dosage of $LiNO_3$ depending on TH_A
Low	High (i.e., high alkali tolerance)	High	• Cement with low–intermediate alkali content can be allowed as high alkali tolerance is indicated by TH_A. • Medium quality fly ash (e.g. alkali content ≤ cement soluble alkali, fly ashes with relatively high CaO contents) can be used • Conventional CF and FA replacement.	Use of: • Low w/c concrete (low permeability). • Ternary blends depending on the severity of ambient conditions
Low	High	Low	Same as above	No need

6.2 DEVELOPMENT OF A NEW ACCELERATED CONCRETE CYLINDER TEST

The Concrete Prism Test (CPT, ASTM C 1293) has been considered as the best index for field performance, but the test duration is a major drawback. Ranc and Debray (1992) first introduced the Accelerated Concrete Prism Test (ACPT) in the early 1990s. The concrete prisms were stored over water at 60°C instead of 38°C. The results show a good correlation between the 38°C and 60°C tests after 56 days of testing period. Other researchers (Grosbois 2000 and Touma et al. 2001) also show a reasonably good correlation between one year concrete prism expansions at 38°C and two to four months prism expansion at 60°C. Although the test duration is shortened by simply increasing the test temperature, a significant reduction in expansion associated with high alkali leaching was noticed in the ACPT compared to the CPT (Folliard et al. 2004 and Ideker et al. 2006). When alkali leaches out of the specimens, the sulfate ions replace the leached alkali hydroxides and decrease the pH of pore solution. This eventually causes the reduction of expansion.

A new, rapid VCMD-based concrete cylinder test [accelerated concrete cylinder test (ACCT)] has been developed in this study to overcome some of the above limitations and come up with a reliable ASR concrete test method. The unique steps that are taken for the proposed test to be considered as a rapid and reliable concrete ASR test method are:

- Introduction of an automatic LVDT based length change measurement system with no involvement of human error.
- Measurements to avoid alkali leaching.
- Testing at relatively high temperature (60°C)–reducing testing time due to faster reaction.
- Testing at varying levels of alkali loadings (alkali-boosted concrete to reduce testing period as well as alkali levels similar to job mix).

The different steps that were involved to develop the new ACCT method are presented below:

6.2.1 Test Equipment

The device used in this study to measure length change of cylindrical concrete specimen over time is the same VCMD that is described in Section 4.1. Figure 6.1 shows the VCMD test setup for ACCT. A 3 × 6 inch concrete cylinder with cast-in place threaded rod is placed inside the container (pot). The specimen is then immersed with soak solution of specific alkalinity (equal to or lower than pore solution alkalinity of the specimen). The LVDT rod is connected to the threaded rod attached to the specimen, which moves inside the LVDT during ASR expansion of the specimen and creates electrical signals. These signals are converted to LVDT displacements (inch) through the data acquisition system and recorded by the attached computer through the LabVIEW program. The detailed test procedure is described later.

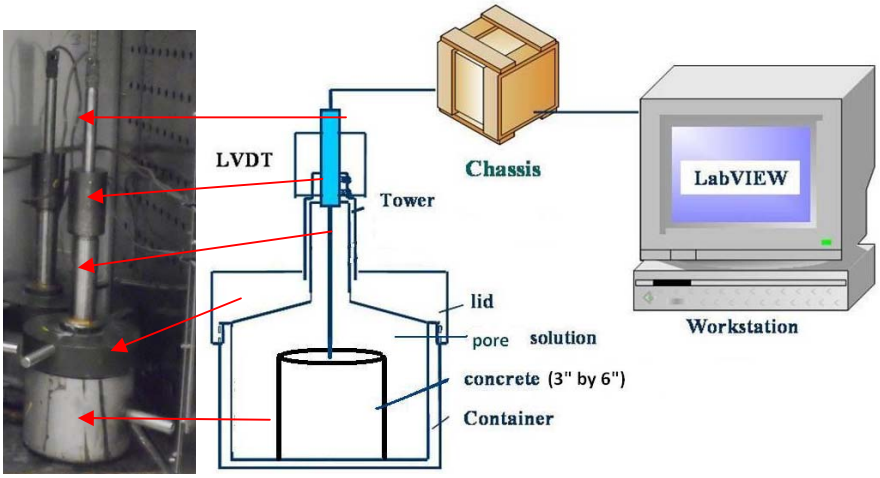

Figure 6.1. VCMD Test Setup for ACCT.

6.2.2 Design of Experiment

The selected factors and their levels are presented in Table 6.3. To establish a comparative assessment, the levels for alkali loadings, cement types and some of the aggregates were selected based on the levels that are used in TxDOT's in-house project. Aggregates are selected to cover a wide range of reactivity (NR to HR). Table 6.4 summarizes the E_a-based reactivity data along with available reactivity data that the ASTM C 1260, ASTM C 1293, modified ASTM C1293, and exposure block for these aggregates had determined. The four levels of alkali loadings (i.e., 3.0, 4.5, 6.7, and 8.9 lb/yard^3) are selected. A low-alkali (CM1 Na_2O_{eq}=0.57 percent) and a high-alkali (CM2 Na_2O_{eq}=0.82 percent) portland cement were chosen in order to reach the desired alkali levels over the range from 3 lb/yard^3 (no additional alkalis) to 8.9 lbs / yard^3 (with the addition of NaOH pellets in the mix) with varying levels of cement factor ± alkali additions. Table 6.5 presents the chemical analyses for the two cements used in this study.

Table 6.3. Factors and Levels in the Design of Experiments.

	Level 1	Level 2	Level 3	Level 4
Alkali Level (lb/yard^3)	3	4.0/4.5	6.7 (0.95 Na_2O_e)	8.9 (1.25 Na_2O_e)
Coarse Aggregate	NR (CA8)	HR (CA1)		
Fine Aggregate	NR (FA5)	MR (FA3)	MR (FA4)	HR (FA6)
Cement Type	CM1	CM2		

Table 6.4. Relevant Reactivity Data of the Tested Aggregates by Different Test Methods.

Aggregate	ASTM C1260 14D Exp., %	E_a based reactivity (Table 5.1)	ASTM C1293 1YR Exp., %	Modified ASTM C1293 1YR Exp., %	Block, % 0.95/1.25 Na_2O_e
Glass	-	HR (4)	-	-	-/-
CA8	0.012	NR (1)	0.01	0.027	0.0026/-
CA1	0.417	HR (4)	0.11	0.078	−/0.2609
FA3	0.317	R (3)	-	0.058	-/
FA6	0.474	HR (4)	-	0.391	-/-
FA5	0.079	NR (1)	0.01	0.035	0.0026/-
FA4	0.242	R (3)	-	0.043	-/-

Table 6.5. Chemical Analysis of the Cements Used.

Composition, Wt%	Na_2O	K_2O	SiO_2	Al_2O_3	Fe_2O_3	CaO	MgO	SO_3	Na_2O_{eq}
Cement 1 (CM1)	0.07	0.76	20.7	5.3	2.9	64.4	0.9	2.9	0.57
Cement 2 (CM2)	0.12	1.06	19.29	5.47	2.71	65.14	1.1	3.13	0.82

6.2.3 Mix Design and Specimen Preparation

All the ACCT mixes are ASTM C1293 type mix with or without alkali boosting. Table 6.6 presents a detailed description of the mix designs. Most of these mixes were tested or are being tested at TxDOT using their modified C1293 method. This procedure will allow researchers to establish a comparative assessment between ACCT and modified C 1293 data.

Table 6.6. Concrete Mix Design for Conducting ACCT.

	Alkali, lb/yard^3	Coarse Aggregate	Fine Aggregate	w/c	CAF	Cement	CF	Additional Alkali (NaOH), lb/yard^3
Mix 1a	4.0	CA8	FA4	0.45	0.76	CM1	7.52	-
Mix 1b	6.7							2.7
Mix 1c	8.9							4.9
Mix 2a	4.0	CA1	FA5			CM1	7.52	-
Mix 2b	4.5					CM2	5.83	-
Mix 2c	6.7					CM1	7.52	2.7
Mix 2d	8.9					CM1	7.52	4.9
Mix 3a	3.0	CA8	FA3			CM1	5.60	-
Mix 3b	4.5					CM2	5.83	-
Mix 3c	6.7					CM2	7.52	0.9
Mix 3d	8.9					CM2	7.52	3.1
Mix 4a	3.0	CA8	FA6			CM1	5.60	-
Mix 4b	4.5					CM2	5.83	-
Mix 4c	6.7					CM2	7.52	0.9
Mix 4d	8.9					CM2	7.52	3.1
Mix 5	4.5	CA1	FA6			CM2	5.83	-
Mix 6	4.5	CA8	FA5			CM2	5.83	-

According to the mix design in Table 6.6, the concretes were mixed by hand following ASTM C192 procedures. The cement and fine aggregates were thoroughly dry blended in a clean stainless steel bowl. The coarse aggregates were then added into the bowl and dry mixing continued until a homogeneous mix of cement, coarse aggregate, and a fine aggregate is achieved. Deionised water was then added and mixing continues for an additional 5 minutes until a homogeneous concrete mix is achieved. Concrete cylinders using each mix (see Table 6.6) were cast for ACCT.

6.2.4 Test Procedure

The new ACCT procedure is briefly described below:

- An 11-inch stainless steel treated rod was embedded on top of each concrete cylinder (measuring 3×6 inches) during specimen casting. After casting, the molds were covered with plastic foil and kept inside a 100 percent RH chamber for seven days at 23°C.
- After seven days, the concrete cylinders were demolded and placed inside the VCMDs (shown in Figure 6.2), which were filled up by soak solution with chemistry that is equal to the pore solution chemistry of each mix (each mix has a specific level of alkalis according to Table 6.6). Pore solution chemistry of each mix in Table 6.6 was determined by squeezing out the pore solution from cement paste specimen (2 × 4 inches) of that mix and analyzing the extracted solution by AAS (presented in detail in Section 6.2.4.1). The

purpose of creating soak solution chemistry = pore solution chemistry is to prevent alkali leaching from the specimen.

- Each VCMD was tightly closed and placed inside an oven at 60°C.
- Expansion measurements were recorded every 15 minutes automatically through data acquisition-computer system over time (49 days).

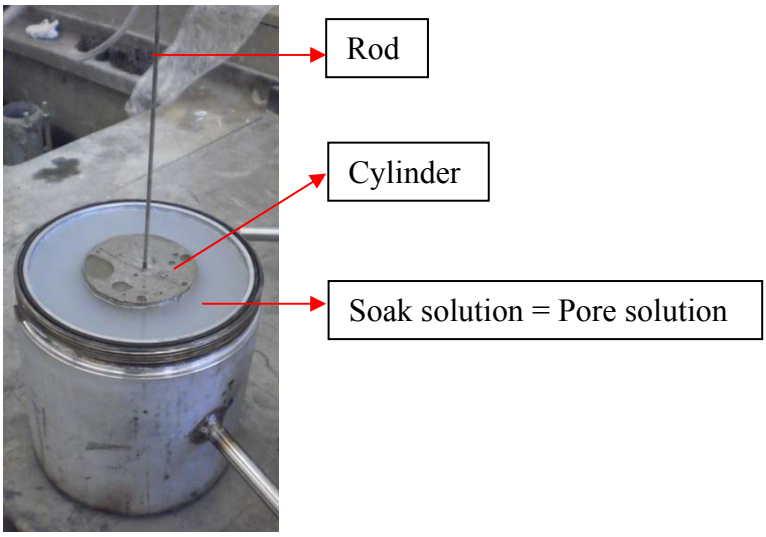

Figure 6.2. Concrete Cylinder in the VCMD.

Initially the concrete specimen expands due to temperature increase from the starting temperature to the target temperature (60°C). The subsequent LVDT readings after temperature stabilization represent displacement due to ASR. Concrete cylinder length changes (initially due to thermal expansion for ~ 4 hours followed by ASR expansion) will make the stainless steel LVDT rod to move up inside the LVDT and electrical signals are generated (Figure 6.1). Therefore, the physical phenomenon (i.e., movement of the rod) is converted into a measurable electrical signal. All LVDTs signals are amplified through the use of signal conditioners and then transferred though a USB cable to a workstation where a program in LabVIEW was developed to display, analyze, and store the generated data (see Figure 6.1). LVDT reading at the stable target temperature represents the reference (initial) LVDT reading for calculating displacement due to ASR. All the LVDT readings after temperature stabilization minus the reference LVDT reading represent displacement due to ASR over time. The displacement due to ASR over time divided by the original length at the reference point multiplied by 100 represents the percent expansion of the concrete cylinder due to ASR over time.

6.2.4.1 Pore Solution Extraction and Analysis

The cement paste cylinders (2 × 4 inches) corresponding to each mix in Table 6.6 were cast and covered with plastic foil, and then stored under 100 percent relative humidity (RH) and at 23°C for seven days. After the seven-day curing, the specimens were de-molded and pore solutions were extracted from each paste specimen. The pore solution extraction from cement

paste specimens was conducted by using a high-pressure squeezing method (Barneyback and Sidney 1981). The extraction method consists of pressing a cement paste cylinder with a loading of 400 lb to extract the liquid contained in the specimen. Figure 6.3 shows the pore-solution extraction apparatus, which consists of a removable base equipped with a drain, a hollow cylinder, and a piston that can be inserted into the cylinder. The specimen is placed within the cylinder, and the piston applies pressure, which gradually increases by means of a hydraulic loading to a maximum of 400 lb. The loading was applied and released twice for all specimens in order to get a sufficient quantity of the pore fluid using a hypodermic syringe inserted through the fluid drain located at the base of the apparatus.

Researchers used an Atomic Absorption Spectrometer (AAS) to analyze the extracted pore solution for Na^+ and K^+ ion concentration. Table 6.7 presents the composition (Na^+ and K^+) of pore solution extracted from the studied cement pastes. A minimum of three cement paste specimens for each mix in Table 6.6 was squeezed to extract pore solution followed by mixing the extracted solutions to get a representative pore solution. This practice also ensures getting enough quantity of solution for chemical analysis. The Na equivalent (Na^+_e) as $Na^+ + 0.59\ K^+$ (French 1980) also represents the total alkali to compare with the TH_A values from E_a. Note that the same alkali loading (6.7 lbs/yard^3) using two different types of cement with varying $Na_2O_{eq.}$ percentages and different amounts of extra alkali addition does not ensure the same pore solution alkalinity (PSA). For example, the PSA with 6.7 (CEM 1) is 0.46 but the PSA with 6.7 (CEM 2) is 0.74. Therefore, cement composition (especially the type of alkali-bearing phases in cement) plays an important role in controlling the PSA and the same alkali loading using different cements do not necessarily provide the same PSA.

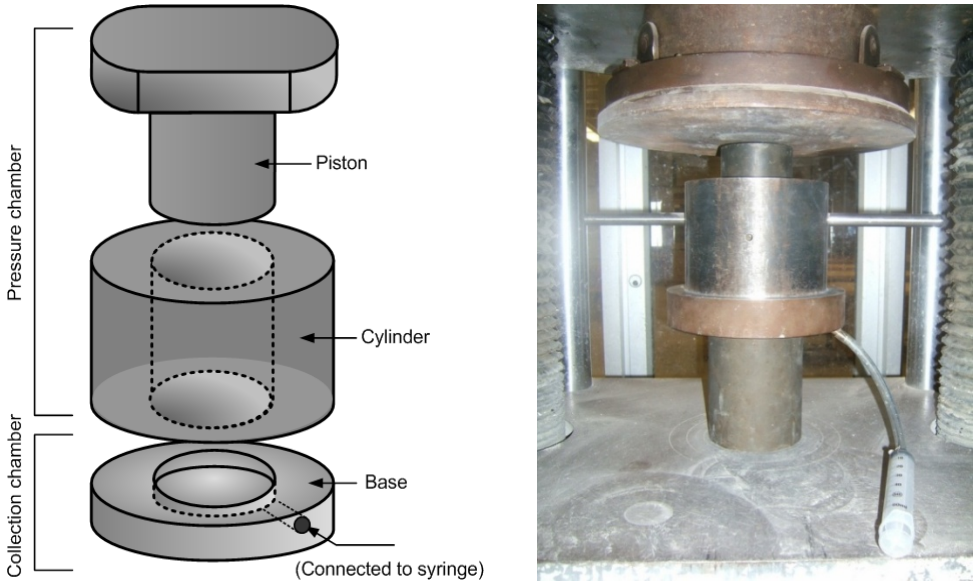

Figure 6.3. Pore-Solution Extraction Apparatus.

Table 6.7. Concentration of the Extracted Pore Solution.

Alkaline level, lb/yard^3	Covers mixes in Table 6.6	Na^+, ppm	K^+, ppm	Na^+, N	K^+, N	Na^+_e, N(PSA)
3.0 (CM1)	3a, 4a	1539	21031	0.07	0.54	0.38
4.0 (CM1)	1a, 2a	1800	19000	0.08	0.49	0.37
6.7 (CM1)	1b, 2c	4898	16100	0.21	0.41	0.46
8.9 (CM1)	1c, 2d	14132	17300	0.61	0.44	0.88
4.5 (CM2)	2b, 3b, 4b, 5, 6	4153	31562	0.18	0.81	0.66
6.7 (CM2)	3c, 4c	6867	28990	0.30	0.74	0.74
8.9 (CM2)	3d, 4d	12755	31865	0.55	0.81	1.04

The water-soluble alkali method is an alternative method to determine pore solution chemistry. This method was primarily developed to determine the soluble alkalis in concrete from existing structure, and can also be applied for fresh concrete. In this method, the cement paste sample is ground to pass a 75 μm sieve. A representative three 10g of the < 75 μm samples are immersed in deionized water at room temperature and left to soak for 24 ± 4 hours. The samples are then filtered, and the solution is made up to 250 ml by adding deionized water as necessary. Using the AAS, the researchers determine the Na and K content and adjust this for the dilution. Table 6.8 presents the composition (Na^+ and K^+) of pore solution that the water-soluble alkali method had determined for the selected paste specimens.

Table 6.8. Concentration of Pore Solution from Water-Soluble Method.

Alkaline level, lb/yard^3	Na^+, ppm	K^+, ppm
3.0 (CM1)	23.4	251.4
4.5 (CM2)	55.4	565.6
6.7 (CM2)	117.8	528.1
8.9 (CM2)	233.8	521.2

Tables 6.7 and 6.8 indicate that the water-soluble method measures significantly lower concentrations of Na^+ and K^+ than those measured with the pore solution extraction method. Pore solution chemistry data in the published literature (Lorenzo et al. 1996; Brouwers and Eijk 2003; Berube et al. 2004; Lothenbach and Winnefeld 2006) are very similar to the alkali concentrations in Table 6.7 that the pore-solution extraction method has determined in this study. Therefore, these pore solution concentrations were used to generate the soak solutions for the concrete cylinder test that correspond to each mix in Table 6.6. The quantities of NaOH and KOH pellets needed to generate an artificial solution of the same composition for each mix in Table 6.7 were first calculated and then dissolved in deionised water to prepare the soak solutions.

6.2.5 Mix-Design Verification

Based on Table 6.1, if the pore solution alkalinity (Table 6.7) is higher than the TH_A determined from aggregate-solution (determined in Chapter 5, Table 5.2), the aggregate will react (degree depends on aggregate reactivity and pore solution alkalinity). On the other hand, if the pore solution alkalinity (PSA) is lower than the TH_A, the aggregate will not react or react very slowly. Table 6.9 compares the PSAs of the selective mixes and TH_A of the reactive aggregates in those mixes. For example, the TH_A of the reactive fine aggregate (FA3) in Mix 3 is 0.47N and the pore solution alkalinities for 3a, 3b, 3c, and 3d mixes are 0.38, 0.66, 0.74, and 1.04N respectively (Table 6.9). Only the concrete cylinder with alkaline level 3.0 lb/yard^3 (0.38N) is lower than the TH_A (0.47 N). Therefore, it can be expected that the reactive fine aggregate (FA3) in mix 3a will not show any ASR, but the same aggregate in mixes 3b, 3c, and 3d where PSA > TH_A will react and give ASR expansion in cylinder test. The higher the PSA the higher the expansion will be. For Mixes 1 and 2, the corresponding reactive aggregates can also be expected to react when the PSA is higher than TH_A and gives expansion as a function of alkalinity. The concrete validation testing (next section) using these mixes will verify the expected expansion behavior based on PSA-TH_A relationship (Table 6.9).

Table 6.9. TH_A of the Reactive Aggregates and Pore Solution Alkalinity (PSA) Comparison.

Alkaline level, lb/yard^3	Covers mixes (Table 6.6)	TH_A, N	(PSA), N	Expected Concrete Cylinder Expansion Behavior
3.0 (CM1)	3a	0.47	0.38	No expansion
4.0 (CM1)	1a	0.46	0.37	No expansion
	2a	0.37	0.37	May (L) or may not expand
4.5 (CM2)	2b	0.37	0.66	Will expand (M)
	3b	0.47	0.66	Will expand (L-M)
6.7 (CM1)	1b	0.46	0.46	May or may not expand
	2c	0.37	0.46	Will expand (L-M)
6.7 (CM2)	3c	0.47	0.74	Will expand (M)
8.9 (CM1)	1c	0.46	0.88	Will expand (H)
	2d	0.37	0.88	Will expand (H)
8.9 (CM2)	3d	0.47	1.04	Will expand (VH)

6.2.6 Mix-Design Validation by VCMD Concrete Cylinder Test

This section presents the concrete validation testing results for the selected mixes from Table 6.6. Mortar cylinders made of highly reactive pure glass balls were tested first to validate the proposed concrete cylinder test before testing actual concrete mixes.

6.2.6.1 Mortar Bar and Cylinder Test with Borosilicate Glass Balls

Using the proposed method, researchers tested the mortar cylinders (3 × 6 inches) made of highly reactive borosilicate glass balls (0.25″size used in the aggregate-solution test in Chapter 5)

to verify its applicability to measure ASR expansion. The team also cast mortar bars (measuring 1″ × 1″ × 11.25″) using the same mortar mix, and conducted an expansion measurement using the conventional length comparator in order to have a comparative assessment between the proposed cylinder method and the conventional mortar bar method (e.g., C 1260). The mortar mix used alkali level 8.9 lb/yard^3 (equivalent to $Na_2O_{eq.}$ = 1.25 percent) with 40 percent glass. The curing conditions (i.e., 1 day fog-room curing before de-molding) and testing conditions (i.e., 80°C, immersing in 1N NaOH solution) were the same for both mortar bar and cylinder tests. Although the proportion of cement: glass ball is not similar to a conventional cement-sand mortar, the other conditions (i.e., 1N NaOH, 80°C) are the same as ASTM C 1260. Figure 6.4 shows the expansion of glass-mortar bars and cylinders at 80°C over time. Figure 6.5 shows the macro-crack pattern of the cylinder and nature of micro-crack under microscope.

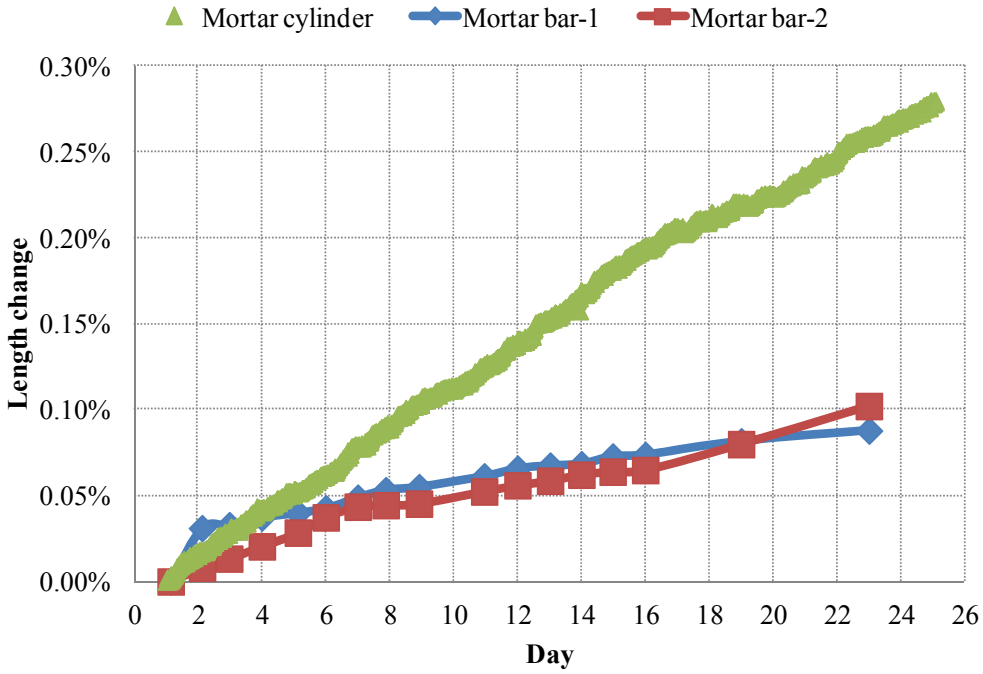

Figure 6.4. The Expansion of Glass-Mortar Bars and Cylinder.

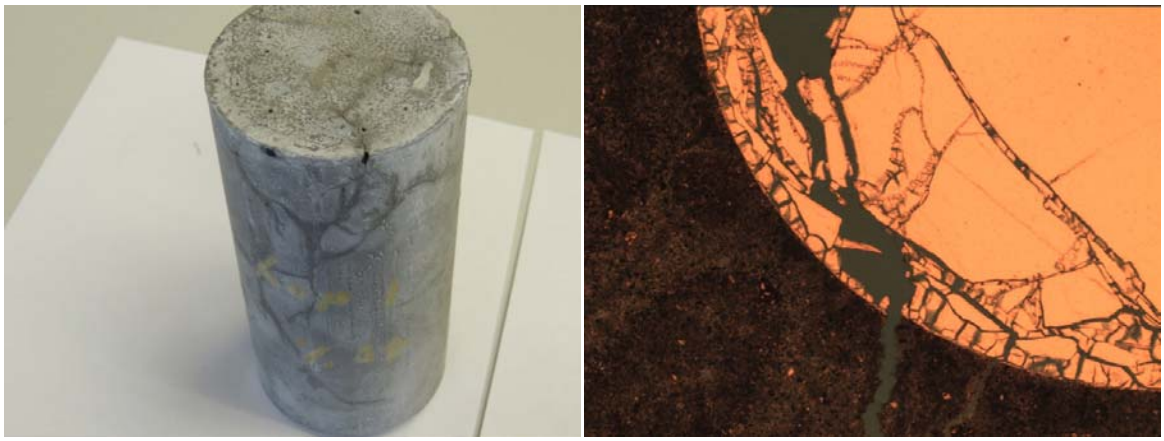

(a) (b)

Figure 6.5. (a) Crack Patterns in the Tested Cylinder, (b) Nature of Microcracks and Presence of ASR Gel in a Reacted Glass Ball, Mortar Thin Section, under Microscope.

Here are some observations regarding Figures 6.4 and 6.5:

- The measurement of the mortar bar expansion using a length comparator shows lower expansion than the expansion that the VCMD mortar cylinder test had measured (Figure 6.4). Although finding an exact cause(s) for this difference in expansion was not a main focus of this study, it is anticipated that a combined effect of difference in specimen dimension and mode of data collection possibly created this kind of difference in expansion measurements. The main purpose of the study involving mortar made of glass balls (pure phase) was to investigate whether the new concrete cylinder test is rapid and reliable. There is an indication that VCMD cylinder test has an advantage of measuring high expansion in a short period of time (i.e., rapid in nature).
- Note that the VCMD cylinder test collected data automatically through the LVDT data acquisition system, whereas the length comparator was used to collect data manually for the mortar bar. The test temperature and measuring temperature in a conventional mortar bar method are not the same, and this may cause some error in expansion measurements. As the data collection in VCMD cylinder test is automatic through the LVDT (no human error) under constant temperature (no error due to temperature difference), the reliability of the VCMD cylinder test should be high.
- The following confirm the presence of a high degree of ASR:

    - Presence of macrocracks in the cylinder (Figure 6.5a).
    - Presence of microcracks in a reacted glass ball (Figure 6.5b).
    - Microcrack passing through both the reacted glass ball and paste (Figure 6.5b).
    - Presence of ASR gel at the periphery of the reacted glass ball (Figure 6.5b).

    This above ASR features (both macro and micro-scale) supports the high expansion measurement (Figure 6.4) in the cylinder test. Therefore, the proposed VCMD-based

cylinder test is capable of measuring ASR expansion in a short period of time. Based on the discussion points in the above item (second bullet, about the VCMD cylinder test), it is expected that the reliability of the cylinder test should also be high. The reliability and repeatability aspects of the concrete cylinder test are discussed further with greater details based on the actual concrete testing results (discussed below).

6.2.6.2 Accelerated Concrete Cylinder Test (ACCT)

A finally adjusted mix based on the analogy in Sections 6.1 and 6.2.5 will most probably not initiate any ASR in the field or cause little ASR without any measurable distress during the expected service life. However, it is recommended to validate the performance of the adjusted mix by conducting the ACCT in the laboratory. More concrete data will verify the applicability of the different options (i.e., Options 1, 2, 3 in section 6.1) with high reliability. Some selective concrete mixes (mixes 1 to 4) have been tested using the ACCT and compared with the modified ASTM C1293 for validation purposes.

The selected mixes in Table 6.6 were tested using ACCT at 60°C and varying levels of alkalinity. For each test corresponding to each mix (Table 6.6), the soak chemistry was equal to pore solution chemistry (Table 6.7). Figures 6.6 to 6.9 show the expansion curves over time at varying levels of alkalinity for different mixes. For all mixes, the higher the alkali loading, the higher the level of expansion is. A comparative assessment between expected expansion behaviors based on PSA-TH_A relationship (Table 6.9) and actual concrete cylinder expansion measurements (Figures 6.6–6.9) leads to the following observations

- For the main mix 1, no expansion was expected for sub-mix 1a [PSA (0.40N) < TH_A (0.46)] but all other sub-mixes were expected to expand (i.e., 1b may or may not and 1c high expansion). Figure 6.6 shows that the measured concrete expansion is in agreement with the predicted expansion behavior. However, sub-mix 1b expanded more than the predicted behavior. Some amount of uncertainly in determining TH_A may be responsible for this kind of discrepancy.
- For the main mix 2, all three sub-mixes were expected to expand with little expansion for sub-mix 2a, low-medium for sub-mix 2c, and high for sub-mix 2d. The concrete expansion measurements in Figure 6.7 supported this expectation. It seems when coarse aggregate is reactive and fine aggregate is non-reactive (mix 2), the magnitude of expansion stays in the lower side in the specified testing period. Modified C 1293 data in Table 6.4 also shows the similar expansion with this reactive coarse aggregate.
- For the main mix 3, the prediction was no expansion for sub-mix 3a followed by 3b (L-M), 3c (M), and 3d (VH) with increasing order of expansion. Concrete expansion measurements in Figure 6.8 supported this expected expansion behavior. Again, fine aggregate is reactive in mix 3.
- The TH_A for the reactive fine aggregate used in mix 4 is not determined. It seems the TH_A for this aggregate should be relatively low. A low TH_A (possibly lower than fine

aggregate in mix 3) in combination with high aggregate reactivity (Table 6.4) may be responsible for this kind of high expansion in Figure 6.9.

Based on these observations, it can be concluded that the direct concrete expansion measurements of these mixes validated the predicted expansion behaviors of the tested mixes (Table 6.9). The magnitude of expansion depends on:

- The reactivity of the aggregate.
- Whether coarse or fine aggregate is reactive.
- The difference between PSA and TH_A (i.e., the higher the positive difference of PSA minus TH_A, the higher the level of expansion).

Therefore, based on these three parameters, one can design a mix without concrete validation testing, which should perform in the field without any ASR or with negligible ASR. However, mix design development through all four stages in Option 1 ensures high reliability and safety.

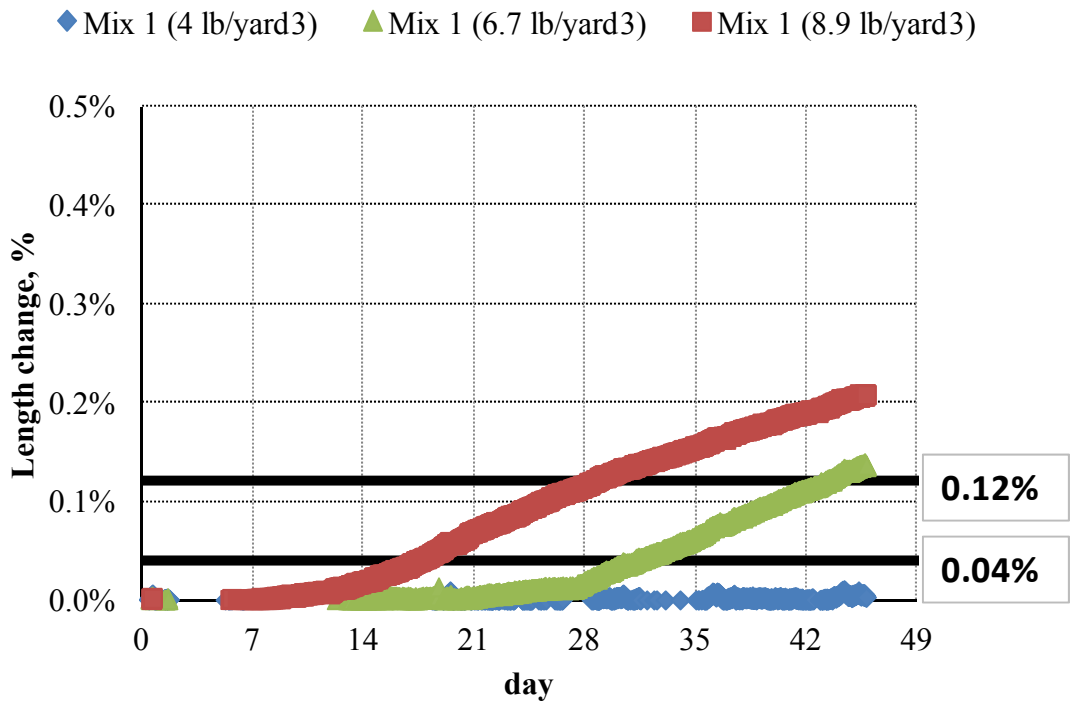

Figure 6.6. Expansion Curves of ACCT (Mix 1) Over Time at Varying Levels of Alkalinity.

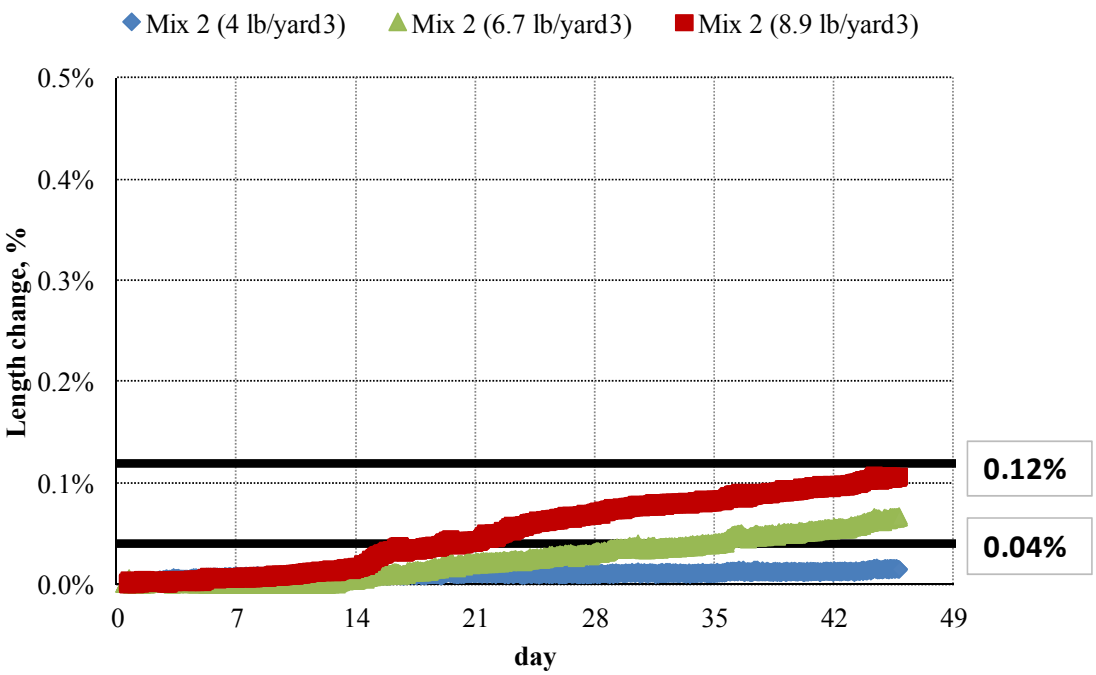

Figure 6.7. Expansion Curves of ACCT (Mix 2) over Time at Varying Levels of Alkalinity.

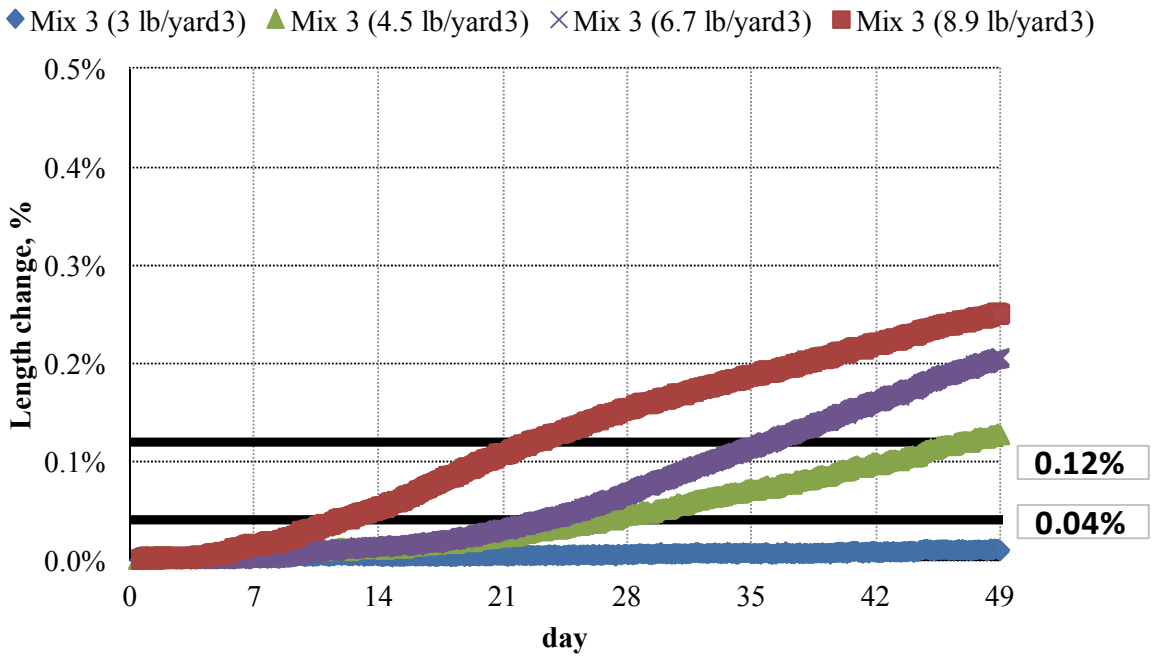

Figure 6.8. Expansion Curves of ACCT (Mix 3) over Time at Varying Levels of Alkalinity.

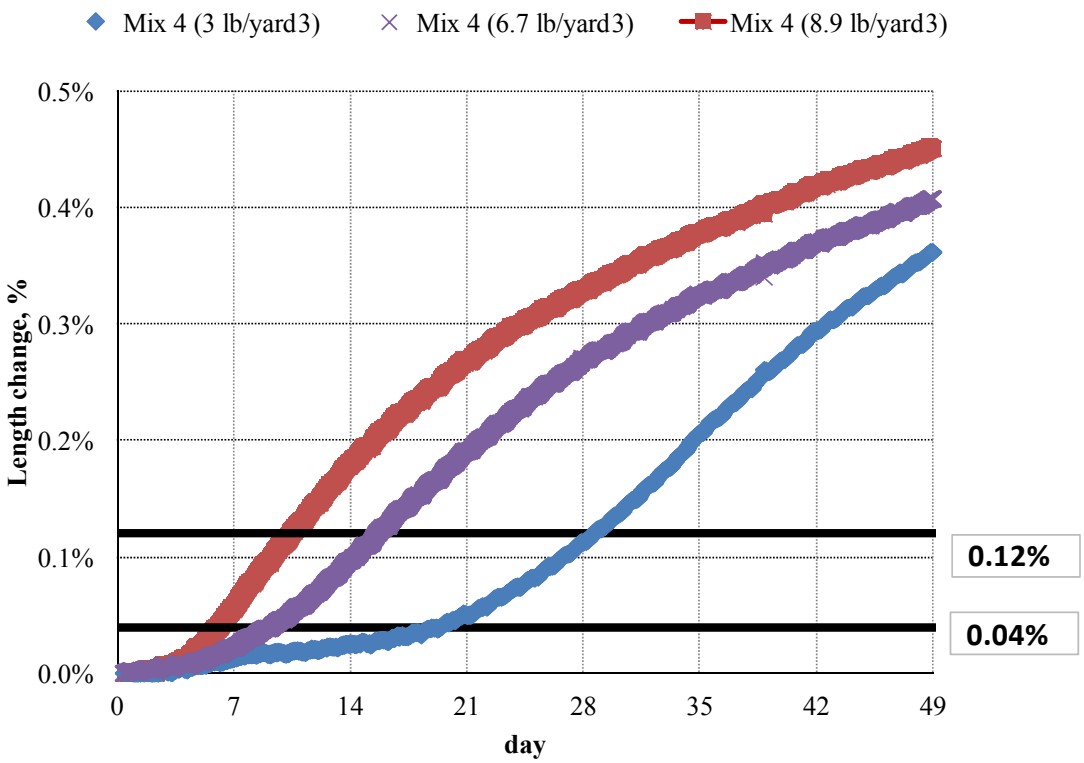

Figure 6.9. Expansion Curves of ACCT (Mix 4) over Time at Varying Levels of Alkalinity.

Mix 4 with alkaline levels 3, 6.7, and 8.9 lb/yard^3 was used to cast two cylinders for each alkaline level to verify the repeatability (within the lab) of ACCT test results. The expansion corresponding to two replicas were used to calculate the coefficient of variation (COV) and the expansion results are presented in Figure 6.10. The majority of expansion-based COV is within 10 percent after the 28-day expansion for the tested mixes at all levels of alkalinity, which indicates that the results are highly repeatable.

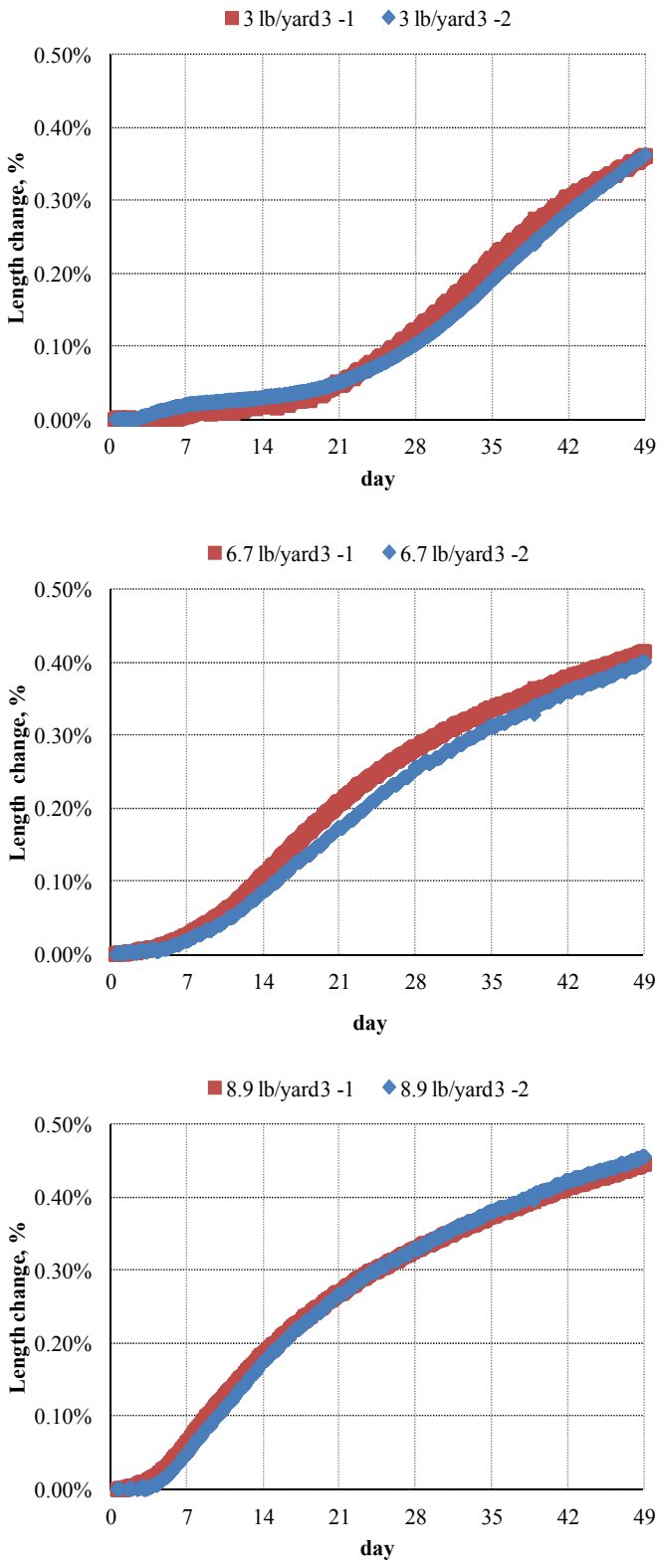

Figure 6.10. Expansion of Mix 4 with Different Alkaline Levels.

Many researchers have proposed the expansion limits of ACPT at 60°C. Proposed expansion limits at 60 °C were found from a range of 0.02 percent to 0.08 percent at 8 weeks (Ranc and Debray 1992; Bolotte 1992; Touma et al. 2001) and 0.03 percent to 0.04 percent at 13 weeks (Bolotte 1992; Touma et al. 2001). CSA in Canada (CSA A23.2-14A, 2004) proposed the most recent expansion limits for the ACPT. From their results, if the expansion of concrete prisms at 60 °C is less than 0.04 percent at the end of one year, the aggregate is classified as an ASR non-reactive. Marginally reactive aggregates will result in expansions between 0.04 percent and 0.12 percent. If the expansion is higher than 0.12 percent, the aggregate is considered as a highly reactive. Figure 6.11 shows the expansion curves of all mixes at each alkali level.

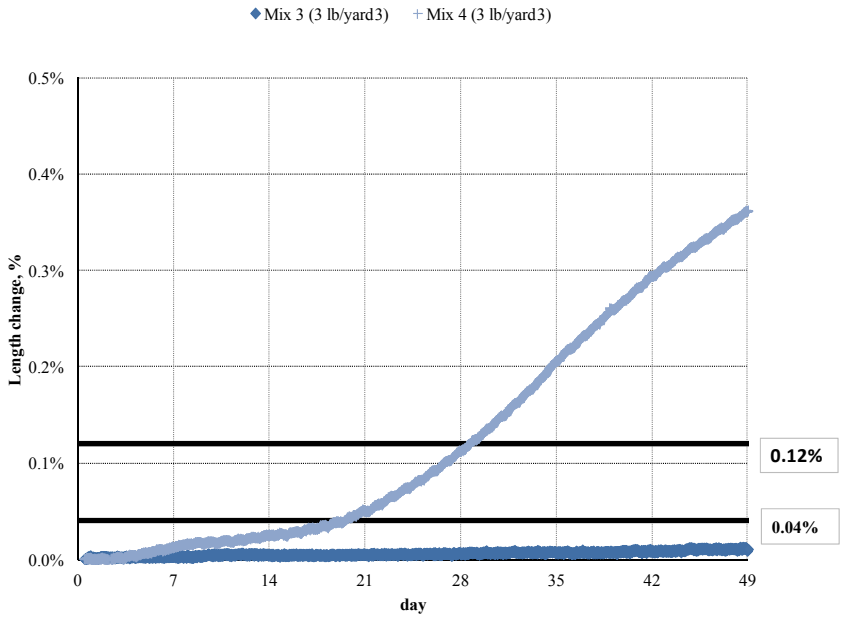

(a)

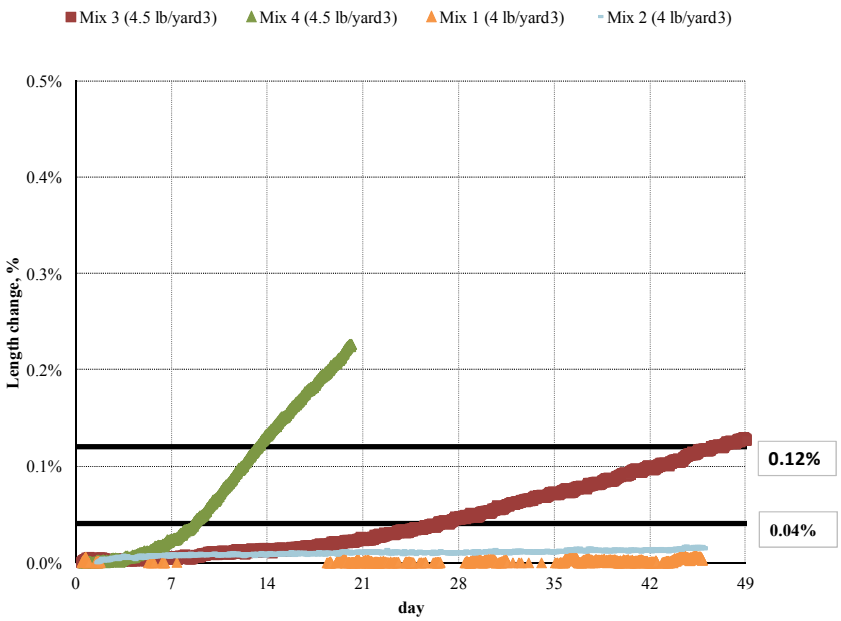

(b)

Figure 6.11. Expansion Curve of ACCT at Each Alkali Level (a) 3, (b) 4 and 4.5 lb/yard^3, (c) 6.7 lb/yard^3, and (d) 8.9 lb/yard^3.

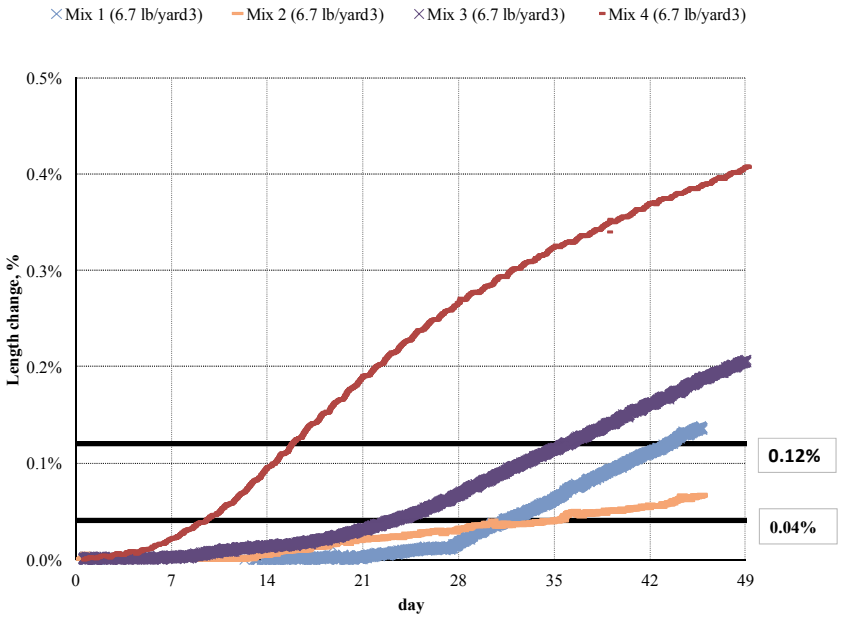

(c)

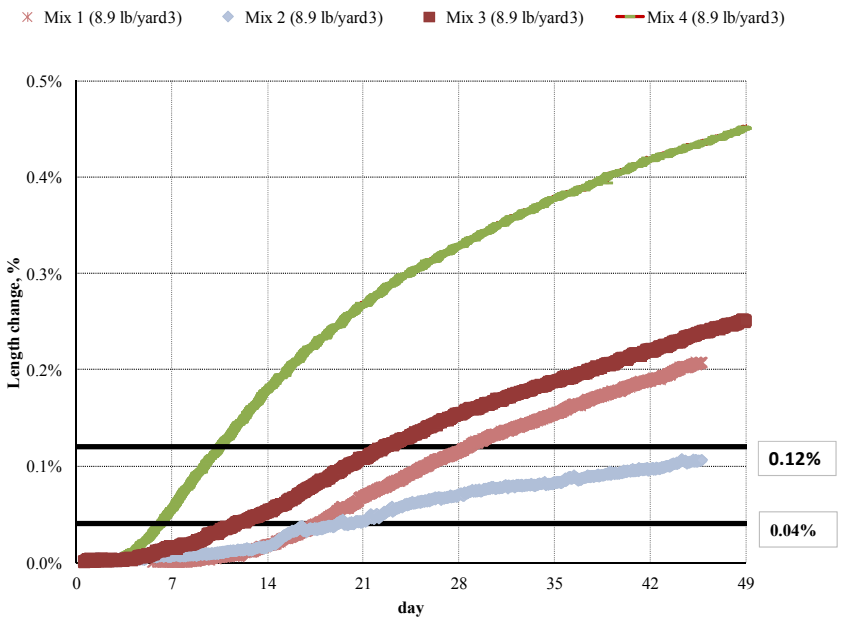

(d)

Figure 6.11. Expansion Curve of ACCT at Each Alkali Level (a) 3, (b) 4 and 4.5 lb/yard^3, (c) 6.7 lb/yard^3, and (d) 8.9 lb/yard^3 (cont'd.).

Expansion limits of 0.04 percent and 0.12 percent are shown as solid horizontal lines in Figure 6.11. Table 6.10 summarizes the aggregate reactivity based on the ACCT expansions in Figure 6.11 and compares with CSA criteria, E_a, and modified ASTM C1293 data. For all mixes (Mixes 1 to 4) with high alkali levels (4.5, 6.7, 8.9 lb/yard^3 with Na_2O_e > 0.6%), the expansion limit of 0.12 percent and 0.04 percent can be reached within a month (14–35 days, Table 6.10). The alkaline levels 8.9 lb/yard^3 (1.25 percent Na_2O_e) in Figure 6.11 (d) is same as conventional concrete prism (ASTM 1293). If the same expansion limit of 0.04 percent and the same alkaline level 1.25 percent Na_2O_e in CPT is applied in this study, the AACT have identified these aggregates as reactive aggregates at 21 days (Table 6.10). The ACCT-based reactivity also matches with E_a-based reactivity and modified ASTM C1293 values along with the TH_A–PSA relationship. This suggests that ACCT in VCMD can be used as a rapid and reliable concrete test.

Table 6.10. Aggregate Reactivity Based on the ACCT Expansion.

Main Mix	Sub-mix	Alkali Loading (lb/yard^3)	TH_A (N)	PSA (N)	Testing Period of ACCT	E_a-based Reactivity	Modified ASTM C1293 (TxDOT)
Mix 4	4d	8.9	< 0.37	1.04	14	HR	0.391
	4c	6.7		0.74	21		
	4b	4.5		0.66	14		
	4a	3.0		0.38	31		

Mix 3	3d	8.9	0.47	1.04	14	R	0.058
	3c	6.7		0.74	28		
	3b	4.5		0.66	28		
	3a	3.0		0.38	NI-R till 49 days of testing		
Mix 2	2d	8.9	0.37	0.88	21	R	0.078
	2c	6.7		0.46	35		
	2b	4.5		0.66	21		
	2a	4.0		0.37	NI-R till 49 days of testing		
Mix 1	1c	8.9	0.46	0.88	21	R	0.043
	1b	6.7		0.46	35		
	1a	4.0		0.40	NI-R till 49 days of testing		

NI-R: Not Indented as Reactive

Here are some observations related to E_a based reactivity prediction vs. concrete expansion.

If one aggregate is identified as reactive based on E_a (i.e., a low value of E_a), it will show measurable expansion above the specified limits in the ACCT (basis for correct identification) provided PSA $\geq TH_A$.

- For example, sub-mixes 1a, 2a, and 3a (Table 6.10) are not identified as reactive till 49 days of testing possibly because PSA $\leq TH_A$ for all these three sub-mixes, although the aggregates are reactive based on E_a.
- All other sub-mixes (e.g., 3b, 3c, 3d, 2b, 2c, 2d, 1b, and 1c) are characterized by PSA $\geq TH_A$ and shows expansion measurements by ACCT.

Based on the results in Table 6.10, it seems that ACCT with alkali loading 4.5 lbs/yard^3 could be a good choice to pass/fail a concrete mix with the same CSA expansion limits. A concrete mix with a conventional cement factor (e.g., CF = 6–7) will be sufficient to achieve 4.5 lbs/yard^3 alkali loadings if the $Na_2O_{eq.}$ of the cement is relatively high (e.g., $0.6 < Na_2O_{eq.} \leq 0.82$). However, if the $Na_2O_{eq.}$ of the cement is low (e.g., 0.55), a high CF ± additional alkalis may be needed in order to achieve 4.5 lbs/yard^3 alkali loadings. Figure 6.12 shows the expansion curve of mixes 2 to 6 using alkali loading 4.5 lb/yard^3. It indicates that a straight cement concrete mix with alkali loading 4.5 lb/yard^3 is sufficient to delineate reactivity at 28 days. Therefore, ACCT with relatively low alkali loadings (as opposed to high alkali loadings, i.e., 6.7–8.9 in the current CPT test) can be effective to identify the reactive mix in a relatively short period of time. It may be close to testing a job mix if a job mix is a straight cement mix.

Job mix generally contains supplementary cementitious materials (e.g., fly ash) and other ASR-preventing admixtures, and will take a longer period of time to show any measurable expansion in the ACCT. That is, if the job mix is still reactive after taking mix design controls and special protection measures as in Table 6.2. Figure 6.13 shows the expansion curves for the mixes with low alkali loadings (i.e., mixes 3 and 4 with alkali loading 3.0 lb/yard^3). Mix 3 (lower

reactive than mix 4) takes around 4 months to cross the 0.04 percent expansion limit. Mix 4 reaches the same level of expansion at relatively early age. This suggests that the ACCT using VCMD needs less time for a reactive aggregate even with a concrete mix with a very low alkali loading. This indicates that the possibility of testing a job mix using the proposed ACCT with a relatively longer testing time (not yet established but it should be around 3–4 months) is actually high. Further research is needed to test several job mixes and assign a representative testing period.

The same mix 3 is identified as reactive (i.e., expansion above 0.04 percent) at 28 days with 4.5 lbs/yard^3 and 14 days with 8.9 lbs/yard^3 (Table 6.10). Therefore, mix 3 was identified as invariably reactive irrespective of alkali loadings. Increase of alkali loadings make it faster to make the same judgment in this case. Further research is needed to verify this observation. If this is found to be true, then adding a little alkali to the job mix could be allowed to reduce the testing time and the VCMD-based cylinder test will emerge as a potential method to test job mix in the laboratory and effectively formulate an ASR-resistant mix with high reliability.

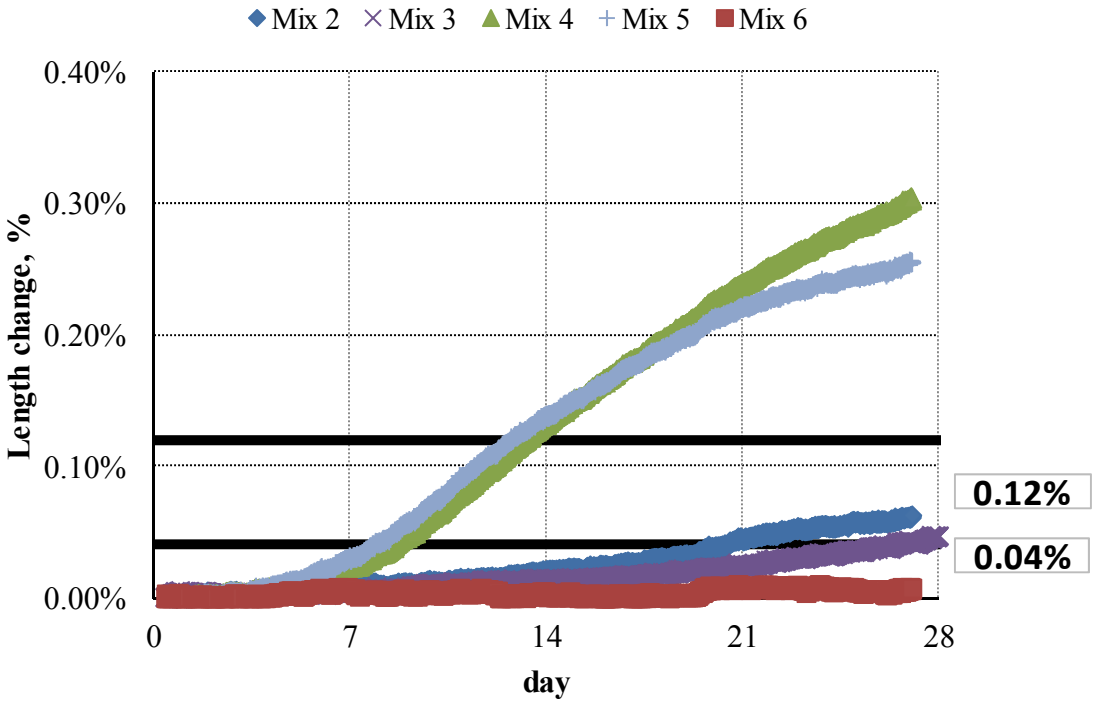

Figure 6.12. Expansion Curves of ACCT (Mixes 2 to 6 with Alkali Level 4.5 lb/yard^3) over Time.

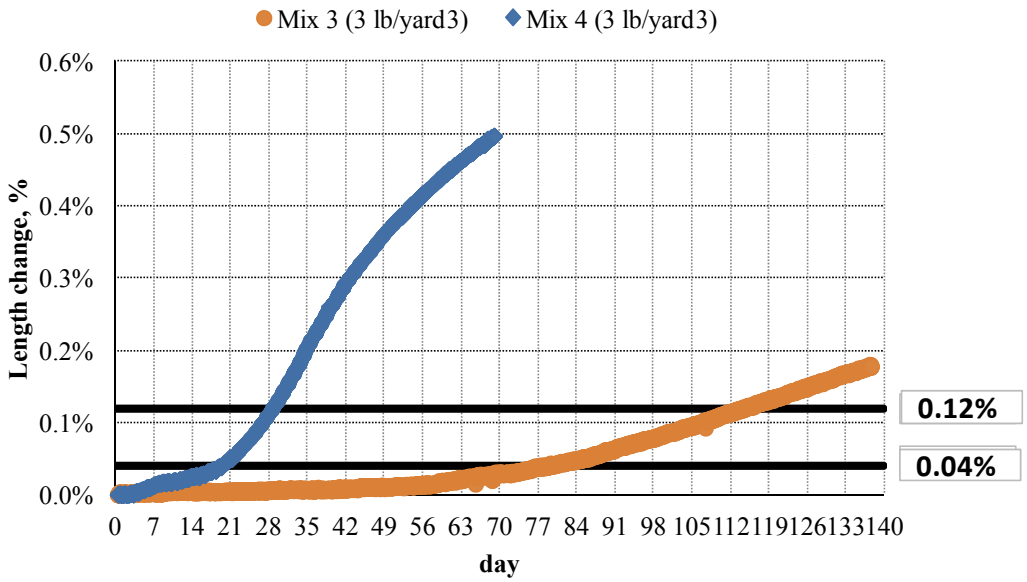

Figure 6.13. Expansion Curves of ACCT (Mixes 3 and 4 with Alkali Level 3.0 lb/yard^3) over Time.

Soak Solution Chemistry

The changes of soak solution chemistry were monitored to verify the leach-proof situation as well as the possibility of ions migration from soak solution to the specimen. An increase of OH-, Na+, and K+ ions concentrations in soak solution represents leaching of these ions from the specimen. On the other hand, a reduction in concentration of these ions in soak solution indicates ion migration from the soak solution to the specimen while ASR is in progress in the specimen.

Case 1: Pore solution = soak solution

The results are shown in Figures 6.14 and 6.15 for the change of OH-, Na+, and K+ concentrations of soak solution of mixes 3 and 4 with alkaline levels 4.5, 6.7, and 8.9 lb/yard3 due to ASR after the testing period of 49 days.

a. Initially, the ionic concentrations in pore solution and soak solution are equal, which does not allow ion migration between pore solution and soak solution. As ASR progresses, Na^+, K^+, and OH^- concentrations go down in the pore solution of the specimen, which triggers ion migration from the soak solution to the pore solution. The decrease in Na^+ (2% reduction for Mix 3 and 13% reduction for Mix 4), K^+ (8-9% reduction for both the mixes), OH^- (13% for Mix 3 and 7.5% for Mix 4) concentrations in soak solution after the test (Figures 6.14 and 6.15) suggests ion migration from soak solution to the specimen. However, the degree of reduction of

the ions in soak solution is not that high. It seems the effect of leach-proof situation on the measured expansion is more pronounced than the effect due to ions migration from the soak solution into the specimens. However, a continuous increase of expansion instead of gradually approaching an asymptotic shape may be supported by ingress of ions from soak solution. Further research is needed to verify these explanations. Note that this effect is very pronounced in the case of ASTM C 1260 where the soak solution is 1N NaOH, which is way higher than the mortar bar pore solution.

b. This situation in item (a) causes an accelerating effect on the test result itself. However, further work is needed to compare the data between soak solution = pore solution and soak solution < pore solution (discussed below) situation and then decide whether pore solution = soak solution is acceptable.

c. Testing with pore solution = soak solution or soak solution > pore solution can be used as a method of simulating a field situation where an external source of alkalis (e.g., sea water ingress, deicing chemicals) and alkali redistribution (i.e., concentration of alkalis in certain zones within the main concrete body due to intense ambient T and RH variations) are significant factors.

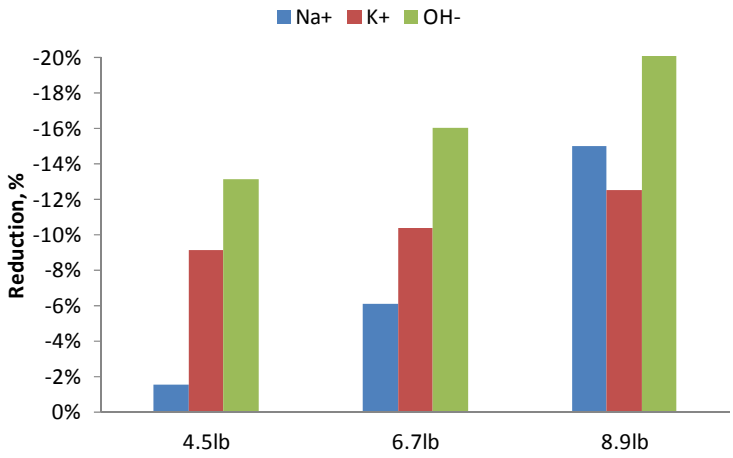

Figure 6.14. The Change of Na^+, K^+, and OH^- of Soak Solution of Mix 3 with Alkali Levels 4.5, 6.7, and 8.9 lb/yard^3 after Testing Period of 49 Days.

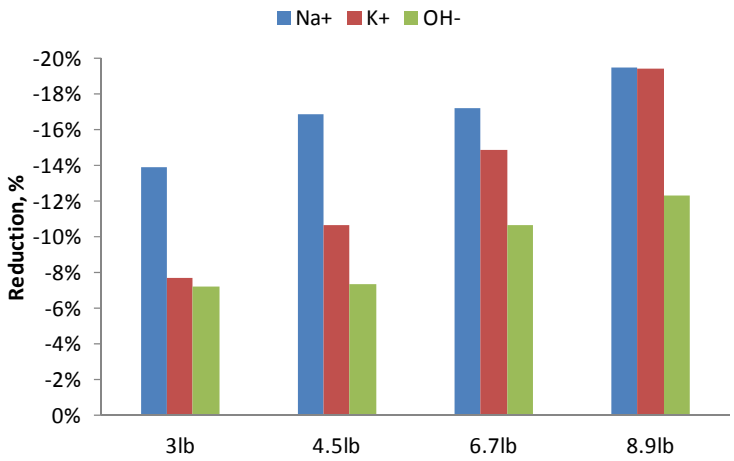

Figure 6.15. The Change of Na^+, K^+, and OH^- of Soak Solution of Mix 4 with Alkali Levels 3, 4.5, 6.7, and 8.9 lb/yard^3 after Testing Period of 49 Days.

Case 2: soak solution << pore solution (soak solution ½ or ¼ of the pore solution)

- At the beginning, some ions may leach out from the specimens to the soak solution as soak solution chemistry is lower than specimen pore solution chemistry. At later stages when ions decrease in the pore solution due to a significant amount of ASR (for a long period of time), some ions may migrate from the soak solution to the pore solution. If this happens, then there will be no change (significant or negligible) in the soak solution chemistry after the test. It is expected that the absolute expansion (ultimate expansion) in this situation will be lower than that measured with pore solution = soak solution condition. The testing period will increase in this situation. It is necessary to test a mix with alkali loading 4.5 lb/yard3 (i) using a soak solution with half the original concentration, and (2) using a soak solution having a quarter of the original concentration to verify this phenomena. The ions ingress from soak solution to the specimen is relatively low in case of low alkali loading (4.5 lb/yard^3) mixes. Therefore, further research is needed to decide whether reduced testing time with pore solution = soak solution is acceptable, or whether a relatively high testing period with soak solution << pore solution is the way to go.

TH_A Based on ACCT at Varying Levels of Alkalinity

For comparison purposes, the concrete expansion over time (till 49 days) of mixes 1 to 3 with varying levels of alkalinity was used to determine TH_A. Figure 6.16 shows the alkalinity vs. concrete expansion relationship of these three mixes. The expansion limit of 0.04 percent was superimposed on these plots to determine TH_A for the reactive aggregates used in these mixes.

The TH_A for mixes 1, 2, and 3 are 0.39, 0.4, and 0.47N respectively, which are similar to the TH_A determined aggregate-solution test (0.46, 0.37, and 0.47N respectively). This suggests that determination of TH_A from E_a vs. alkalinity relationship in aggregate-solution test is reliable and that long duration concrete tests at multiple levels of alkalinity might not be needed.

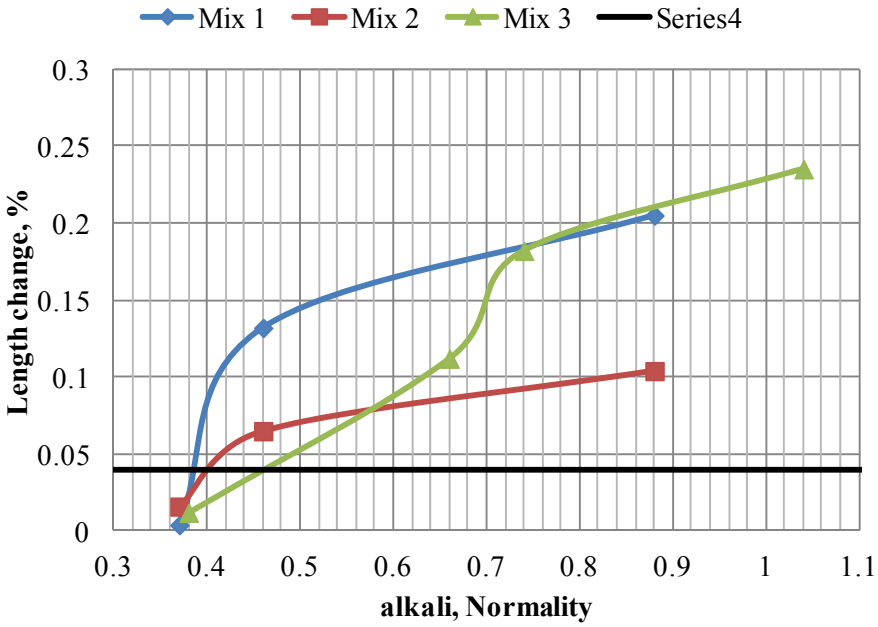

Figure 6.16. Effect of Alkalinity on the Expansion of Mixes 1 to 3.

6.2.6.3 Use of VCMD Concrete Test to Judge the Efficacy of Using Fly Ash

Mix 4 with alkaline level 4.5 lb/yard^3 with and without fly ash was conducted to validate the adjusted mix in VCMD. Fly ash F replaced 25 percent of cement in the mix, and pore solution was extracted to generate the soak solution. Table 6 shows the chemistry of extracted pore solution with 25 percent fly ash replacement. The pore solution is reduced from 0.66N to 0.43N (Table 6.11) when 25 percent of cement was replaced with fly ash. It can be expected that the expansion can be reduced due to a reduction of alkali concentration in pore solution. Figure 6.17 shows the expansion curves of mix 4 with and without fly ash. The expansion is reduced from 0.3 percent to 0.06 percent (around 80 percent reduction). Note that the PSA of fly ash mixture is still probably not below the TH_A of the reactive aggregate in the mix; as a result, the expansion (i.e., 0.06 percent) is not below 0.04 percent. Either fly ash replacement levels need to be increased (if it is allowable) or other mitigating measures in conjunction with the addition of fly ash need to be used. This is an indication that the proposed concrete cylinder test can be effectively used to determine fly ash contents, cement contents, and contents of ternary blends (if recommend in a particular situation based on the guidelines listed in Table 6.2) in order to make the PSA below TH_A and develop safe ASR-resistant mixes.

Table 6.11. Concentration of the Extracted Pore Solution of Mix 4 with 25% Fly-Ash Replacement.

Alkaline Level	Na^+, ppm	K^+, ppm	Na^+, N	K^+, N	Na^+_e, N
4.5 lbs./yard^3 (with 25% fly ash)	2260	21800	0.10	0.56	0.43
4.5 lbs./yard^3 (without fly ash)	4153	31562	0.18	0.81	0.66

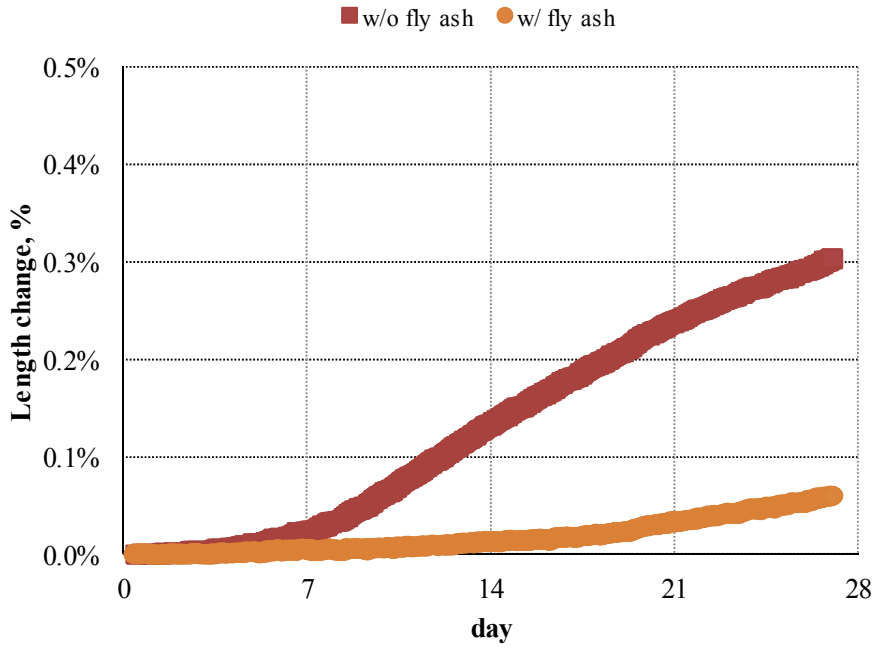

Figure 6.17. Expansion of Mix 4 with and without Fly Ash Replacement.

6.3 SUMMARY

The observations based on the results and discussion of this chapter are summarized below:

- A procedure to design an ASR-resistant concrete mix based on activation energy, threshold alkalinity, pore solution chemistry and concrete validation testing is developed. The guidelines to select mix-design controls and special protection measures depending on E_a, TH_A and severity of ambient conditions are developed.

- Since measuring activation energy is established as a reliable method to predict aggregate alkali silica reactivity, all four stages (Option 1) are recommended for aggregates belonging to false positive and negative categories. The four stages are:

  - Determination of Ea and TH_A from aggregate-solution test.
  - Determination of pore solution alkalinity (PSA).
  - Mix design adjustment based on TH_A–PSA relationship (i.e., PSA needs to be below TH_A in order to prevent / minimize ASR).
  - Mix design validation through concrete testing.

- For the aggregates where the reactivity prediction based on the current test methods is satisfactory, activation energy measurement through aggregate-solution test may not be needed. However, mix design verification/validation through direct VCMD concrete testing is highly recommended.

- The proposed test method was developed to measure expansion of concrete cylinder due to ASR at a temperature of 60°C. Making soak solution chemistry equal to pore solution chemistry ensures no leaching test condition. Although testing period is not yet fully established, the proposed VCMD cylinder test takes around 1 month (21–35 days) to identify a reactive straight cement concrete mix with varying alkali loadings (i.e., 8.9–4.5 lbs/yard^3). However, the time needed to test a slowly reactive straight cement mix with lower alkali loadings (e.g., 3.0–4.0 lbs/yard^3) is relatively high and yet to be established.
- The results indicated that the situation of pore solution = soak solution causes an accelerating effect that could be used to make the test rapid. Further research is needed to decide whether reduced testing time with pore solution = soak solution is acceptable, or whether a relatively high testing period with soak solution << pore solution is the way to go.
- Since the data collection in the VCMD cylinder test is automatic through LVDT (no human error) under constant temperature (no error due to temperature difference), the reliability of the VCMD cylinder test is high.
- The ACCT with relatively low alkali loadings (as opposed to high alkali loadings, i.e., 6.7–8.9 in the current CPT test) and at 60°C can effectively be used to pass/fail a concrete mix in a relatively short period of time. It may be close to testing a job mix if a job mix is a straight cement mix.
- The VCMD-based cylinder test has the ability to emerge as a potential method to test job mix in the laboratory and effectively formulate ASR-resistant mix with high reliability. The possibility of the proposed ACCT testing a job mix (e.g., a typical ASR mitigated mix) with a relatively longer testing time (not yet established but it should be around 3-4 months) is actually high. Further research is needed to test several job mixes and assign a representative testing period. The results indicated that adding little alkali to the job mix could be allowed to reduce the testing time.

- Further research is needed to verify the applicability of the current expansion limit (i.e., 0.04 percent) in the proposed cylinder test. This can be accomplished by generating more concrete data using different mixes with varying reactivity, followed by a comparative assessment between the proposed cylinder test, a modified ASTM C1293, and exposure block data (calibration).

CHAPTER 7: CONCLUSIONS AND RECOMMENDATIONS

This section summarizes the main findings of this study and offers recommendations for further investigation of ASR aggregate and concrete testing.

7.1 CONCLUSIONS

Based on the results obtained from this study, the primary findings include:

Aggregate-Solution Testing, Measuring E_a and Developing E_a-Based Classification System

The observations related to measuring activation energy and developing E_a-based aggregate classification system from aggregate-solution tests are summarized below:

- From the glass balls-solution tests (closed system), researchers observed that the VCMD measures net solution volume contraction due to ASR over time. This same solution volume contraction over time was invariably observed in all aggregate-solution tests. The pure phase experiments using glass balls were used to validate the VCMD test method as a proof of concept.
- The net solution volume contraction in a closed system condition of the VCMD is due to the combined effects of

  - Si-O-Si bond breaking and dissolution–solution volume decreases.
  - Consumption of reactants such as water and ionic species–solution volume decreases.
  - Product formation and expansion–solution volume increases.
  - Solution goes into micropores (pore developed due to the formation of high-volume, less dense ASR products) and microcracks–the degree of micropore and microcrack formation is related to the degree of ASR–solution volume decreases.
  - Incomplete absorption–negligible but may cause slight solution volume decrease.

- It was explained in Chapter 4 that aggregate absorption should achieve more than 95 percent AC during sample preparation time and before starting the VCMD test for ASR. It is unlikely that the absorption (filling the remaining most inaccessible pores by solution) will continue during the VCMD testing period (i.e., four days). Even if it continues, it would be very negligible. Therefore, the effect of aggregate absorption in measuring net solution volume contraction over time in the VCMD test is very negligible. The main phenomenon in creating net solution volume contraction is ASR.
- A kinetic-type model was developed to model the measured non-linear type solution volume change over time. By fitting the model volume change data to the measured volume data over time, the characteristics parameters (i.e., $\varepsilon 0$, β, $t0$, ρ) are calculated. The β (rate constant) values at multiple temperatures (minimum 3 temperatures) are then determined and activation energy is calculated by plotting $\ln(\beta)$ versus $(1/T)$. Based on the rate theory, the slope of the linear regression is equal to $(-Ea/R)$ where R is the universal gas constant and E_a is the activation energy.
- As the device measures the net combined effects of the different steps of ASR (i.e., breaking Si-O-Si bond, dissolution, product formation, swelling, etc.) in the form of net solution volume change over time, it is better to use the term “compound activation

energy." Moreover, aggregates are multi-phase and sometimes very heterogeneous materials. The distribution of the reactive constituents inside the aggregate is in general inhomogeneous in nature. The activation energy that the proposed method will measure should not be confused with the activation energy of a single (one step) chemical reaction of a pure phase in Chemistry.

- The VCMD-based test can reliably predict aggregate alkali silica reactivity in a short period of time in terms of measuring activation energy. A representative E_a can be determined by testing as-received aggregates (i.e., field aggregates) with 0.5N NaOH + $Ca(OH)_2$ solution (similar to concrete pore solution) and with permissible repeatability. This helps further reduction of testing time and reduces the gap between lab and field.
- The majority of COV based on rate constant is within 10 percent, which indicates the results are highly repeatable (see Figure 5.4 and Appendix D).
- The E_a-based method has correctly identified the aggregates that the AMBT method has passed/failed but that the CPT had failed/passed in a short period of time (see Figure 5.4 in Chapter 5). This is the main benefit of the VCMD-based test method.
- A good correlation between E_a-based aggregate reactivity and C 1260 (14 days expansion)/C 1293 (1-year concrete prism expansion) (see Table 5.1, Figure 5.3, and Chapter 5) indicates that the proposed method has the merits to be considered as a rapid and reliable ASR test method on one hand, and have the potential to be considered as an alternative method to the current AMBT method on the other hand.
- ASR E_a can serve as a single chemical material parameter to represent alkali silica reactivity of aggregate. The E_a-based aggregate classification can serve as a potential screening parameter in an aggregate quality control program.
- Measuring low E_a (high reactivity) of an aggregate using the VCMD is supported by the higher consumption of Na+ (Figures 5.7 and 5.8) and/or greater reduction of OH- (Figures 5.5 and 5.6) in the test solution. Therefore, the test solution monitoring method has supported the VCMD test results as a supporting tool.
- Similarly, the microstructural studies on the reacted aggregate particles by SEM-EDS have also supported the activation energy-based reactivity prediction.
- An apparent relationship between compound activation energy (E_a) and alkalinity was observed, i.e., the higher the alkalinity, the lower the E_a. An attempt was made to model this relationship between E_a and alkalinity, and determine threshold alkalinity (TH_A) for each aggregate (see Table 5.2). In general, the higher the reactivity (i.e., the lower the E_a) the lower the TH_A. A reactive aggregate can practically behave as non-reactive or very slow reactive if concrete pore solution alkalinity can be maintained below the TH_A.

Development of a Procedure for Formulating ASR Resistant Concrete Mix

- A procedure to design an ASR-resistant concrete mix based on activation energy, threshold alkalinity, pore solution chemistry and concrete validation testing is developed. The five stages that are involved in developing an ASR resistant mix are listed below:

    - Determination of E_a and TH_A from aggregate-solution test.
    - Development of an ASR-resistant mix by applying both mix design controls and special protection measures (as needed) depending on activation energy-based

reactivity prediction, TH_A, and some consideration on the severity of ambient conditions.
  - Determination of pore solution alkalinity (PSA) using the pore solution extraction method or any other suitable method.
  - Mix design adjustment/verification based on TH_A-PSA relationship: PSA needs to be below TH_A in order to prevent/minimize ASR.
  - Mix design validation through concrete testing–A new accelerated concrete cylinder test (ACCT) using VCMD was developed to test concrete mixes in a short time.

- All these five stages are recommended (until enough data are generated and better understanding is achieved) for aggregates that belong to false positive and negative categories. If the pore solution extraction method is not available, the dependency on concrete validation testing will be high in order to develop a safe ASR-resistant mix with high reliability. As activation energy-based reactivity prediction is reliable and dependable, an expert can design ASR-resistant mix based on E_a-based reactivity, TH_A, and knowledge gained based on concrete validation testing without pore solution data and concrete validation testing. This practice may be acceptable, but some amount of risk will be involved.
- For the aggregates where the reactivity prediction based on the current test methods is satisfactory, activation energy measurement through aggregate-solution test may not be needed. However, mix design verification/validation through direct VCMD concrete testing is highly recommended.
- The proposed ACCT method was developed to determine the length change of concrete cylinder (3 × 6 inches) due to ASR at a temperature of 60°C. Making soak solution chemistry equal to pore solution chemistry ensures no leaching test condition. Although the testing period is not yet fully established, the proposed VCMD cylinder test takes around 1 month (21–35 days) to identify a reactive straight cement concrete mix with varying alkali loadings (i.e., 8.9–4.5 lb/yard^3). However, the time needed to test a slowly reactive straight cement mix with lower alkali loadings (e.g., 3.0–4.0 lb/yard^3) is relatively high and yet to be established (e.g., 3–4 months for aggregate with medium-slow reactivity).
- Because the data collection in the VCMD cylinder test is automatic through LVDT (no human error) under constant temperature (no error due to temperature difference), the reliability of the VCMD cylinder test is high. Creating a leach-proof situation in the VCMD cylinder test is another advantage that enhances the reliability of the VCMD cylinder test.
- ACCT with relatively low alkali loadings (4.5 lb/yard^3 as opposed to high alkali loadings, i.e., 6.7–8.9 lb/yard^3 in the current CPT test) and at 60°C can effectively be used to pass/fail a concrete mix in a relatively short time. It may be close to testing a job mix.
- The VCMD-based cylinder test has the ability to emerge as a potential method to test job mix (e.g., a mix with typical ASR mitigation measures) in the laboratory and effectively formulate an ASR-resistant mix with high reliability. Further research is needed to test several job mixes and assign a representative testing period.

7.2 RECOMMENDATIONS

Further Research

The following are the areas of further research using the Aggregate-Solution Test.

- The activation energy-based aggregate classification system is developed based on testing a limited number of aggregates (i.e., 16 aggregates) in this study. Therefore, the ranges are arbitrary in nature at this time. To establish an effective ASR aggregate classification system, the assignment of more refined activation energy ranges through testing a greater number of aggregates is highly warranted.
- More aggregates that the AMBT method has passed/failed but that the CPT had failed/passed are needed in order to establish the benefit (i.e., consistent identification of aggregates that belong to false positive and negative categories) of the VCMD-based procedure. Identification of the critical aggregates (those belonging to false positive and negative categories) from the TxDOT database followed by the VCMD aggregate-solution test to determine E_a, TH_A is highly warranted in order to correctly identify the reactivity of these aggregates.
- It is necessary to generate E_a at one or two additional levels of alkalinity (e.g., 0.25–0.3N NH + CH and/or 0.7N NH + CH) and improve the TH_A calculation procedure in order to increase the reliability of the proposed approach of TH_A determination.
- Develop a procedure to determine optimum dosages of Li-compounds–one approach could be the dosage needed to make E_a falls in the non-reactive or slowly reactive ranges. The other approach could be through concrete testing using the proposed ACCT method (described below).

The following are the areas of further research for further improvement of the proposed concrete test method and procedure for developing an ASR-resistant concrete mix:

- More concrete testing and assign an effective testing period that can be used to test concrete mixes of varying reactivity (i.e., from slowly reactive to highly reactive).
- It is proposed that the ACCT with relatively low alkali loadings (i.e., 4.5 lb/yard^3) and 60°C can effectively be used to pass/fail a concrete mix in a relatively short time. It is necessary to do more testing to verify its efficacy and assign an effective testing period.
- The results indicated that the situation of pore solution = soak solution causes an accelerating effect for the ASR, which could be used to make a test rapid. Further research on modification of soak solution (e.g., soak solution ½, ¼ of pore solution alkalinity, lime-saturated water, etc.) and its effect on concrete expansion is needed to decide whether a reduced testing time with pore solution = soak solution is acceptable, or a relatively high testing period with soak solution << pore solution is way to go.
- The possibility of testing a job mix (e.g., a typical ASR-mitigated mix) by the proposed ACCT is high. Further research is needed to test several job mixes and assign a representative testing period that should cover concrete mixes with wide range of reactivity. The results indicated that adding a little alkali to the job mix could be allowed to reduce the testing time. Generating supporting evidence through concrete testing with and without alkali boosting would justify this step.

- Verification of different options (e.g., options 1, 2 and 3 in Chapter 6) that are proposed to develop ASR-resistant concrete mixes using the proposed ACCT method.
- Assigning replacement levels of fly ash to control ASR by using the proposed concrete testing–the replacement levels needed to reduce the expansion at the recommended testing period below the recommended limits.
- Assigning optimum dosage of Li-compounds to control ASR using the proposed VCMD concrete cylinder test.
- Further research is needed to verify the applicability of the current expansion limit (i.e., 0.04 percent) in the proposed cylinder test. This can be accomplished by generating more concrete data using different mixes with varying reactivity, followed by a comparative assessment between the proposed cylinder test, TxDOT-modified ASTM C1293, and exposure block data (a better way to do calibration).
- Measurement of ASR expansion using concrete specimens of different dimensions (i.e., a cylinder of 3 × 6 inches, prism of 3 × 3 × 4.7 inches, and prism of 4 × 4 × 11.25 inches) in VCMD at different temperatures (i.e., 38^{o}C and 60^{o}C) and under alkali leach-proof condition should be helpful in understanding the effects of specimen sizes and temperatures on the concrete expansion behavior. It will allow establishing a comparison between conventional C 1293 data and the VCMD cylinder test using the same specimen size and under the same temperature conditions, but with no leaching and automatic data collection with the VCMD cylinder test.
- It is reported that testing concrete at 60°C is associated with increased sulfate concentration and reduction of OH^- ions in the pore solution, which causes reduction in expansion. This needs to be verified.

Proposed Implementation Plan

It is recommended to implement the VCMD method through the following activities:

1. Establish repeatability (within the Lab) and reproducibility (between the labs) of the VCMD test.

    a. Provide equipment to five labs (cost ~ $2600.00/ each) within TxDOT. Two can be given to TxDOT (Austin) and three can be given to three district labs.
    b. Provide the necessary training and workshops to the representative operator for all the labs.
    c. Select some aggregate materials with a good record of reactivity based on the current methods as well as the VCMD method (this study), and conduct VCMD testing.
    d. Repeat six replicas per sample within the lab.
    e. Reproduce between the labs. COV percent will be determined based on the average E_a of each lab (for a total of five labs).
    f. Develop a precision and bias statement.

2. Field Validation–The current TxDOT exposure blocks will be useful to validate the performance under field conditions. Proper planning is necessary to select aggregate types and mix design matching with the mix design of the TxDOT's current exposure block.

3. Guidelines that are developed in Chapter 6 for developing ASR-resistant concrete mixes will be refined and updated based on the above findings.
4. Specification recommendation–shadow specification will be prepared based on the final guidelines (Step 3) on developing ASR-resistant mixes; TxDOT will decide if it is needed to incorporate the shadow specification in the construction specification. The guidelines will be based on both activation energy-based reactivity prediction and formulating ASR-resistant mix based on E_a, TH_A, pore solution chemistry (may not be needed), and concrete validating testing using the proposed VCMD-based concrete cylinder test.

REFERENCES

Abraitis, P. K., D. J. Vaughan, F. R. Livens, J. Monteith, D. P. Trived, and J. S. Small (1998). Dissolution of a complex borosilicate glass at 60^{o}C: The influence of pH and proton adsorption on the congruence of short-term leaching. Mat. Res. Soc. Symp. Proc., Vol. 506.

Abraitis, P.K., F.R. Livens, J.E. Monteith, J.S. Small, D.P. Trivedi, D.J. Vaughan, and R.A. Wogelius (2000). Appl. Geochem., 15, p. 1399–1416.

Adams, M. P., B. Gray, J. H. Ideker, J. E. Tanner, A. Jones, and B. Fournier (2012). Applicability of Standard Alkali-Silica Reactivity Testing Methods for Recycled Concrete Aggregate. In Proceedings of the 14th International Conference on Alkali-Aggregate Reaction in Concrete, CD-ROM, Austin, Texas.

Alexander, G. B., W. M. Heston, and R. K. Iler (1954). The Solubility of Amorphous Silica in Water. J. Am. Chem. Soc., Vol. 58 (6), p. 453-455.

ASTM C 1260-07 (2008): Standard Test Method for Potential Alkali Reactivity of Aggregates (Mortar-Bar Method). American Society for Testing Materials, West Conshohocken, Annual Book of ASTM Standards (04.02): Concrete and Aggregates: 677-681.

ASTM C 1293-08a (2008): Standard Test Method for Determination of Length Change of Concrete Due to Alkali-Silica Reaction. American Society for Testing Materials, West Conshohocken, Annual Book of ASTM Standards (04.02): Concrete and Aggregates: 682-688.

ASTM C 150-12 (2012): Standard Specification for Portland Cement. ASTM International, Annual Book of ASTM Standards, American Society for Testing Materials, West Conshohocken, Annual Book of ASTM Standards (04.01): Concrete and Aggregates: 157-165.

ASTM C1567-07 (2008): Standard Test Method for Determining the Potential Alkali-Silica Reactivity of Combinations of Cementitious Materials and Aggregate (Accelerated Mortar-Bar Method). ASTM International, American Society for Testing Materials, West Conshohocken, Annual Book of ASTM Standards (04.02): Concrete and Aggregates: 776-781.

ASTM C1608-07 (2012): Standard Test Method for Chemical Shrinkage of Hydraulic Cement Paste. ASTM International, American Society for Testing Materials, West Conshohocken, Annual Book of ASTM Standards (04.01): Concrete and Aggregates: 692-695.

ASTM C 227-03 (2008): Standard Test Method for Potential Alkali Reactivity of Cement-Aggregate Combinations (Mortar-Bar Method). American Society for Testing Materials, West Conshohocken, Annual Book of ASTM Standards (04.02): Concrete and Aggregates: 152-156.

ASTM C 289-07 (2008): Standard Test Method for Potential Alkali Reactivity of Aggregate (Chemical Method). American Society for Testing Materials, West Conshohocken, Annual Book of ASTM Standards (04.02): Concrete and Aggregates: 179-185.

ASTM C 295-03 (2008): Standard Guide for Petrographic Examination of Aggregate for Concrete. American Society for Testing Materials, West Conshohocken, Annual Book of ASTM Standards (04.02): Concrete and Aggregates: 199-206.

ASTM C 33-07 (2008): Standard Specification for Concrete Aggregates. American Society for Testing Materials, West Conshohocken, Annual Book of ASTM Standards (04.02): Concrete and Aggregates: 12-22.

ASTM C441-05 (2008): Standard Test Method for Effectiveness of Mineral Admixture or Ground Blast-Furnace Slag in Preventing Excessive Expansion of Concrete Due to the Alkali-Silica Reaction. American Society for Testing Materials, West Conshohocken, Annual Book of ASTM Standards (04.02): Concrete and Aggregates: 250-252.

ASTM C856-04 (2008): Standard Practice for Petrographic Examination of Hardened Concrete. American Society for Testing Materials, West Conshohocken, Annual Book of ASTM Standards (04.02): Concrete and Aggregates: 438-454.

Barisone, G. and G. Restivo (2000). Alkali–silica reactivity of some Italian opal and flints tested using a modified mortar bar test, in: M.A. Bérubé, B. Fournier, B. Durand (Eds.), 11th International Conference on Alkali–Aggregate reaction in Concrete, p. 239–245.

Barneyback, R.S. and D. Sidney (1981). Expression and Analysis of Pore Fluids from Hardened Cement Pastes and Mortars. Cem. Concr. Res., (11), p. 279-285.

Barringer, W.L. (2000). Application of Accelerated Mortar Bar Tests to New Mexico Aggregates. Proceedings of 11th International Conference on Alkali-Aggregate Reactions in Concrete, Quebec City, Quebec, Canada, p. 563-572.

Bates, J. K., C. R. Bradley, E. C. Buck, J. C. Cunnane, W. L. Ebert, X. Feng, J. J. Mazer, and D. J. Wronkiewicz (1994). High-level Waste Borosilicate Glass: A Compendium of Corrosion Characteristics, Volume II, U.S. Department of Energy.

Bektas, F., L. Turanli, T. Topal, and M.C. Goncuoglu (2004). Alkali reactivity of mortars containing chert and incorporating moderate-calcium fly ash. Cem. Concr. Res. 34, p. 2209–2214.

Bérubé, M. A., B. Durand, D. Vezina, and B. Fournier (2000). Alkali-Aggregate Reactivity in Quebec. Canada, Journal of Civil Engineering, Vol. 27 No. 2, p. 226-45.

Bérubé, M. A., J. Duchesne, J.F. Dorion, and M. Rivest (2002). Laboratory assessment of alkali contribution by aggregates to concrete and application to concrete structures affected by alkali–silica reactivity. Cem. Concr. Res., 32, p. 1215–1227.

Bérubé, M. A., C. Tremblay, B. Fournier, M. D. Thomas, and D.B. Stokes (2004). Influence of lithium-based products proposed for counteracting ASR on the chemistry of pore solution and cement hydrates. Cem. Concr. Res., 34, p. 1645–1660.

Bleszynski, R.F. and M.D.A. Thomas (1998). Microstructural studies of alkali–silica reaction in fly ash concrete immersed in alkaline solutions. Adv. Cem. Based Mater., 7, p. 66–78.

Bolotte, B. (1992). Development of an Accelerated Performance Test on Concrete for Evaluating its Resistance to AAR. Proc. of the 9th Int. Conf. on AAR in Concrete, London (UK), The Concrete Society, p. 110-116.

Bonakdar, A., B. Mobasher, S. K. Dey, and D. M. Roy (2010). Correlation of Reaction Products and Expansion Potential in Alkali-Silica Reaction for Blended Cement Materials ACI Journal, 107 (4), p. 380-386.

Brandt, M.P. and R.E. Oberholster (1983). Study of Tygerberg Formation Aggregate for Potential Alkali-Reactivity, Implications of Test Methods and Applications of the Findings in Practice. SCIR Research Report No. 580, p. 96.

Broekmans, M.A.T.M. (2002). The alkali–silica reaction: mineralogical and geochemical aspects of some Dutch concretes and Norwegian mylonites. PhD. Thesis, in, University of Utrecht, p. 144.

Brouwers, H. J. H. and R. J. van Eijk (2003). Alkali concentrations of pore solution in hydrating OPC. Cem. Concr. Res., 33, p. 191–196.

Brouxel, M. (1993). The alkali–aggregate reaction rim: Na2O, SiO2, K2O and CaO chemical distribution, Cem. Concr. Res., 23, p. 309–320.

Buck, A.D. and K. Mather (1987). Methods for controlling effects of alkali–silica reaction in concrete. Army Engineer Waterways Experiment Station Vicksburg MS Structures Lab, Accession no ADA178479, p. 69.

Callister (Jr.), W.D. (2007). Materials Science and Engineering An Introduction: John Wiley & Sons, Inc., New York.

Carrasquillo, R.L. and J. Farbiaz (1988). Alkali-Aggregate Reaction in Concrete Containing Fly Ash: Final Report. Center of Transportation Research, Research Report # 450-3F.

Chatterji, S. (1989). Mechanisms of alkali-silica reaction and expansion. Proc., 8th Int. Conf. on Alkali-Aggregate Reaction in Concrete, Kyoto, p. 101-105.

Chatterji, S., A. D. Jensen, N. Thaulow, and P. Christemsens (1986). Studies of alkali silica reaction. Part 3. Mechanisms by which NaCl and Ca(OH)2 affect the reaction. Cem. Concr. Res., 16(2), p. 246-254.

Constantiner, D. and S. Diamond (2003). Alkali release from feldspars into pore solutions. Cem. Concr. Res., 33, p. 549–554.

CSA A23.2–14A (2004). Potential expansivity of aggregates (procedure for length change due to alkali–aggregate reaction in concrete prisms at 38 °C). Concrete Materials and Methods of Concrete Construction/Methods of Test and Standard Practices for Concrete, Mississauga, ON, Canada, p. 246–256.

De Grosbois, M. (2000). Evaluation of the Potential Alkali-Reactivity of Concrete Aggregates: Performance of Testing Methods and A Producers Point of View, Proceedings, 11th International Conference of Alkali-Aggregate Reactivity in Concrete, Quebec City, QC, Canada, p. 267-276.

Diamond, S., (1976). A Review of Alkali-Silica and Expansion Mechanisms: 2. Reactive Aggregate. Cem. Concr. Res., Vol. 6, No. 4, p. 549-560.

Diamond, S. (1981). Effect of Two Danish Fly Ashes on Alkali Contents of Pore Solutions of Cement-Fly Ash Pastes. Cem. Concr. Res., Vol. 11, No. 3, p. 383-394.

Diamond, S. (1983). Alkali-Reactions in Concrete-Pore Solution Effects. Proceedings of the Sixth International Conference on Alkalis in Concrete, p. 155–166.

Diamond, S. (1997). Alkali Silica Reactions-Some Paradoxes. Cement and Concrete Composites, Vol. 19, p. 391-401.

Diamond, S. (2000). Chemistry and other characteristics of ASR gels, in: M.-A. Bérubé, B. Fournier, B. Durand (Eds.), 11th International Conference on Alkali Aggregate Reactions in Concrete, Québec, Canada, p. 31–40.

Diamond, S. and M. Penko (1992). Proceedings G.M. Idorn International. Symposium. Durability of Concrete, ACI SP-131, p. 153.

Diamond, S. and N. Thaulow (1974). A study of expansion due to alkali–silica reaction as conditioned by the grain size of the reactive aggregate. Cem. Concr. Res. 4, p. 591–607.

Dove, P.M., and J.D. Rimstidt (1994). Silica–water interactions, in: P.J. Heaney, C.T. Prewitt, G.V. Gibbs (Eds.), Silica: physical behaviour, geochemistry and materials applications Reviews in Mineralogy, Mineralogical Society of America, p. 259–308.

Dunant, C.F. and K.L. Scrivener (2012). Effects of aggregate size on alkali–silica-reaction induced expansion. Cem. Concr. Res., 42 (6), p. 745–751.

Fernandes, I., F. Noronha, and M. Teles (2004). Microscopic analysis of alkali–aggregate reaction products in a 50-year-old concrete. Mater. Charact. 53, p. 295–306.

Folliard, K. J., J.H. Ideker, M.D.A. Thomas, and B. Fournier (2004). Assessing aggregate reactivity using the Accelerated Concrete Prism Test. Seventh CANMET/ACI International

Conference on Recent Advances in Concrete Technology, Supplementary Papers, Las Vegas, Nevada, p. 269–283.

Folliard K.J., M.D.A. Thomas, B. Fournier, K.E. Kurtis, and J.H. Ideker (2007). The Use of Lithium to Prevent or Mitigate Alkali-Silica Reaction in Concrete Pavements and Structures. Publication No. FHWA-HRT-06-133, Office of Infrastructure Research and Development, Federal Highway Administration: p. 47.

Folliard, K. J., R. Barborak, T. Drimalas, L. Du, S. Garber, J. Ideker, T. Ley, S. Williams, M. Juenger, B. Fournier, and M. D.A. Thomas (2006). Preventing ASR/DEF in New Concrete. Report No. 0-4085-5, Center for Transportation Research, University of Texas at Austin, Austin, TX.

French, W. J. (1980). Reactions between aggregates and cement paste-an interpretation of the pessimum. the Quarterly Journal of Enfineering Geology, 13 (4), p. 231-247.

Fournier, B., R. Chevrier, M. DeGrosbois, R. Lisella, K. Folliard, J. Ideker, M. Shehata, M. Thomas, and S. Baxter (2004). The accelerated concrete prism test (60°C): variability of the test method and proposed expansion limits, in:M. Tang,M. Deng (Eds.), 12th International Conference on Alkali–Aggregate Reaction in Concrete, International Academic Publishers—World Publishing Corporation, Beijing, China, p. 314–323.

Garcia-Diaz, E., D. Bulteel, Y. Monnin, P. Degrugilliers, and P. Fasseu (2010). ASR pessimum behaviour of siliceous limestone aggregates. Cem. Concr. Res., v 40, n 4, p. 546-549.

Garcia-Diaz, E., J. Riche, D. Bulteel, and C. Vernet (2006). Mechanism of damage for the alkali silica reaction. Cem. Concr. Res. 36, p. 395–400.

Gao, X. X., S. Multon, M. Cyr, and A. Sellier (2013). Alkali–silica reaction (ASR) expansion: Pessimum effect versus scale effect. Cem. Concr. Res., 44, p. 25–33.

Gillott, J.E. (1975). Alkali–aggregate reactions in concrete, Eng. Geol. 9, p. 303–326.
Glasser, L.S. D. and N. Kataoka (1981). The chemistry of alkali-aggregate reaction. Proceedings of the 5th ICAAR, Cape Town, South Africa, p. 7.

Gillott, J.E., M.A.G. Duncan, and E.G. Swenson (1973). Alkali-Aggregate Reaction in Nova Scotia. IV. Character of the Reaction. Cement Concrete Research, Vol. 3, p. 521-535.

Gogte, B.S. (1973). An evaluation of some common Indian rocks with special reference to alkali–aggregate reactions, Eng. Geol. 7, p. 135–153.

Grattan-Bellew, P.E. (1989). Test Methods and Criteria for Evaluating the Potential Reactivity of Aggregates. Proceedings of the Eighth International Conference on Alkali-Aggregate Reaction in Concrete, Kyoto, Japan, p. 279-294.

Grattan-Bellew, P.E. (1994). Alkali contribution from limestone aggregate to pore solution of old concrete. ACI Mater. J., Am. Concr. Inst., 91, p. 173–177.

Grattan-Bellew, P.E. (1997). A Critical Review of Ultra-Accelerated Tests for Alkali-Silica Reactivity. Cement and Concrete Composites, Vol. 19, p. 403-414.

Grattan-Bellew, P.E. (2001). Petrographic and Technological Methods for Evaluation of Concrete Aggregates, in: V.S. Ramachandran, J.J. Beaudoin (Eds.), Handbook of analytical techniques in concrete science and technology Principles, Techniques, and Applications, Noyes Publications, p. 63–98.

Han, S. and M. Tang (1984). Alkali-aggregate reaction under high temperature, high pressure and high alkali content. Journal of Nanjing Institute of Chemical Technology, 2, p. 1–10.
Hobbs, D.W. in: T. Taylor (Ed.) (1988). Alkali-Silica Reaction in Concrete. London, p. 22–27.

Hasson, G., D. Zollinger, and R. Lytton (2010). Determination of the Main Parameters of Alkali Silica Reaction Using System Identification Method. Journal of Materials in Civil Engineering, Vol. 22, No. 9, p. 865-873.

Hobbs, D.W. (1988). Alkali–silica Reaction in Concrete, Thomas Telford Ltd, London.
Hansen, W. C. (1944). Studies relating to the mechanism by which the alkali-aggregate reaction proceeds in concrete. Journal of the American Concrete Institute, 15(3), p. 213-227.

Hobbs, D.W. and W.A. Gutteridge (1979). Particle size of aggregate and its influence upon the expansion caused by the alkali-silica reaction. Magazine of Concrete Research, 31 (109), p. 235–242.

Hooton, R.D. (1986). Effect of Containers on ASTM C 441—Pyrex Mortar Bar Expansions. Proceedings of the Seventh International Conference on Alkali-Aggregate Reaction in Concrete, p. 351–357.

Ichikawa, T. (2009). Alkali–silica reaction, pessimum effects and pozzolanic effect. Cem. Concr. Res., 39 (8), p. 716–726

Ichikawa, T. and M. Miura (2007). Modified model of alkali-silica reaction, Cem. Concr. Res., v 37, n 9, p. 1291-1297.

Ideker, J.H., K.J. Folliard, B. Fournier, and M.D.A. Thomas (2006). The role of "non-reactive" aggregates in the Accelerated (60 °C) Concrete Prism Test, in: B. Fournier (Ed.), Proceedings from the Marc-André Bérubé Symposium on alkali–aggregate reactivity in concrete, 8th CANMET/ACI International Conference on Recent Advances in Concrete Technology, CANMET, Montreal, Canada, p. 45–70.

John, D. A., A.B. Poole, and I. Sims (1998). Concrete Petrography—A Handbook of Investigative Techniques. Arnold, U.K, p. 474.

Johnston, D.P, D. Stokes, and R. Surdahl (2000). A Kinetic-Based Method for Interpreting ASTM C 1260. Cement Concrete Aggregate, Vol. 22, No. 2, p. 142-149.

Kagimoto, H., I. Inoshita, and M. Kawamura (2004). Threshold OH− concentration in pore solution of mortar using alkali reactive aggregates, in: M. Tang, M. Deng (Eds.), 12th International Conference on Alkali–Aggregate Reaction in Concrete, Beijing, China, p. 728–735.

Kawamura M. and K. Iwahori (2004). ASR Gel Composition and Expansive Pressure in Mortars Under Restraint. Cem. Concr. Res., Vol. 26, p. 47-56.

Kawamura, M., K. Takemoto, and S. Hasaba (1983). Application of quantitative EDXA analyses and microhardness measurements to the study of alkali-silica reaction mechanisms. Proceedings of the Sixth International Conference on Alkalis in Concrete, p. 167–174.

Kawamura, M., N. Arano, and T. Terashima (1998). Composition of ASR gels and expansion of mortars, in: M. Cohen, S. Mindess, J. Skalny (Eds.), Materials Science of Concrete: Special Volume, The Sidney Diamond Symposium, American Ceramic Society, Westerville, OH, p. 261-276.

Knudsen, T. and N. Thaulow (1975). Quantitative microanalyses of alkali–silica gel in concrete. Cem. Concr. Res.. 5. P. 443–454.

Kollek, J.J., S.P. Varma, and C. Zaris (1986). Measurement of OH− concentrations of pore fluids and expansion due to alkali–silica reaction in composite cement mortars. 8th International Congress on the Chemistry of Cement, Rio de Janeiro, p. 183–189.

Kuroda, T., S. Inoue, A. Yoshino, and S. Nishibayashi (2004). Effects of particle size, grading and content of reactive aggregate on ASR expansion of mortars subjected to autoclave method, in: M. Tang, M. Deng (Eds.), 12th International Conference on Alkali-Aggregate Reaction in Concrete, International Academic Publishers, Beijing, China, p. 736–743.

Kuroda T., S. Nishibayashi, S. Inoue, and A. Toshino (2000). Effects of the Particle Size of reactive Fine Aggregate and Accelerated Test Conditions on ASR Expansion of Mortar Bar. Transactions of the Japan Concrete Institute, Vol. 22, p. 113-118.

Lindgård, J., Ö. Andiç-Çakır, I. Fernandes, T. F. Rønning, M.D.A. Thomas (2012). Alkali–silica reactions (ASR): Literature review on parameters influencing laboratory performance testing, Cem. Concr. Res. 42, p. 223–243.

Lorenzo, P., S. Goni, S. Hernandez, and A. Guerrero (1996). Effect of Fly Ashes with High Total Alkali Content in the Alkalinity of the Pore Solution of Hydrated Portland Cement Paste, J. Am. Ceram. Soc. 97 (2), p. 470-474.

Lothenbach, B. and F. Winnefeld (2006). Thermodynamic modelling of the hydration of Portland cement. Cem. Concr. Res., 36, p. 209–226.

Lu, D., B. Fournier, and P. Grattan-Bellew (2006). Effect of aggregate particles size on determining alkali–silica reactivity by accelerated tests, J. ASTM Int. 3, p. 11.

Lu, D., B. Fournier, P. Grattan-Bellew, Y. Lu, Z. Xu, and M. Tang (2008). Expansion behavior of Spratt and Pittsburg limestones in different test procedures, in: M.A.T.M. Broekmans, B.J.Wigum (Eds.), 13th International Conference on Alkali–Aggregate Reactions in Concrete, Trondheim, Norway, p. 619–627.

Ludwig, U. (1981). Effects of Environmental Conditions on Alkali-Aggregate Reaction and Preventive Measures. Proceedings, 8th International Conference on Alkali-Aggregate Reaction in Concrete, Kyoto, Japan, p. 583-596.

McGowan, J. K. and H. E. Vivian (1952). Studies in cement-aggregate reaction: Correlation between crack development and expansion of mortars. Australian Journal of Applied Science, 3, p. 228–232.

Mehta, P.K. and P.J.M. Monteiro, (1992). Concrete: Structure, Properties, and Materials (2nd Edition.). Prentice Hall, Upper Saddle River, New Jersey.

Mindess, S., J.F. Young, and D. Darwin, (2003). Concrete, Prentice Hall, Upper Saddle River, New Jersey.

Moisson, M., M. Cyr, E. Ringot, and A. Carles-Gibergues (2004). Efficiency of reactive aggregate powder in controlling the expansion of concrete affected by alkali–silica reaction (ASR), in: M. Tang, M. Deng (Eds.), 12th International Conference on Alkali-Aggregate Reaction in Concrete, International Academic Publishers, Beijing, China, p. 617–624.

Morey, G. W., R. O. Fournier, and J. J. Rowe (1964). The solubility of amorphous silica at 25 ^{o}C. J. of Geophysical Research, Vol. 69 (10), p 1995-2002.

Mukhopadhyay, A.K. and D.G. Zollinger (2009). Development of Dilatometer Test Method to Measure Coefficient of Thermal Expansion (CoTE) of Aggregates. Journal of Materials in Civil Engineering, Vol. 21, Issue 12.

Mukhopadhyay, A. K., C. Shon, and D. Zollinger (2006). Activation Energy of Alkali-Silica Reaction and Dilatometer Method. In Transportation Research Record: Journal of Transportation Research Board, No. 1979, Transportation Research Board of the National Academies, Washington D.C., p. 1-11.

Mukhopadhyay, A. K., G. Hassan, K. W. Liu, and D. Zollinger (2012). A New Kinetic Type Rapid Aggregate ASR Test Method. In Proceedings of the 14th International Conference on Alkali-Aggregate Reaction in Concrete, CD-ROM, Austin, Texas.

Mukhopadhyay, A. K., H. Ghanem, C. S. Shon, D. Zollinger, D. Gress, and D. Hooton (2009). Mitigation of ASR in Concrete-Combined Materials Test Procedure. IPRF Report (DOT/FAA-01-G-003-2, accessible at http://www.iprf.org/products/IPRF-03-2-Final%20Report-12.7.09.pdf)

Mukhopadhyay A.K., S. Neekhra and D.G. Zollinger (2004). New Mineralogical Approach to Predict Aggregate and Concrete Coefficient of Thermal Expansion (CoTE). Presented (04-4167, Compendium of papers CD-ROM) in Transportation Research Board, Washington D.C.

Multon, S., M. Cyr, A. Sellier, N. Leklou, and L. Petit (2008). Coupled effects of aggregate size and alkali content on ASR expansion. Cem. Concr. Res. 38, p. 350–359.

Nilsson, L. O.(2006). Modelling moisture conditions in cementitious materials—some present challenges. 2nd International Symposium on Advances in Concrete through Science and Engineering, Quebec City, Canada.

Nixon, P.J. and I. Sims (1992). RILEM TC106 Alkali Aggregate Reaction–Accelerated Tests Interim Report and Summary of Survey of National Specifications. Proceedings of the Ninth International Conference on Alkali-Aggregate Reaction in Concrete, Concrete Society, Slough, England, Vol. 2, p. 731–738.

Olafsson H. and N. Thaulow (1983). Alkali-Silica Reactivity of Sands, Comparison of Various Test Methods. Proceedings of the 6th International Conference on Alkalis in Concrete.

Ostertag, C. P., C. Yi, and P. Monteiro (2007). Effect of Confinement on Properties and Characteristics of Alkali-Silica reaction Gel. ACI Materials Journal, 104-M30, p. 276–282.

Pedneault, A., (1996). Development of Testing and Analytical Procedures for the Evaluation of the Residual Potential of Reaction, Expansion, and Deterioration of Concrete Affected by ASR. M.Sc. Memoir, Laval University, Québec City, Canada, p. 133.

Pierce, E. M., E.A. Rodriguez, L.J. Calligan, W.J. Shaw, and B.P. McGrail (2008). Appl. Geochem., 23, p. 2559–2573.

Ponce, J. M. and O. R. Batic (2006). Different manifestations of the alkali-silica reaction in concrete according to the reaction kinetics of the reactive aggregate. Cem. Concr. Res., 36, p. 1148–1156.

Poole, A.B. (1992) Alkali-silica reactivity mechanisms of gel formation and expansion. Proceedings of the 9th ICAAR, In: Concr. Soc. Publ. CS104 1 (editor): London, England, p. 782–789.

Powers, T. C., and H. H. Steinour (1955). An investigation of some published researches on alkali-aggregate reaction: I. the chemical reactions and mechanism of expansion. Journal of the American Concrete Institute, 26(6), p. 497–516.

Prezzi, M., P. J. M. Monteiro, and G. Sposito (1997). Alkali-silica reaction - Part 1: Use of the double-layer theory to explain the behavior of the reaction product gels. ACI Journal, 94(1), p. 10-17.

Ramyar, K., A. Topal, and Ö. Andiç-Çakır (2005). Effects of aggregate size and angularity on alkali–silica reaction, Cem. Concr. Res., 35, p. 2165–2169.

Ranc, R. and Debray, L (1992). Reference Test Methods and a Performance Criterion for Concrete Structures. The 9th International Conference on Alkali-Aggregate Reaction in Concrete, London, U.K., p. 824-831.

Regourd., M. (1989). Products of reaction and petrographic examination, 8th International Conference on Alkali–Aggregate Reactions in Concrete, Kyoto, p. 445–456.

Regourd, M., and H. Hornain (1986). Microstructure of reaction products, in: P.E. Grattan-Bellew (Ed.). 7th International Conference on Alkali–Aggregate Reactions in Concrete, Ottawa, p. 375–380.

RILEM TC 191-ARP (2003): Alkali-reactivity and prevention—assessment, specification and diagnosis of alkali-reactivity. RILEM recommended test method AAR-1: detection of potential alkali-reactivity of aggregates—petrographic method. Mater. Struct. 36, p. 480–496.

Rivard, P., M. A. Bérubé, J.-P. Ollivier, and G. Ballivy (2003). Alkali mass balance during the accelerated concrete prism test for alkali–aggregate reactivity, Cem. Concr. Res., 33, p. 1147–1153.

Rodrigues, F. A., P. J. M. Monteiro, and G. Sposito (1999). The alkali-aggregate reaction: The surface charge density of silica and its effect on the expansive pressure. Cem. Concr. Res., 29(4), p. 527-53.

Rogers, C.A. and R.D. Hooton (1989). Leaching of Alkalis in Alkali-Aggregate Reaction Testing. Proceedings of the Eight International Conferences on Alkali-Aggregate Reaction, p. 327–332.

Sarkar, S.L., D.G. Zollinger, A.K. Mukhopadhyay and L. Seungwook (2004). Appendix 1 Handbook for Identification of Alkali-Silica Reactivity, Airfield Pavement, Advisory Circular No. 150/5380-8, U.S. Department of Transportation Federal Aviation Administration.

Shayan, A., A. Xu, H. Morris (2008). Comparative study of the concrete prism test (CPT 60°C, 100% RH) and other accelerated tests, in: M.A.T.M. Broekmans, B.J. Wigum (Eds.), 13th International Conference on Alkali–Aggregate Reactions in Concrete, Trondheim, Norway, p. 391–400.

Shao, Y., T. Lefort, S. Moras, and D. Rodriguez (2000). Studies on concrete containing ground waste glass. Cem. Concr. Res., 30 (1), p. 91–100.

Shayan, A. (1992). The pessimum effect in an accelerated mortar bar test using 1 M NaOH solution at 80°C. Cem. Concr. Compos. 14, p.249–255.

Shayan, A. (2002). Value-added Utilisation of Waste Glass in Concrete, in: IABSE Symposium Melbourne.

Shehata, M.H. and M.D.A. Thomas (2000). The Effect of Fly Ash Composition on the Expansion of Concrete Due to Alkali Silica Reaction. Cem. Concr. Res., Vol. 60, No. 7, p. 1063-1072

Shehata, M.H. and M.D.A. Thomas (2006). Alkali release characteristics of blended cements. Cem. Concr. Res., 36, p. 1166–1175.

Shon, C. S., A.K. Mukhopadhyay, and D.G. Zollinger (2007). Alkali-Silica Reactivity of Aggregate and Concrete Evaluated by Dilatometer Method: Performance-Based Approach. Journal of the Transportation Research Board, No. 2020, p. 10-19.

Shon, C. S., D.G. Zollinger, and S.L. Sarkar (2003). Application of Modified ASTM C 1260 Test for Fly Ash-Cement Mixtures, Journal of the Transportation Research Board 1834, p. 93-106.

Shon, C. S., S. Lim, A.K. Mukhopadhyay, D.G. Zollinger, and S.L. Sarkar (2002). New Aggregate Characterization Tests for Thermal and ASR Reactivity Properties. Proceedings, 10th International Conference for Aggregates Research (ICAR) Annual Symposium.

Shon, C. S., S.L. Sarkar, and D.G. Zollinger (2004). Testing the Effectiveness of Class C and Class F Fly Ash in Controlling Expansion due to Alkali-Silica Reaction Using Modified ASTM C 1260 Test Method, Journal of Materials in Civil Engineering Vol. 16, No. 1, p. 20-27.

Sibbick, R.G. and C.L. Page (1992). Threshold alkali contents for expansion of concretes containing British aggregates. Cem. Concr. Res., 22, p. 990–994.

Sorrentino, D., J.Y. Clement, and J.M. Golberg (1992). A New Approach to Characterize the Chemical Reactivity of the Aggregates. Proceedings, 9th International Conference on Alkali-Aggregate Reaction in Concrete, Slough, England, p. 1009-1016.

Stanton, D.E. (1940). Expansion of concrete through reaction between cement and aggregate. American Society of Civil Engineers, 66, p. 1781–1811.

Tang, M.S. and H. Su-Fen, (1980). Effect of Ca(OH)2 on Alkali-Silica Reaction, Proceedings of the Eight International Congress of Cement Chemistry. Paris, France, Vol. 2, p. 94–99.

Tatematsu, H. and T. Sasaki, (1989). Proposal of a New Index for a Modified Chemical Method. Proceedings, 8th International Conference on Alkali-Aggregate Reaction in Concrete, Kyoto, Japan, p. 333-338.

Thaulow, N., U.H. Jakobsen, and B. Clark (1996). Composition of alkali silica gel and ettringite in concrete railroad ties: SEM-EDX and X-ray diffraction analyses. Cem. Concr. Res., 26, p. 309–318.

Thomas, M., B. Fournier, K. Folliard, J. Ideker, and M. Shehata (2006). Test methods for evaluating preventive measures for controlling expansion due to alkali–silica reaction in concrete. Cem. Concr. Res., 36, p. 1842–1856.

Touma, W., D. Fowler, R. Carrasquillo, K. J. Folliard, and N. R. Nelson (2001). Characterizing the Alkali-Silica Reactivity of Aggregates Using ASTM C 1293, ASTM C 1260, and Their Modifications. Journal of the Transportation Research Board, Transportation Research Board, No. 1757, p. 157-165.

Turriziani, R., (1986). Internal Degradation of Concrete: Alkali Aggregate Reaction. Reinforcement Steel Corrosion, Proceedings of the 8th International Congress on the Chemistry of Cement, Rio de Janeiro, Brazil, September, Vol. I, p. 388-442.

Uomoto, T, Y. Furusawa, and H. Ohga (1992). A Simple Kinetics Based Model for Predicting Alkali Silica Reaction. In Proceedings of the 9th International Conference on Alkali-Aggregate Reaction in Concrete, London, England, Vol.2, p. 1077-1084.

Utton, C. A., R.J. Hand, P.A. Bingham, N.C. Hyatt, S.W. Swanton, and S.J. Williams (2013). Dissolution of vitrified wastes in a high-pH calcium-rich solution. J. of nuclear Materials, Vol. 433, p. 112-122.

Verstraete, J., L. Khouchaf, D. Bulteel, E. Garcia-Diaz, A.M. Flank, and M.H. Tuilier (2004). Amorphisation mechanism of a flint aggregate during the alkali-silica reaction: X-ray diffraction and X-ray absorption XANES contributions, Cem. Concr. Res., v 34, n 4, p. 581-586.

Vivian, H.E. (1947). The effects on mortar expansion of reactive component in the aggregate. Studies in cement–aggregate reactions, part 10, CSIRO Bull. 256, p. 13–20.

Vivian, H.E., (1981). A Working Appraisal of Alkali-Aggregate Reaction in Concrete. Proceedings of the 5th International Conference on Alkali-Aggregate Reaction in Concrete, Cape Town, South Africa, Paper S252/14.

Wang, H. and J.E. Gillott (1991). Mechanisms of alkali-silica reaction and significance of calcium hydroxide. Cem. Concr. Res., 21, p. 647–654.

Wenk, H.R., P.J. Monteiro, and K. Shomglin (2008). Relationship between aggregate microstructure and mortar expansion. A case study of deformed granitic rocks from the Santa Rosa mylonite zone, J. Mater. Sci. 43, p. 1278–1285.

Woods, H. (1968). Durability of Concrete Construction. Monograph, vol. 4, American Concrete Institute, Detroit, Michigan.

Zhang, C., A. Wang, M. Tang, B. Wu, and N. Zhang (1999). Influence of aggregate size and aggregate size grading on ASR expansion. Cem. Concr. Res. 29. P. 1393–1396.

Zhang, X. and G.W. Groves (1990). The alkali–silica reaction in OPC-silica glass mortar with particular reference to pessimum effects. Adv. Cem. Res., 3 (9), p. 9–13.

APPENDIX A – STANDARD TEST METHOD FOR DETERMINATION OF COMPOSITE ACTIVATION ENERGY OF AGGREGATE DUE TO ALKALI-SILICA REACTION (CHEMICAL METHOD)

Test Procedure for

Standard Test Method for Determination of Composite Activation Energy of Aggregates Due to Alkali-Silica Reaction (Chemical Method)

TxDOT Designation: Tex-XXX-E

Date: October 2013

1. SCOPE

1.1 This test method covers chemical determination of the reactivity of an as-received aggregate in terms of measuring composite activation energy of alkali silica reaction where aggregate reacts with alkaline solution of chemistry similar to pore solution chemistry of Portland-cement concrete.

1.2 This test is intended to offer a rapid and reliable ASR standard test method. A test method where as-received aggregates are immersed in alkaline solution and allowed to react at different temperatures. The test measures solution volume change (i.e., volume contraction) in a closed system over time (till 4–5 days) as the reaction between aggregates and solution proceeds.

1.3 The test method is developed to determine aggregate composite activation energy (CAE) of ASR. CAE is a measure of aggregate alkali-silica reactivity and is a potential screening parameter to develop CAE based aggregate classification system. The lower the CAE the higher is the reactivity.

1.4 The test method reliably predicts aggregate alkali reactivity in a short period of time and can be effectively used as an alternative to the current test method (ASTM C 1260).

2. DEFINITION

2.1 Dry Unit Weight-as defined in ASTM Test Method C 138 for fine and coarse aggregates.

2.2 For definitions of other terms relating to concrete or aggregates, see ASTM Terminology C 125.

3. APPARATUS

3.1 Scales—The scales and weights used for weighing materials shall conform to the requirements prescribed in Specification C 1005.

3.2 Crushing Equipment—A small jaw crusher or other suitable equipment capable of crushing aggregate to pass a 1 ½" sieve.

3.3 Sieves— A 25.4-mm (1"), 12.5-mm (1/2"), 4.75-mm (No. 4), 2.36-mm (No. 8), 1.18-mm (No. 16), 600-µm (No. 30), 300-µm (No. 50), 150-µm (No. 100) sieve.

3.4 De-Airator/Vacuum Pump—A small vacuum pump or other suitable equipment to apply a vacuum pressure of 30 in-Hg.

3.5 Vibrating Table—A vibrating table with variable-speed control keeps sample material loose.

3.6 Glassware—All glass apparatus and vessels should be carefully selected to meet the particular requirements for each operation. Standard volumetric flasks, burets, and pipets should be of precision grade.

3.7 The VCMD device (Figure 1, Note 1) consists of a stainless steel pot (Figure 1a), a brass lid (Figure 1a), a stainless steel hollow tower (Figure 1b), a brass housing to hold linear variable differential transducer (LVDT) with perfect vertical alignment (Figure 1c and 1d), and a stainless steel float (Figure 2). A detailed drawing of the individual parts (Figs. 1a, b, c, and d) and assembled view with all these parts together (Figure 1) are presented below. One end of Tower (Figure 1b) is screwed into the lid (Figure 1a) and the other end screwed into the LVDT housing (Figure 1c) with O-rings in all three junctions (i.e., (i) between the pot and lid, (ii) between the lid and tower and (iii) between the tower and LVDT housing). The LVDT (Note 2) is placed into the center hole of the LVDT housing and pushed into a O-ring (2-112 buna-n) placed at the bottom of the LVDT. With the proper tightening of the six set screws (come though the side of the housing), a perfect vertical alignment of the LVT is ensured.

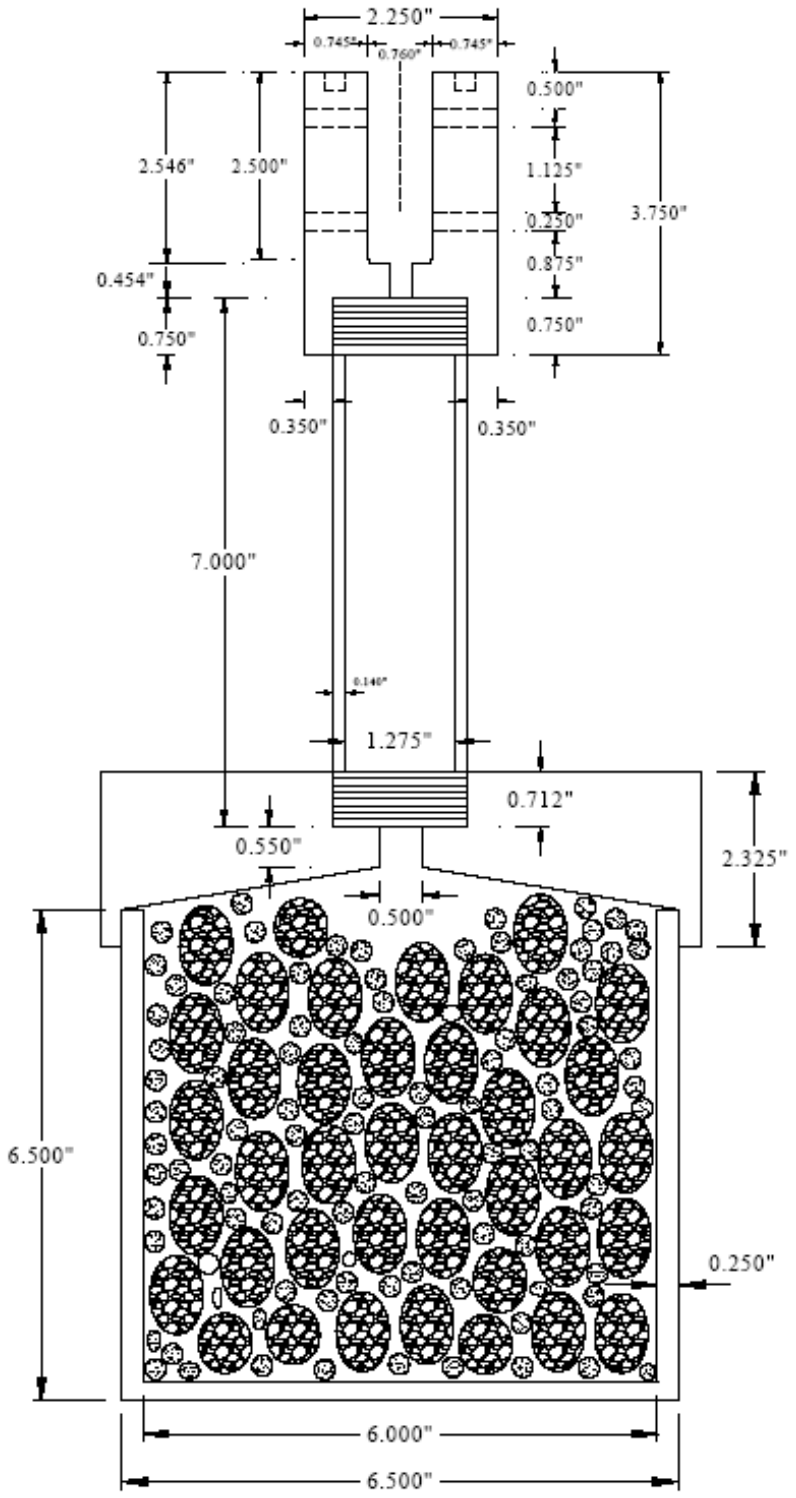

Figure 1 Cross-Sectional View of the Device

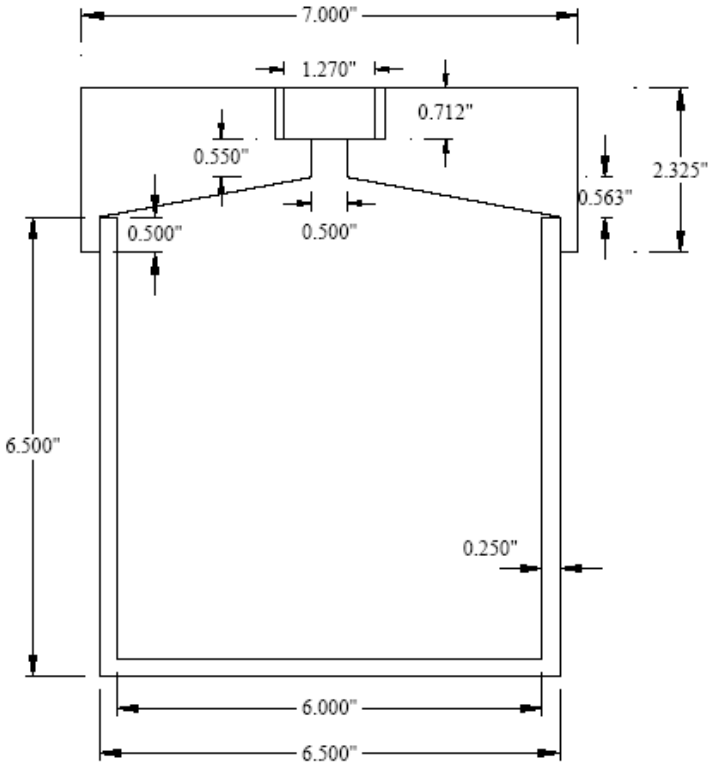

Figure 1a Stainless Steel Pot + Brass Lid

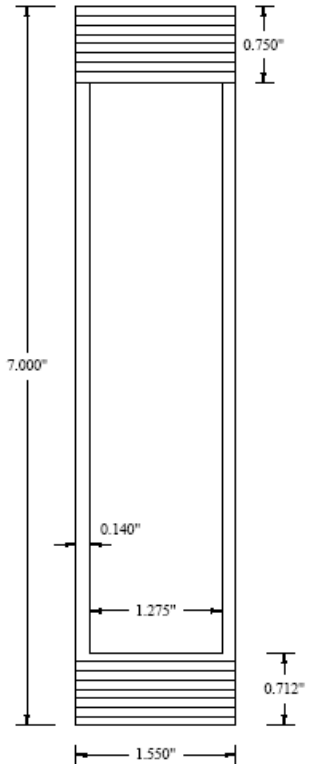

Figure 1b Stainless Tower

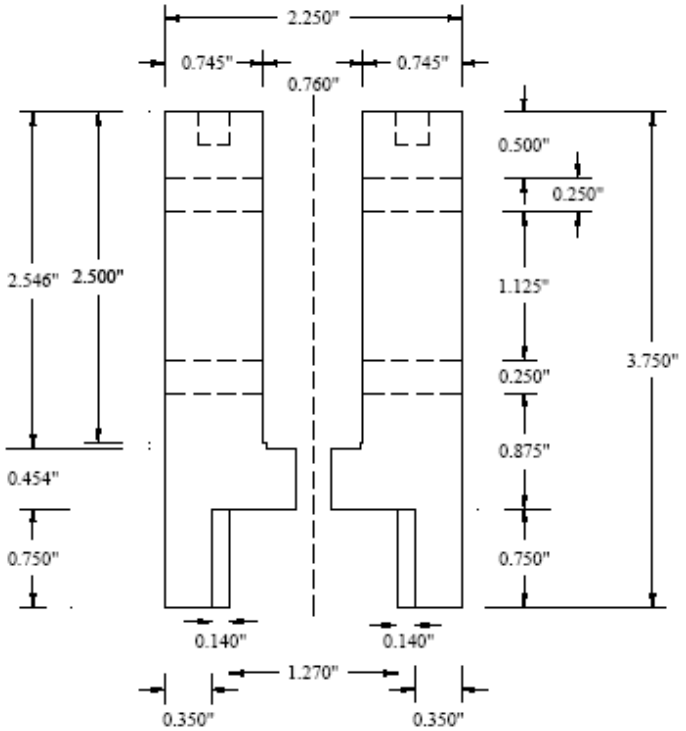

Figure 1c LVDT Housing

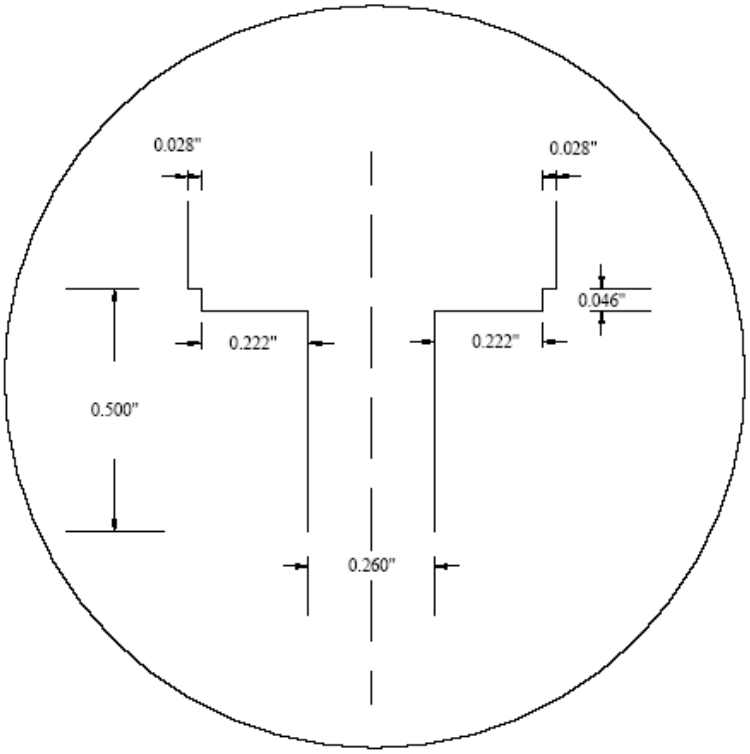

Figure 1d Detailed Drawings of the Central Part of the Housing in Figure 1c

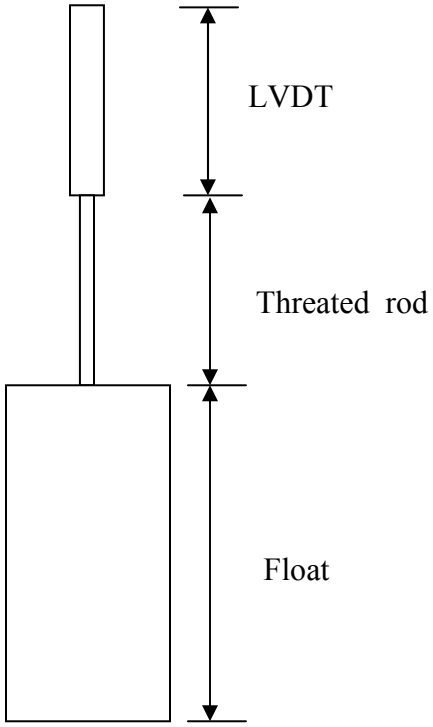

Figure 2 A Schematic Diagram of the Float System

3.8 Oven-A convection oven with temperature control in the range of 40.0 to 100.0±1.0°C.

3.9 The combinations of number of oven and VCMD to measure activation energy at one level of alkalinity are summarized in Table 3 (X1).

Note 1-The pot is made of Stainless steel: "1.4401 X5CrNiMo17-12-2 316 S31600" (ASTM C 182). The type of brass used for the lid is the Naval brass (ASTM B 21); similar to admiralty brass; is a 40 percent zinc brass and 1 percent tin. The tower is made from Stainless steel S31600 (ASTM C 182).

Note 2- The LVDT should have a nominal linear range of ±1 inch and operating temperature range up to 150°C.

4. REAGENTS AND MATERIALS

4.1 Sodium Hydroxide (NaOH)-UPS or technical grade may be used, provided the Na^+ and OH^- concentrations are shown by chemical analysis to lie between 0.49N and 0.51N.

4.2 Calcium Hydroxide ($Ca(OH)_2$)- UPS or technical grade may be used.

4.3 Purity of water-De-ionized or distilled water is recommended (ASTM D 1193).

4.4 Soak Solution-Each liter of solution shall contain 20.0 g of NaOH dissolved in 900 ml of water, and shall be diluted with additional deionized or distilled water to obtain 1.0 L of solution. Additional 1 g of $Ca(OH)_2$ per liter need to be added in order to saturate the solution.

Warning-Before using NaOH, review (1) the safety precautions for using NaOH; (2) first aid for burns; and (3) the emergency response to spills, as described in the manufacturer's Material Safety Data Sheet or other reliable safety literature. NaOH can cause very severe burns and injury to unprotected skin and eyes. These should include full-face shields, rubber aprons, and gloves impervious to NaOH. Gloves should be checked periodically for pin holes.

5. SAMPLE PREPARATION

5.1.1 Obtain as-received bulk aggregate sample and wash in accordance with ASTM D75. Dry the aggregate samples to essentially constant mass, preferably in an oven at 110 ± 5°C (230 ± 9°F) in accordance with Test Method C 29. A fixed representative gradation is selected for both coarse and fine aggregates (Tables 1 and 2) in order to compare the results between different aggregates. As a result, the oven dried aggregates need to be sieved out in order to separate the different

size fractions (Tables 1 and 2). To prepare a test sample, recombine these size fractions according to the gradation requirement in Tables 1 and 2 for fine and coarse aggregates, respectively.

5.2 Dry unit weight-as defined in Test Method C 138 for fine and coarse aggregates.

5.3 Number of Samples – Test three samples (at least two) for each temperature to verify repeatability. Each test sample is around 8 to 9 lb depending on the dry unit weight of aggregate (ASTM C 29).

TABLE 1 Grading Requirements for Fine Aggregates

Sieve Size		Mass, %
Passing	Retained on	
9.5 mm (3/8")	4.75 mm (No. 4)	4
4.75 mm (No. 4)	2.36 mm (No. 8)	13
2.36 mm (No. 8)	1.18 mm (No. 16)	17
1.18 mm (No. 16)	600 μm (No. 30)	38
600 μm (No. 30)	300 μm (No. 50)	23
300 μm (No. 50)	150 μm (No. 100)	5

TABLE 2 Grading Requirements for Coarse Aggregates

Sieve Size		Mass, %
Passing	Retained on	
9.5 mm (1 1/2")	25.4 mm (1")	2
25.4 mm (1")	12.5 mm (1/2")	43
12.5 mm (1/2")	4.75 mm (No. 4)	54
4.75 mm (No. 4)	2.36 mm (No. 8)	1

6. PROCEDURE

6.1 Determine the weight of the test sample based on the unit weight (sub-section 7.2) to fill 80% of the pot volume (~ 8-9 lb)

6.1.1 Add alkaline solution (0.5N NaOH + saturated $Ca(OH)_2$) [sub-section 6.4] to the pot till the aggregate sample is immersed. For fine aggregates, poking the aggregate with a metal rod will accelerate penetration of the solution to the bottom of the pot. Gently tap the side of the pot to remove any large air bubbles.

6.2 Screw the lid onto the pot with proper placement of the O-ring. Make sure the lid is properly seated and tightened. Add some more solution through the tower to the pot to ensure that the aggregate sample is fully immersed. Screw the tower with the lid.

6.3 Connect vacuum system to the tower. Turn on the vacuum pump and wait until vacuum of at least 25-inch Hg is achieved within 5 minutes. An attainment of the above vacuum is an indication of the leak-proof situation of the pot-lid-tower assembled system. If the expected vacuum is not achieved, it possibly indicates some leaking though the pot-lid junction and the following actions, i.e., (i) tightening the lid and / or (ii) remove the lid followed by rechecking/replacing the O-ring followed by reassemble and vacuum test again should be performed in order to ensure leak-proof situation. Turn off the vacuum pump when proper vacuum is achieved.

6.4 Keep the pot to stand overnight under room temperature to allow aggregate saturation. Rubber stopper or cork can be placed at the top of the tower to reduce solution loss due to evaporation.

6.5 Place the pot on vibro-deairator and connect to vacuum system to the tower. Vacuum under low vibration for 2 hours to remove air bubbles and ensures further saturation. The vacuum of at least 25-inch Hg is required. Repeat the same procedure (sub-section 8.4) if the expected vacuum is not achieved.

6.6 Place the pot in the oven and heat it to a temperature of 60°C with rubber stopper or cork at the top of the tower. It takes around 3 hours to reach 60°C from the room temperature (23°C).

6.7 Remove the pot from the oven and place it on vibro-deairator and connect to the vacuum system again in order to apply a second stage of vacuuming at high temperature under light vibration for 45 minutes. This facilitates further removal of air bubbles that may generate during heating and ensures an almost fully saturation stage. The vacuum of at least 25-inch Hg is required (as in sub-section 8.6).

6.8 Remove the pot from vibro-vacuum system and place inside the oven.

6.9 The stainless steel float with threaded and LVDT rod (Figure 2) is weighted and then inserted through the tower. The LVDT housing is then placed at the top of the tower. Insert the LVDT into the housing and ensure perfect vertical alignment (Note 3).

6.10 View float level (i.e., measure of solution level) from the LVDT displacement reading on the computer and adjust alkaline solution level (remove LVDT and pour or remove solution through the tower) in order to achieve appropriate initial level (Note 4).

6.11 Finally, the LVDT is securely placed in the LVDT housing using set of screws (section 5.7) and ensure a perfect vertical alignment.

6.12 Set up the oven temperature to the selected target temperature (60 or 70 or 80°C) and let the computer record the solution volume change in a form of float movement through LVDT-data acquisition system over time (4 days).

Note 3- The free movement of the float is assured by rotating the LVDT. This removes any sticking issues due to improper placement of the float system.

Note 4- An initial float level of -0.9 to -0.8 is the best to accommodate high net solution volume expansion (thermal expansion) due to temperature change from the starting temperature (temperature after second stage vacuum, i.e., sub-section 8.8) to the target temperatures (60, 70, and 80°C) with a LVDT of −1 to 1 inch measurement range.

6.13 Terminate the test and remove the device from the oven. Allow the device to cool down before removing the LVDT. Unscrew the set screws from the side of the LVDT housing and remove the LVDT housing (Note 5).

6.14 Unscrew the lid from the pot (Note 6). Remove the sample from the pot and thoroughly clean the pot, lid, and tower (Note 7).

6.15 Repeat the procedures (8.1-8.15) for the remaining two temperatures.

Note 5-When remove the housing from the tower, use care to avoid bending the thread and / or LVDT rod connecting the float to the LVDT. Dry and weigh the float and compare the mass to the initial mass. If the mass has increased by more than a few tenths of a gram, the float most likely has a leak. Check that the O-ring between the pot and lid is not cracked or otherwise damaged, discolored or dirty. Make sure that the groove on which the O-ring sits is clean.

Note 6-It may be necessary to tap on the handles with a rubber mallet to break the lid loose.

Note 7- Scrub the inside of the pot with steel wool and water. DO NOT use soap or detergent. Rinse all parts thoroughly with de-ionized or distilled water after cleaning.

7. CALCULATION

7.1 Reference Reading- Average of 1 hour LVDT reading at the thermally stabilized period (It takes around 5 to 8 hrs for the alkaline solution to reach the target temperature and be stabilized at that temperature) represents the reference level (Figure 3 X2.) or initial level for ASR.

7.2 Calculate the displacement due to ASR (Δh) (Figure 3 X2.).

7.3 Multiply the calibrated displacement by the area of the tower and divide by the volume of the sample to obtain the change in solution volume due to ASR. Calculate the volume change at percentage as follows:

$$V(\%) = \frac{\Delta V_{ASR}}{V_{Aggregate}} \times 100$$

$$\Delta V_{ASR} = r^2 \pi \Delta h$$

where:

V(%)= Percent volume change of solution due to ASR.

ΔV_{ASR}= Measured volume change of solution due to ASR.

$V_{Aggregate}$= Initial volume of aggregate (80% of the pot).

r= Radius of the tower

7.4 Activation Energy -A kinetic-type model (Note 9) below is used to model measured non-linear type volume change data over time. By fitting the model to measured volume change data over time, the reaction rate (β) is calculated.

$$\varepsilon = \varepsilon_0 \cdot e^{-(\frac{\rho}{t - t_0})}$$

where:

ε_0 = ASR ultimate volume change.

β = Rate constant.

t_0 = Theoretical Initial time of ASR (hr).

ρ = Time corresponding to a volume change ($\varepsilon_0/\varepsilon$).

7.5 The rate constant (β) values at multiple temperatures (minimum 3 temperatures) are then determined and Ea is calculated by plotting ln(β) versus (1/T).

7.6 The slope of the linear regression is equal to (-Ea/R) based on rate theory, where R is the universal gas constant and Ea is the activation energy (KJ/mol).

7.7 Data from at least three temperatures must be generated at the recommended testing period of 4 days to determine aggregate activation energy (Note 10).

Note 8- Plot the LVDT displacement of each float versus time. Check for sticking of the LVDT which will appear as a flat line in the plot often followed by a large change in displacement

Note 9- A computer program is developed for activation energy calculation. The program can be downloaded via Texas A&M Transportation Institute. The computer system requires MATLAB 7.11.0.584 (R2010b) and Microsoft Office Excel 2007.

Note 10-The activation energy is the energy barrier that has to overcome to initiate ASR taking into account the combined effect of alkalinity, temperature,

and time. The concept of ASR Ea can be considered as a composite single parameter of alkali silica reactivity of different reactive component(s) in aggregate. The use of term “composite activation energy” will be more appropriate than “activation energy” for heterogeneous and multi-phase aggregate materials.

8. REPORT

8.1 Report the following information:

8.1.1 Type and source of aggregate.

8.1.2 A plot of measured and calculated solution volume change over time at three different temperatures.

8.1.3 Rate constant of solution volume change at three temperatures.

8.1.4 Calculated activation energy for the material.

9. PRECISION AND BIAS

9.1 Within-Laboratory Precision-It has been found that the average within-laboratory coefficient of variation for materials with reaction rate at the same test conditions is within 10%. The reaction rate within the same laboratory under the same condition should not differ by more than 15%.

9.2 Bias-Since there is no accepted reference material for determining the bias of this test method, no statement is being mad.

APPENDIX
(Nonmandatory Information)

X1. Table 3 Combinations of Oven and VCMD

Option	60°C	70°C	80°C	No. of VCMDs	No. of Oven	No. of Days	Activation Energy
1	3	3	3	9	3	5	3 replicas
2	2	2	2	6	3	5	2 replicas
3	1	1	1	3	3	5	without replicas
4	1	1	1	3	1	15	3 replicas for a single aggregate E_a without replicas for 3 aggregates
5	3	3	3	8	2	15	1^{st} aggr. -E_a with 3 replicas 2^{nd} aggr. - E_a with 3 replicas 3^{rd} aggr. - E_a with 2 replicas
						10	1^{st} aggr. - E_a with 3 replicas 2^{nd} aggr. - E_a W/O replicas

Options 1 and 2 are the ideal combinations; 3 and 4 are minimum requirements for determination of activation energy; 5 is the current combination for this test.

X2. Reference Reading

Average of 1 hour LVDT reading at the thermally stabilized period after the target temperature is reached represents the reference / initial level for ASR. Subtract the subsequent LVDT displacement values from the reference level to obtain the displacement (Δh) due to ASR.

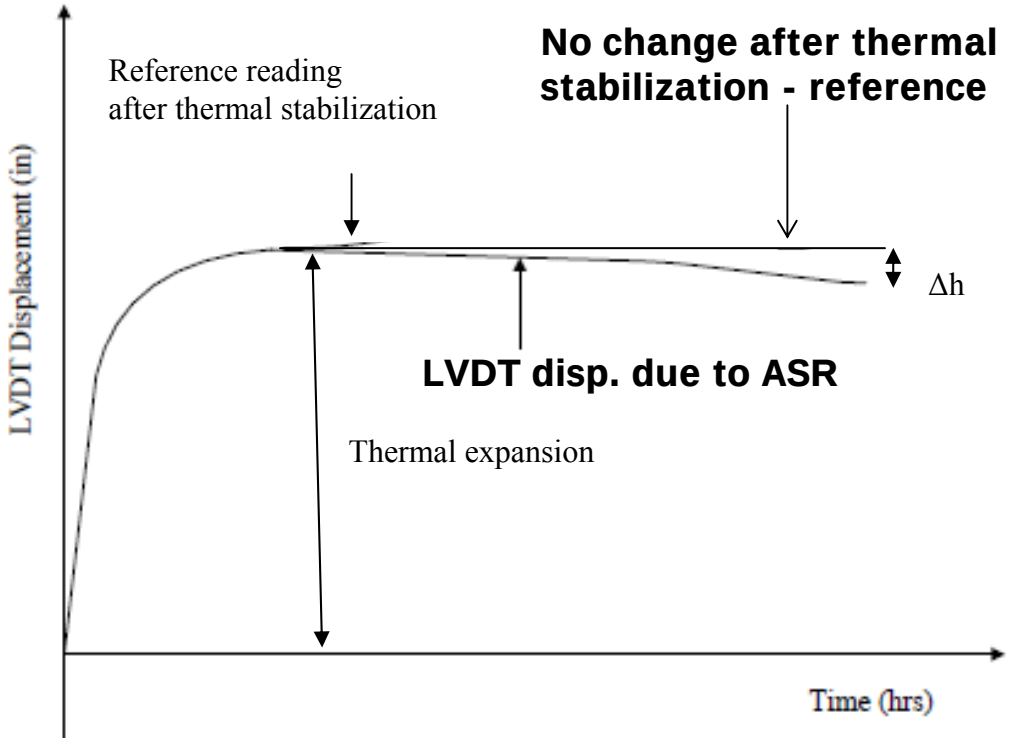

Figure 3 A Schematic Draw of Reference Reading

APPENDIX B – AVERAGE SOLUTION VOLUME CHANGE OVER TIME AT DIFFERENT TEMPERATURES AND ALKALINITIES FOR THE TESTED AGGREGATES

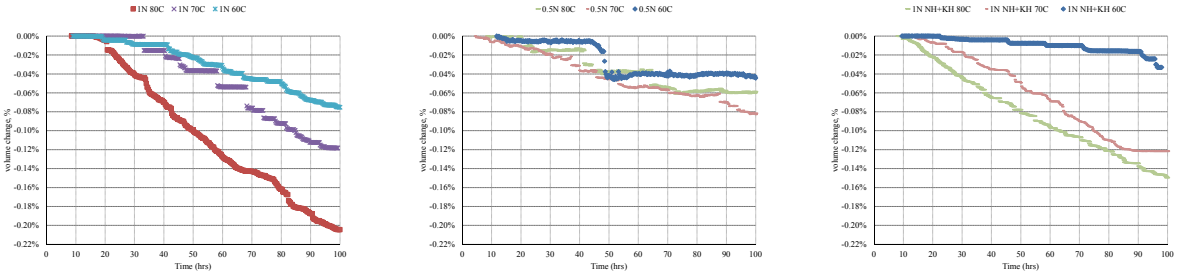

Figure B1 Solution Volume Change with 3 Alkalinities (1N NH + CH, 0.5N NH + CH, and 1N NH + KH + CH) at 3 Temperatures (60, 70, and 80°C) for Borosilicate Glass

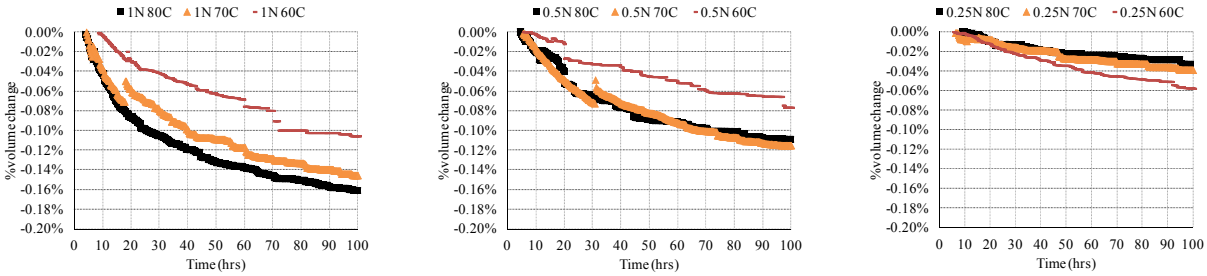

Figure B2 Solution Volume Change with 3 Alkalinities (1, 0.5, and 0.25N NH + CH) at 3 Temperatures (60, 70, and 80°C) for FA1

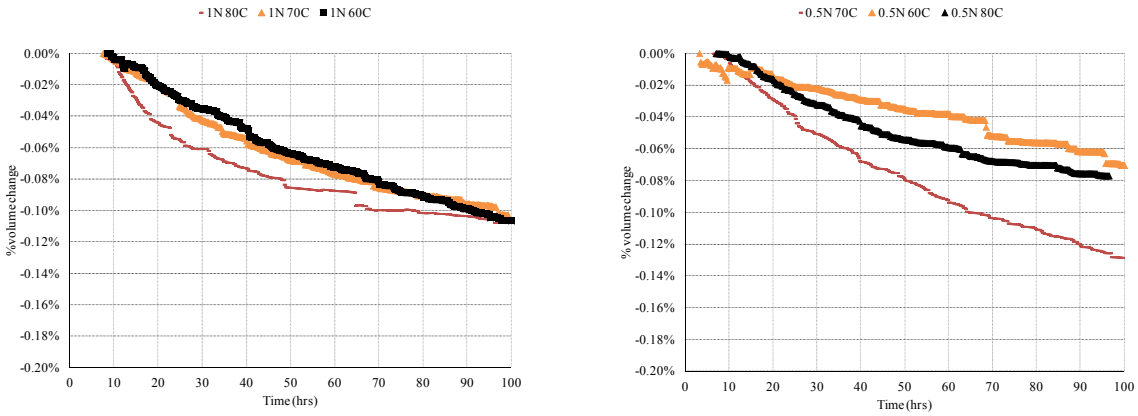

Figure B3 Solution Volume Change with 2 Alkalinities (1 and 0.5N NH + CH) at 3 Temperatures (60, 70, and 80°C) for FA2

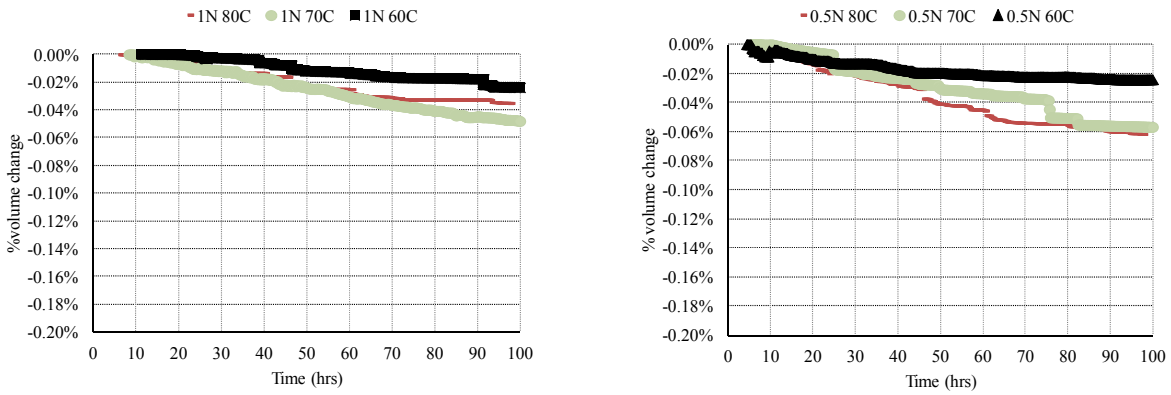

Figure B4 Solution Volume Change with 2 Alkalinities (1 and 0.5N NH + CH) at 3 Temperatures (60, 70, and 80°C) for FA3

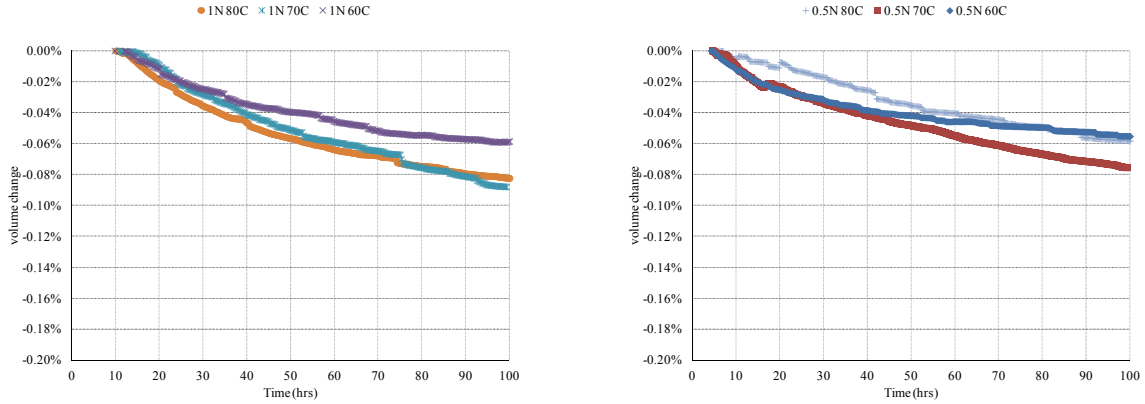

Figure B5 Solution Volume Change with 2 Alkalinities (1 and 0.5N NH + CH) at 3 Temperatures (60, 70, and 80°C) for FA4

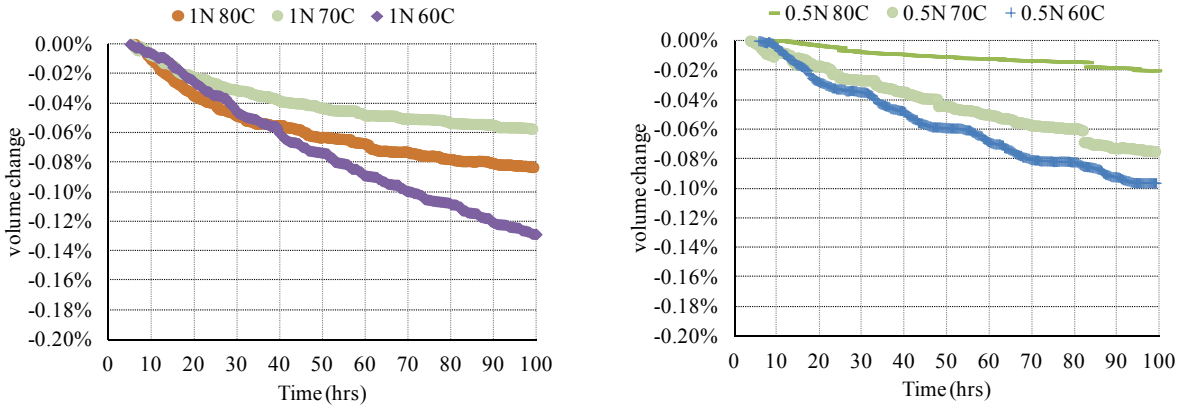

Figure B6 Solution Volume Change with 2 Alkalinities (1 and 0.5N NH + CH) at 3 Temperatures (60, 70, and 80°C) for FA5

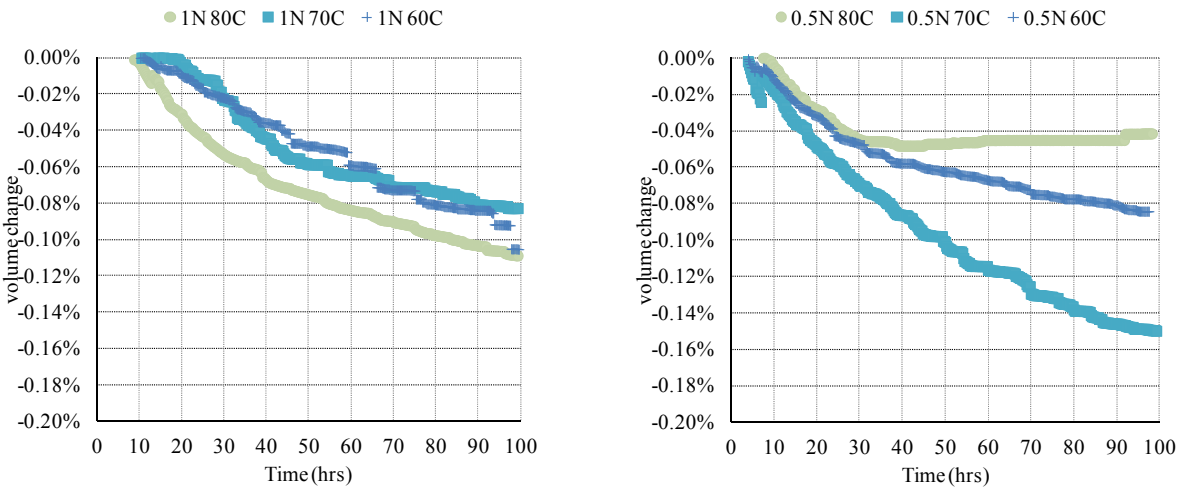

Figure B7 Solution Volume Change with 2 Alkalinities (1 and 0.5N NH + CH) at 3 Temperatures (60, 70, and 80°C) for CA1

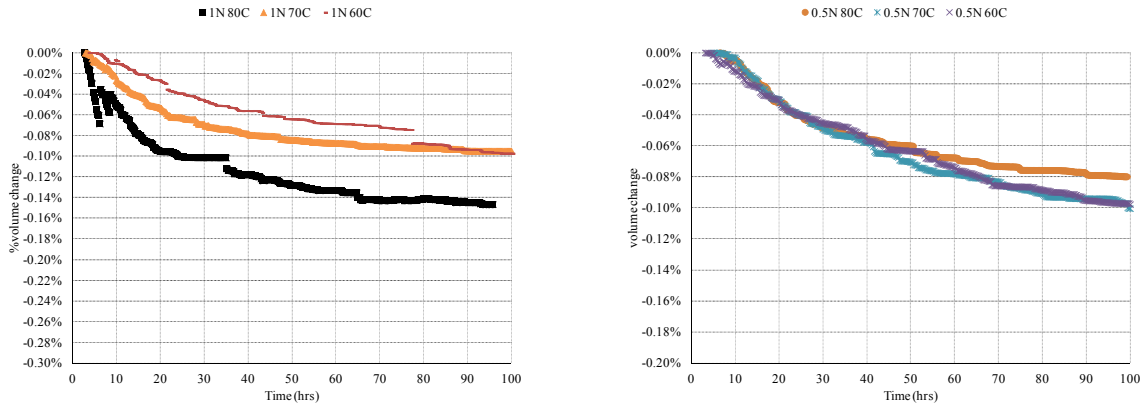

Figure B8 Solution Volume Change with 2 Alkalinities (1 and 0.5N NH + CH) at 3 Temperatures (60, 70, and 80°C) for CA2

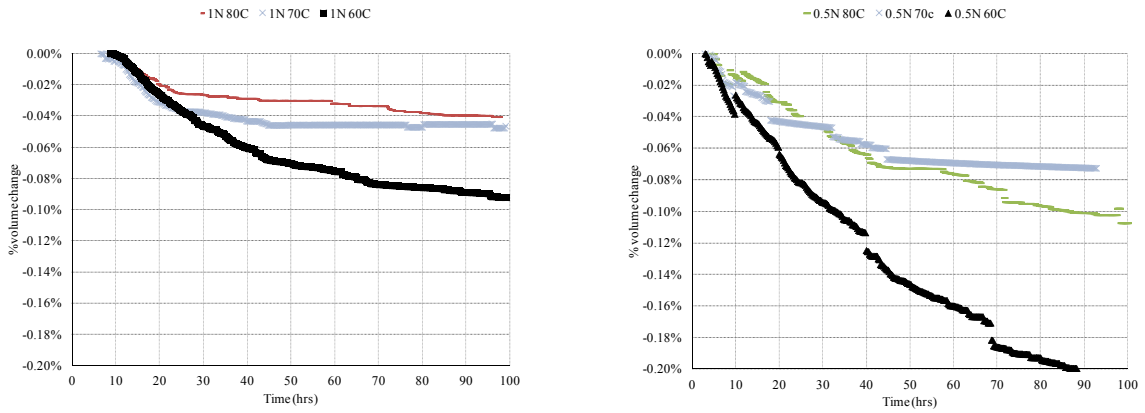

Figure B9 Solution Volume Change with 2 Alkalinities (1 and 0.5N NH + CH) at 3 Temperatures (60, 70, and 80°C) for CA3

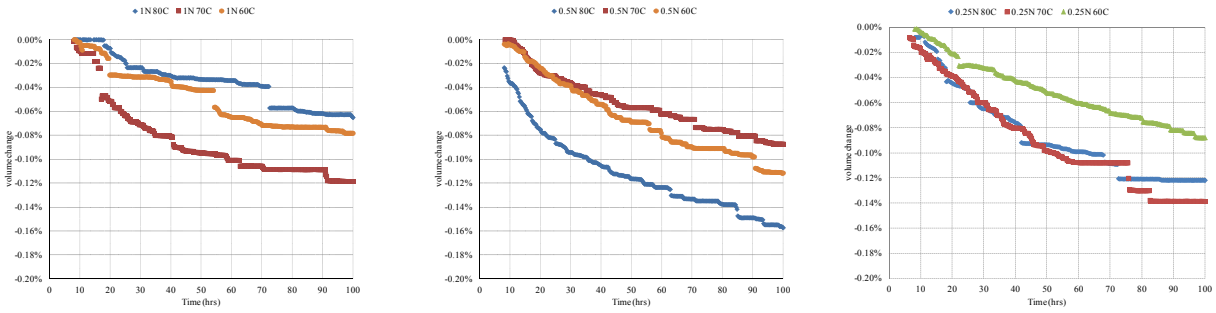

Figure B10 Solution Volume Change with 3 Alkalinities (1, 0.5, and 0.25N NH + CH) at 3 Temperatures (60, 70, and 80°C) for CA4

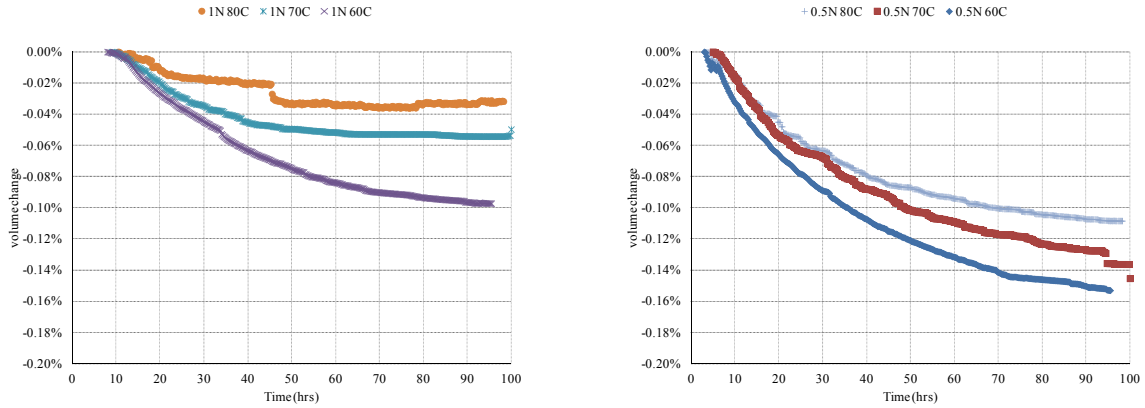

Figure B11 Solution Volume Change with 2 Alkalinities (1 and 0.5N NH + CH) at 3 Temperatures (60, 70, and 80°C) for CA5

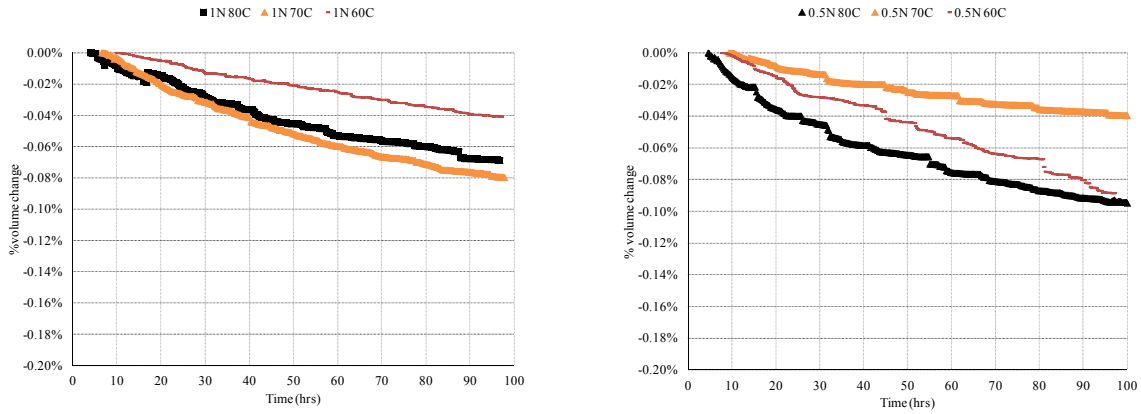

Figure B12 Solution Volume Change with 2 Alkalinities (1 and 0.5N NH + CH) at 3 Temperatures (60, 70, and 80°C) for CA6

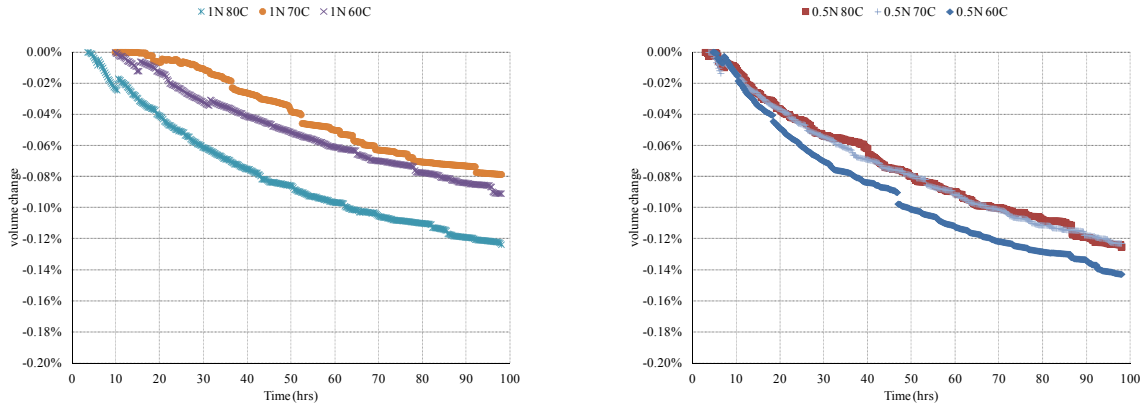

Figure B13 Solution Volume Change with 2 Alkalinities (1 and 0.5N NH + CH) at 3 Temperatures (60, 70, and 80°C) for CA7

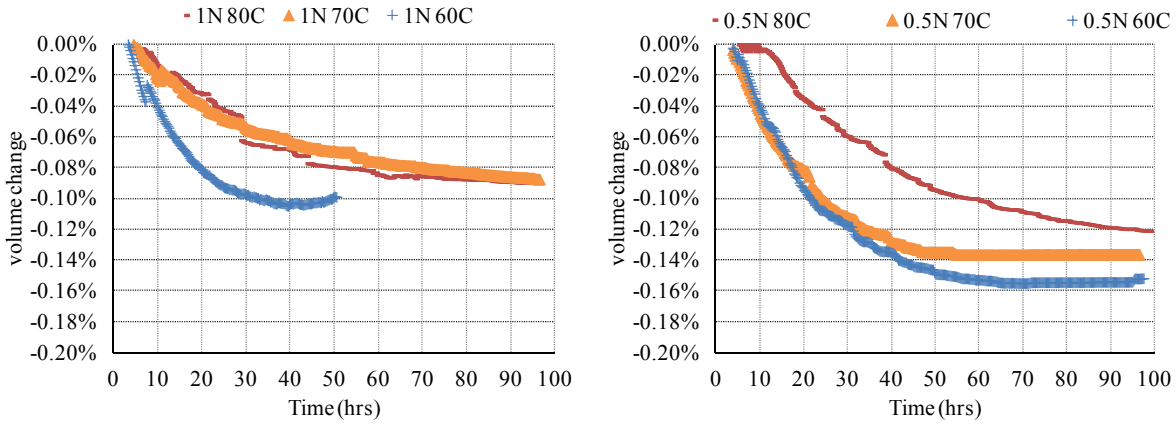

Figure B14 Solution Volume Change with 2 Alkalinities (1 and 0.5N NH + CH) at 3 Temperatures (60, 70, and 80°C) for CA8

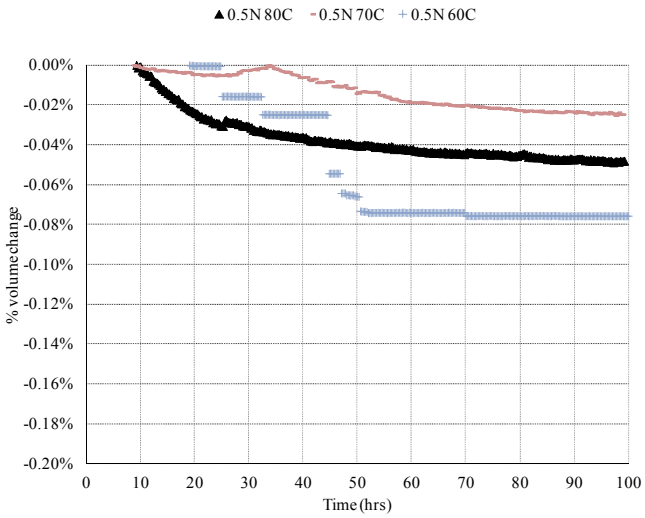

Figure B15 Solution Volume Change with 0.5N NH + CH at 3 Temperatures (60, 70, and 80°C) for FA6

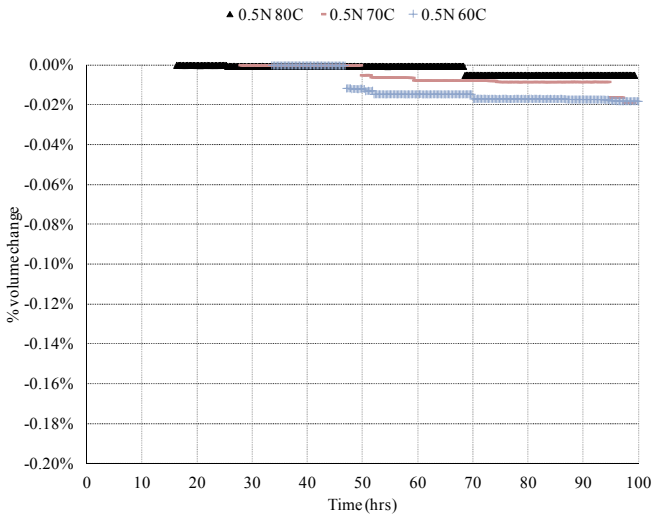

Figure B16 Solution Volume Change with 0.5N NH + CH at 3 Temperatures (60, 70, and 80°C) for FA7

APPENDIX C – MEASURED AND CALCULATED SOLUTION VOLUME CHANGE OVER TIME DUE TO ASR AND ACTIVATION ENERGY CALCULATION AT DIFFERENT LEVELS OF ALKALINITIES

Solution normality	Volume change over time and Ea calculation	Ea (KJ/mole)
1N NH + CH	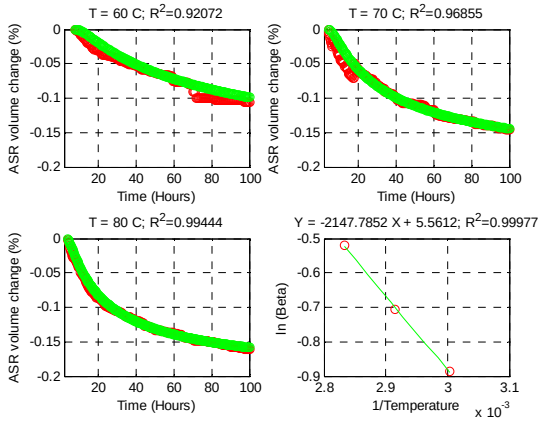	17.86
0.5N NH + CH	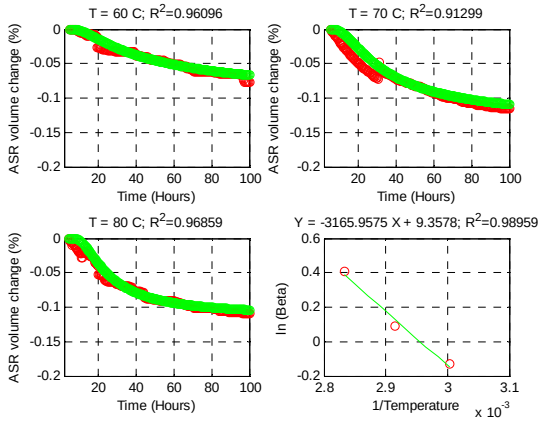	26.32
0.25N NH + CH	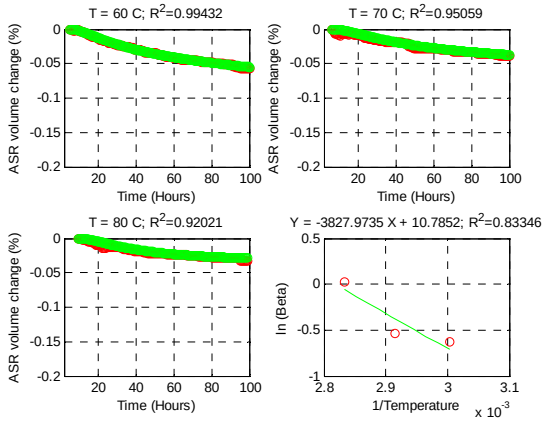	31.83

Figure C1 Measured (Red) and Modeled (Green) Solution Volume Change over Time due to ASR and Associated Ea Calculation for FA1 at 1, 0.5, and 0.25 NH + CH Solution

Solution normality	Volume change over time and Ea calculation	Ea (KJ/mole)
1N NH + CH	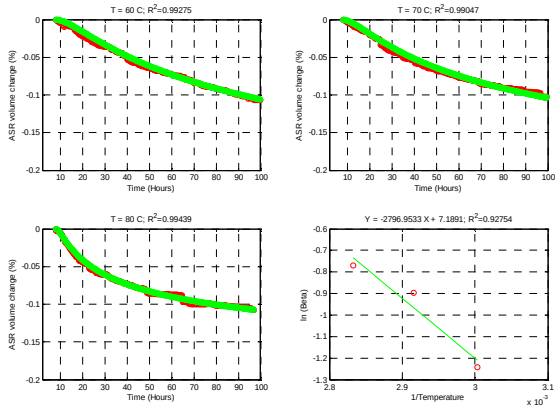	23.25
0.5N NH + CH	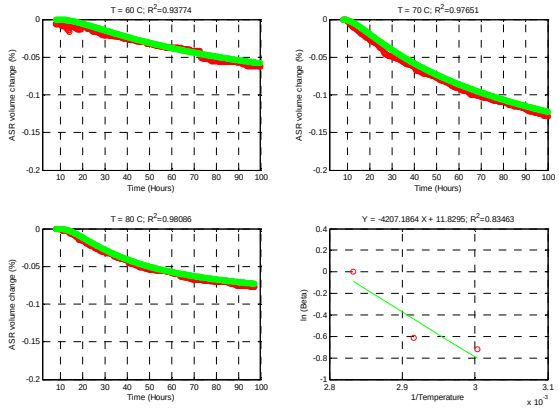	34.98

Figure C2 Measured (Red) and Modeled (Green) Solution Volume Change over Time due to ASR and Associated Ea Calculation for FA2 at 1 and 0.5 NH + CH Solution

Solution normality	Volume change over time and Ea calculation	Ea (KJ/mole)
1N NH + CH	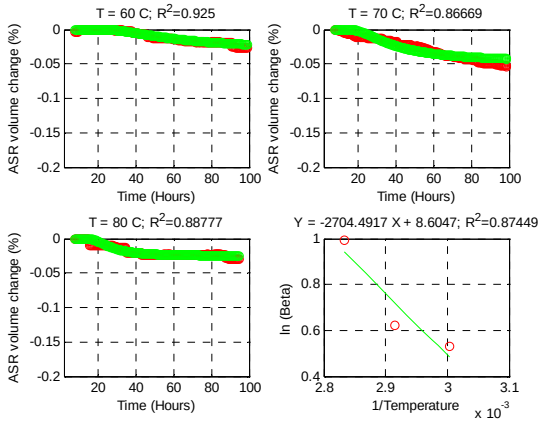	22.49
0.5N NH + CH	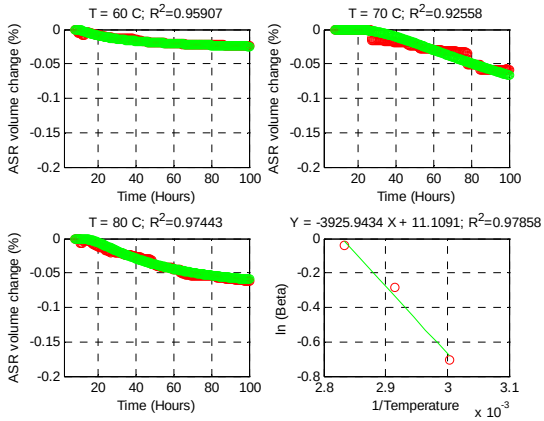	32.64

Figure C3 Measured (Red) and Modeled (Green) Solution Volume Change over Time due to ASR and Associated Ea Calculation for FA3 at 1 and 0.5 NH + CH Solution

Solution normality	Volume change over time and Ea calculation	Ea (KJ/mole)
1N NH + CH	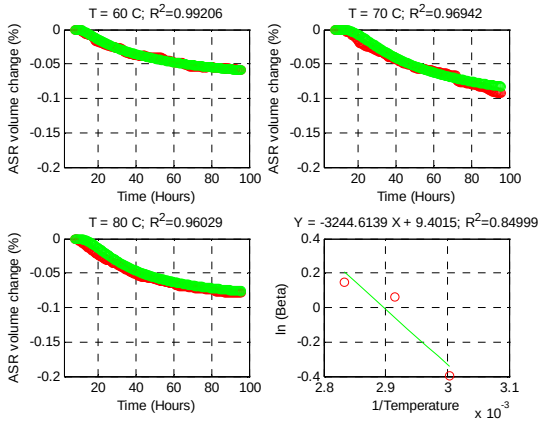	26.98
0.5N NH + CH	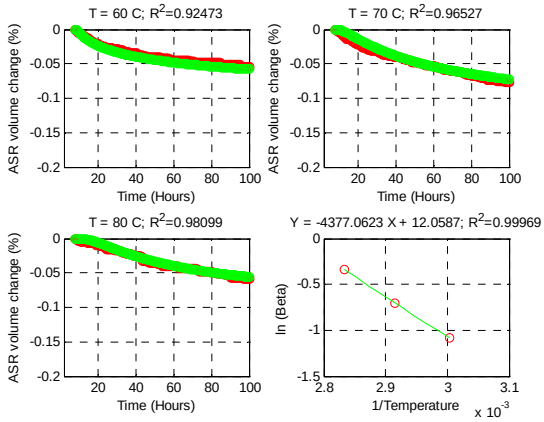	36.39

Figure C4 Measured (Red) and Modeled (Green) Solution Volume Change over Time due to ASR and Associated Ea Calculation for FA4 at 1 and 0.5 NH + CH Solution

Solution normality	Volume change over time and Ea calculation	Ea (KJ/mole)
1N NH + CH	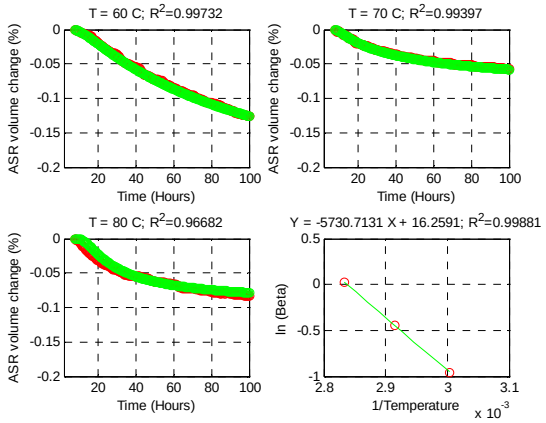	47.65
0.5N NH + CH	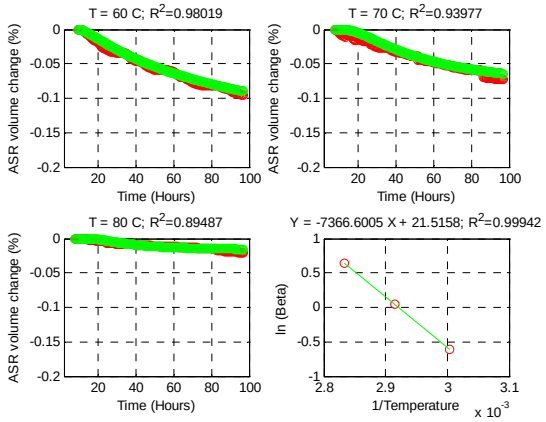	61.25

Figure C5 Measured (Red) and Modeled (Green) Solution Volume Change over Time due to ASR and Associated Ea Calculation for FA5 at 1 and 0.5 NH + CH Solution

Solution normality	Volume change over time and Ea calculation	Ea (KJ/mole)
1N NH + CH	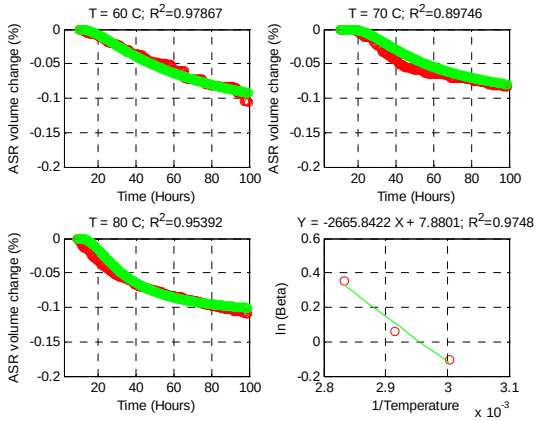	22.16
0.5N NH + CH	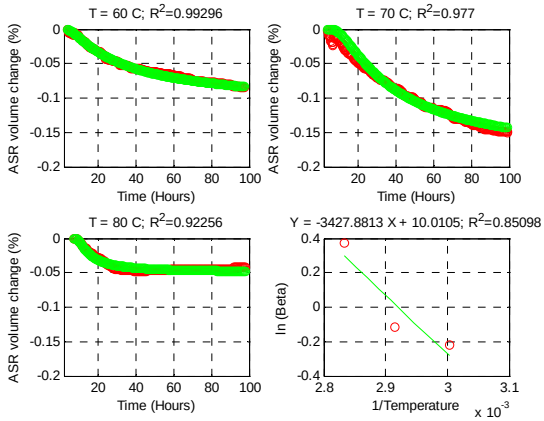	28.50

Figure C6 Measured (Red) and Modeled (Green) Solution Volume Change over Time due to ASR and Associated Ea Calculation for CA1 at 1 and 0.5 NH + CH Solution

Solution normality	Volume change over time and Ea calculation	Ea (KJ/mole)
1N NH + CH	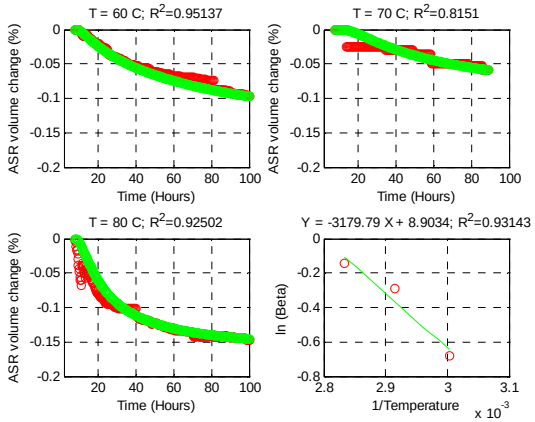	26.44
0.5N NH + CH	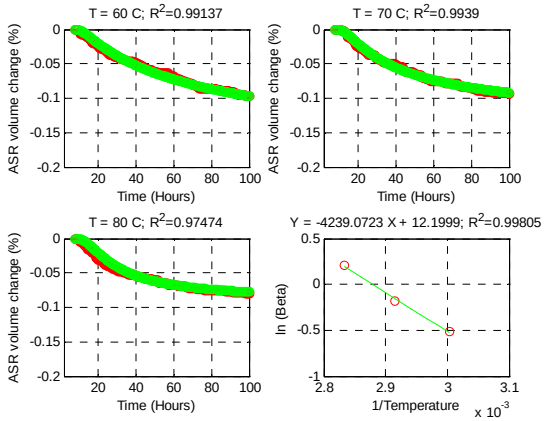	35.24

Figure C7 Measured (Red) and Modeled (Green) Solution Volume Change over Time due to ASR and Associated Ea Calculation for CA2 at 1 and 0.5 NH + CH Solution

Solution normality	Volume change over time and Ea calculation	Ea (KJ/mole)
1N NH + CH	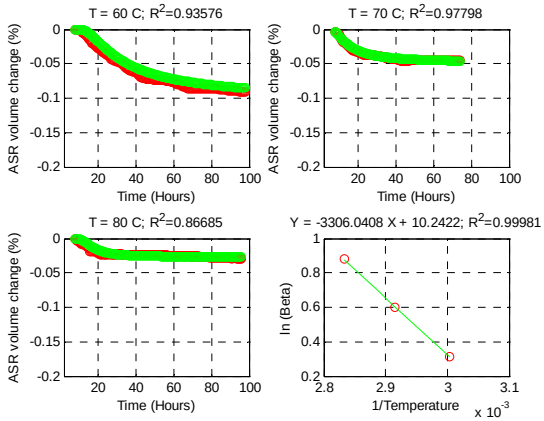	27.49
0.5N NH + CH	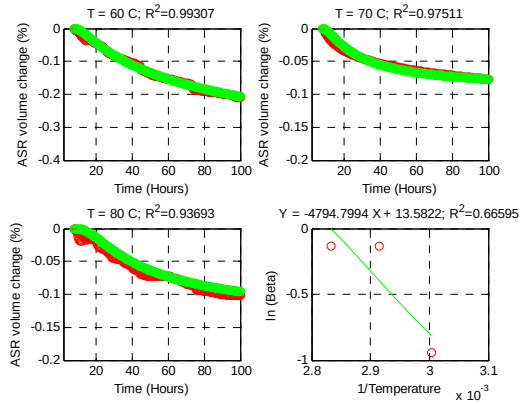	39.86

Figure C8 Measured (Red) and Modeled (Green) Solution Volume Change over Time due to ASR and Associated Ea Calculation for CA3 at 1 and 0.5 NH + CH Solution

Solution normality	Volume change over time and Ea calculation	Ea (KJ/mole)
1N NH + CH	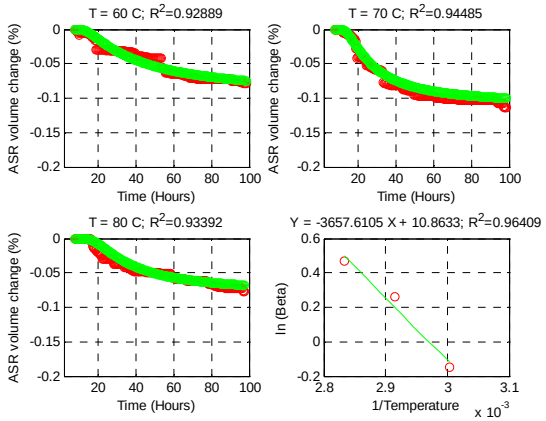	30.41
0.5N NH + CH	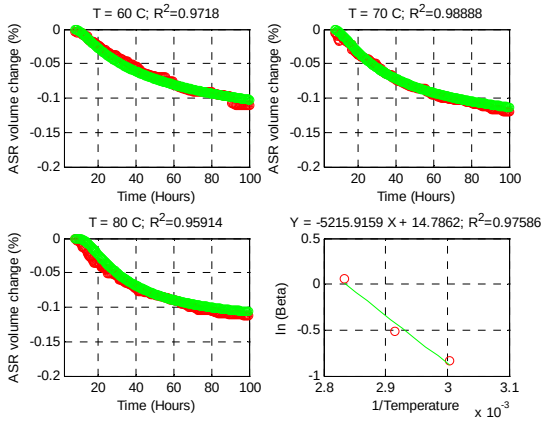	43.37
0.25N NH + CH	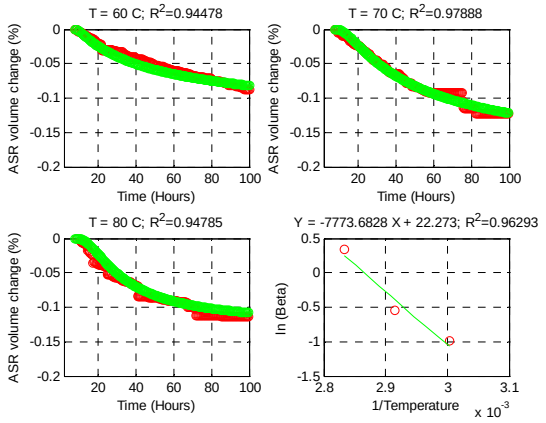	64.63

Figure C9 Measured (Red) and Modeled (Green) Solution Volume Change over Time due to ASR and Associated Ea Calculation for CA4 at 1 and 0.5 NH + CH Solution

Solution normality	Volume change over time and Ea calculation	Ea (KJ/mole)
1N NH + CH	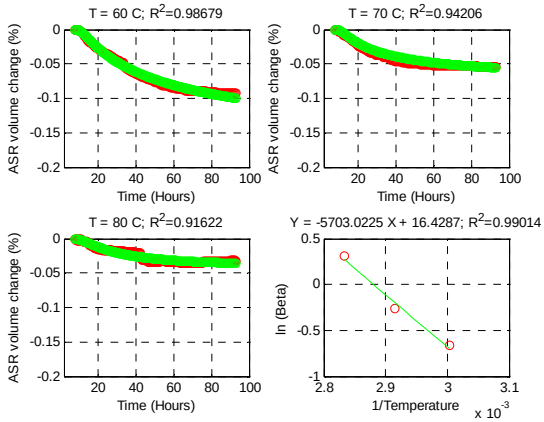	47.41
0.5N NH + CH	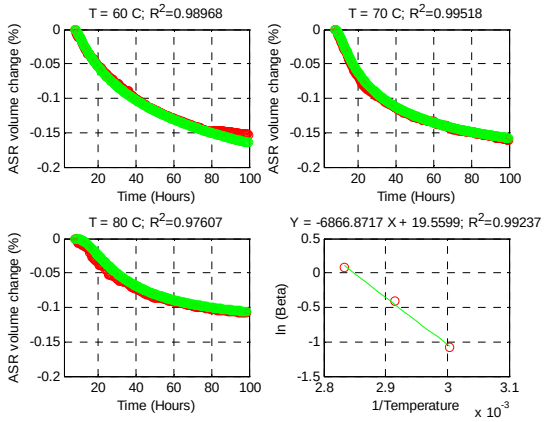	57.09

Figure C10 Measured (Red) and Modeled (Green) Solution Volume Change over Time due to ASR and Associated Ea Calculation for CA5 at 1 and 0.5 NH + CH Solution

Solution normality	Volume change over time and Ea calculation	Ea (KJ/mole)
1N NH + CH	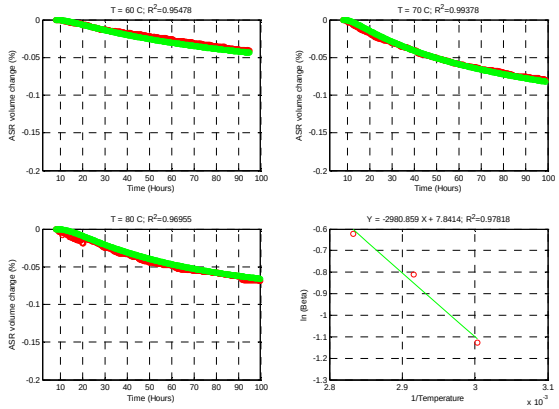	24.78
0.5N NH + CH	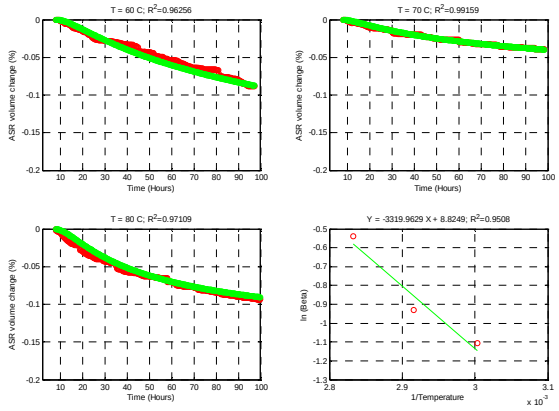	27.60

Figure C11 Measured (Red) and Modeled (Green) Solution Volume Change over Time due to ASR and Associated Ea Calculation for CA6 at 1 and 0.5 NH + CH Solution

Solution normality	Volume change over time and Ea calculation	Ea (KJ/mole)
1N NH + CH	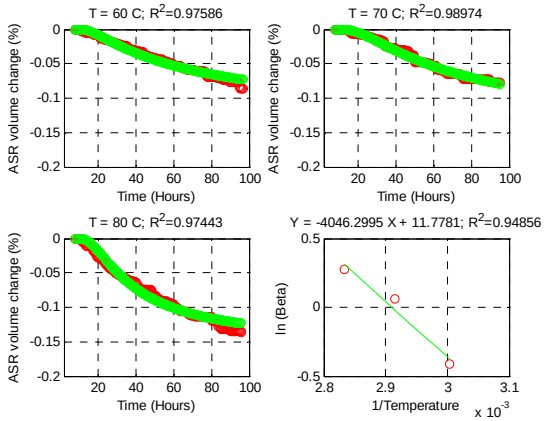	33.64
0.5N NH + CH	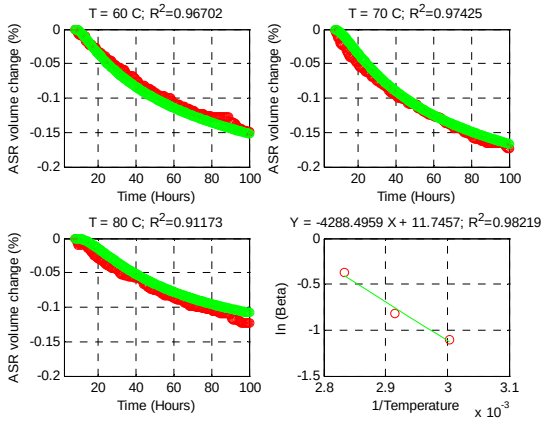	35.65

Figure C12 Measured (Red) and Modeled (Green) Solution Volume Change over Time due to ASR and Associated Ea Calculation for CA7 at 1 and 0.5 NH + CH Solution

Solution normality	Volume change over time and Ea calculation	Ea (KJ/mole)
1N NH + CH	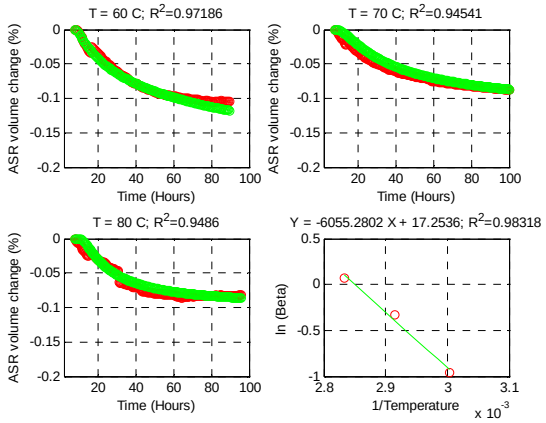	50.34
0.5N NH + CH	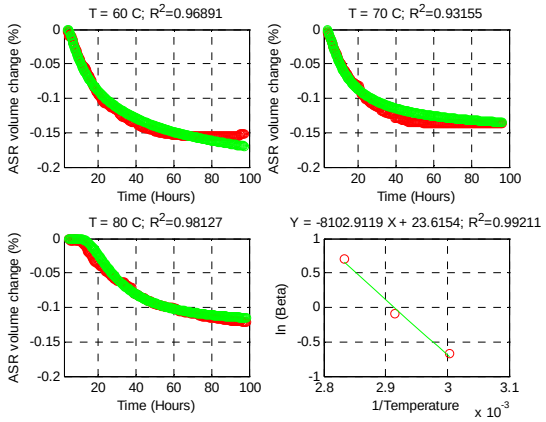	67.37

Figure C13 Measured (Red) and Modeled (Green) Solution Volume Change over Time due to ASR and Associated Ea Calculation for CA8 at 1 and 0.5 NH + CH Solution

Solution normality	Volume change over time and Ea calculation	Ea (KJ/mole)
0.5N NH + CH	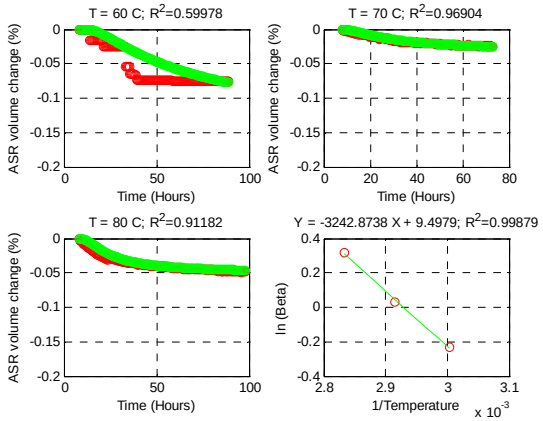	26.96

Figure C14 Measured (Red) and Modeled (Green) Solution Volume Change over Time due to ASR and Associated Ea Calculation for FA6 at 0.5 NH + CH Solution

APPENDIX D – ALL SOLUTION VOLUME CHANGE OVER TIME DATA AT DIFFERENT TEMPERATURES AND ALKALINITIES FOR THE TESTED AGGREGATES AND REPEATABILITY CALCULATION

Measured (red) and modeled (green) solution volume change over time at different temperatures and alkalinities for all the repeated tests are presented in Figures D1 to D13. The associated rate constants based on the modeled (green) curves are calculated to verify the repeatability and summarized in Tables D1 to D13 for all aggregates.

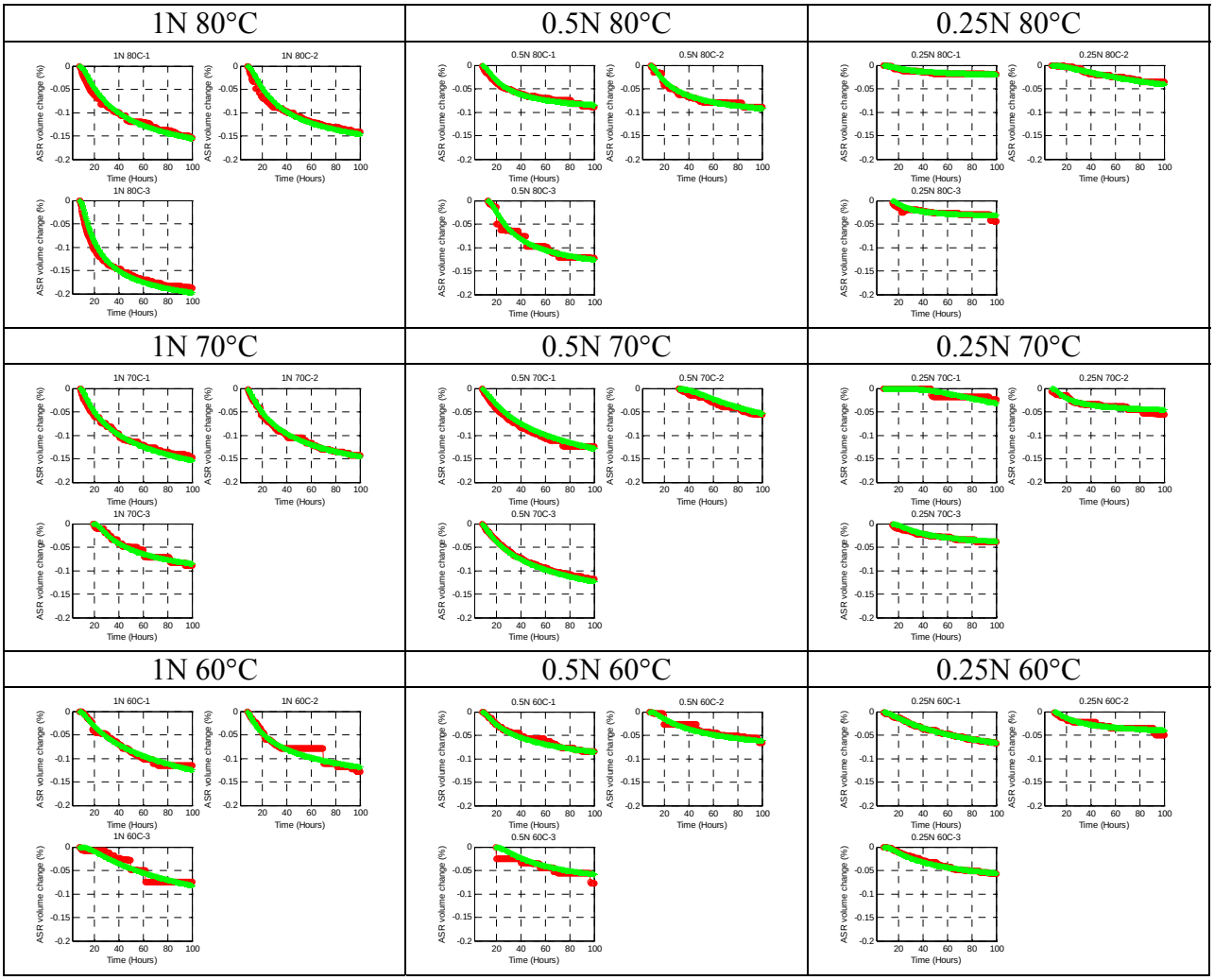

Figure D1 Measured (Red) and Modeled (Green) Solution Volume Change over Time for FA1 with 3 Alkalinities (1, 0.5, and 0.25N NH + CH) at 3 Temperatures (60, 70, 80°C)

Table D1 Calculated Rate Constant Based on the Modeled Curve (Green) in Figure D1 for FA1

	β				mean	COV.
Temperature, °C		**test1**	**test2**	**test3**		
80	1N	0.5842	0.6195	0.6134	0.6057	3.12%
	0.5N	0.5964	0.6062	0.6014	0.6013	0.81%
	0.25N	0.5792	0.6009	0.6038	0.5946	2.26%
70	1N	0.4954	0.5069	0.5345	0.5123	3.92%
	0.5N	0.4842	0.4835	0.5107	0.4928	3.15%
	0.25N	0.4108	0.4309	0.4067	0.4161	3.11%
60	1N	0.3968	0.4237	0.4468	0.4224	5.92%
	0.5N	0.3776	0.3645	0.3872	0.3764	3.03%
	0.25N	0.3143	0.3322	0.3253	0.3239	2.79%

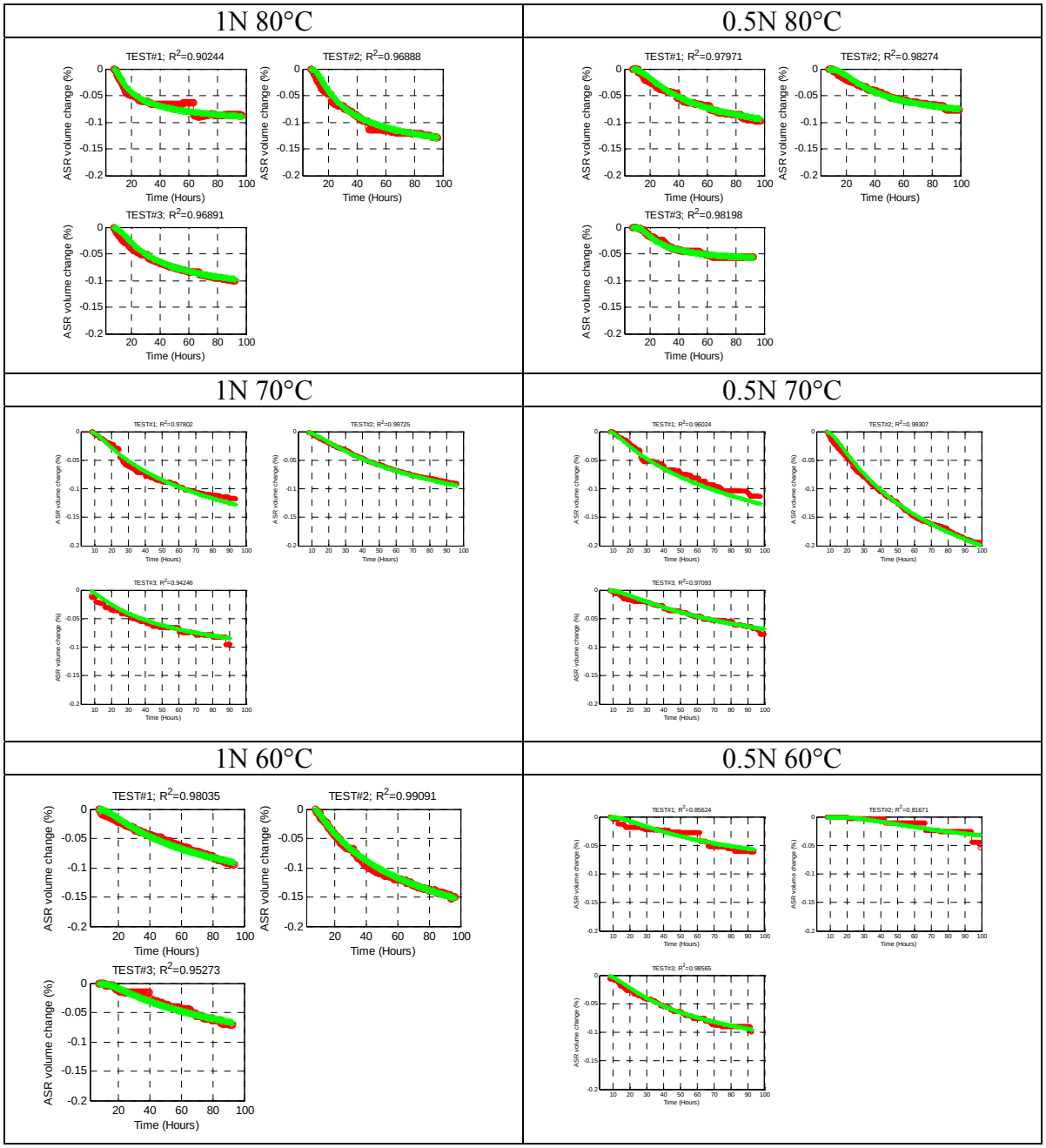

Figure D2 Measured (Red) and Modeled (Green) Solution Volume Change over Time for FA2 with 2 Alkalinities (1 and 0.5N NH + CH) at 3 Temperatures (60, 70, 80°C)

Table D2 Calculated Rate Constant Based on the Modeled Curve (Green) in Figure D2 for FA2

	β				mean of 3	COV.
Temperature, °C		test1	test2	test3		
80	1N	0.7058	0.7888	0.6497	0.7148	9.79%
	0.5N	1.0449	0.9979	1.1317	1.0582	6.41%
70	1N	0.4331	0.4343	0.3975	0.4216	4.96%
	0.5N	0.4067	0.3742	0.3418	0.3742	8.67%
60	1N	0.3967	0.3703	0.4453	0.4041	9.41%
	0.5N	0.4827	0.5525	0.5287	0.5213	6.81%

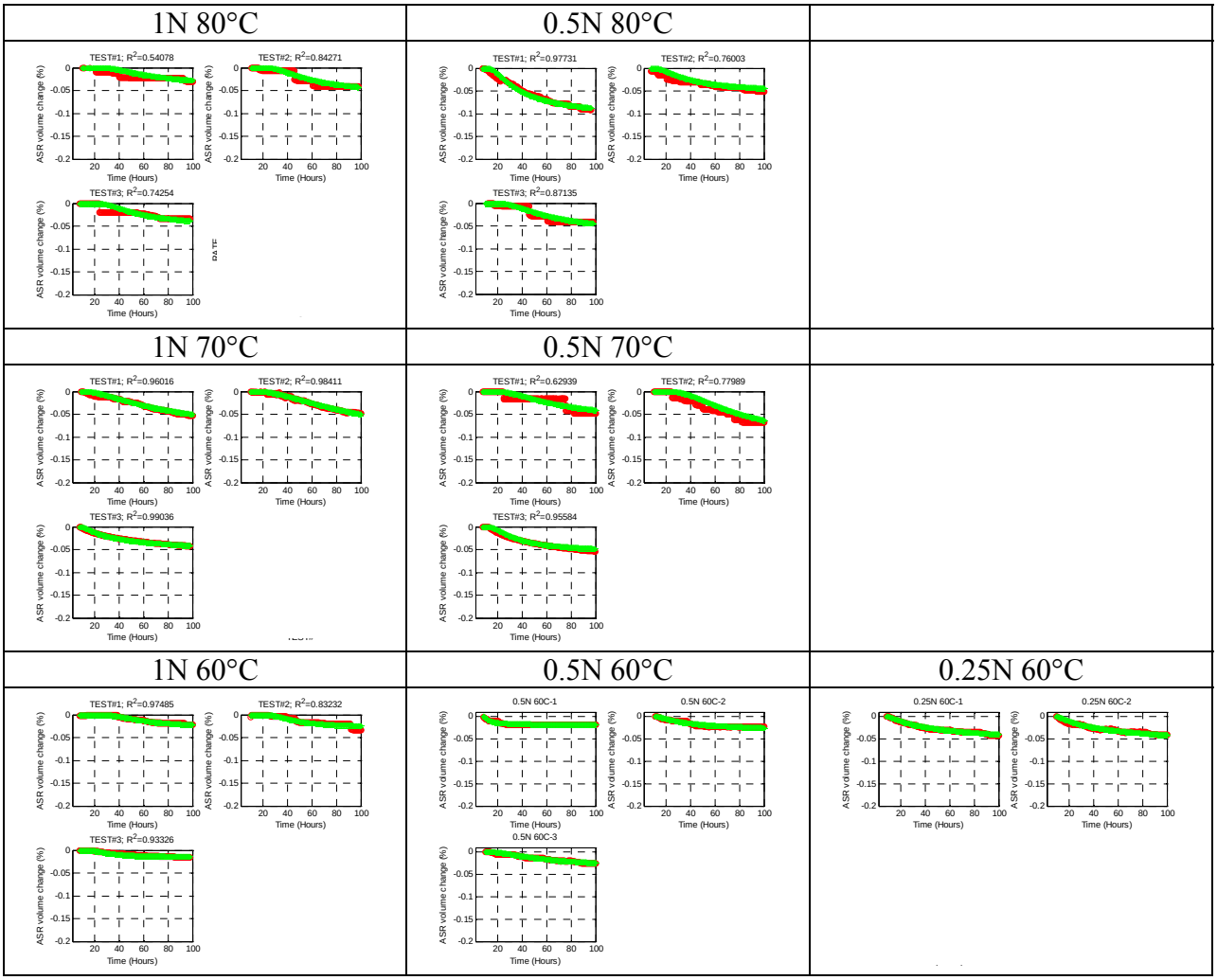

Figure D3 Measured (Red) and Modeled (Green) Solution Volume Change over Time for FA3 with 3 Alkalinities (1, 0.5 and 0.25N NH + CH) at 3 Temperatures (60, 70, 80°C)

Table D3 Calculated Rate Constant Based on the Modeled Curve (Green) in Figure D3 for FA3

	β				mean	COV.
Temperature, °C		test1	test2	test3		
80	1N	2.0763	1.8154	1.8116	1.9011	7.98%
	0.5N	1.2058	1.2911	1.3948	1.2972	7.30%
70	1N	0.6553	0.6243	0.553	0.6109	8.59%
	0.5N	1.6858	1.5363	1.5995	1.6072	4.67%
60	1N	2.3667	2.3405	2.2128	2.3067	3.57%
	0.5N	0.9568	0.8001	0.8658	0.8742	9.00%
	0.25N	0.4695	0.4703		0.4699	0.12%

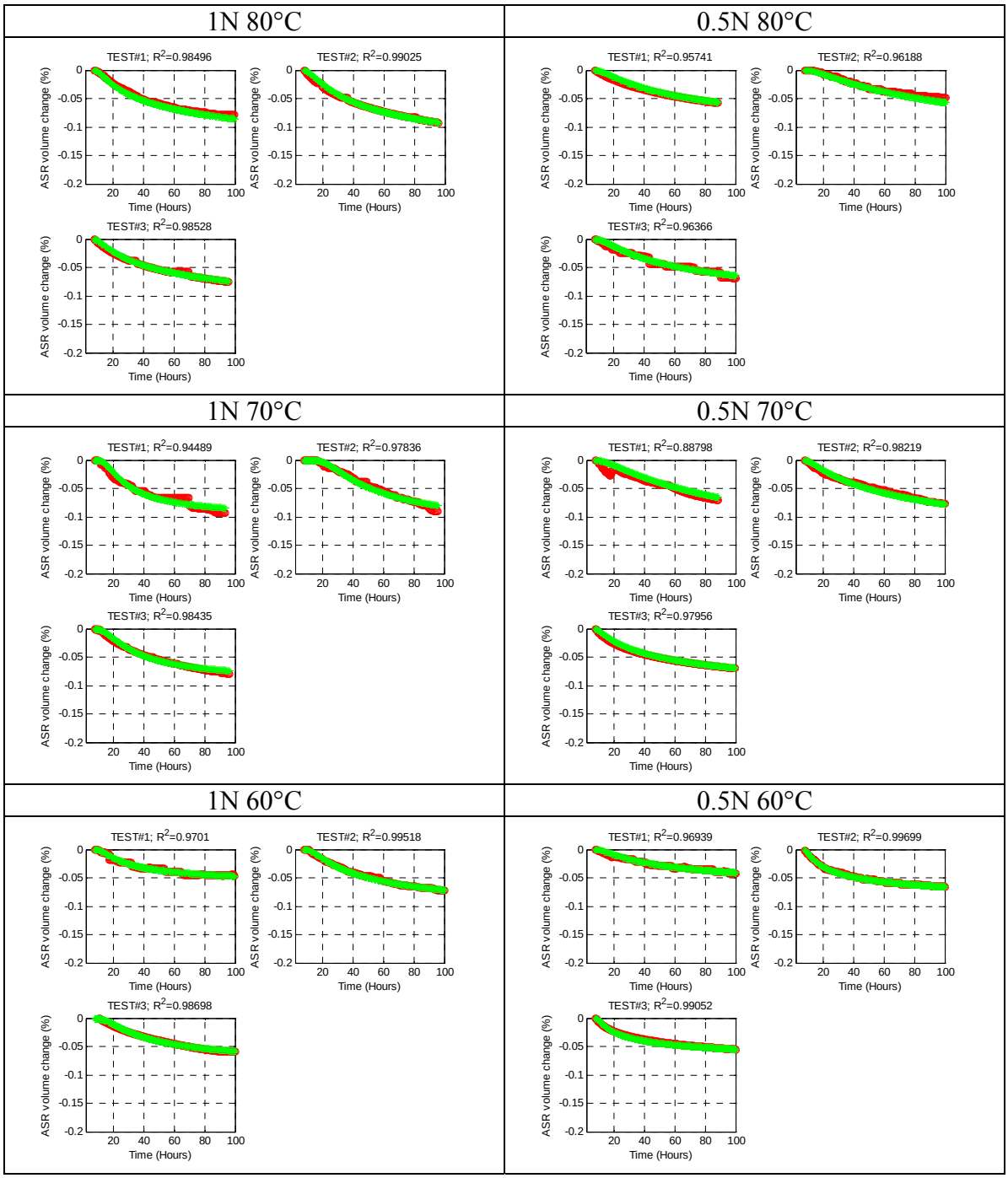

Figure D4 Measured (Red) and Modeled (Green) Solution Volume Change over Time for FA4 with 2 Alkalinities (1 and 0.5N NH + CH) at 3 Temperatures (60, 70, 80°C)

Table D4 Calculated Rate Constant Based on the Modeled Curve (Green) in Figure D4 for FA4

	β				mean	COV.
Temperature, °C		**test1**	**test2**	**test3**		
80	1N	0.4127	0.4131	0.4001	0.4086	1.81%
	0.5N	0.5183	0.5628	0.4991	0.5267	6.20%
70	1N	1.4079	1.2426	1.4394	1.3633	7.75%
	0.5N	0.3211	0.3507	0.3971	0.3563	10.75%
60	1N	1.0373	0.9809	1.1602	1.0595	8.65%
	0.5N	0.4378	0.4961	0.484	0.4726	6.51%

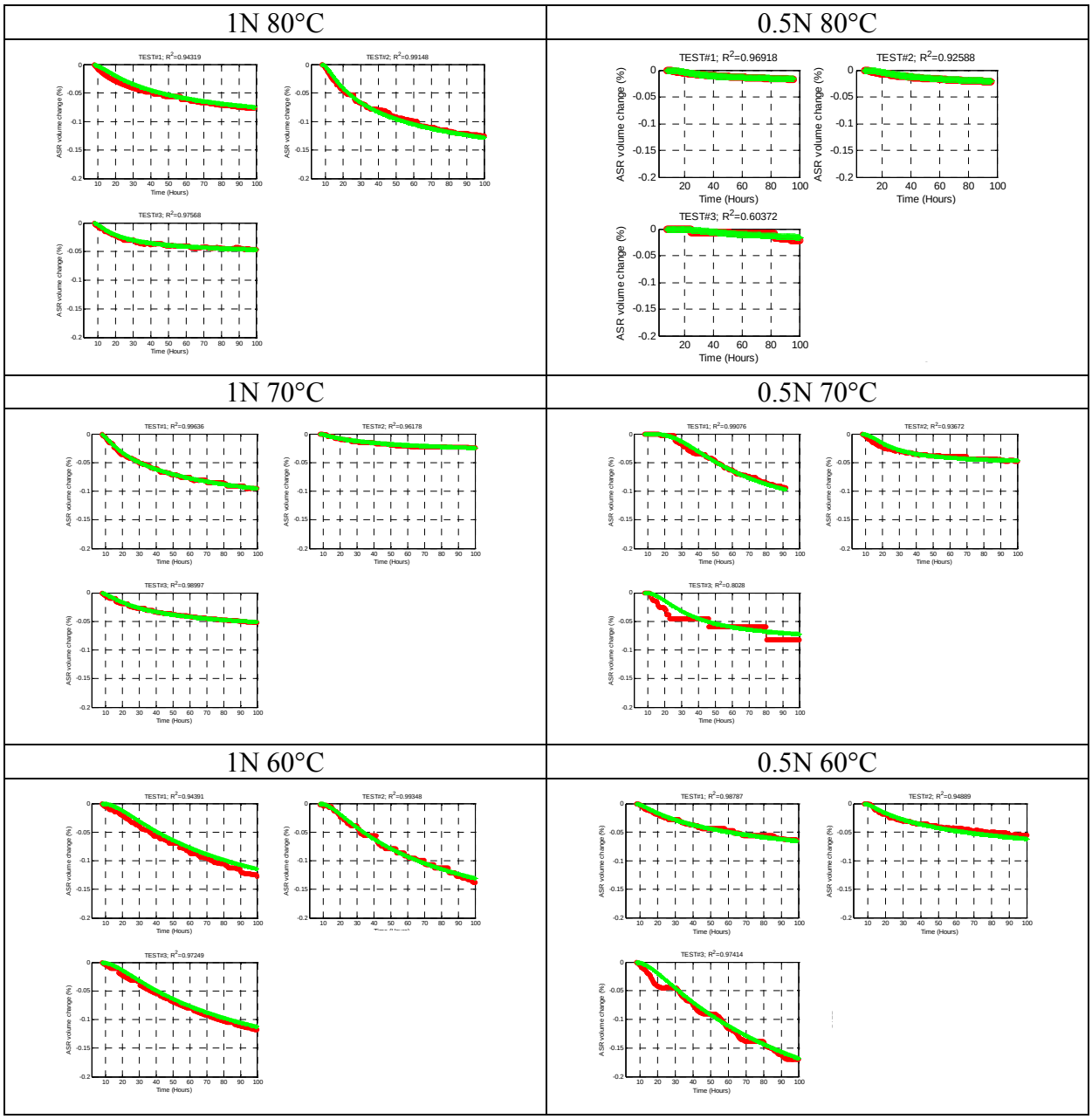

Figure D5 Measured (Red) and Modeled (Green) Solution Volume Change over Time for FA5 with 2 Alkalinities (1 and 0.5N NH + CH) at 3 Temperatures (60, 70, 80°C)

Table D5 Calculated Rate Constant Based on the Modeled Curve (Green) in Figure D5 for FA5

	β				mean	COV.
Temperature, °C		test1	test2	test3		
80	1N	0.5458	0.5448	0.6434	0.5780	9.80%
	0.5N	1.0655	1.0419	1.1912	1.0995	7.30%
70	1N	0.4869	0.4287	0.4829	0.4662	6.97%
	0.5N	1.4461	1.2625	1.516	1.4082	9.30%
60	1N	0.5897	0.6514	0.5557	0.5989	8.10%
	0.5N	0.4388	0.4589	0.3911	0.4296	8.11%

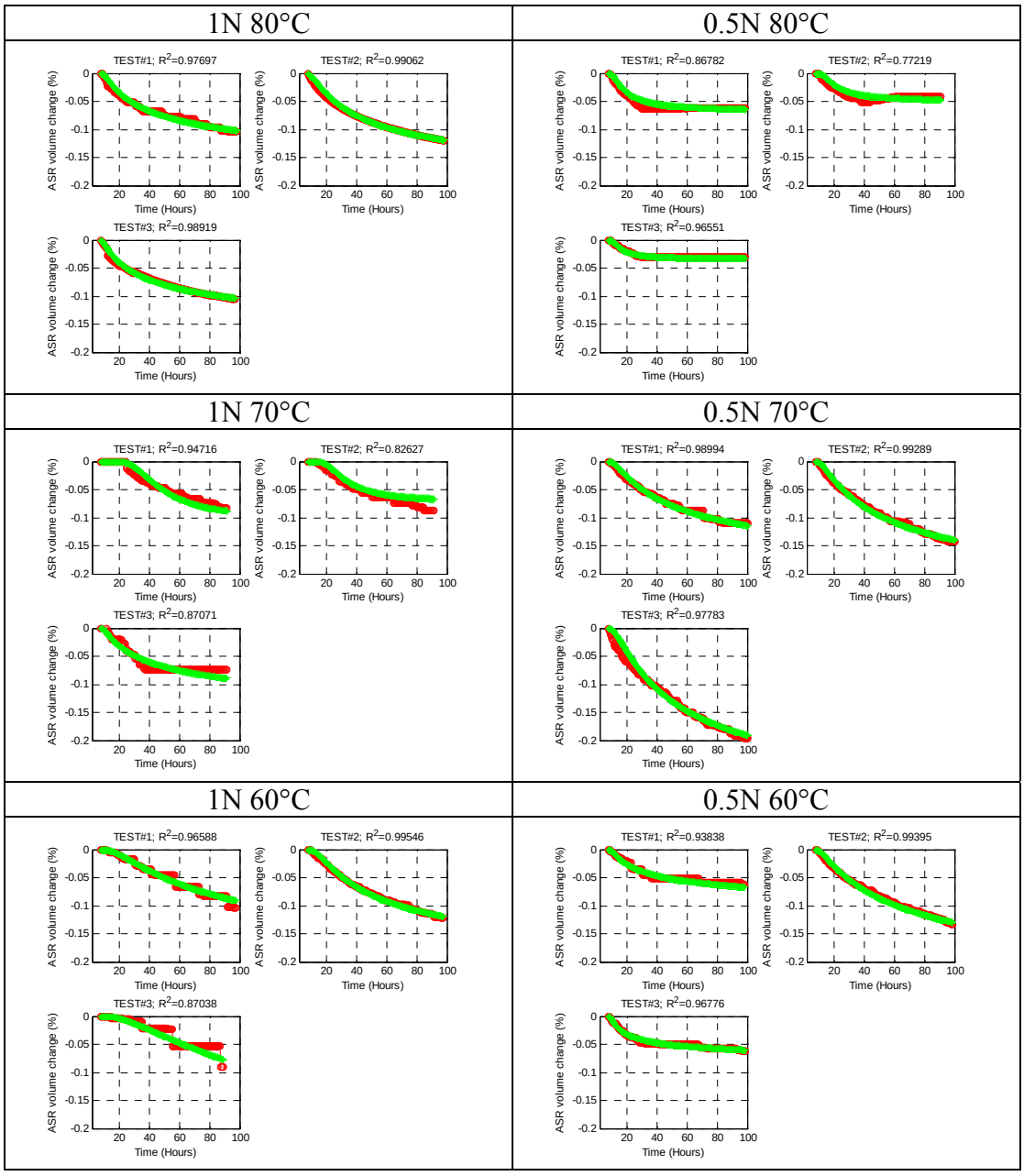

Figure D6 Measured (Red) and Modeled (Green) Solution Volume Change over Time for CA1 with 2 Alkalinities (1 and 0.5N NH + CH) at 3 Temperatures (60, 70, 80°C)

Table D6 Calculated Rate Constant Based on the Modeled Curve (Green) in Figure D6 for CA1

	β				mean	COV.
Temperature, °C		**test1**	**test2**	**test3**		
80	1N	0.5443	0.4599	0.4504	0.4849	10.66%
	0.5N	1.3119	1.6959	1.5701	1.5260	12.83%
70	1N	2.2579	2.4291	1.8542	2.1804	13.54%
	0.5N	0.564	0.6029	0.5015	0.5561	9.20%
60	1N	0.6944	0.7421	0.7189	0.7185	3.32%
	0.5N	0.5092	0.4898	0.4963	0.4984	1.98%

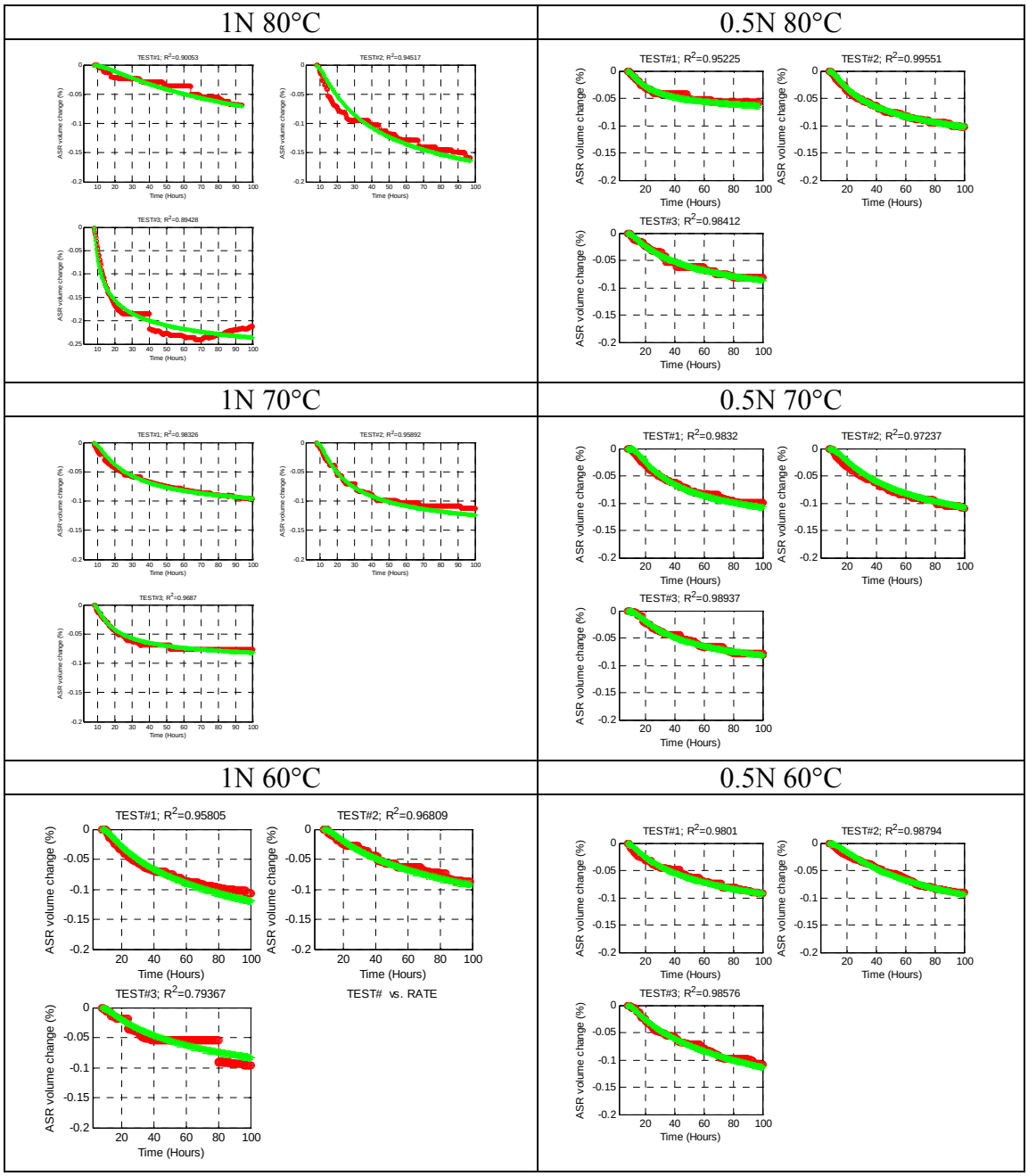

Figure D7 Measured (Red) and Modeled (Green) Solution Volume Change over Time for CA2 with 2 Alkalinities (1 and 0.5N NH + CH) at 3 Temperatures (60, 70, 80°C)

Table D7 Calculated Rate Constant Based on the Modeled Curve (Green) in Figure D7 for CA2

Temperature, °C	β				mean	COV.
		test1	test2	test3		
80	1N	0.4414	0.4457	0.4496	0.4456	0.92%
	0.5N	0.5728	0.5457	0.5683	0.5623	2.58%
70	1N	0.6528	0.7064	0.7712	0.7101	8.35%
	0.5N	0.7733	0.6349	0.7348	0.7143	10.00%
60	1N	0.432	0.4047	0.3883	0.4083	5.41%
	0.5N	0.4263	0.4097	0.3738	0.4033	6.65%

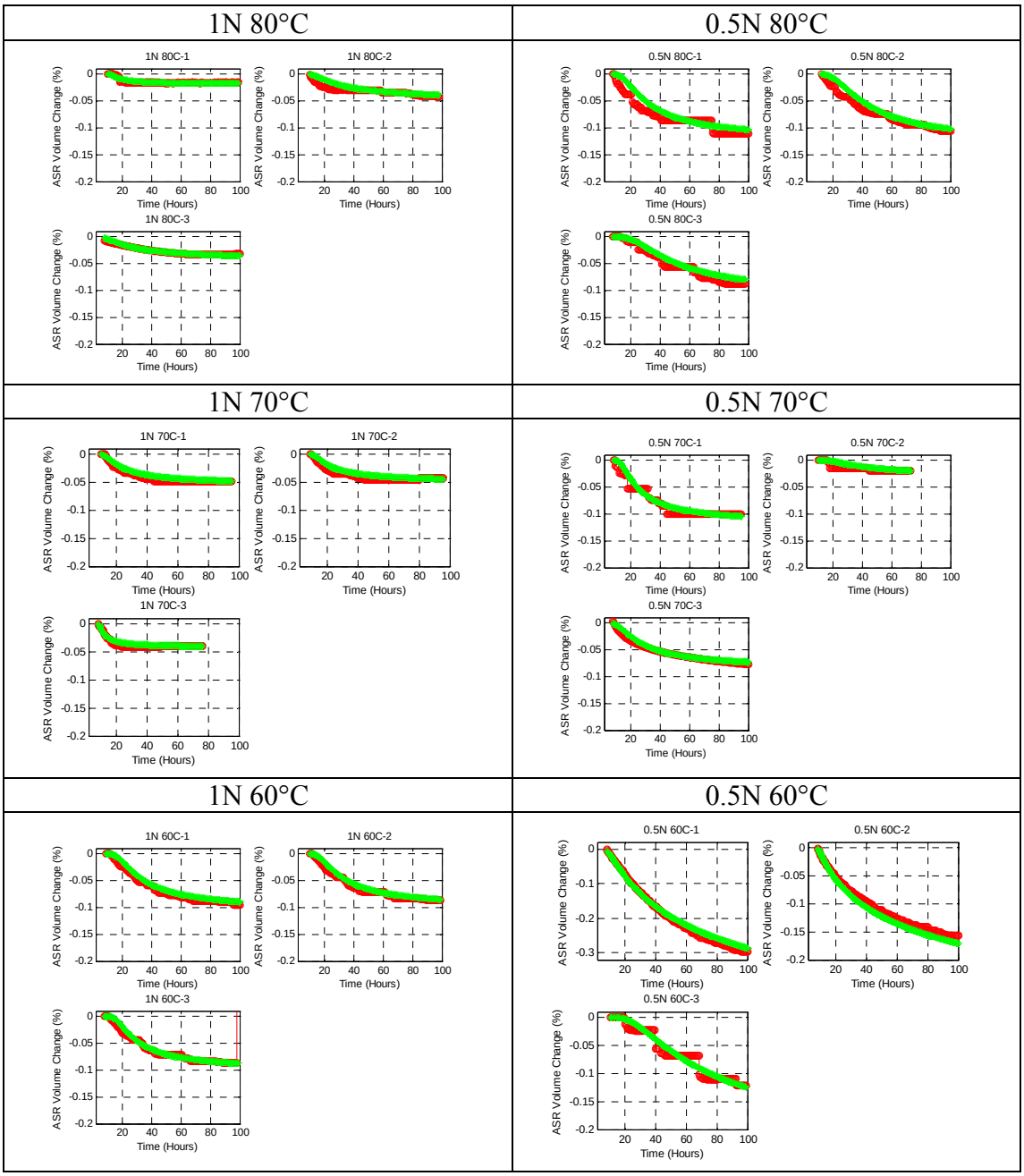

Figure D8 Measured (Red) and Modeled (Green) Solution Volume Change over Time for CA3 with 2 Alkalinities (1 and 0.5N NH + CH) at 3 Temperatures (60, 70, 80°C)

Table D8 Calculated Rate Constant Based on the Modeled Curve (Green) in Figure D8 for CA3

	β				mean	COV.
Temperature, °C		**test1**	**test2**	**test3**		
80	1N	0.9583	0.865	1.0517	0.9583	9.74%
	0.5N	1.3043	1.2332	1.4871	1.3415	9.76%
70	1N	1.518	1.3416	1.3226	1.3941	7.73%
	0.5N	1.2116	1.1167	1.3263	1.2182	8.62%
60	1N	1.3907	1.2561	1.4155	1.3541	6.33%
	0.5N	0.202	0.254	0.2437	0.2332	11.81%

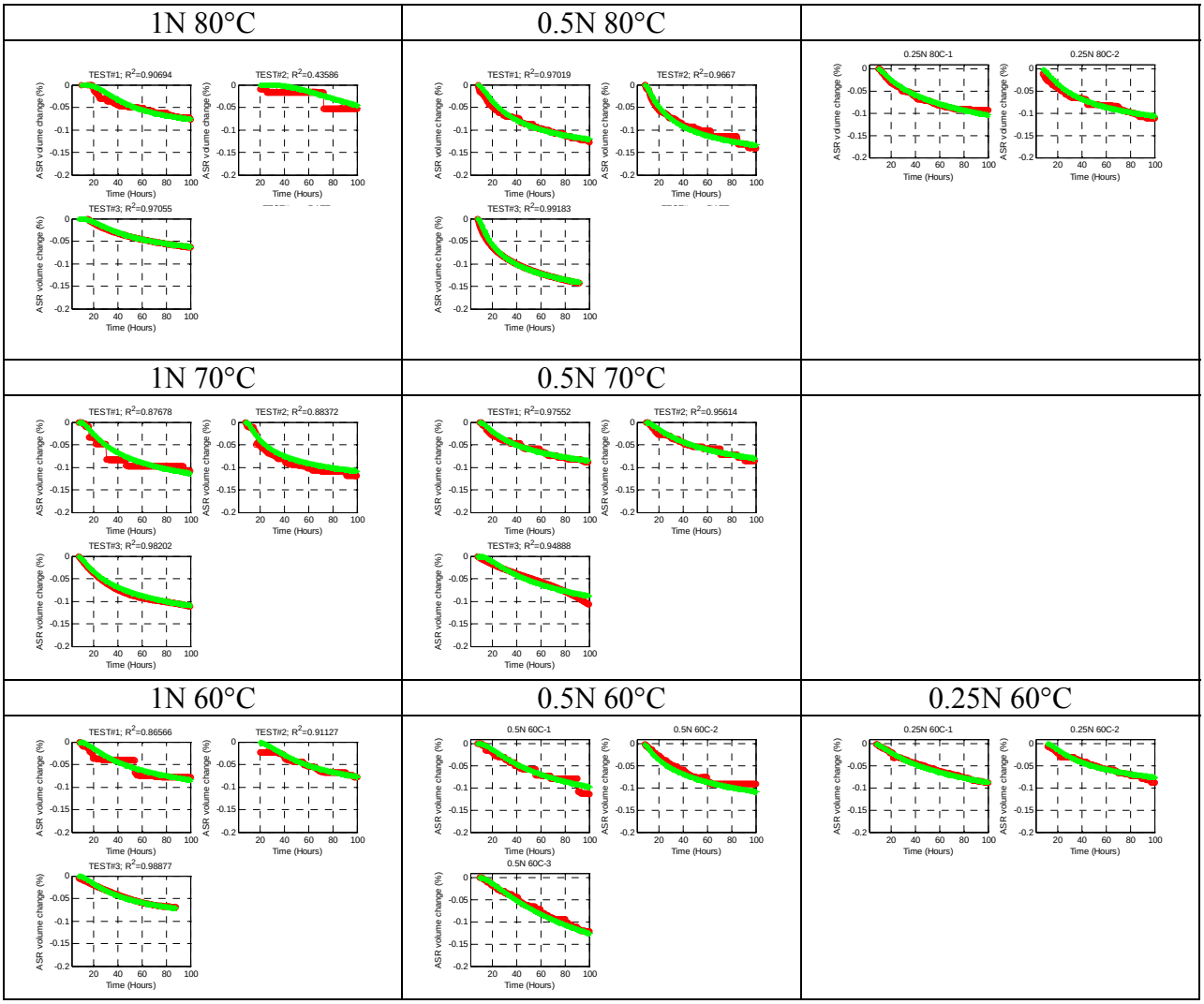

Figure D9 Measured (Red) and Modeled (Green) Solution Volume Change over Time for CA4 with 3 Alkalinities (1, 0.5, and 0.25N NH + CH) at 3 Temperatures (60, 70, 80°C)

Table D9 Calculated Rate Constant Based on the Modeled Curve (Green) in Figure D9 for CA4

	β				mean	COV.
Temperature, °C		test1	test2	test3		
80	1N	0.9143	0.9145	0.8938	0.9075	1.31%
	0.5N	0.5533	0.5601	0.467	0.5268	9.85%
	0.25N	0.4717	0.45		0.4609	3.33%
70	1N	0.6668	0.5908	0.5489	0.6022	9.93%
	0.5N	0.5806	0.5111	0.5299	0.5405	6.65%
60	1N	0.5758	0.5712	0.4889	0.5453	8.97%
	0.5N	0.3613	0.4297	0.4019	0.3976	8.65%
	0.25N	0.3419	0.3217		0.3318	4.30%

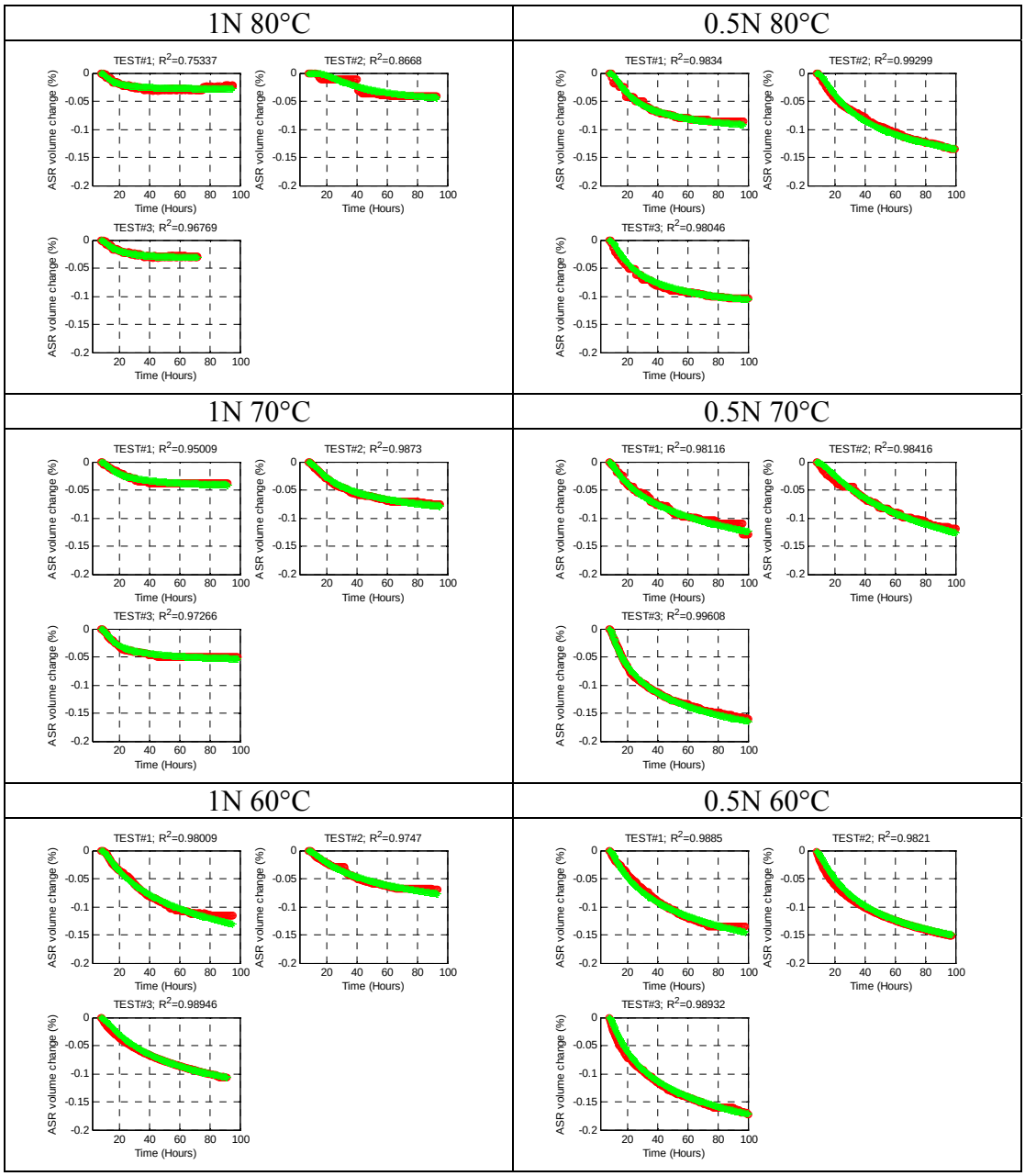

Figure D10 Measured (Red) and Modeled (Green) Solution Volume Change over Time for CA5 with 2 Alkalinities (1 and 0.5N NH + CH) at 3 Temperatures (60, 70, 80°C)

Table D10 Calculated Rate Constant Based on the Modeled Curve (Green) in Figure D10 for CA5

	β				mean	COV.
Temperature, °C		**test1**	**test2**	**test3**		
80	1N	1.3975	1.2784	1.4792	1.3850	7.29%
	0.5N	0.8449	0.7014	0.7346	0.7603	9.88%
70	1N	0.8098	0.7052	0.8182	0.7777	8.09%
	0.5N	0.3843	0.3372	0.4099	0.3771	9.78%
60	1N	0.41	0.4437	0.3827	0.4121	7.41%
	0.5N	0.3739	0.4481	0.4009	0.4076	9.21%

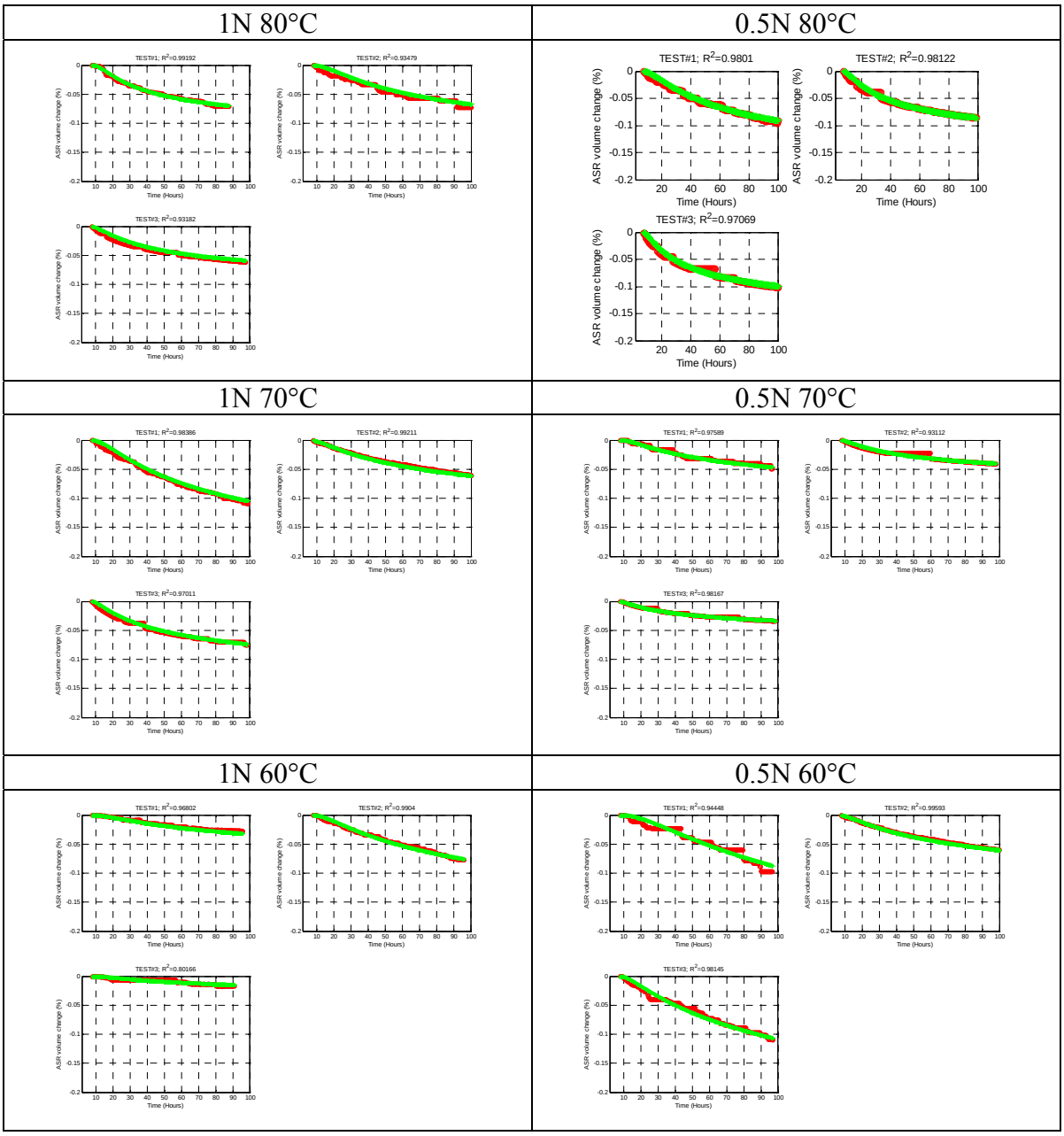

Figure D11 Measured (Red) and Modeled (Green) Solution Volume Change over Time for CA6 with 2 Alkalinities (1 and 0.5N NH + CH) at 3 Temperatures (60, 70, 80°C)

Table D11 Calculated Rate Constant Based on the Modeled Curve (Green) in Figure D11 for CA6

	β				mean	COV.
Temperature, °C		**test1**	**test2**	**test3**		
80	1N	0.6197	0.5263	0.5289	0.5583	9.53%
	0.5N	0.3915	0.4302	0.4192	0.4136	4.82%
70	1N	0.4384	0.4055	0.4434	0.4291	4.80%
	0.5N	0.5034	0.4554	0.5092	0.4893	6.03%
60	1N	0.5177	0.4456	0.4432	0.4688	9.03%
	0.5N	0.3877	0.4122	0.4333	0.4111	5.55%

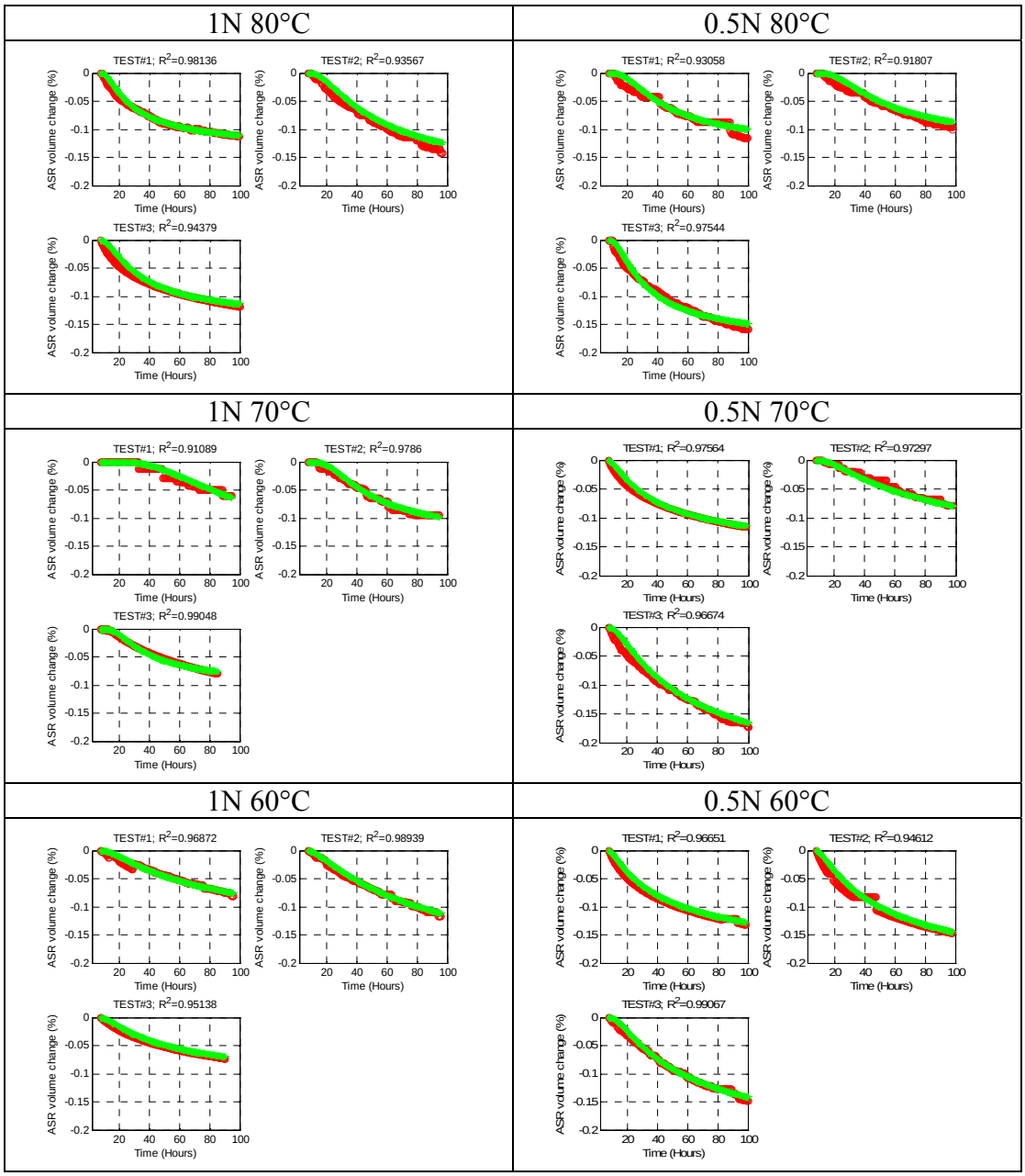

Figure D12 Measured (Red) and Modeled (Green) Solution Volume Change over Time for CA7 with 2 Alkalinities (1 and 0.5N NH + CH) at 3 Temperatures (60, 70, 80°C)

Table D12 Calculated Rate Constant Based on the Modeled Curve (Green) in Figure D12 for CA7

	β				mean	COV.
Temperature, °C		**test1**	**test2**	**test3**		
80	1N	0.8318	1.0191	0.8221	0.8910	12.46%
	0.5N	1.5932	1.4526	1.3634	1.4697	7.88%
70	1N	1.1526	1.4464	1.1802	1.2597	12.88%
	0.5N	0.5327	0.6363	0.5518	0.5736	9.61%
60	1N	0.478	0.4678	0.5055	0.4838	4.03%
	0.5N	0.4651	0.4542	0.5337	0.4843	8.90%

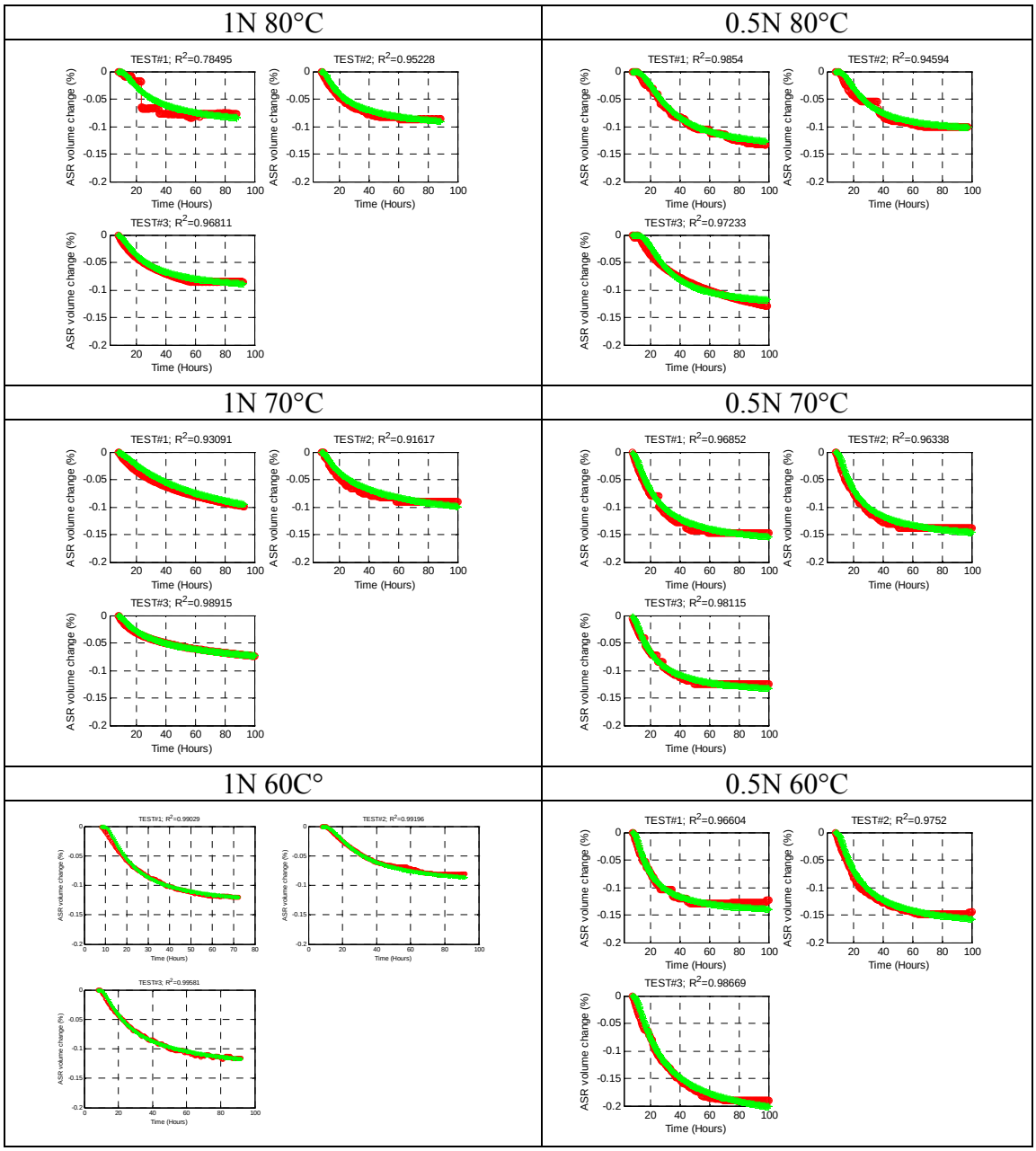

Figure D13 Measured (Red) and Modeled (Green) Solution Volume Change over Time for CA8 with 2 Alkalinities (1 and 0.5N NH + CH) at 3 Temperatures (60, 70, 80°C)

Table D13 Calculated Rate Constant Based on the Modeled Curve (Green) in Figure D13 for CA8

	β				mean	COV.
Temperature, °C		**test1**	**test2**	**test3**		
80	1N	0.767	0.7529	0.7686	0.7628	1.13%
	0.5N	1.8588	1.8607	1.6755	1.7983	5.92%
70	1N	0.443	0.5449	0.4724	0.4868	10.77%
	0.5N	0.9658	0.9695	1.125	1.0201	8.91%
60	1N	1.0647	1.2581	1.0332	1.1457	10.89%
	0.5N	0.9865	0.8676	0.8131	0.8891	9.97%